P-199

[redacted]

Copy Number 31

NASA CR 182125

NASA

LARGE SCALE ADVANCED PROP-FAN (LAP) HIGH SPEED WIND TUNNEL TEST REPORT

By: William A. Campbell
Peter J. Arseneaux
Harry S. Wainauski

HAMILTON STANDARD DIVISION
UNITED TECHNOLOGIES CORPORATION

Prepared for

National Aeronautics and Space Administration
NASA-Lewis Research Center
Contract NAS3-23051

NASA CR 182125

NASA

LARGE SCALE ADVANCED PROP-FAN (LAP) HIGH SPEED WIND TUNNEL TEST REPORT

By: William A. Campbell
Peter J. Arseneaux
Harry S. Wainauski

HAMILTON STANDARD DIVISION
UNITED TECHNOLOGIES CORPORATION

Prepared for

National Aeronautics and Space Administration
NASA-Lewis Research Center
Contract NAS3-23051

CONTENTS

CONTENTS (Continued)

ILLUSTRATIONS

ILLUSTRATIONS (Continued)

ILLUSTRATIONS (Continued)

ILLUSTRATIONS (Continued)

TABLES

1.0 ABSTRACT

High Speed Wind Tunnel Testing of the SR-7L Large Scale Advanced Prop-Fan (LAP) is herein reported. The LAP is a 2.74 meter (9.0 FT) diameter, 8-bladed tractor type rated for 4475 KW (6,000 SHP) at 1698 RPM. It was designed and built by Hamilton Standard under contract to the NASA Lewis Research Center. The LAP employs thin swept blades to provide efficient propulsion at flight speeds up to Mach .85.

Testing was conducted in the ONERA S1-MA Atmospheric Wind Tunnel in Modane, France. The test objectives were to confirm the LAP was free from high speed classical flutter, determine the structural and aerodynamic response to angular inflow, measure blade surface pressures (static and dynamic) and evaluate the aerodynamic performance at various blade angles, rotational speeds and flight Mach numbers.

The measured structural and aerodynamic performance of the LAP correlated well with analytical predictions thereby providing confidence in the computer codes used for design. There were no signs of classical flutter throughout all phases of the test up to and including the 0.84 maximum Mach number achieved. Steady and unsteady blade surface pressures were successfully measured for a wide range of Mach numbers, inflow angles, rotational speeds and blade angles.

No barriers were discovered that would prevent proceeding with the PTA (Prop-Fan Test Assessment) Flight Test Program scheduled for early 1987.

2.0 SUMMARY

This report describes the procedures followed and results obtained during High Speed Wind Tunnel Testing of the SR-7L Large Scale Advanced Prop-Fan (LAP). The LAP is a 2.74 meter (9 foot) diameter, 8 bladed advanced propeller designed to attain high propulsive efficiency at flight speeds up to Mach .85. The Prop-Fan achieves this superior speed and efficiency by employing thin swept blades and high disc loading. The High Speed Wind Tunnel Test was conducted in the ONERA S1-MA Large Atmospheric Wind Tunnel facility in Modane, France.

Testing was accomplished during two separate tunnel entries. This was necessitated by a test rig failure during the first entry. Prior to interruption of the test in early 1986, all structural dynamic, aerodynamic performance and a limited amount of blade steady pressure testing was completed. Testing resumed in early 1987, and culminated in the completion of the steady and unsteady blade pressure tests. A complete chronological history of both tunnel entries is provided in Appendix A.

The purpose of the Wind Tunnel Test was to confirm the LAP was free from high speed classical flutter, determine the structural and aerodynamic response to angular inflow, measure blade surface pressures (both steady and unsteady) and evaluate the aerodynamic performance at various blade angles, rotational speeds and Mach numbers. Results from these tests would assist in determining the readiness of the LAP and its instrumentation systems for follow-on Prop-Fan Test Assessment (PTA) flight testing. The Wind Tunnel Test was accomplished in two phases. In the first phase, structural dynamic and aerodynamic performance data were collected concurrently, for the 2, 4 and 8 blade configurations, over a wide range of blade angles, Mach numbers and rotational speeds. Due to rig constraints, structural dynamic evaluation of the LAP operating at a fixed angle of attack was limited to the 2 bladed Prop-Fan configuration at a 3° inflow angle. During the second phase of testing, a specially fabricated static pressure tapped blade was employed to map the blade surface steady pressure distribution for a range of operating conditions. Due to drive system power limitations, testing was accomplished utilizing a two bladed Prop-Fan configuration to provide blade loadings simulating the take-off, cutback and design cruise conditions. The final phase of testing, also utilizing the two blade configuration for reasons mentioned above, employed another specially instrumented blade incorporating high frequency response pressure transducers. Data from these transducers was used to define and evaluate the blade surface unsteady pressure distribution for the same operating conditions run during the steady pressure test. Unsteady pressure testing included evaluating the effects of a wake in the propeller inflow at a 3° angle of attack.

2.0 (Continued)

Results from the High Speed Wind Tunnel Test demonstrated that the SR-7L Prop-Fan was free of high speed blade flutter over the entire operating envelope tested. Additionally, all measured blade surface and blade shank strains were well below allowables set prior to testing. Good correlation was found between measured and analytically predicted 1P strain sensitivities for the SR-7L blade. Results confirmed that 1P strain peaks inboard on the blade and lessens near the tip, and that, in general, blade strains were found to increase with power and Mach number. Measured aerodynamic performance for the four blade configuration corresponded well with analytical predictions over the entire range of points tested. Though good agreement for the eight blade configuration was found at Mach numbers of .70 and .73, performance was slightly underpredicted at .5 Mach number. Steady and unsteady blade surface pressure measurements were successfully collected for a wide range of Mach numbers, rotational speeds, blade angles and inflow angles. In addition to confirming the presence of tip edge and leading edge vortex flows at Mach numbers of zero and .2, shock waves were evident at the trailing edge at .7 and .78 Mach number. Unsteady pressure responses were clearly present as evidenced by a dominant 1-P response in the angular inflow data and significant 2-P response in the wake inflow data. Sinusoidal response was evident on the pressure (face) side of the blade for all cases examined for angular inflow conditions and on the suction (camber) side under low loading conditions. Under high loading conditions, the suction (camber) side exhibited non-sinusoidal response resulting from the presence of tip and leading edge vortices.

3.0 INTRODUCTION

The Prop-Fan, a high speed, high efficiency aircraft propulsion concept was launched during the "Oil Crunch" days of the mid 1970's. In response to the national need to reduce fuel consumption, Congress directed NASA to address a series of aircraft related technologies aimed at increasing the fuel efficiency of airline operation. In response, NASA created the Aircraft Energy Efficiency (ACEE) program which addressed fuel savings through advancements in both airframe and engine technology. The element of the ACEE program offering the greatest potential fuel savings was the Advanced Turboprop Program (ATP) as described in Reference 1. The NASA Lewis Research Center had total responsibility for the ATP project which is summarized in Reference 2. The objective of the ATP was to demonstrate technology readiness for efficient, reliable and acceptable operation of advanced turboprop-powered commercial transports at cruise speeds up to Mach 0.8 and at altitudes above 9,800 meters (30,000 ft.) while maintaining cabin comfort levels (noise and vibration) comparable to those of modern turbofan-powered aircraft. The technology would also apply to possible new military aircraft for a variety of missions. Out of this project evolved the Prop-Fan concept.

Although high propulsive efficiency from turboprops was nothing new, the standards of high cruise speed and cabin comfort set by the contemporary turbofan powered aircraft were beyond the capability of any turboprop powered aircraft. The Prop-Fan concept evolved to satisfy the requirements of high speed and altitude with improved efficiency while maintaining a high degree of cabin comfort. It is characterized by the large number of blades (8 or 10), thin airfoil sections, and swept blade planforms (Figure 3-1).

Once the concept and its benefits were defined, NASA conducted a systematic program to verify that the predicted benefits could be achieved and that there were no unsolvable problems in implementing the concept. The potential benefits of the Prop-Fan propulsion concept have been investigated in numerous propulsion and aircraft systems studies conducted by the airframe and engine manufacturers under NASA sponsorship (References 3 thru 9). These studies have shown that the inherent efficiency advantage that turboprop propulsion systems have achieved at lower cruise speeds may now be extended to the higher speeds of todays turbofan and turbojet powered aircraft. By applying swept wing/reduced diameter technology to the design of propeller blades, and by achieving higher disc loadings through the use of a greater number of blades, it was found that the inherent fuel efficiency of the propeller can be extended to speeds up to .85 Mn. The efficiency of the Prop-Fan should allow aircraft to be designed that are 15% to 25% more efficient than today's most technologically advanced turbofan powered airlines (Reference 10).

Since 1975, Hamilton Standard has been deeply involved with the NASA Lewis Research Center in the development of the Prop-Fan. Until recently, this effort utilized a series of .622 meter (2 ft.) diameter models which incorporated differing numbers of blades as well as changes in blade shape. These models underwent exhaustive testing in several wind tunnels at NASA and

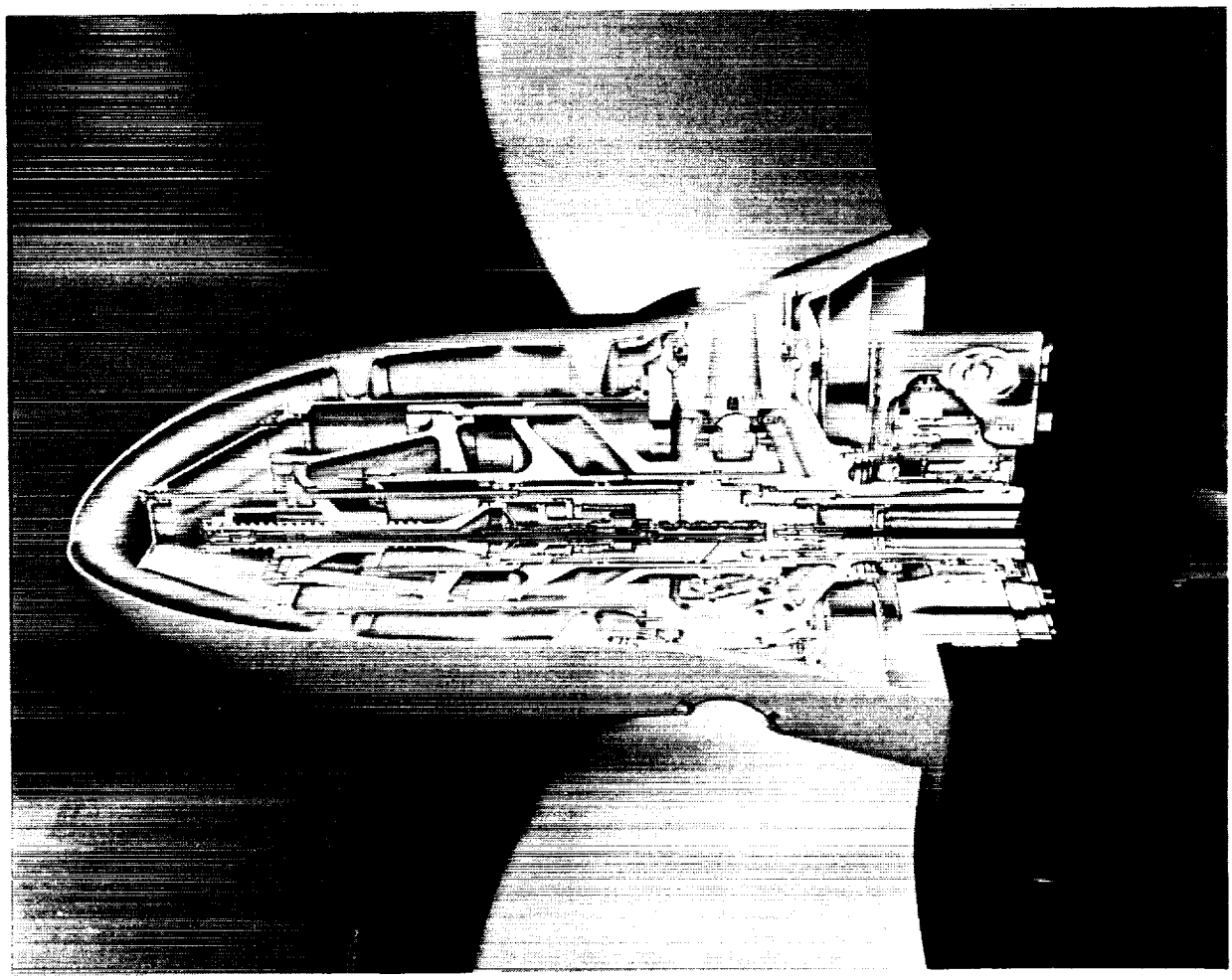

FIGURE 3-1. PROP-FAN CONCEPT

3.0 (Continued)

United Technologies as well as on a NASA Jetstar acoustic research vehicle. In these tests the targeted efficiencies were demonstrated, the source noise was characterized, and structural dynamics verified. Detailed descriptions of these tests and results have been the subject of numerous technical papers; a summary of which can be found in References 11 and 12.

Although the results of the aerodynamic performance and source noise tests can be confidently scaled from model to product size, the structure of the solid homogeneous model blades is so different from that envisioned for a product that extrapolation of model structural behavior is unacceptable. The verification of the structural integrity of a large-scale Prop-Fan then becomes the final major technical hurdle to be crossed before industry acceptance of the Prop-Fan as a viable aircraft propulsion scheme. This verification was initiated in 1983, when Hamilton Standard, under the sponsorship of NASA Lewis Research Center, embarked on a program to build and test a 2.74 meter (9 foot) diameter, 8-bladed Prop-Fan. This Prop-Fan was designated the SR-7L or the Large Scale Advanced Prop-Fan (LAP). The major elements of the LAP program are depicted in the summary schedule shown in Figure 3-2. Detail design and fabrication of the Prop-Fan components (blades, hub and blade retention, spinner, pitch change mechanism, pitch control and instrumentation system) was initiated early in 1983 building on a preliminary design conducted
under an earlier contract. Various bench tests of each component then followed to verify key design characteristics.

Design, fabrication and test of an aeroelastically scaled .622 meter (2 foot) Prop-Fan model was included in the LAP program to obtain an early assessment of the Prop-Fan's aeroelastic characteristics. This model has been designated SR-7A. Other objectives of the SR-7A testing included the measurement of aerodynamic performance and noise.

Testing of the SR-7L rotor under the LAP program included in-house whirl, static and high speed wind tunnel tests. Whirl Rig Testing was successfully conducted on the G-5 rig at Hamilton Standard. The objectives of the test were to measure the stiffness of the blade retention system, evaluate the control dynamic characteristics of the blade pitch change system and determine the wear rate on blade actuation and retention hardware. Whirl Rig Testing was conducted using stub weights to simulate the Prop-Fan blades. The stubs provided appropriate centrifugal loading but generated essentially no thrust or drag. The Static Rotor Testing, with SR-7L blades installed, was successfully conducted at the Wright Aeronautical Laboratory at Wright Patterson Air Force Base in Dayton, Ohio (Reference 13). The goals of the Static Rotor Test were to measure the static aerodynamic performance of the LAP, assess stall flutter characteristics and investigate the structural behavior and integrity of the SR-7L blades for static operating conditions. The final component of the LAP test program, High Speed Wind Tunnel Testing, is the subject of this report.

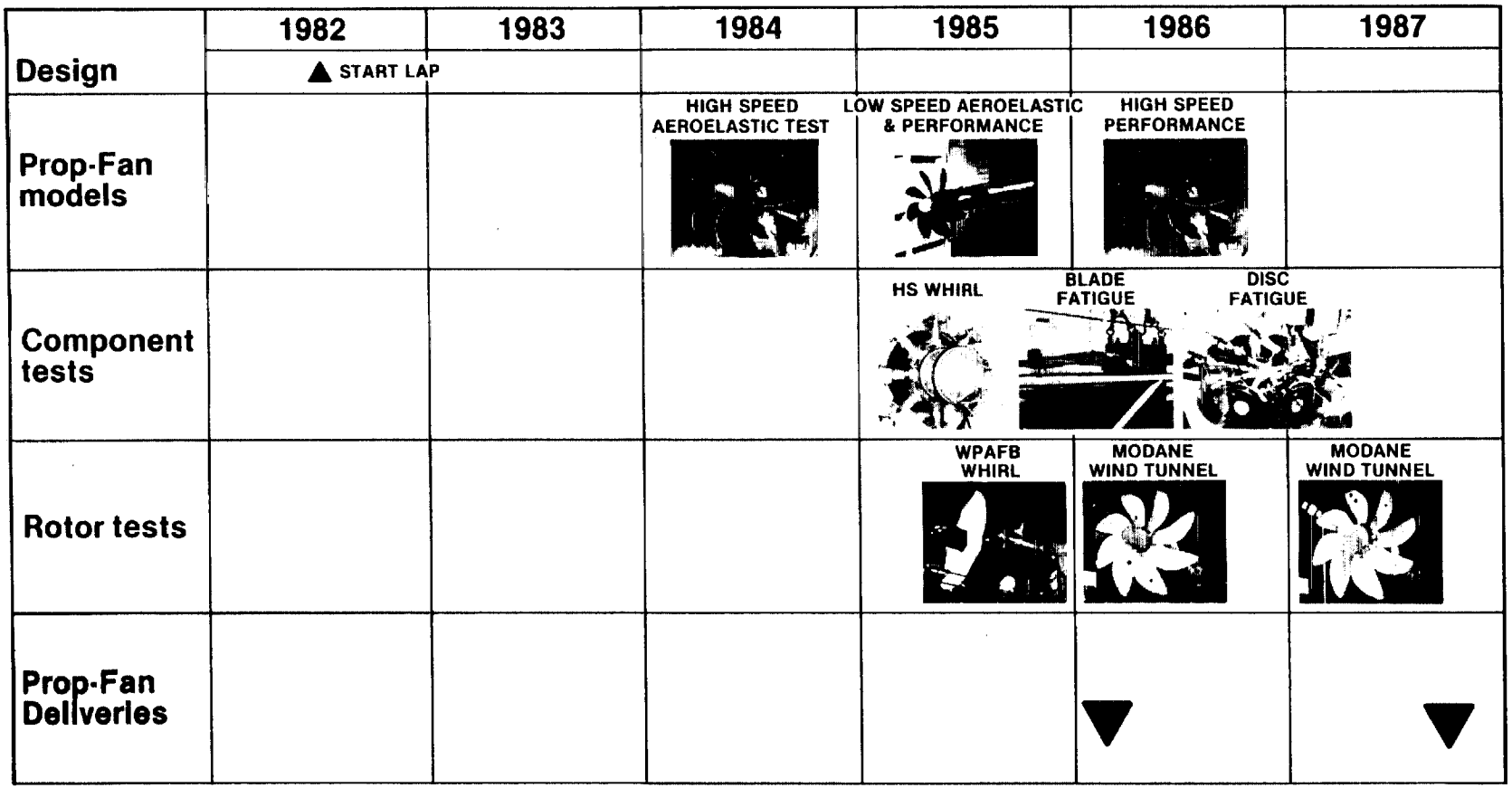

FIGURE 3-2. LARGE SCALE ADVANCED PROP-FAN (LAP) PROGRAM ELEMENTS

3.0 (Continued)

The LAP program is complemented by another NASA sponsored program, the Prop-Fan Test Assessment (PTA) program, which takes the large scale Prop-Fan (developed under the LAP program) and mates it with an Allison Gas Turbine supplied gas generator and gearbox to form a Prop-Fan propulsion system. The major elements of the PTA program are depicted in Figure 3-3. Following completion of the Static Engine Test at Rohr's Brown Field Facility, the quick engine change (QEC) nacelle will be mated to the wing of Gulfstream II aircraft which will ultimately serve as the flight test vehicle for the Prop-Fan.

This report addresses the procedures and results of the High Speed Wind Tunnel Test conducted at the ONERA S1-MA Atmospheric Wind Tunnel in Modane, France. This facility was selected for three reasons. First, it is capable of reaching high cruise Mach numbers. Second, it is sufficiently large (8 meter or 26.25 ft. diameter test section) to avoid excessive wall interference effects; and third, it has an existing model drive system. Although the power capability of the drive is only about one fourth of what the Prop-Fan is designed to absorb, proper blade loading can be reached by running with a partial set of blades (eight, four, and two blade configurations). The specific objectives of the test are listed below.

- To conduct a careful and controlled search for any evidence of classical flutter. Because of the greater air density of the wind tunnel, it is possible to more closely approach the flutter threshold than at the 10,668 meter (35,000 ft) flight altitude. At design Mach number the wind tunnel operates at an effective altitude of about 4,267 meters (14,000 ft). Analytic predictions and tests of the SR-7A model strongly suggested that classical flutter would not be encountered.

- To measure steady and unsteady surface pressure on the blade as well as overall Prop-Fan performance. One blade was instrumented with 465 static taps (20 chordal at 13 radial stations on the camber side and 16 chordal at 13 radial stations on the face side of the blade) to obtain a complete pressure map. Another blade had 26 dynamic pressure sensors (7 chordal at the 35 inch station and 6 chordal at the 49 inch station, for each side of the blade) to assess unsteady effects. These measurements will provide benchmark data for understanding the physics of transonic flow over the blades and for verification of analytic computer codes.

- To determine the structural and aerodynamic response of the Prop-Fan to angular inflow. Analysis of data from this simple, known angular inflow condition will significantly contribute to the understanding of Prop-Fan behavior in the more complex, airplane installed flow field.

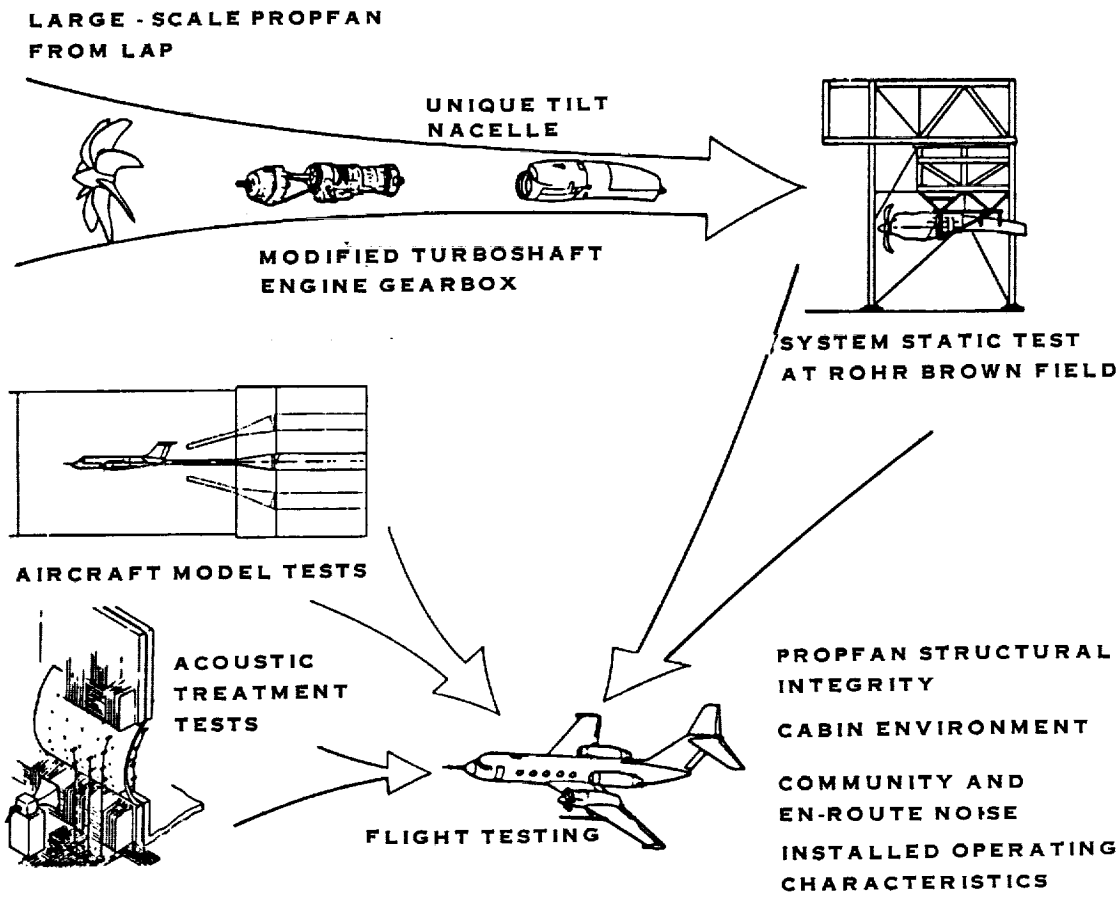

FIGURE 3-3. PROP - FAN TEST ASSESSMENT (PTA) PROGRAM ELEMENTS

4.0 PROP-FAN DESCRIPTION

4.1 General Description

The Large Scale Advanced Prop-Fan shown in Figure 4-1, is a 2.74 meter (9 ft.) diameter 8 bladed tractor type Prop-Fan rated for 4474 KW (6,000 HP) at 1698 RPM. To achieve the program objective of verifying large scale Prop-Fan structural integrity, a number of design requirements and goals were established as summarized in Figure 4-2. The requirements include characteristics judged essential to meeting the program objective as well as design features established from prior work. The goals, on the other hand, represent design targets and were judged less important to the program objective. The LAP is designed to be mounted on a standard 60A splined propeller shaft for an existing turboprop gearbox. It has a hydraulically actuated blade pitch change system and a hydromechanical pitch control that allows the Prop-Fan to operate in a speed governing mode or, with minor modifications, in a Beta Control mode, as was the case in this test. Beta Control mode operation was chosen to provide the operator the capability to select desired blade pitch angles while running. A pitchlock feature is also incorporated in the actuator. This feature maintains the propeller blade angle in the event of a loss of system operating oil pressure. The design of the actuator and control is based on proven technology used in Hamilton Standard's military and commercial propellers. A brief description of each of the major elements of the LAP as depicted in Figure 4-1, is presented below.

4.2 SR-7L Blade

Features of the structural configuration of the SR-7L blade are shown in Figure 4-3. These include a central aluminum spar which forms the structural "backbone" of the blade, a multi-layered glass-cloth-reinforced shell overhanging the leading and trailing edge of the spar, a nickel sheath which covers the leading edge of the outer two-thirds of the blade, and a non-operational integral heater in the inboard leading edge area. Though the scope of the LAP testing never included utilization of the blade heaters, it was decided to install the heaters to evaluate the structural response of a blade closely resembling that of a typical blade configuration. The remaining internal cavities are filled with low-density rigid foam. The outboard portion of the spar is intentionally moved toward the blade leading edge to increase stability by reducing overhung mass in the tip trailing edge, while at the same time increasing the integrity of the leading edge from the standpoint of resistance to foreign object damage.

The blade design makes use of a NACA Series 16 airfoil outboard and a Series 65 circular arc airfoil inboard. Each blade has an activity factor of 227.3 with 45° of blade sweep at the tip. The blades were designed with predeflection so that the blades will assume the desired aerodynamic shape at the cruise operating condition (Reference 14).

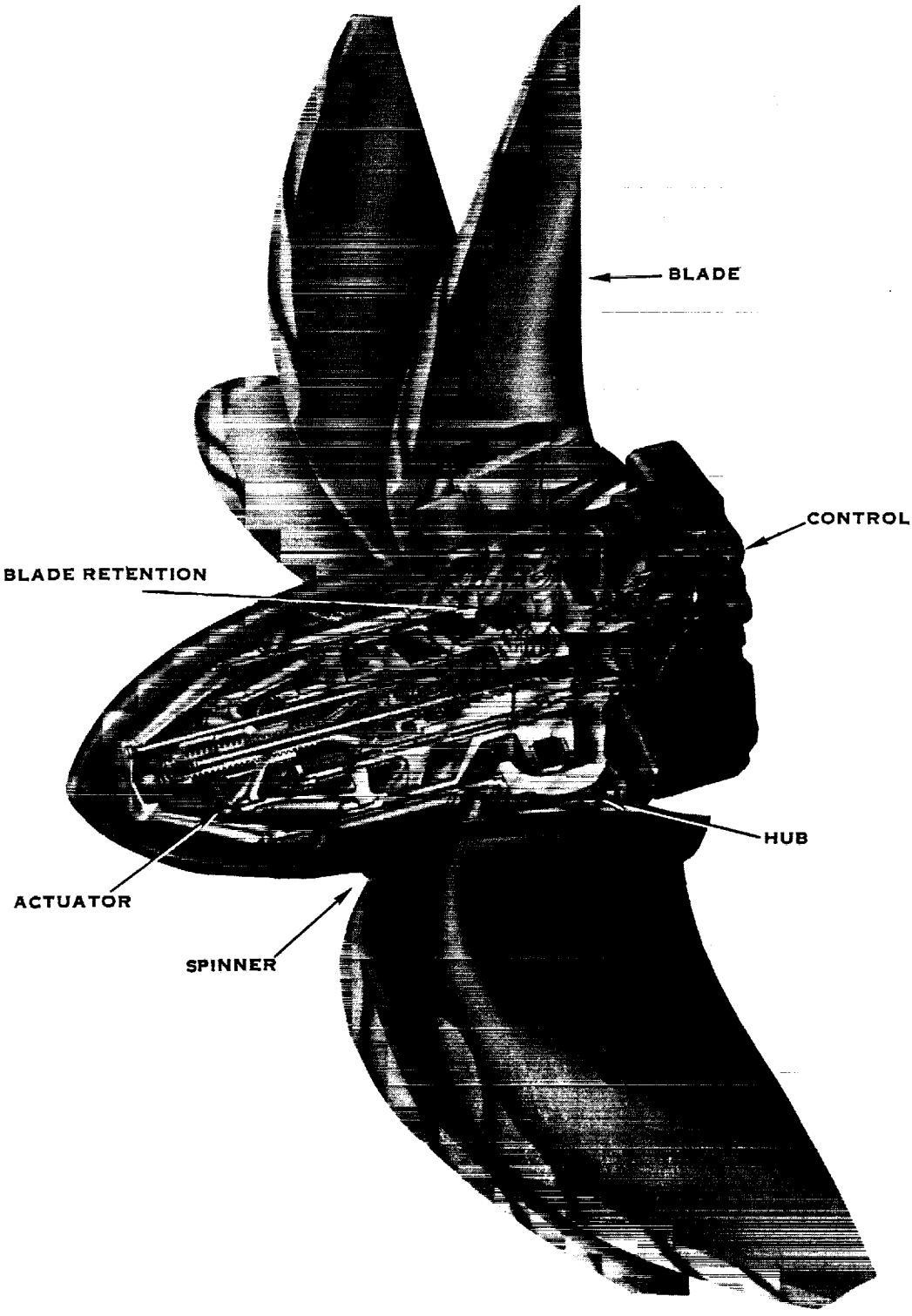

FIGURE 4-1. LARGE-SCALE ADVANCED PROP-FAN

UNITED TECHNOLOGIES HAMILTON STANDARD

DESIGN REQUIREMENTS

- **Configuration**

Diameter	2.74 meter (9 ft)
Number of blades	8

- **Design point**

Cruise Mach number	0.8
Altitude	10,668 meters (35,000 ft)
Tip speed	244 meters/sec (800 ft/sec)
Power loading ($SHP/_D2$)	32

- **Structural integrity**

  Flutter free over normal flight envelope ($M \leq 0.8$)
  Stresses within allowable limits
  Overspeed tolerance
  Critical speed margins

- **Safety features**
  Leading edge projection
  Lighting protection
  Icing protection (installed but not operational)
  Overspeed protection

- **Reverse thrust capability**

DESIGN GOALS

• Net efficiency (isolated nacelle)	-78.6% AT M = 0.8, 10,668 meters (35,000 ft)(Cruise) -52.0% AT M = 0.2, SL (TO)
• Noise	
Near field (design point cruise, max. free field, 0.8D)	-144 db overall sound pressure level
Far field	-FAR 36 minus 10 db
• Stall flutter	-None at 100% TO power and rpm; M = 0 - 0. 2
• High speed (classical) flutter	-None over extended flight envelope, ($M \leq 0.85$) 105% max operating speed
• Over speed limit (hub, blades, blade retention)	-120% max operating speed - no yield -141% max operating speed - no failure
• Foreign object damage	
Minor-Birds up to 4 oz	-No damage to primary blade structure
Moderate -2" Hail; Birds to 2 lb	-Some loss of material or airfoil distortion; operate at 76% power for 5 minutes
Major-Birds up to 4 lb	-Some loss of material or airfoil distortion; maintain ability to feather
• Blade life	-35,000 hr - replacement with scheduled maint. -50,000 hr - meantime between unscheduled removal

FIGURE 4-2. DESIGN REQUIREMENTS AND GOALS SUMMARY

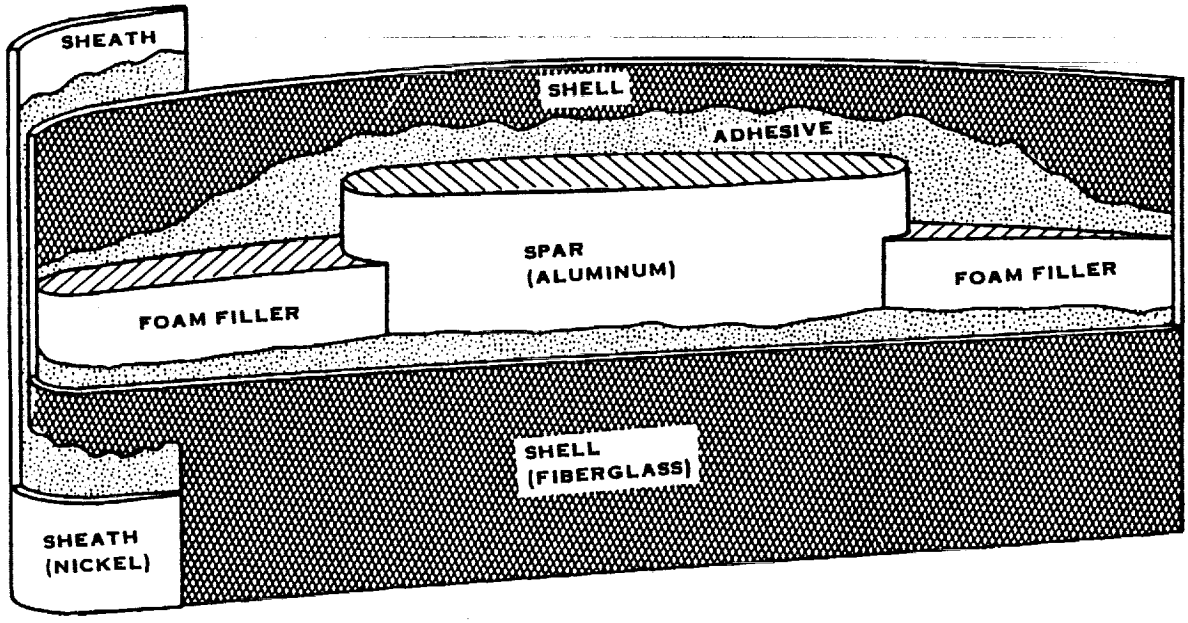

FIGURE 4-3. FEATURES OF THE SR-7L BLADE CONSTRUCTION

4.2 (Continued)

Although some improvements in sweep/stress/stability trade-offs were predicted through the use of advanced composites, it was decided not to include these in the final blade design. Their use would require the development of new manufacturing technology, both in terms of suitable construction methods and processes, and lengthy development of design allowables to reflect the manufacturing process.

It was felt that the scope of the program would be best served by utilizing the service-proven combination of an aluminum spar enveloped with a fiberglass shell for which processes and stress allowables are well known.

4.3 Pitch Change Actuator

The pitch change system is comprised of two components, a pitch change actuator and a control. The pitch change actuator is the prime mover for blade angle change and is located within the Prop-Fan hub as shown in Figure 4-4. Its primary components are an internal stationary piston, a translating outer cylinder with an integral yoke to engage each of the blade trunnions and a pitchlock and servo assembly which contains a four-way metering beta valve assembly, a pitchlock screw, a ground adjustable low pitch stop, a servo piston and a ball screw to drive the pitchlock screw and beta valve (Reference 15).

As stated earlier, the LAP was modified to operate in the Beta Control mode throughout all phases of the wind tunnel test. This was accomplished through the use of an electromechanical controller (D.C. motor and gearhead) mounted on the front of the dome as shown in Figure 4-5. The controller provides the rotary input to the pitchlock servo directly, replacing the rotary input from the half area servo. In order to give the D.C. motor full control of the blade angle, the servo and ballscrew must be disconnected from the pitchlock screw by removing the quill shaft. This disables the control signal and allows the motor to work directly on the pitchlock screw without having to fight the servo output. This permits the operator to remotely position blade angle as desired while running.

The actuator was designed to present state-of-the-art technology and low development risk technique that has been used on a number of existing propeller systems. The design uses mostly steel for the load carrying members and all surfaces subject to sliding seal wear are chrome plated to increase durability. The actuator was designed to conservative stress and deflection levels to minimize development effort while maintaining a reasonable but not minimum weight.

The pitch change mechanism was designed such that all malfunctions will either cause the system to pitchlock or go to feather. An additional safety feature on the LAP is a ground adjustable low pitch stop. This limits the minimum blade angle under all circumstances.

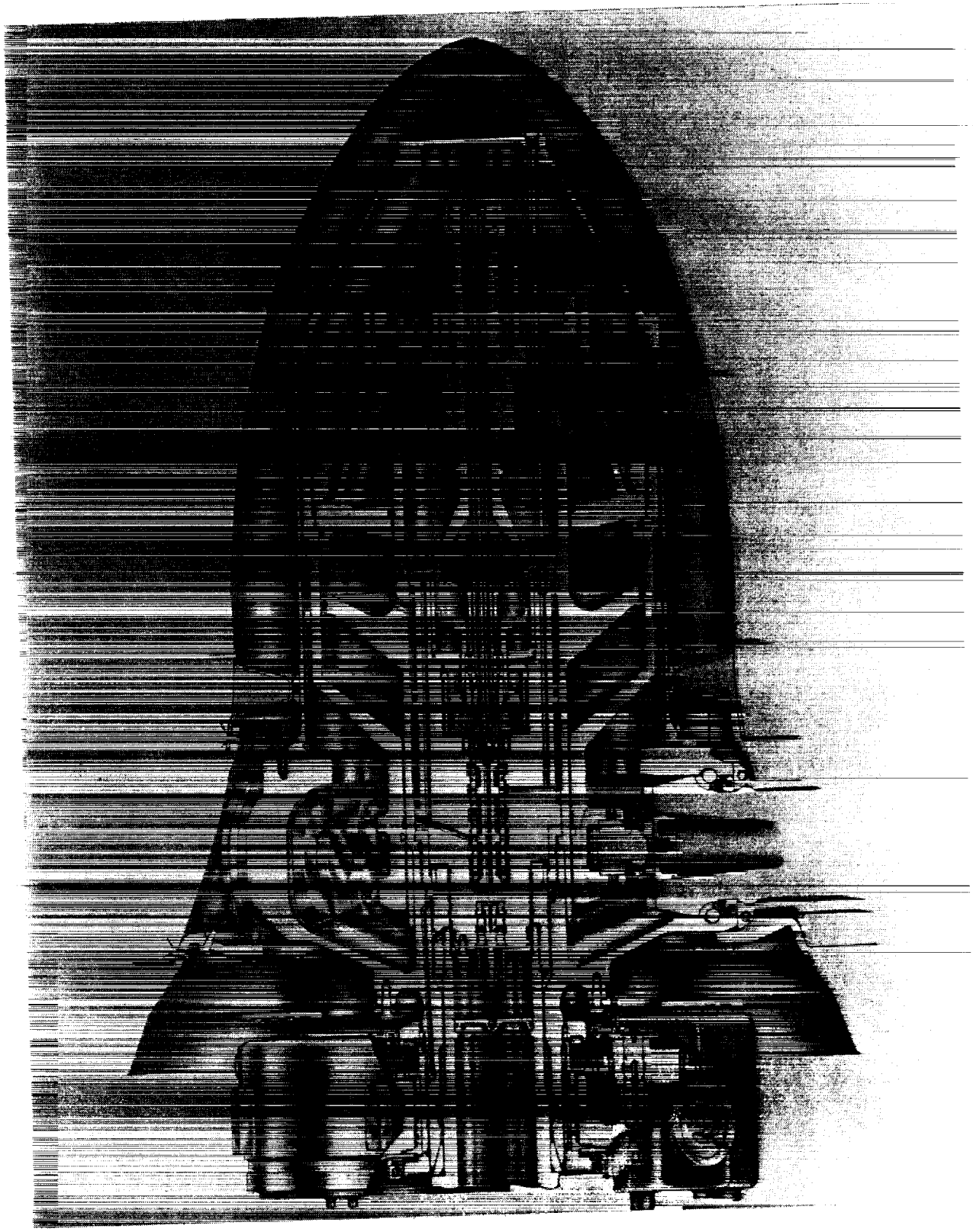

FIGURE 4-4 LAP PITCH CHANGE ACTUATOR

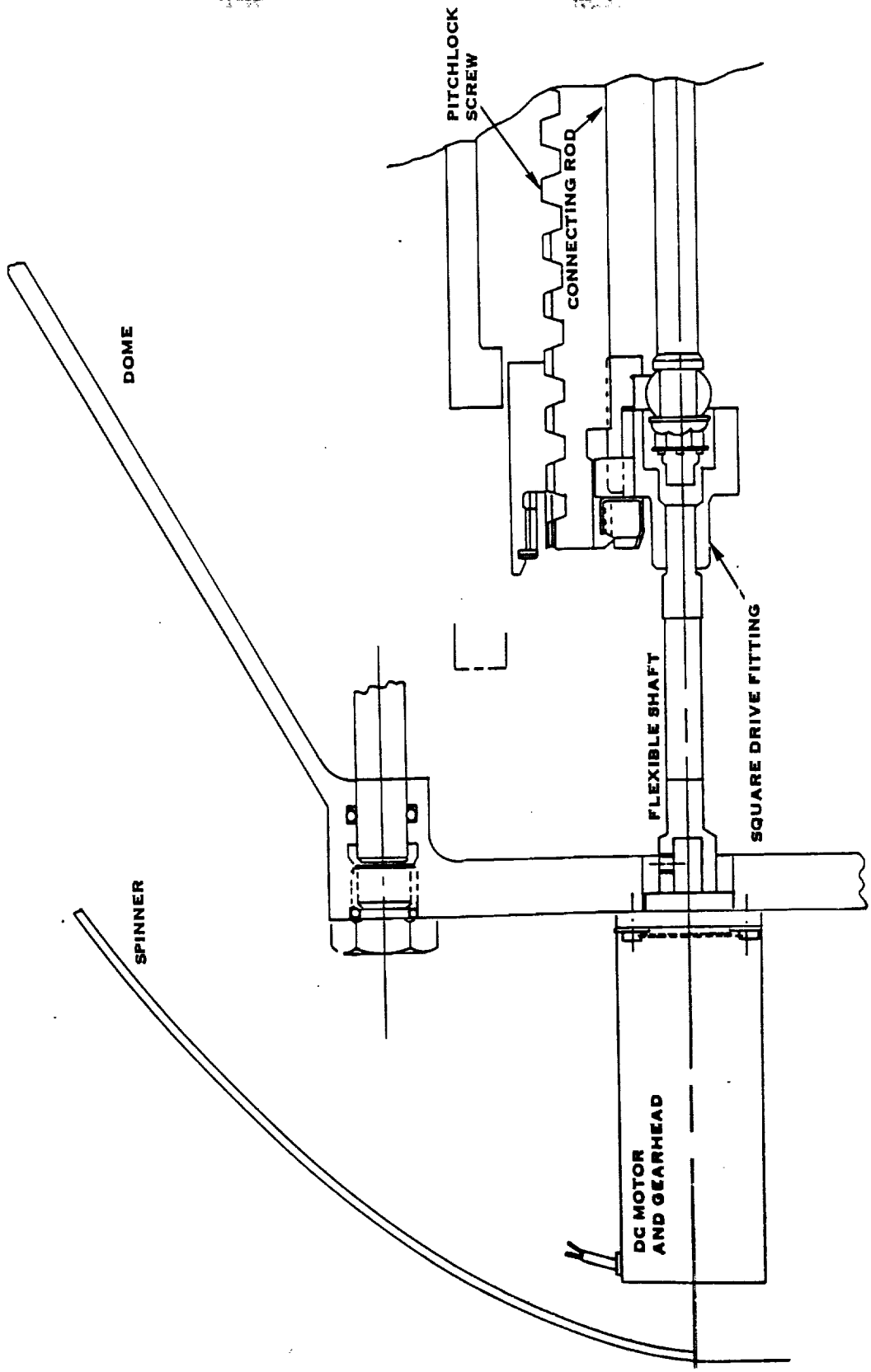

FIGURE 4-5. MOTOR DRIVEN PITCH CONTROL MECHANISM

4.4 Pitch Control

To minimize cost and development time, it was decided to utilize a modified version of an existing turboprop propeller control. Based on the type of engine and gearbox planned for use with the LAP, the control selected was a modified 54460 control (Figure 4-6). The 54460 hydromechanical integral oil control, which is currently in use on the Grumman E-2 and C-2 aircraft, was modeled after the Lockheed C-130 and P-3 controls. Since the first production unit in 1956, there have been over 12,000 built and they have logged over 80,000,000 operating hours.

The primary function of the LAP control, as modified for wind tunnel testing, was to generate the hydraulic pressure necessary to assure proper actuator operation. Two gear type pumps located in the stationary control and driven by the Prop-Fan shaft provided the system hydraulic pressure.

4.5 Hub and Blade Retention

The LAP hub assembly forms a semi-rigid link between the blades, which provide the thrust, and the engine shaft, which provides the torque (Reference 16). The hub and tailshaft is a one piece forged component which is carburized, heat treated and machined (Figure 4-7). A single row ball bearing retains each of the eight blades in the hub, while the tailshaft secures the Prop-Fan to the engine shaft through two cone seats that are preloaded against each other by the Prop-Fan retaining nut. The hub also forms the support for the pitch change actuator system, the control and the spinner.

The retention transmits the loads from the blades to the hub while accommodating changes in blade pitch. The single row ball bearing retention provides ease of maintenance by allowing individual blade replacement without disassembly of the hub. It has a through hardened inner race which seats against the aluminum blade shank and an outer race which is integral with the barrel. The outer race is carburized to achieve the hardness necessary to support the ball loads. The balls are kept apart from each other by an elastomeric separator. The rotational speed of the Prop-Fan keeps the retention submerged in oil which is contained in the hub by eight blade seals (Reference 17).

4.6 Spinner

The LAP spinner and rear bulkhead assembly is essentially a reinforced fiberglass/epoxy shell, supported by the hub and actuator, and incorporating an aerodynamic shape to facilitate proper air flow around the blade roots (Figure 4-8). Its primary function is to insure proper Prop-Fan aerodynamic performance. The rear bulkhead, which mounts on the rear of the hub arms, is the main structural support for the spinner and provides a mounting surface for much of the instrumentation hardware in the rotating field.

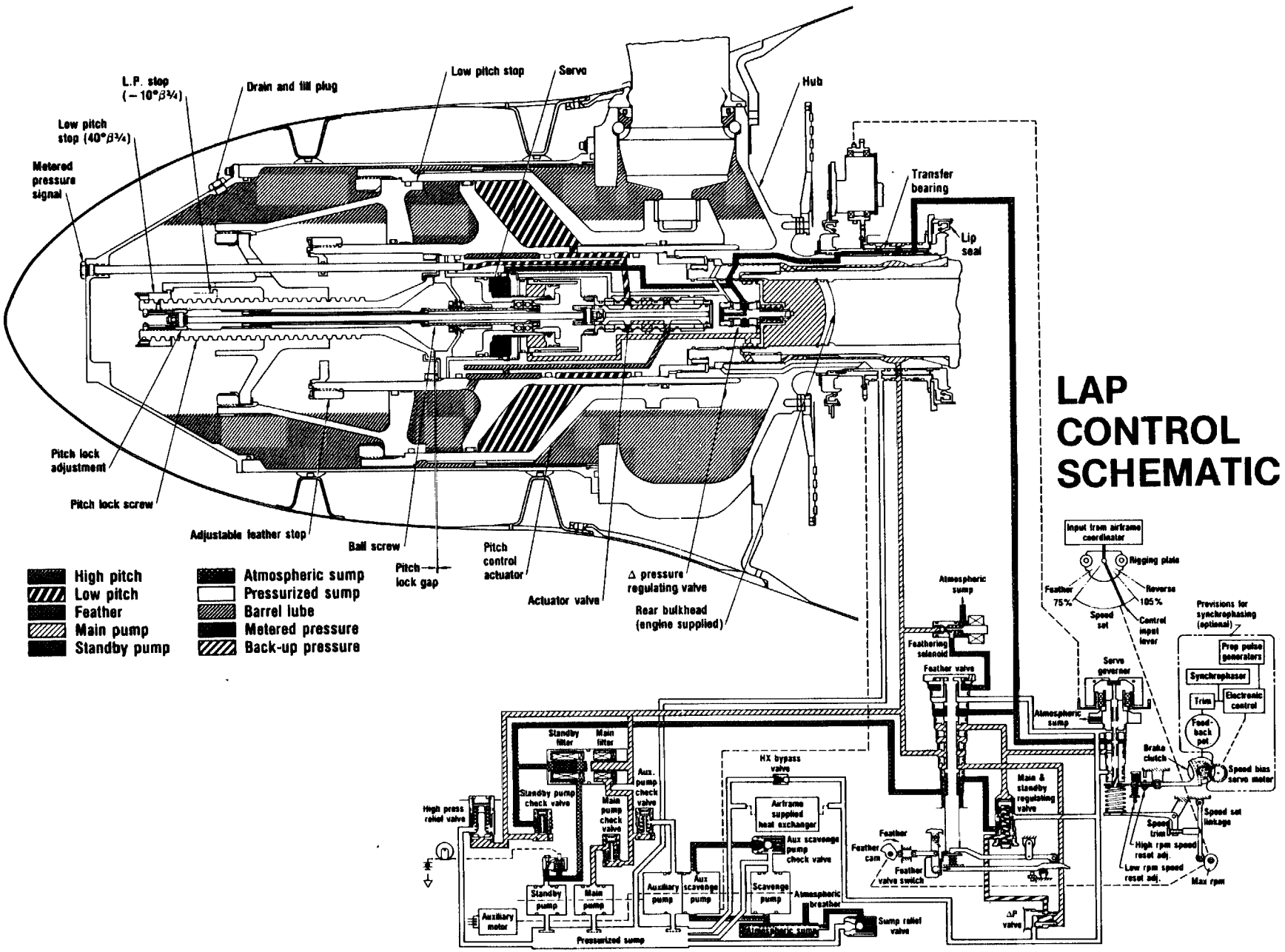

LAP CONTROL SCHEMATIC

FIGURE 4-6. LAP CONTROL SCHEMATIC

FIGURE 4-7. SR-7L HUB

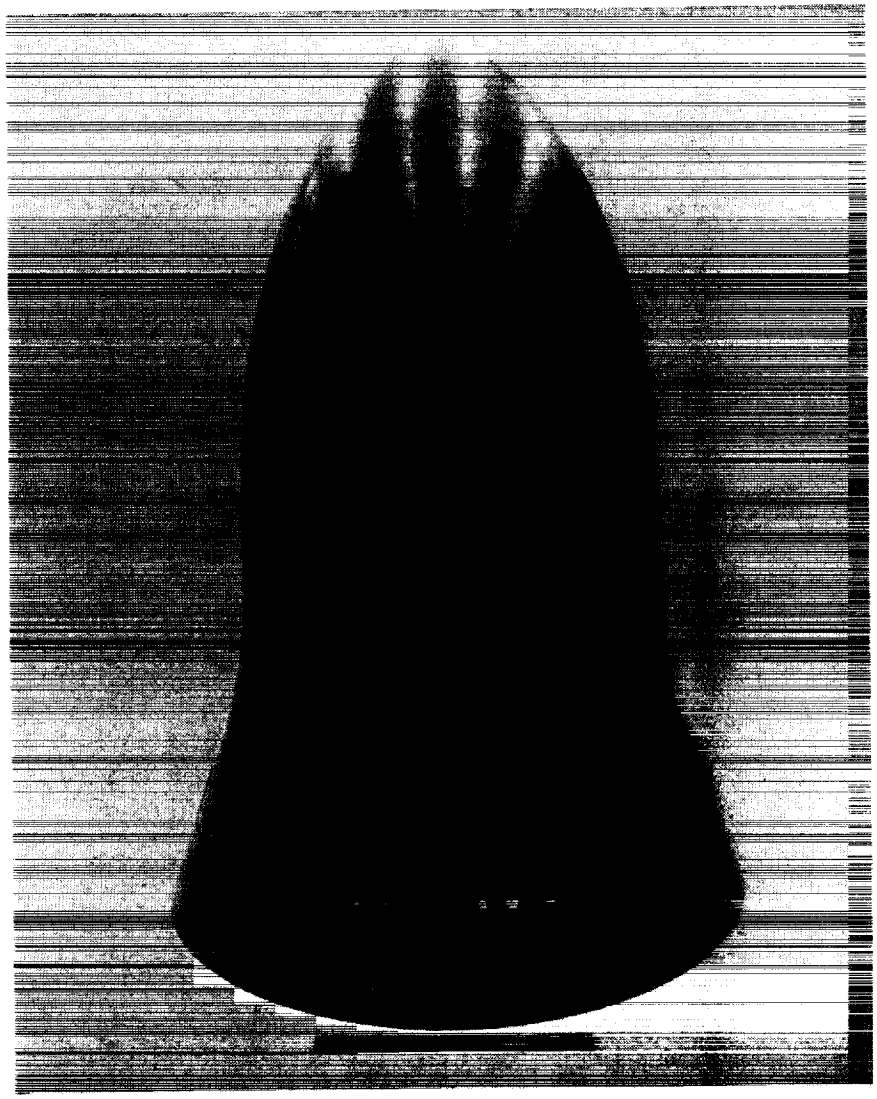

FIGURE 4-8 SR-7L SPINNER

5.0 INSTRUMENTATION DESCRIPTION

5.1 General Description

In order to accomplish the objectives set forth in the Plan of Test, three separate instrumentation arrangements were employed to gather and record the desired data. For the structural dynamic and aerodynamic performance tests, the system described in sections 5.1.1 and 5.1.2 was used. For the blade surface steady pressure test, a system description is provided in section 5.2 and for the unsteady pressure test, the system used is presented in section 5.3. Figure 5-1 provides a summary listing of all the instrumentation, rotating and stationary, and indicates whether it was provided by H.S. or ONERA. Additional detailed descriptions of the key data gathering deviced required for specific phases of the test are presented in the appropriate Test Procedure section of this report.

Common to all three instrumentation arrangements was the frequency modulated multiplex electronic data acquisition system (DAS), as shown in Figure 5-2, and several Prop-Fan system diagnostic monitoring devices.

5.1.1 Electronic Data Acquisition Systems (DAS)

The electronic data acquisition system for the LAP provided the capacity to transmit 33 channels of information from the electronic measurement devices on the rotating side of the Prop-Fan to the data collection and monitoring equipment in the stationary field. This was accomplished by employing an eight ring platter-type slip ring assembly which provided the electrical interface for the DAS between the rotating Prop-Fan assembly and the non-rotating control.

As illustrated in Figure 5-2, three rings were utilized to transmit data to the stationary field. One of the three carried the output of a potentiometer which was mounted as shown in Figure 5-3 and used for monitoring blade angle position. The other two rings transmitted the remaining 32 channels of information which consisted of signals from two miniature pressure transducers for monitoring actuator high and low pitch pressures and combinations of up to 30 blade strain or unsteady pressure signals, as determined by the particular test being conducted. Transmittal of these 32 signals on only two slip rings necessitated the use of FM multiplexing. The DC signals from the strain gages and pressure transducers in the rotating field were divided into two groups of sixteen. The signals were then converted to frequency modulated signals by two groups of voltage controlled oscillators. Each group was then multiplexed by a mixer, allowing thirty two channels to be transmitted through two slip rings. The two groups of sixteen channels were each detranslated in the stationary field to four groups of four multiplexed channels (IRIG Standard 1A thru 4A). Each set of four channels was recorded on one track of a standard Honeywell 101 tape recorder. Simultaneously, eight discriminators were used to demodulate any two groups of four channels for real time monitoring of data. One discriminator was tuned to the center frequency of each channel.

H.S. INSTRUMENTATION

ROTATING:

- HIGH AND LOW PITCH OIL PRESSURE MEASUREMENT
- BLADE ANGLE MEASUREMENT
- BLADE VIBRATORY STRAIN MEASUREMENTS
- BLADE SURFACE STEADY AND UNSTEADY PRESSURE MEASUREMENTS

STATIONARY:

- CONTROL SUPPLY PRESSURE MEASUREMENT
- CONTROL SUMP OIL TEMPERATURE MEASUREMENT
- HEAT EXCHANGER ΔP MEASUREMENT
- CONTROL AND SCANIVALVE ACCELEROMETER MEASUREMENTS

INSTRUMENTATION PROVIDED BY ONERA (ALL STATIONARY)

TEST RIG INSTRUMENTATION:

- RIG ACCELEROMETER MEASUREMENTS
- PROP-FAN RPM PICK-UP
- RIG BEARING TEMPERATURE MEASUREMENTS
- BALANCE AND TORQUEMETER MEASUREMENTS (FIGURE 6-10)
- CENTERBODY PRESSURE MEASUREMENTS (FIGURES 7-10, 7-11)
- SPINNER BULKHEAD PRESSURE MEASUREMENTS (FIGURE 7-12)

TUNNEL INSTRUMENTATION:

- STATIC PRESSURE MEASUREMENTS:
  - 4 METERS UPSTREAM OF THE PROP-FAN PLANE OF ROTATION
  - ADJACENT TO THE PROP-FAN PLANE OF ROTATION
- STAGNATION PRESSURE MEASUREMENTS
- AIR DENSITY MEASUREMENT
- STAGNATION TEMPERATURE MEASUREMENT OF FLOW
- STATIC TEMPERATURE MEASUREMENT OF FLOW

FIGURE 5-1. H.S. AND ONERA INSTRUMENTATION LIST

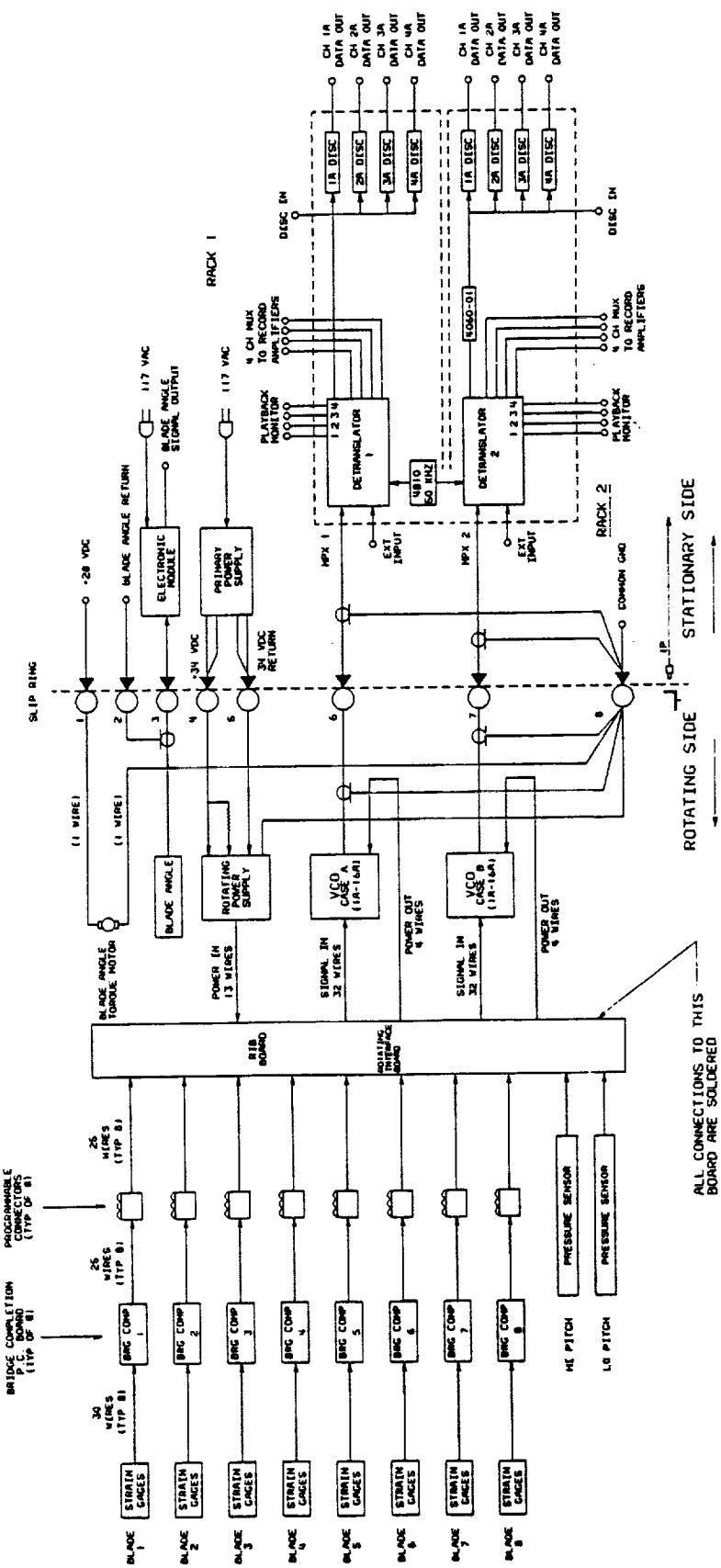

FIGURE 5-2. LAP INSTRUMENTATION SYSTEM SCHEMATIC

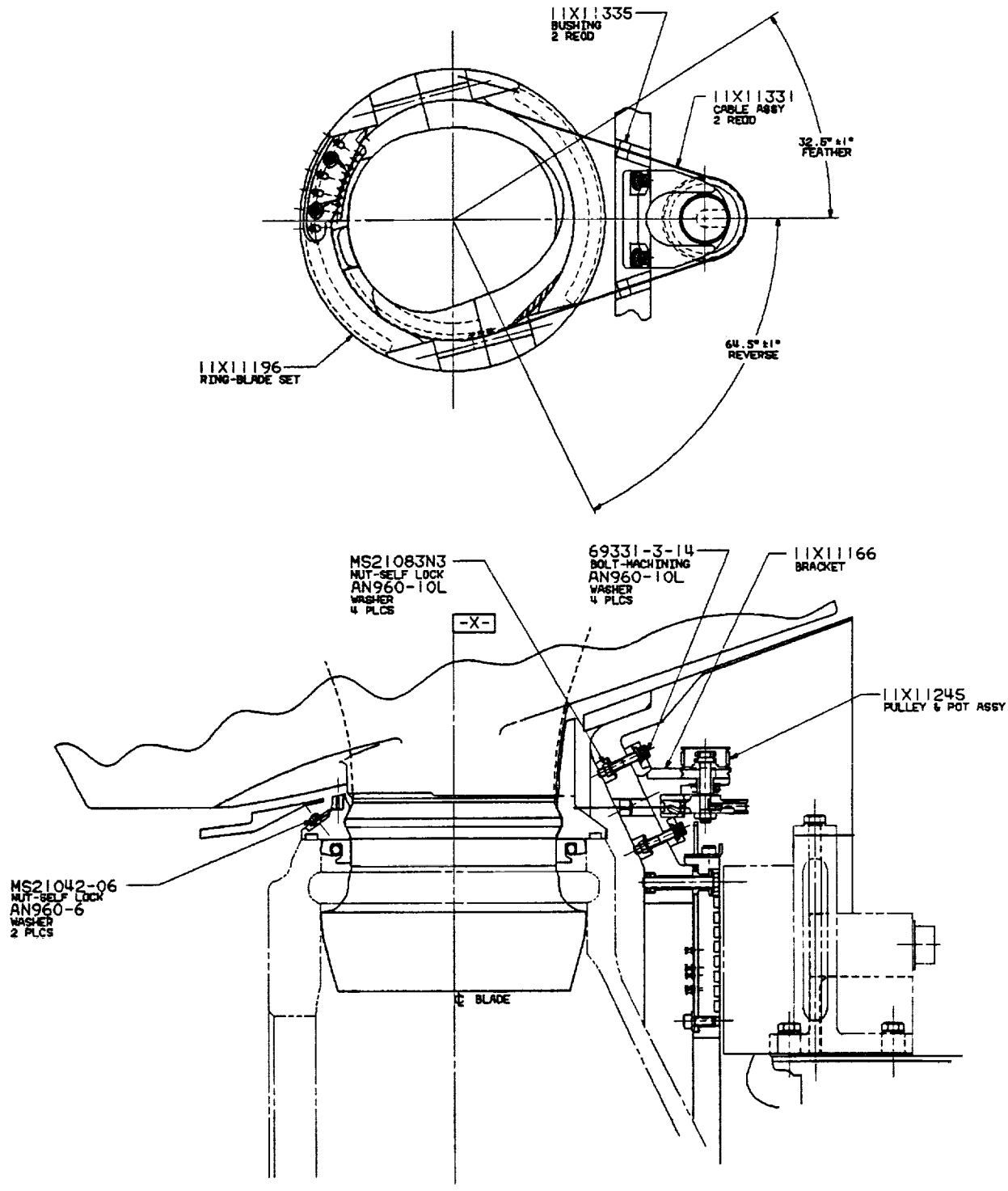

FIGURE 5-3. LAP BLADE PITCH ANGLE MEASUREMENT SYSTEM

5.1.1 (Continued)

The FM electronic instrumentation system provided inherent noise immunity for data transmission. The frequency response for the system was DC to 1000 HZ. Overall accuracy of the system was ±3% RSS. Time correlation between channels was ±13.8 microseconds.

The electronic instrumentation system allowed for up to ten blade shell or shank gages to be installed on any blade, though a maximum of 32 gages could be active at any one time. Strain gaged blades were closely monitored during flutter and critical speed testing as well as measuring strains at various operating conditions. The blade shank strain gages were employed to measure blade bending moments.

A total of sixteen gages could be selected from blades one through four and an additional sixteen gages could be chosen from blades five through eight. Selection of the desired combination of gages was accomplished using eight programmable connectors mounted on the Prop-Fan hub. Programming of the connectors required using jumper wires to connect the sockets of patch boards in the connectors. The bridge completion circuits for the strain gages were located on circuit boards in the blade cuff.

Monitoring of instrumentation during the test was accomplished with an oscilloscope, a spectrum analyzer and a visicorder. The oscilloscope permitted a time domain display of four channels simultaneously. The spectrum analyzer provided the capability to display any one channel in the time or frequency domain. The analyzer also had transient capture and playback features. The visicorder provided a hard copy plot of instrumentation signals versus time.

5.1.2 Prop-Fan Diagnostic Monitoring Instrumentation

In addition to monitoring and collecting data from the rotating field, a number of parameters intended to provide protection for the Prop-Fan system were measured and digitally displayed by the stationary field instrumentation. These included control sump oil temperature, control supply oil pressure, differential pressure across the heat exchanger and control/Scanivalve accelerometer measurements. The control sump temperature was measured by a thermocouple installed inside the oil drain port of the control. Control supply oil pressure was measured by a transducer inside the control. This transducer signal was transmitted via an existing connector on the control. The heat exchanger differential pressure was measured by a ΔP transducer connected across the oil exit and return ports on the aft face of the control. The control vibration was measured by two accelerometers mounted on the propeller control housing. One accelerometer was oriented to sense motion in the horizontal direction and the other to sense motion in the vertical

5.1.2 (Continued)

direction. Additionally, during conduct of the steady pressure test, an accelerometer sensing vertical motion, was installed on the Scanivalve fairing assembly. The "once per revolution" signal was originally planned to be provided by a pickup mounted on the control and triggered by a target on the rotating propeller bulkhead. However, the system eventually used was provided by an eddy current proximity probe targeted on a 59 tooth wheel (on a 60 tooth basis) mounted on the propeller shaft. The rotational speed was averaged over ten revolutions.

5.2 Steady Pressure Measurement System

In addition to employing the instrumentation systems described in section 5.1.1 and 5.1.2, a specially designed pneumatic instrumentation system was used to collect and measure blade airfoil surface steady pressures. This system consisted of a specially fabricated blade with rows of pressure taps installed at thirteen radial stations and a scanivalve mounted on the nose of the Prop-Fan. (See Figure 5-4.) The pressure taps were connected to the scanivalve by 36 capillary tubes run along the acutator dome.

The scanivalve instrumentation system provided 36 channels for transmitting steady pressure data from the surface of the blade to the stationary field.. The scanivalve itself consists of a rotating and a stationary portion. The rotating portion was attached to the front of the actuator dome. The radial tubes from the steady pressure measurement blade were connected to the rotating portion of the scanivalve. Each tube was connected to one channel of the scanivalve. The stationary portion of the scanivalve contained a pressure transducer which monitored one channel of the scanivalve at a time. The stationary portion of the valve protruded through the leading edge of the propeller spinner and was restrained against rotation. Switching of the scanivalve channels to be monitored by the transducer was controlled by a pneumatic signal requiring a clean air source of 150 psi. The scanning rate was adjustable from 0.1 to 10 seconds per channel. The scanivalve was enclosed in an aerodynamically shaped fiberglass fairing to maintain a well behaved inflow to the Prop-Fan. The umbilical, which connected the scanivalve with the control and monitoring equipment outside the tunnel, was enclosed in a conduit with an airfoil shaped cross section. This also minimized disturbance of the inflow to the Prop-Fan.

On line monitoring of the scanivalve pressure transducer signals was accomplished using the digital readout from the scanivalve controller. In addition to recording the measured pressures on magnetic tape, on-site data manipulation and print-out generation was provided by a Fluke DA computer coupled with a plotter and dot matrix printer.

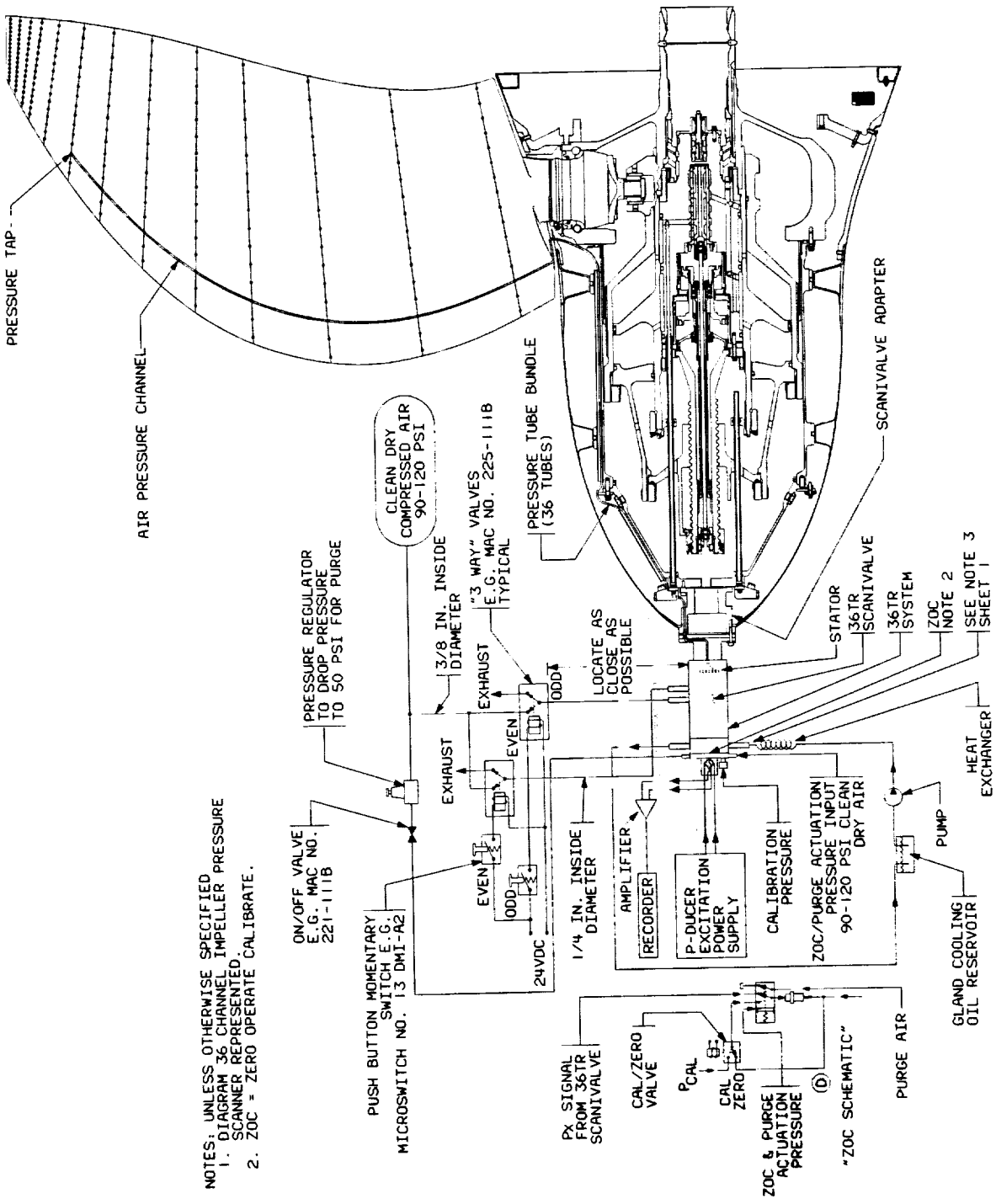

FIGURE 5-4. STEADY PRESSURE MEASUREMENT SYSTEM

5.3 Unsteady Pressure Measurement System

Collection of blade surface unsteady pressure data was accomplished by utilizing a specially instrumented blade, coupled with the instrumentation arrangement described earlier in sections 5.1.1 and 5.1.2. Twenty-six high frequency response pressure transducers were installed in two rows on each side of the blade. The unsteady pressure signals were transmitted from the rotating to the stationary field through the FM multiplex electronic data acquisition system. The signals were monitored on the four-channel oscilloscope and recorded on the IRIG tape recorder.

6.0 TEST FACILITY DESCRIPTION

6.1 Wind Tunnel Description

The LAP High Speed Rotor Test was performed in Chariot No. 3 in the S1-MA Large Wind Tunnel at the Modane-Avrieux Aerothermodynamic Test Center operated by the Office National D'Etudes et des Recherches Aerospatiales (ONERA), France (Figures 6-1 and 6-2). The tunnel is a continuous, closed loop, single return, atmospheric facility incorporating bleed slots in the tunnel walls to allow air exchange capability and tunnel circuit screens to minimize turbulence, as shown in Figures 6-3 and 6-4. Tunnel cooling is accomplished by air exchange with outside air of up to 20% of the test section mass flow rate. The tunnel is driven by two coaxial counter-rotating Pelton water turbines from a water supply with an 865 meter head, sufficient to generate a maximum of 88MW (100,000 HP). The test section velocity can be continuously varied from 8 m/sec to Mach 1.0, well encompassing the range for this test. The curves of Figure 6-5 give a representative sample of the tunnel driving power and Reynolds number as a function of test section Mach number. Tunnel pressure altitude varies from approximately 1,100 meters (3,600 ft.) at low speed, up to 6,000 meters (20,000 ft.) at Mach 1.0. At Mach 0.8 the tunnel operates at an effective pressure altitude of approximately 4,260 meters (14,000 ft.). Stagnation temperature ranges from -20°C to +60°C, depending on the external ambient temperature and the Mach number in the test section.

The tunnel has three interchangeable test sections or chariots which are positioned in the aerodynamic circuit. Each of the chariots contain a different test section shape and size and are specialized for a wide variety of test capabilities. The use of individual chariots allows a test to be conducted in the tunnel while the next test is being set-up in another chariot located in 1 of 2 adjacent mounting stations. The LAP was installed in Chariot No. 3 which has a propeller test rig permanently mounted in its test section (Figure 6-6). The test section is 14 meters long, has a circular cross section with a diameter of about 8 meters and non-permeable walls. Several lateral fillers or inserts were added to the test section specifically for this test to assure the desired range of Mach numbers could be attained. They serve the additional purpose of area compensating for the propeller test rig blockage generated by the 970 mm diameter center body. A more detailed description of the tunnel facilities is contained in References 18 and 19.

6.2 Test Rig Description

The Prop-Fan was installed on the test rig as shown in Figure 6-6. The power source for the Prop-Fan drive system is twin Turbomeca gas turbines driving a common gearbox, enclosed in a streamlined pod located approximately 7 meters downstream of the Prop-Fan plane, as shown in Figure 6-7. The engines were rated for a combined maximum power of 1000 KW (1341) HP at standard conditions (59°F, 29.92 in. Hg.) as depicted in Figure 6-8. Velocity measurements made upstream of the engine inlets indicated no disturbance at the Prop-Fan plane due to the operation of the engines. The gearbox was a

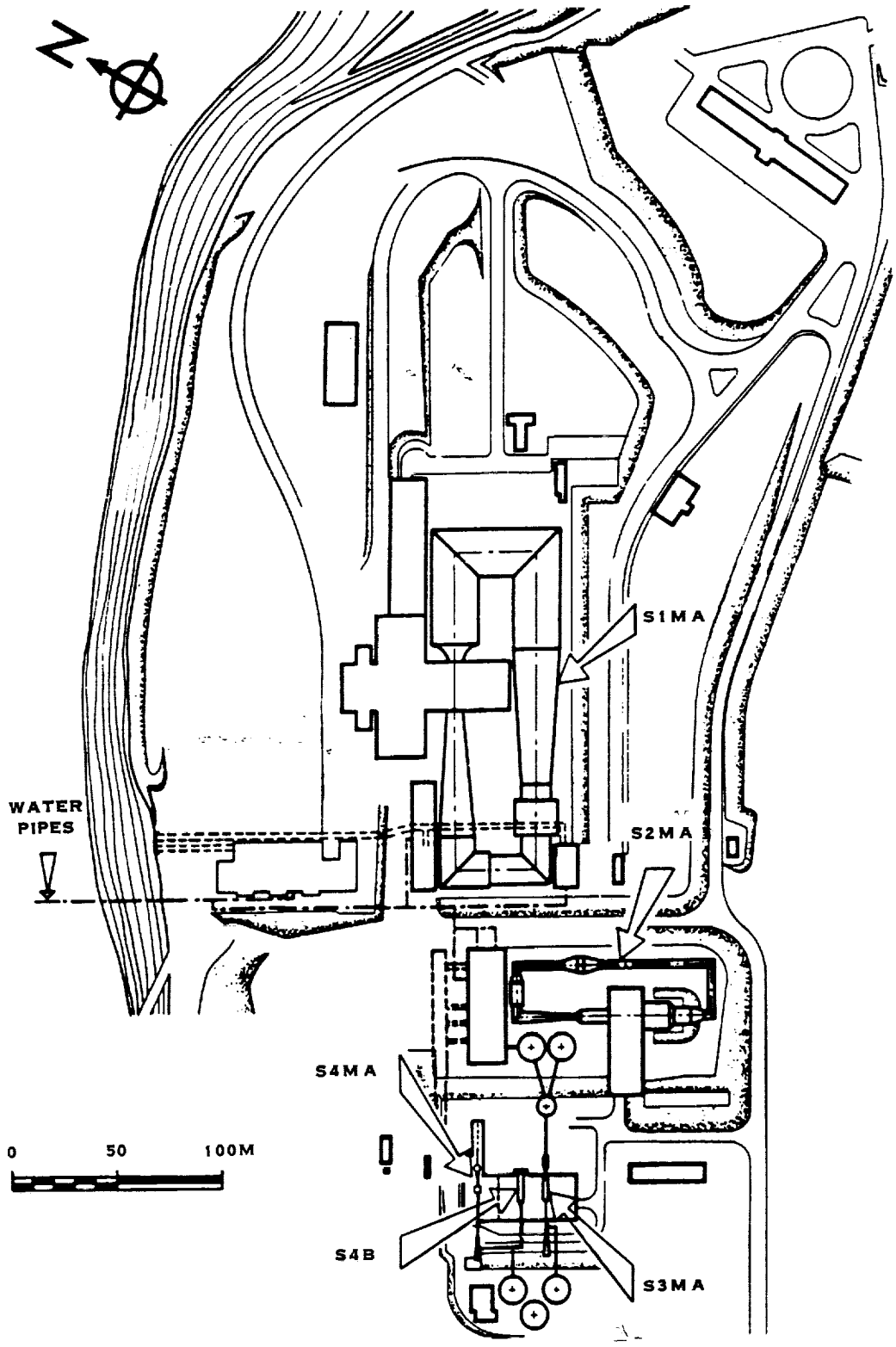

FIGURE 6-1. MODANE - AVRIEUX AEROTHERMODYNAMIC TEST CENTER

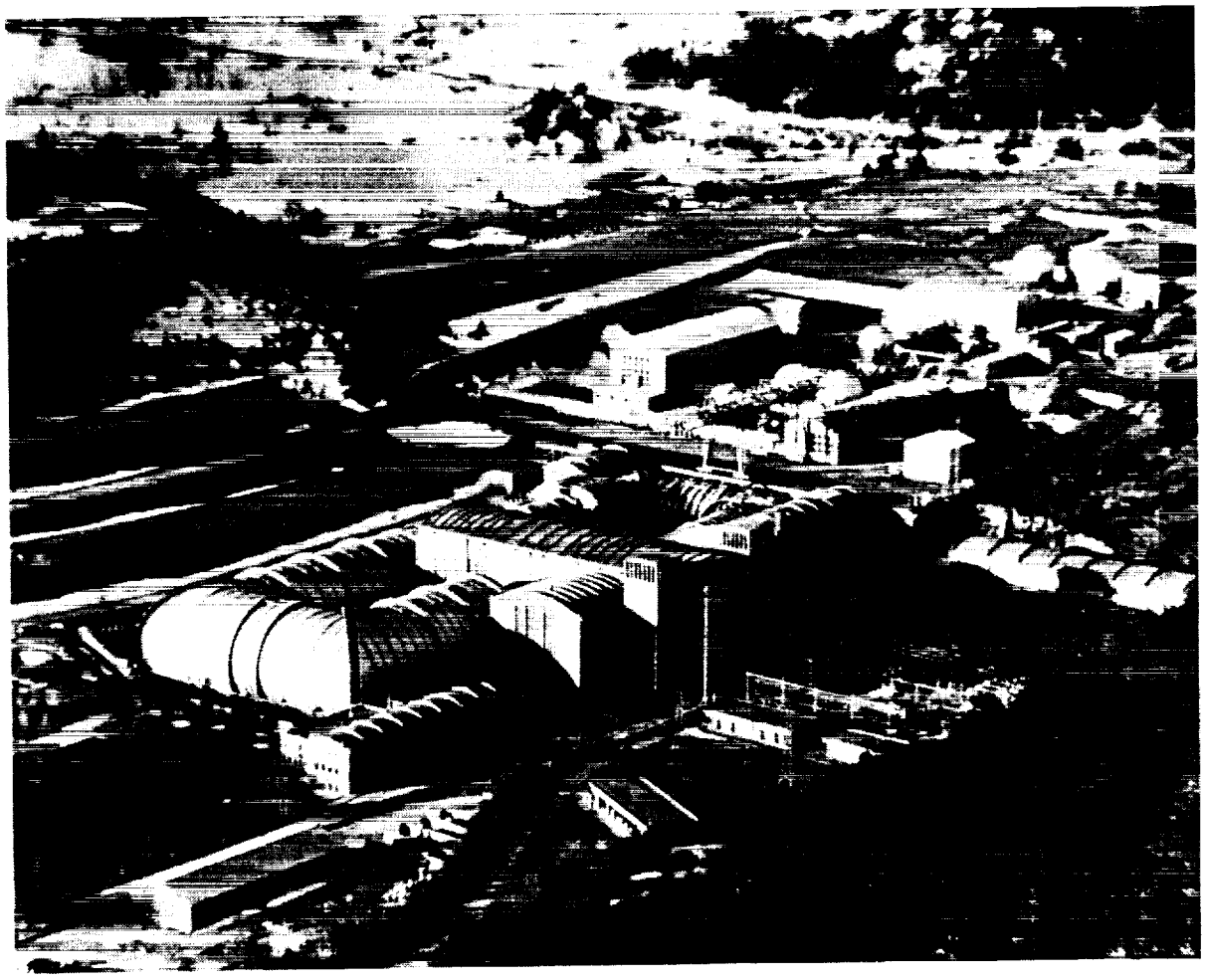

FIGURE 6-2 S1-MA LARGE ATMOSPHERIC WIND TUNNEL

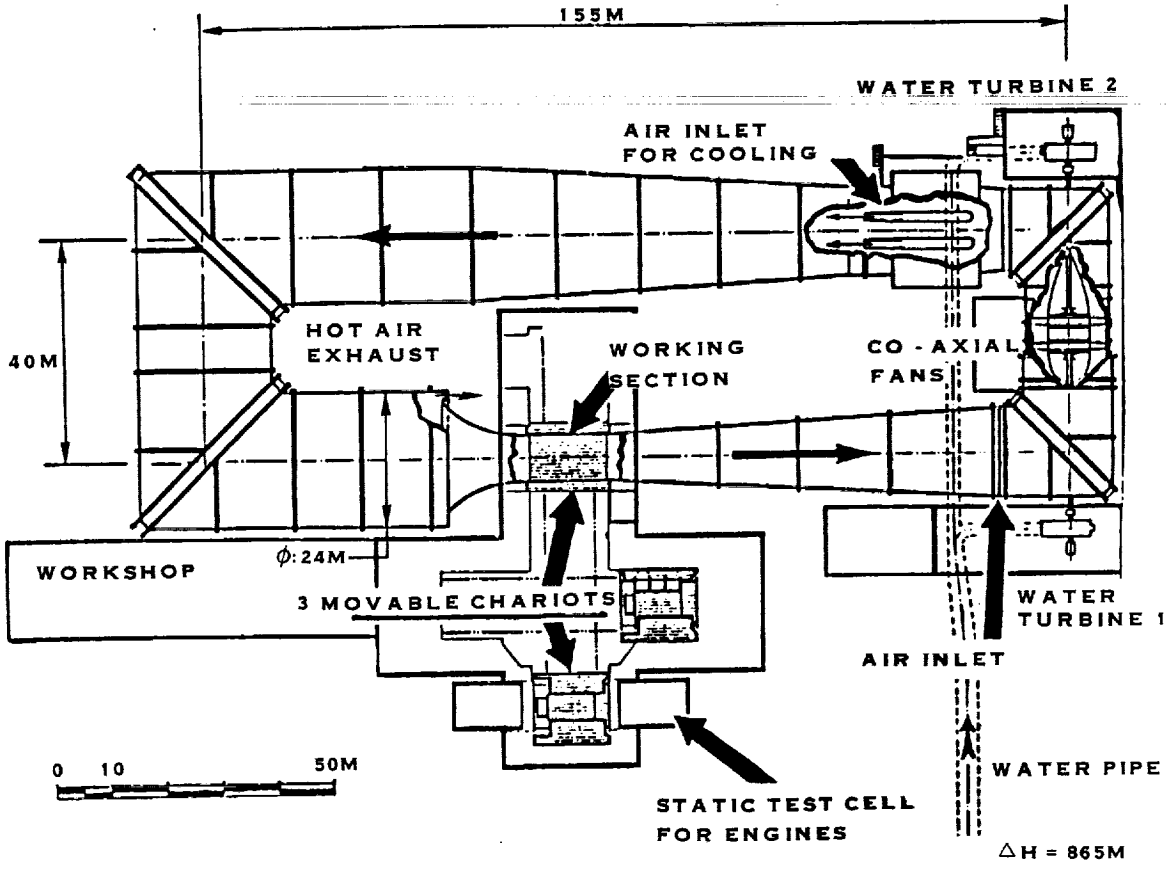

FIGURE 6-3. S1-MA WIND TUNNEL SCHEMATIC

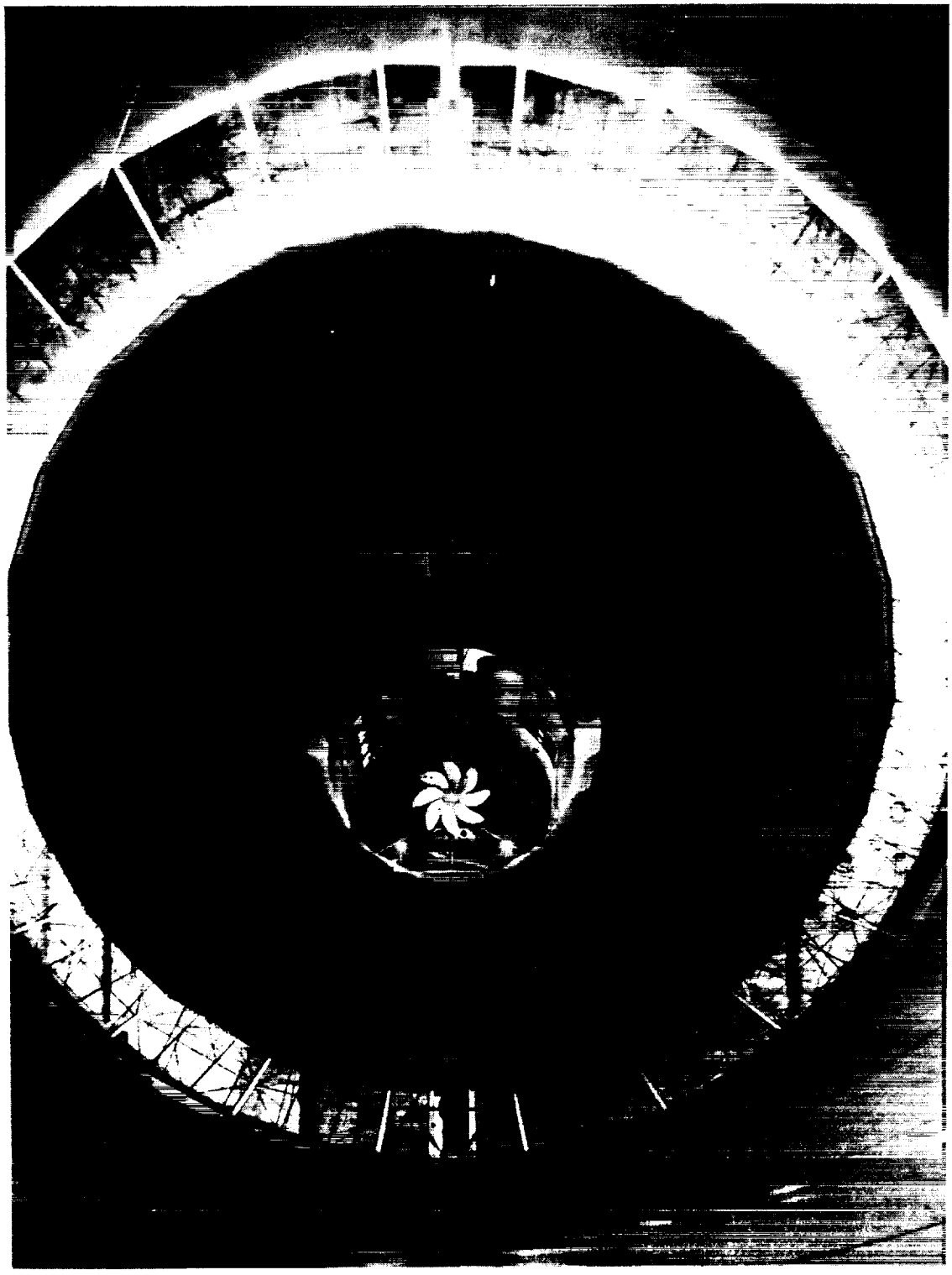

FIGURE 6-4. S1-MA WIND TUNNEL NOZZLE INLET TO TEST SECTION

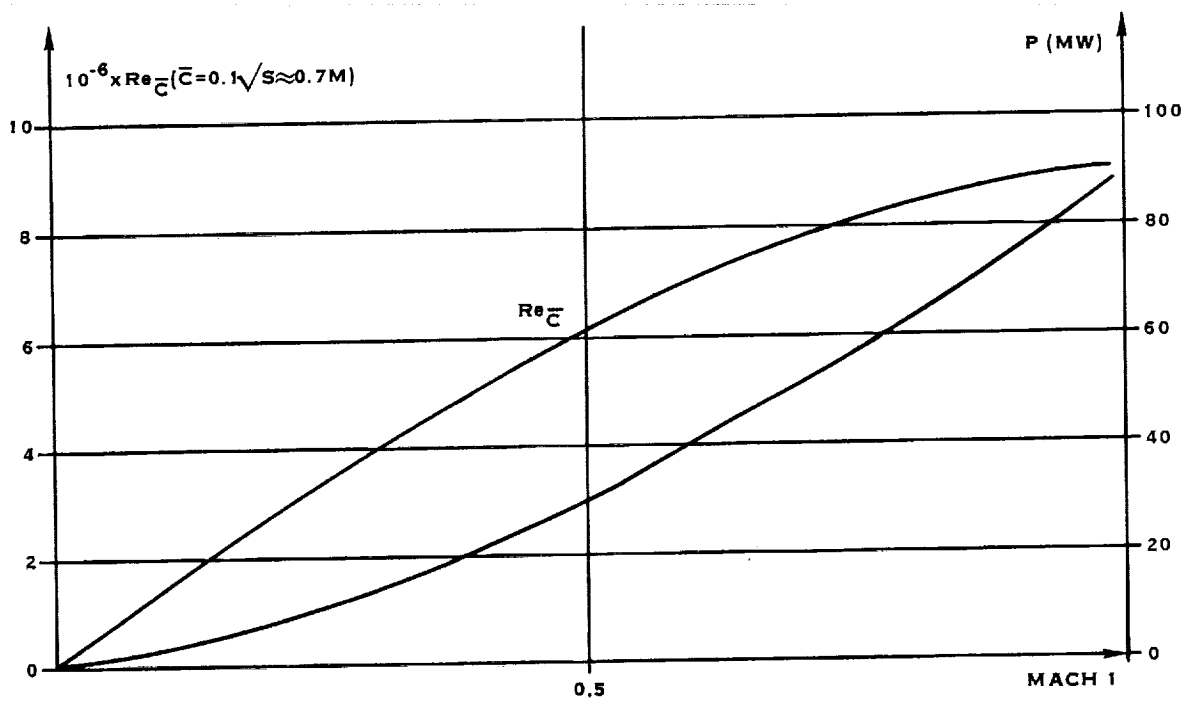

NOTE: THE CHART ABOVE IS FOR A REFERENCE CHORD LENGTH OF 0.7 M

FIGURE 6-5. TUNNEL DRIVING POWER AND REYNOLDS NUMBER AS A FUNCTION OF MACH NUMBER

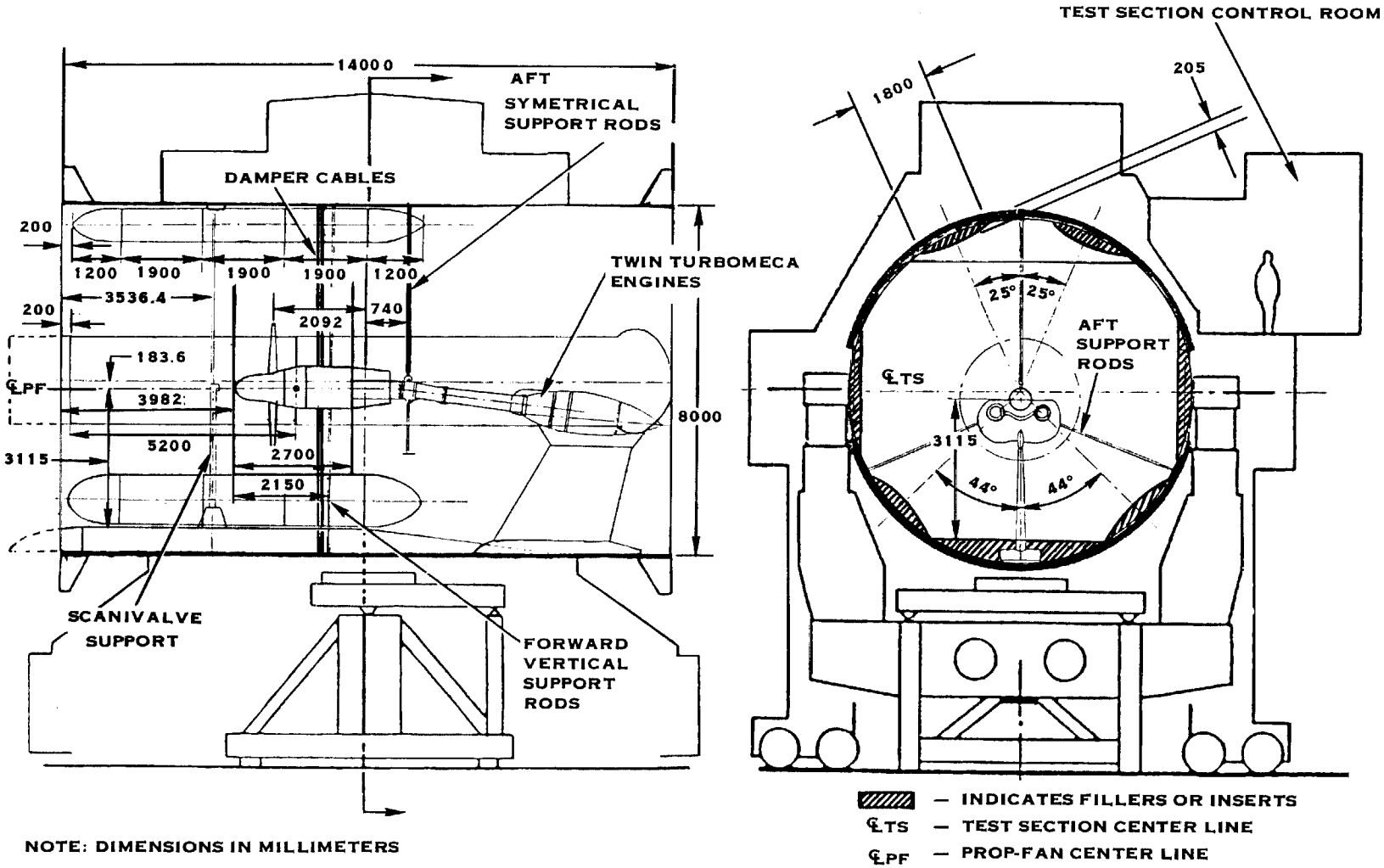

FIGURE 6-6. PROP-FAN INSTALLATION IN TEST SECTION/CHARIOT NO. 3

ORIGINAL PAGE
BLACK AND WHITE PHOTOGRAPH

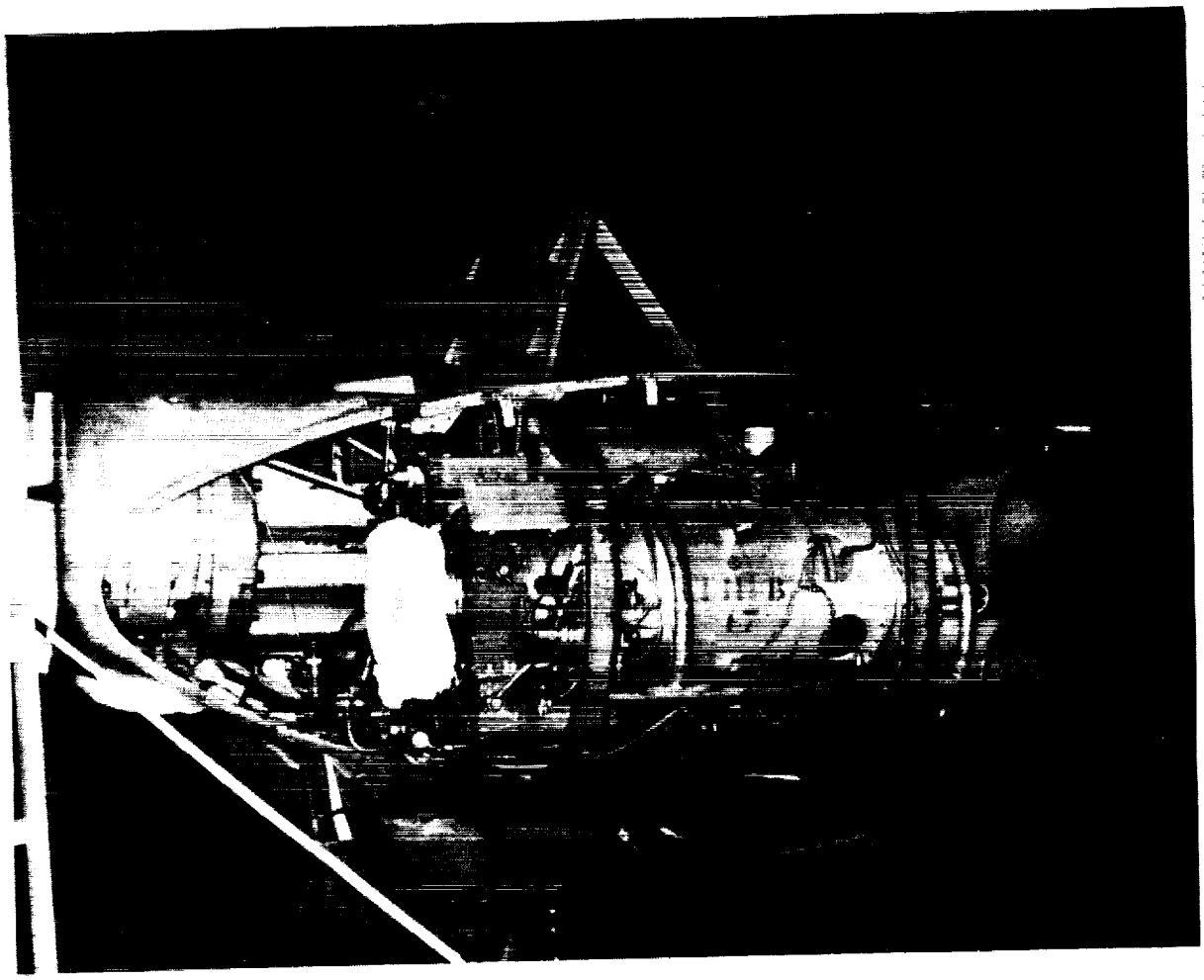

ORIGINAL PAGE IS
OF POOR QUALITY

FIGURE 6-7. PROP-FAN DRIVE SYSTEM ENGINES AND GEARBOX

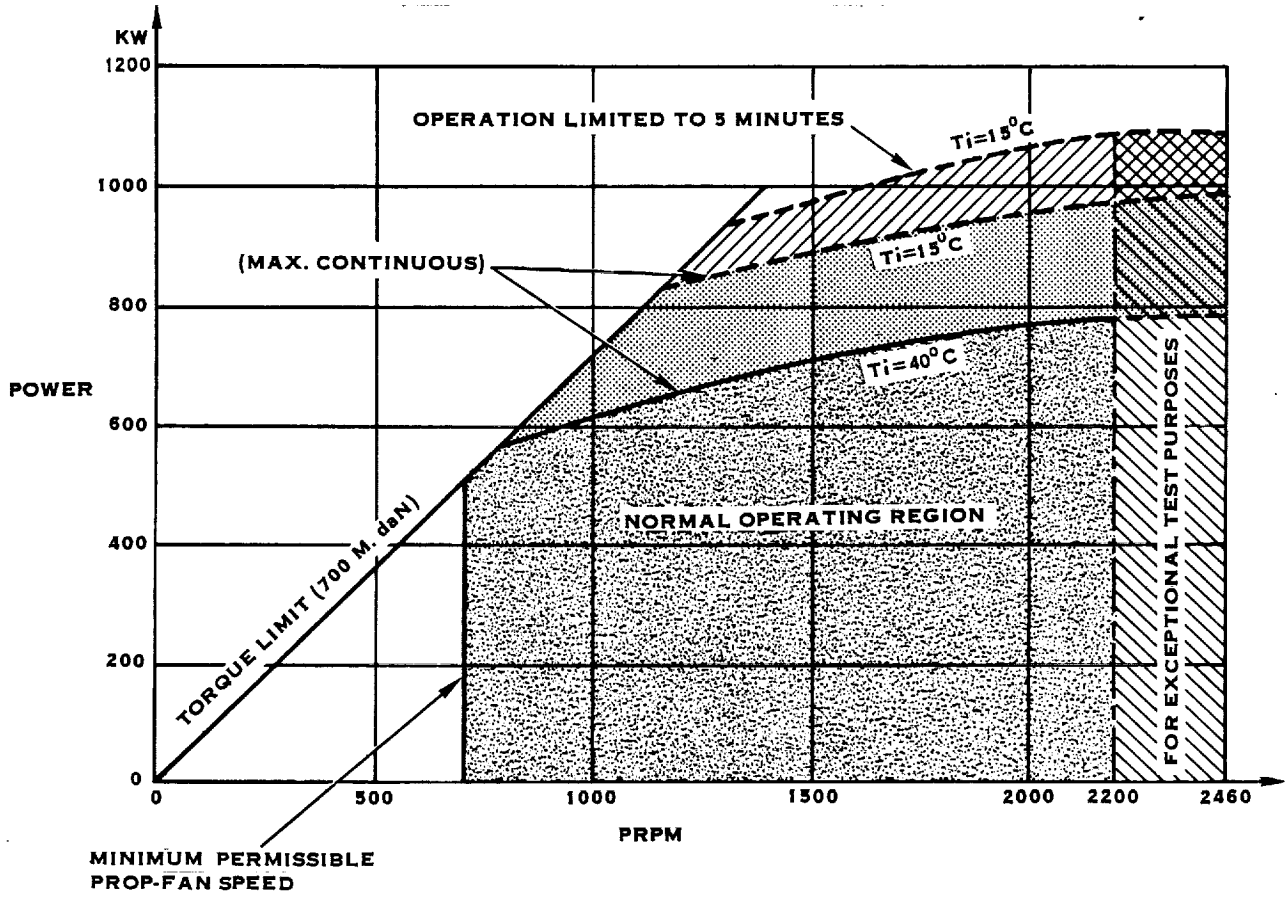

FIGURE 6-8. PROP-FAN TEST RIG POWER LIMITATIONS

6.2 (Continued)

speed reducer providing a reduction in RPM of approximately 3:1 from the engine to the Prop-Fan. Power was transmitted to the Prop-Fan from the gearbox through a long drive shaft and a balance (Figure 6-9). The drive shaft housing was supported by rods and damping cables attached to the tunnel walls. The particular rod and cable arrangement used in each test was dependent upon the type of test being run and the number of blades installed. These arrangements were established during a pre-test vibration survey conducted in the tunnel by ONERA. Universal joints at each end of the drive shaft allowed the Prop-Fan to be operated at various inflow angles relative to the flow through the test section.

A balance and torquemeter, installed in the drive system, allowed the thrust, torque, sides forces and bending moments acting on the Prop-Fan to be measured. A diagram of the balance is shown is Figure 6-10. Forces and moments are transmitted through the balance by six strain gaged elements which are referred to as dynamometers. Thrust, yawing moment and pitching moment are transmitted and measured by the three axial dynamometers (T1, T2 and T3). Balance friction torque and the lateral and vertical forces are transmitted and measured by the three tangential dynamometers (Z1, Z2 and Y). The torque supplied to the Prop-Fan is computed by subtracting the measured friction losses in the balance from the torque measured and transmitted by the torquemeter. All six dynamometers have a capacity of 2000 daN. Two flexible couplings decouple the transmission of the torque from the thrust measurement with one of the couplings being fitted with a gage bridge (torquemeter).

A stationary aerodynamic fairing or centerbody was installed around the drive system. This was also commonly referred to as the minimum body. The minimum body provided a downstream extension of the aerodynamic contour of the Prop-Fan spinner and was designed to reduce the air velocity passing through the root portion of the Prop-Fan rotor. At the inner blade radii the combination of thick airfoil sections and the large number of blades presents significant blockage to the flow, which could result in choking if the velocity was not moderated. The minimum body is approximatly 35% of the diameter of the Prop-Fan rotor. A description of the minimum body pressure tap arrangement is presented in Section 7.0.

6.3 Test Rig Modifications

The LAP Prop-Fan High Speed Wind Tunnel Test was completed following the incorporation of several structural improvements to the propeller test rig drive system. These modifications, as shown in the comparison of Figures 6-11 and 6-12, were added to preclude recurrence of a cone seat fretting corrosion problem encountered early in the testing, which led to an unanticipated interruption of the test. In addition, the modifications in general provided a more structurally sound rig design, better able to handle the loads imparted by the Prop-Fan.

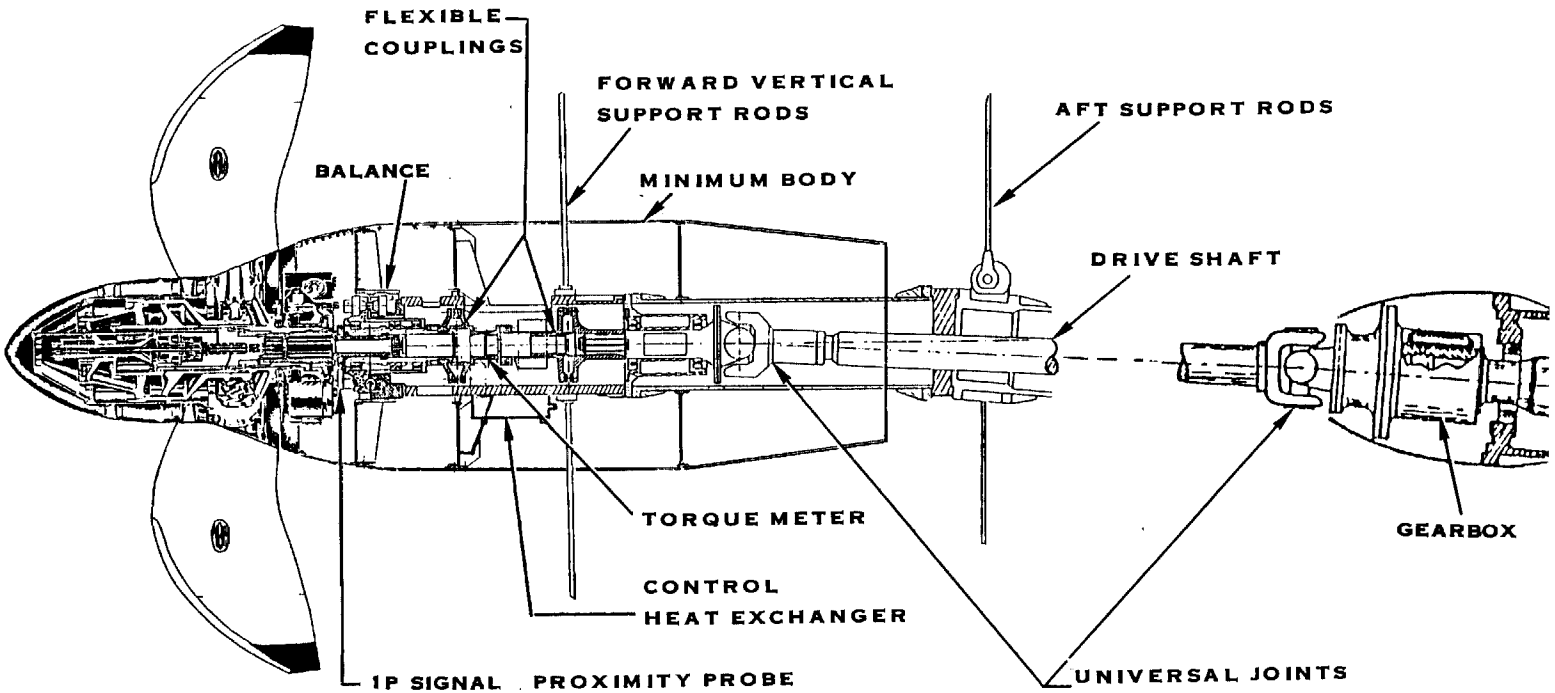

FIGURE 6-9. PROP-FAN DRIVE SYSTEM

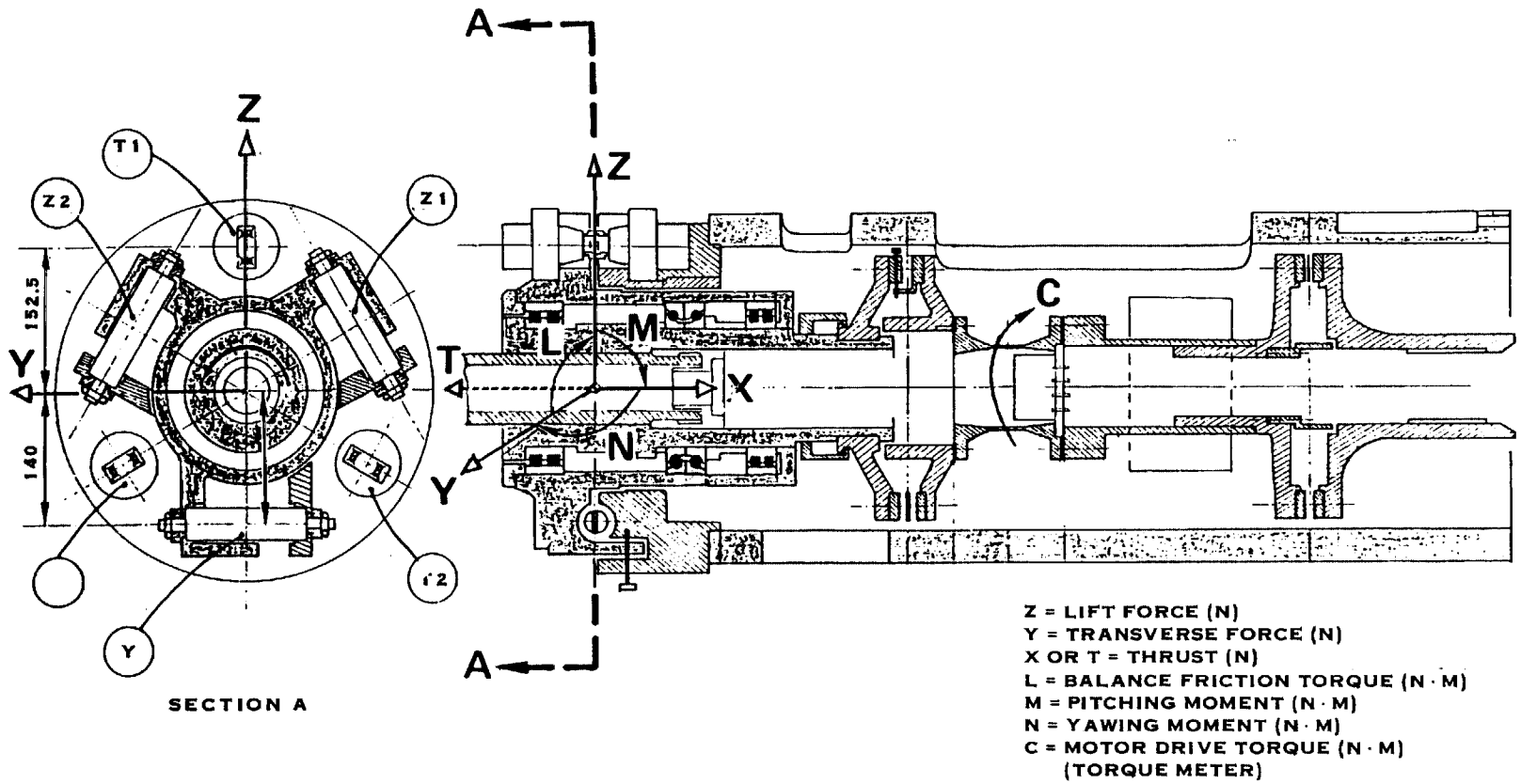

FIGURE 6-10. PROP-FAN TEST RIG DRIVE TRAIN BALANCE SCHEMATIC

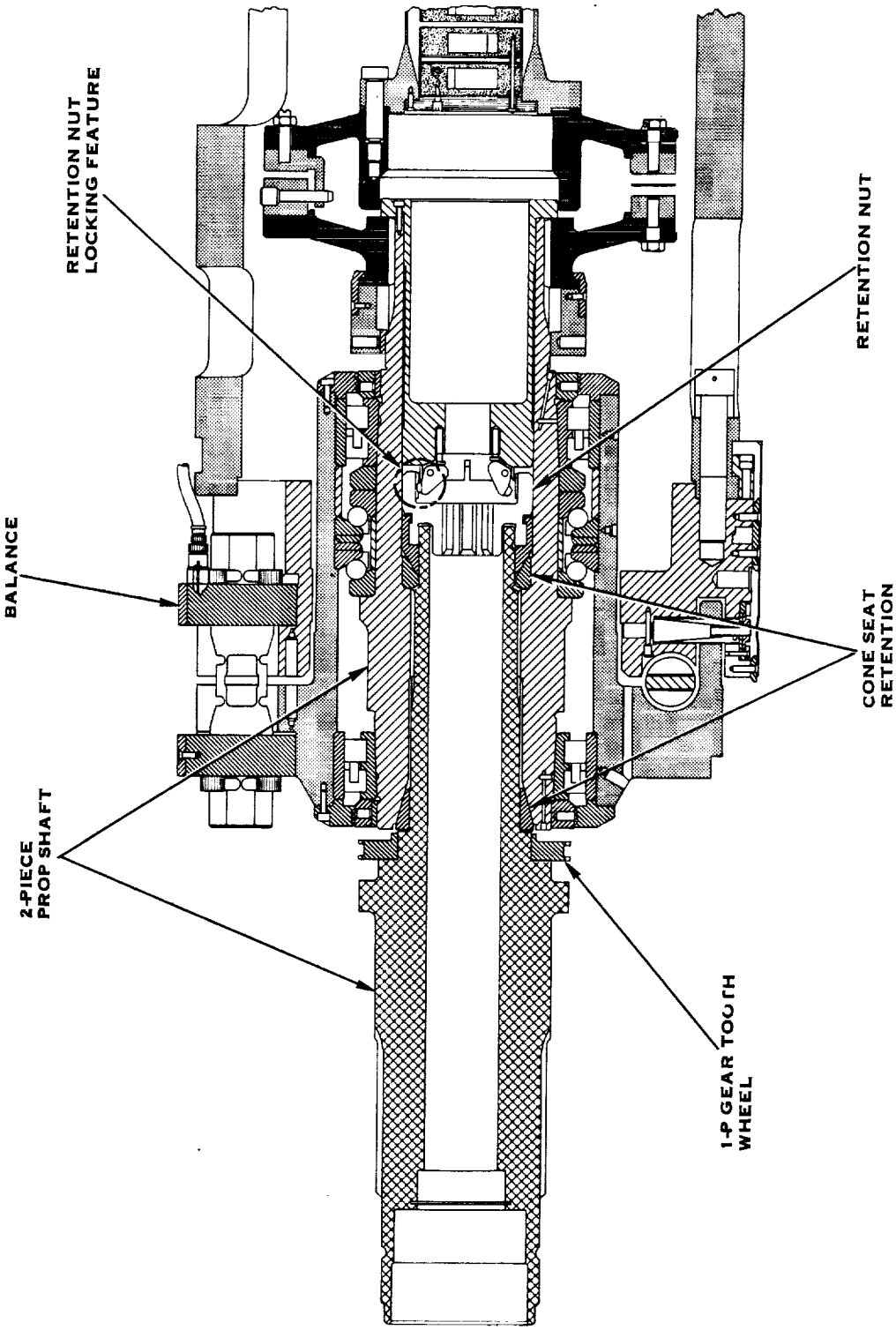

FIGURE 6-11. ORIGINAL TEST RIG CONFIGURATION

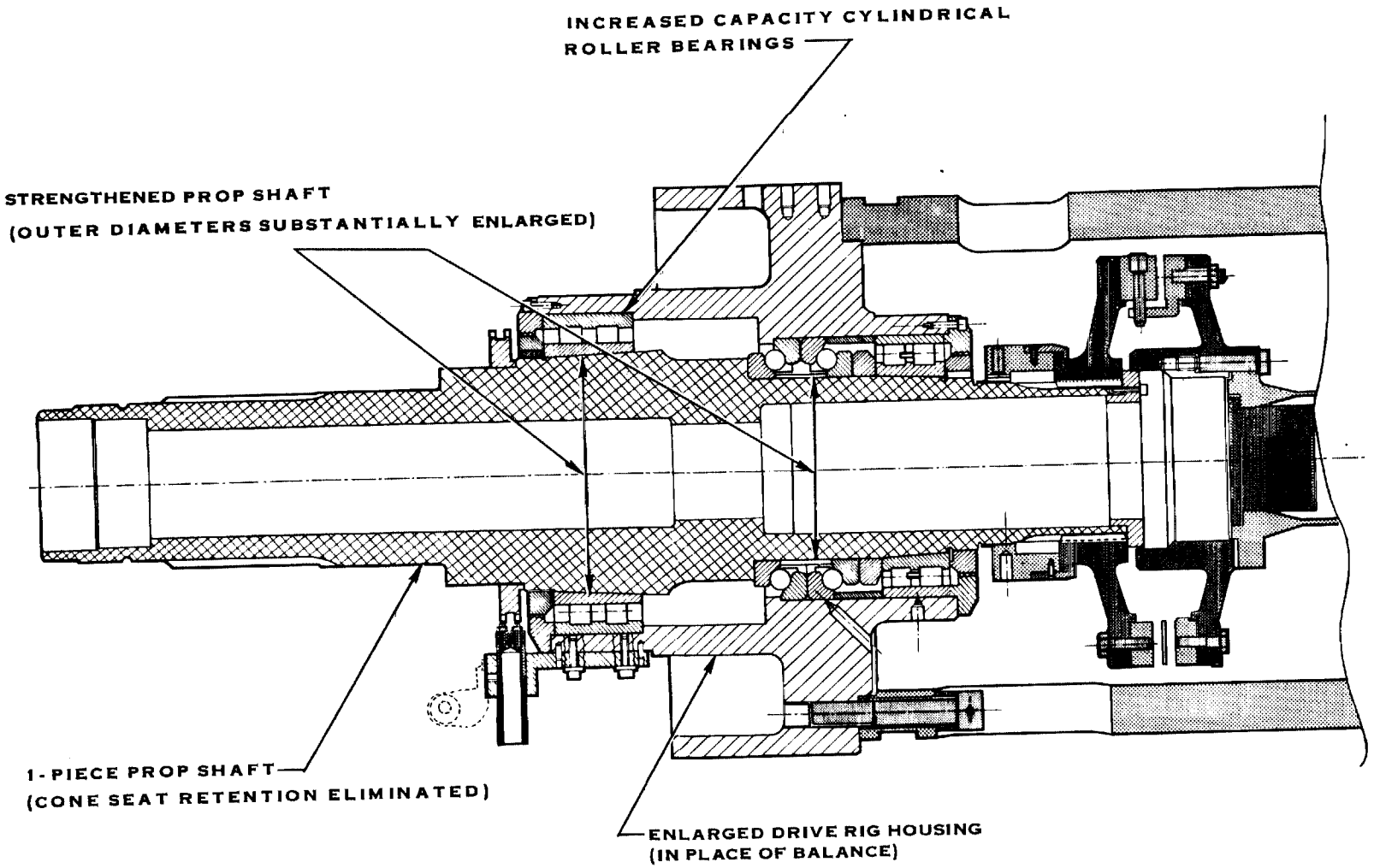

FIGURE 6-12. MODIFIED TEST RIG CONFIGURATION

6.3 (Continued)

The most significant modification to the drive system was the elimination of the cone seat retention configuration on the aft end of the prop shaft. It was this area which experienced the severe fretting corrosion problem early in the test. The new design provides for a one piece prop shaft mounted in a substantially enlarged forward test rig housing incorporating increased capacity cylindrical roller bearings. Since a safe structural operating envelope for the Prop-Fan had been defined earlier in the testing, the balance was removed to provide room for the test rig structural improvements.

7.0 SPINNER AND CENTERBODY DRAG MEASUREMENT

7.1 Test Rig Vibration Survey

Before testing was conducted in the S1-MA wind tunnel, the whirl flutter stability of the Prop-Fan/test rig system was evaluated. Stability of the Prop-Fan/test rig was a major concern because the LAP was the largest assembly ever installed on the test rig.

The Prop-Fan was assembled and installed on the propeller drive system in the tunnel test section in preparation for the vibration survey. To eliminate the possibility of damaging any of the actual LAP blades during this survey, blade stubs were installed in place of the blades. Additional weights were hung from selected blade stubs to account for the weight difference between the stubs and blades. The stubs were shimmed to minimize any movement in the blade retention during the shake test.

The survey was conducted using two electromechanical shakers positioned at various locations along the axis of the minimum body. Data was obtained using two accelerometers mounted on the test rig force balance just aft of the Prop-Fan. The data was used to determine the eigenfrequencies of the various rig vibration modes in the horizontal and vertical planes.

The results of the survey confirmed the need for an unsymmetrical rig support structure which pre-test analytical whirl flutter stability studies had suggested. Though the vibration test demonstrated that the 4 bladed SR-7L would operate whirl flutter free, it was agreed that rig damping characteristics would be closely monitored during all test envelope expansion. In order to incorporate the maximum test rig resistance to whirl flutter onset, several different rig support structure configurations were employed, based on the number of blades installed, as depicted in Figures 7-8, 8-1, 8-2, 10-1 and 11-1.

7.2 Wind Tunnel Corrections

Immediately following completion of the test rig vibration survey, ONERA conducted the wind tunnel calibration test. The purpose of this calibration was to remove the effects of the presence of the test rig on the measured Mach number. The ONERA approach was as follows. First, a compressible flow calculation was performed to establish the axial velocity distribution at the working radius of the blade (.6R) through the plane of rotation of the Prop-Fan. Next, two independent axial velocity surveys were made at the same radial location, utilizing a special pressure tapped pipe and scanivalve system. The results of these surveys are shown in Figures 7-1 thru 7-6. The uncorrected Mach number data represents actual measurements taken, while the corrected Mach number data is the difference between the calculations and the measurements of Figures 7-1 thru 7-6 added to the wall Mach number measured 2 meters (6.56 ft.) upstream of the Prop-Fan plane of rotation. Thus, the corrected Mach number data represents

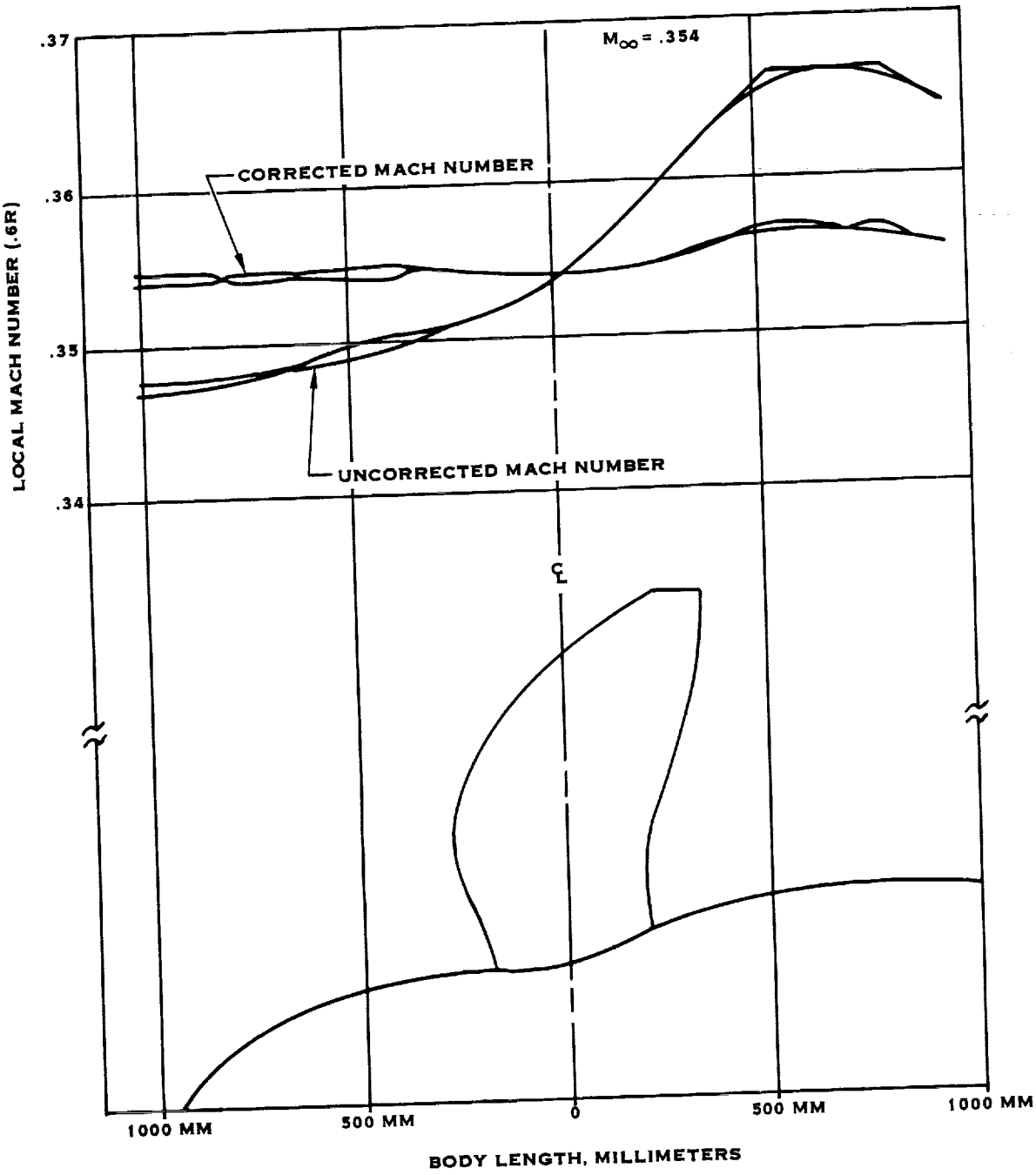

FIGURE 7-1. AXIAL MACH NUMBER DISTRIBUTION FOR FREESTREAM MACH NUMBER .354

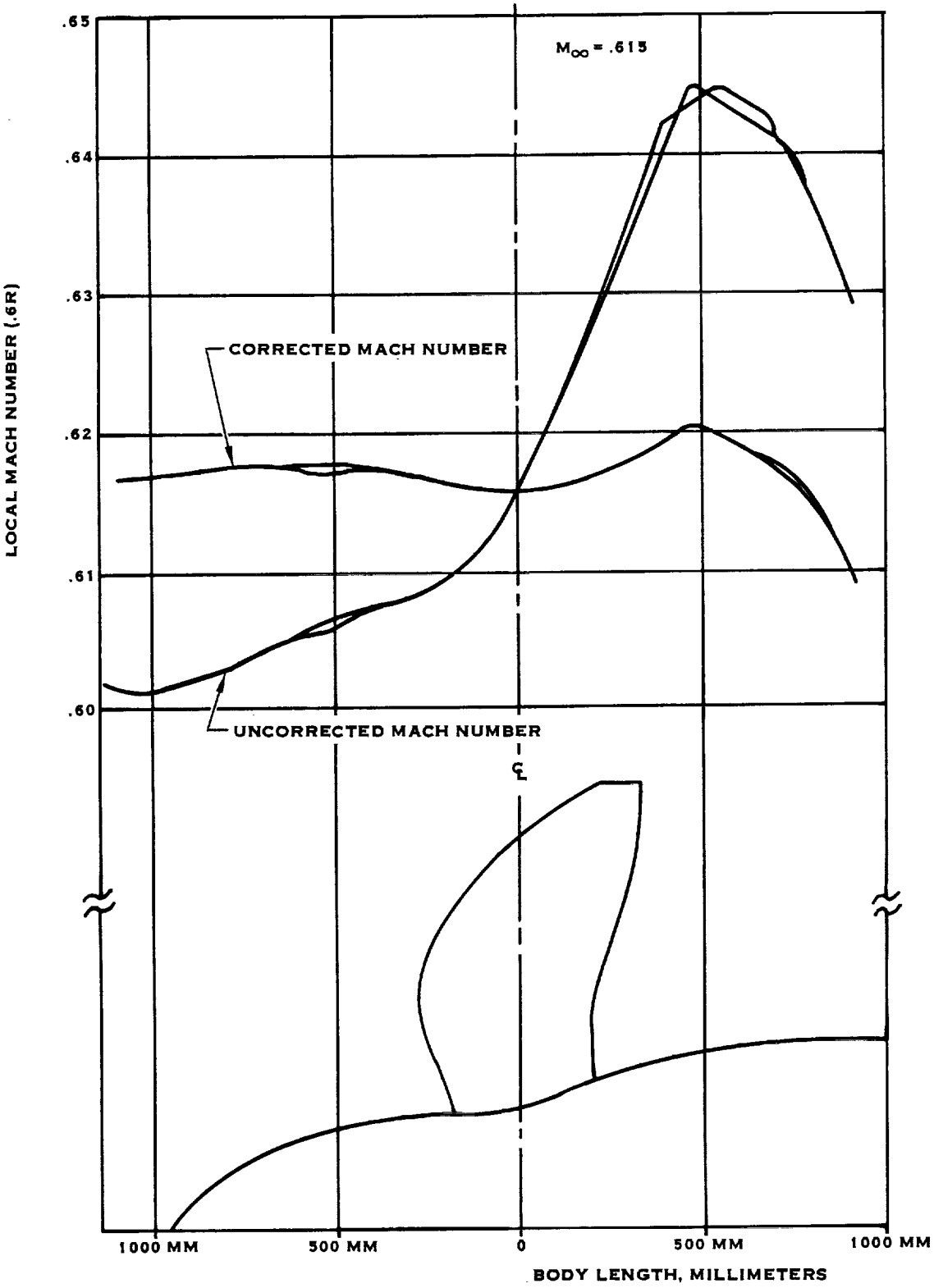

FIGURE 7-2. AXIAL MACH NUMBER DISTRIBUTION FOR FREESTREAM MACH NUMBER .615

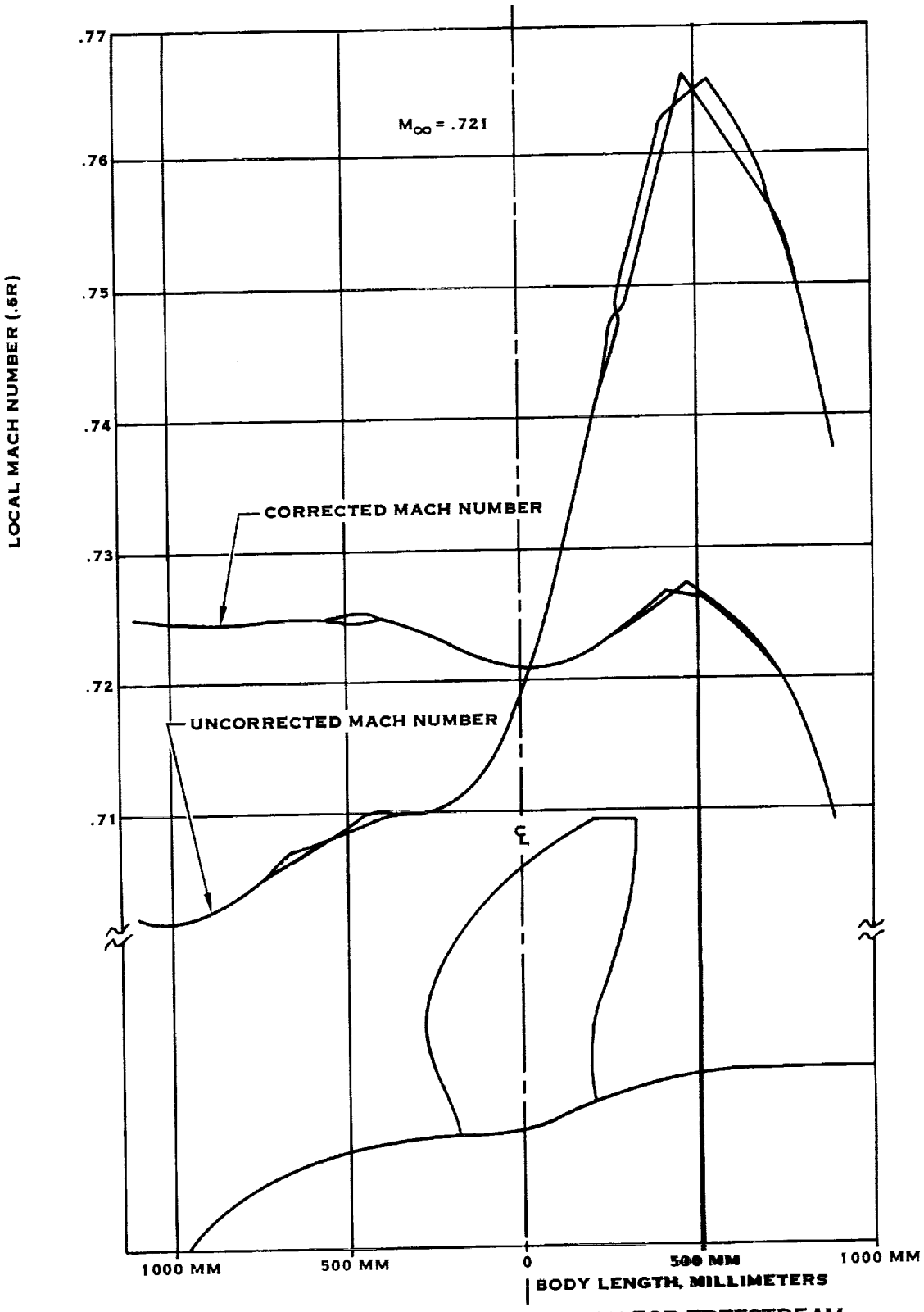

FIGURE 7-3. AXIAL MACH NUMBER DISTRIBUTION FOR FREESTREAM MACH NUMBER .721

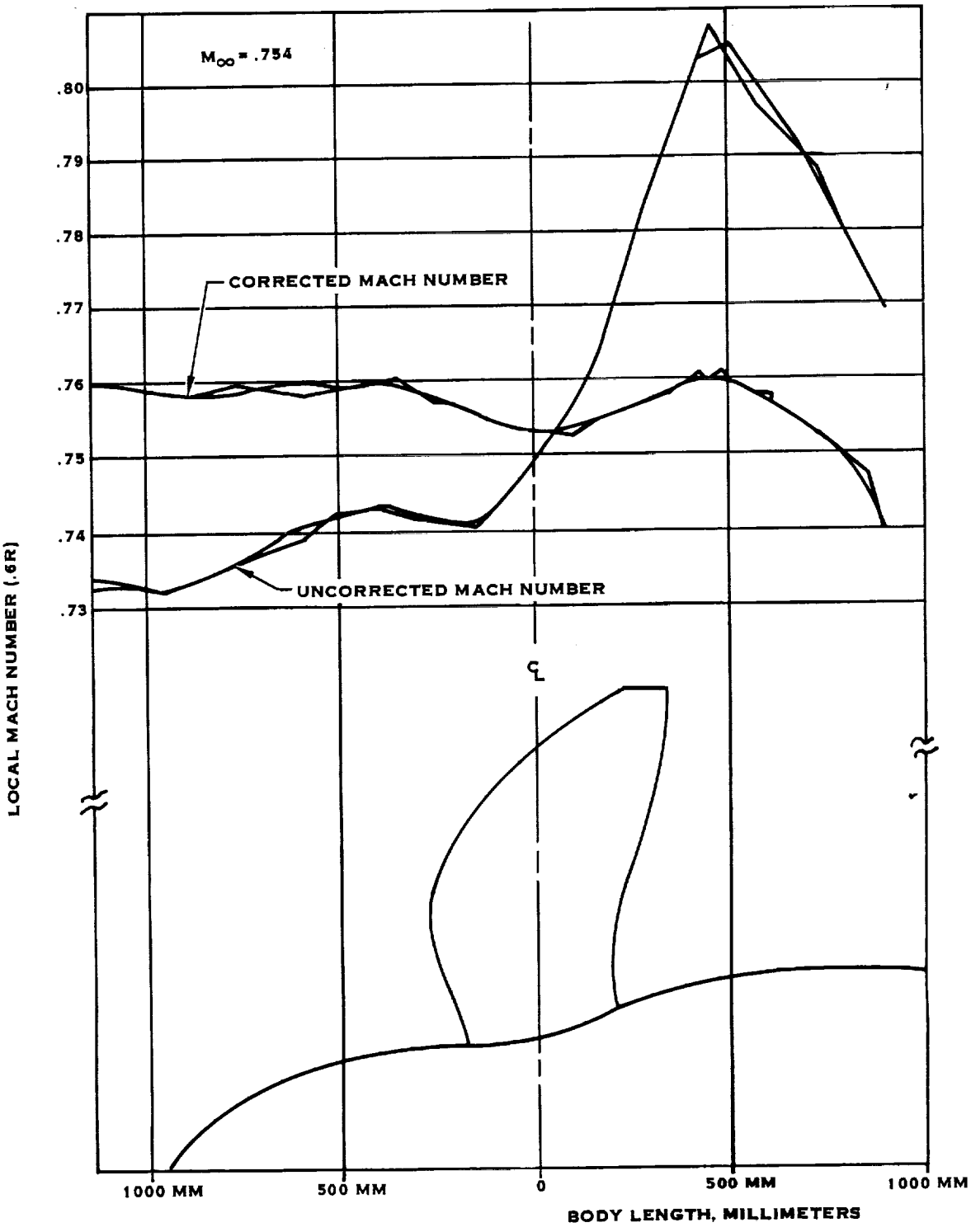

FIGURE 7-4. AXIAL MACH NUMBER DISTRIBUTION FOR FREESTREAM MACH NUMBER .754

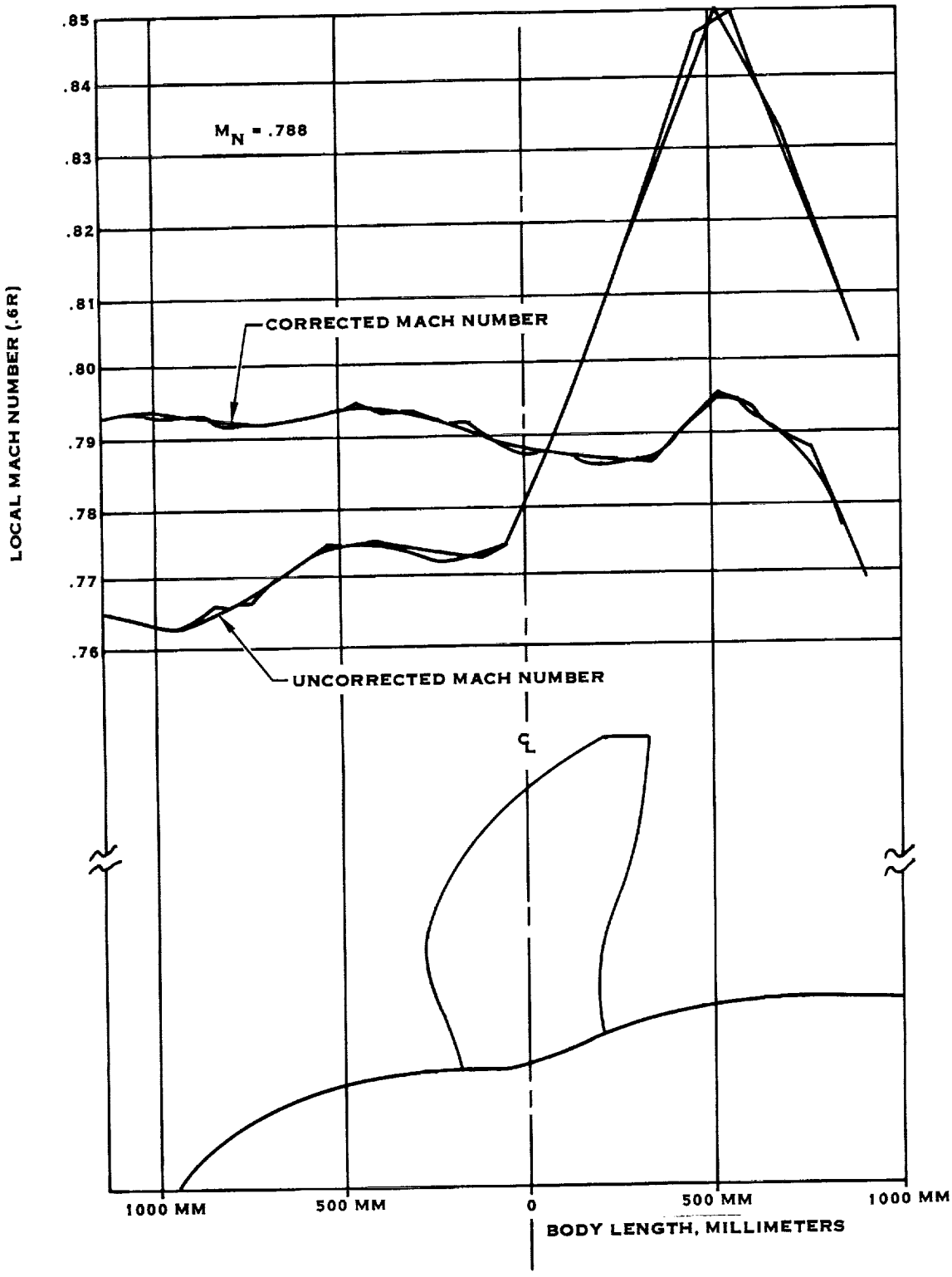

FIGURE 7-5. AXIAL MACH NUMBER DISTRIBUTION FOR FREESTREAM MACH NUMBER .788

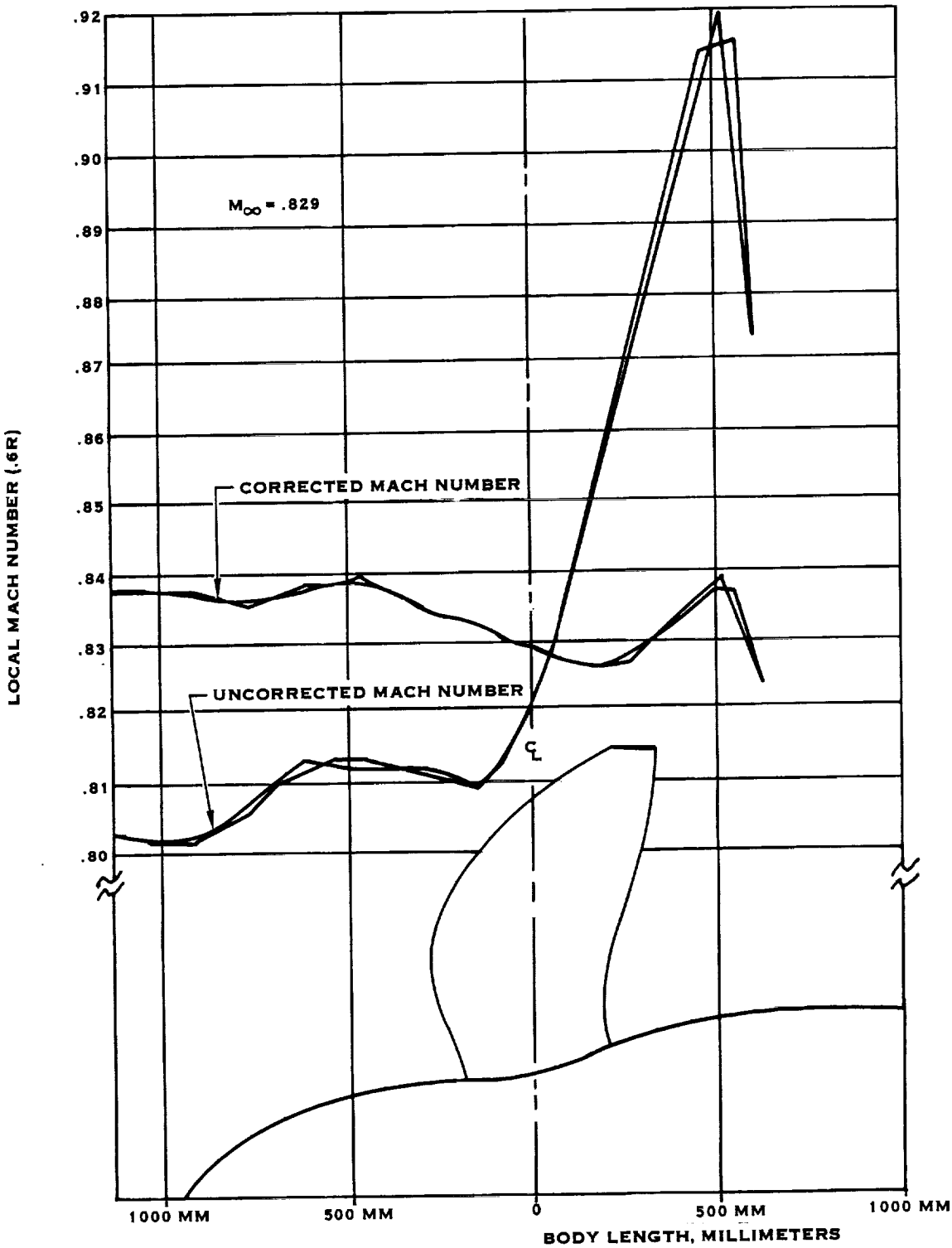

FIGURE 7-6. AXIAL MACH NUMBER DISTRIBUTION FOR FREESTREAM MACH NUMBER .829

7.2 (Continued)

the influence of the tunnel walls on the axial velocity distribution. Note there is very little difference at the lower Mach numbers between the corrected Mach number data and the uncorrected Mach number data as measured at the 2 meter wall location. In addition to the velocity calibration described above, ONERA used the Prandlt-Young correction as discussed in Reference 20 to further adjust the velocity data before computing an advance ratio, J. This correction, as defined below, is a compressible correction to the velocity to account for tunnel wall interference.

$$\frac{V'}{V} = 1 - \frac{\tau_4 \, \alpha_1}{2(1 + 2\,\tau_4)^{1/2}(1 - M_N^{\,2})^{1/2}}$$

or

$$V_{cor} = \left[1 - \frac{\tau_4 \, \alpha_1}{2(1 + 2\,\tau_4)^{1/2}(1 - M_N^{\,2})^{1/2}}\right] V_{meas}$$

where

$$\tau_4 = \frac{\text{THRUST}}{\rho \times \text{DISC AREA} \times V^2}$$

and

$$\alpha_1 = \frac{\text{PROPELLER DISC AREA}}{\text{TUNNEL CROSS-SECTION AREA}}$$

Note that this correction is largest where the thrust is largest and the velocity the smallest, i.e. low Mach number testing.

7.3 Test Rig Corrections

7.3.1 Test Objectives

7.3.1.1 To determine the aerodynamic drag on the Prop-Fan spinner as a function of Mach number for Mach numbers ranging from .2 to .85.

7.3.1.2 To determine the aerodynamic pressure drag on the test rig centerbody as a function of Mach number for Mach numbers ranging from .2 to .85.

7.3.2 Test Procedure

In preparation for the spinner/body tare test, the test rig and associated support structure were set up as depicted in Figures 7-7 and 7-8. In order to isolate and evaluate the affects of the presence of the spinner and centerbody in the flow field, the LAP blades were replaced with blade stubs, whose external contours were machined to match that of the spinner (Figure 7-9).

As defined in Figures 7-10 and 7-11, the forward end of the centerbody serves as an extension of the external contour of the spinner, and was designed to alleviate compressibility losses in the blade root section by reducing the air velocity passing through the central portion of the Prop-Fan rotor. At the inner blade radii, the combination of thick airfoil sections and the large number of blades presents significant blockage which could lead to choked flow. The moderation of velocity caused by the centerbody reduces the possibility of choked flow occuring at the high subsonic Mach numbers at which the LAP operates. Figures 7-10 and 7-11 also define the location of the centerbody surface static pressure taps. There are four rows of twenty-nine taps per row positioned along the length of the centerbody surface. The rows of taps were spaced 90° apart, circumferentially. Figure 7-12 defines the location of an additional set of static pressure taps in the space between the spinner rear bulkhead and centerbody. These taps consisted of four rows, ten taps per row, extending radially outward, located at the centers of equal areas. Each row was oriented 90° apart from another.

Collection of the static pressure measurements from the locations described above, while varying tunnel Mach number, was accomplished using a scanivalve system. Spinner/centerbody drag data was collected at a total of 42 test points. All of the data was collected at zero degree inflow angle. Table 7-I lists the Mach numbers at which data was collected.

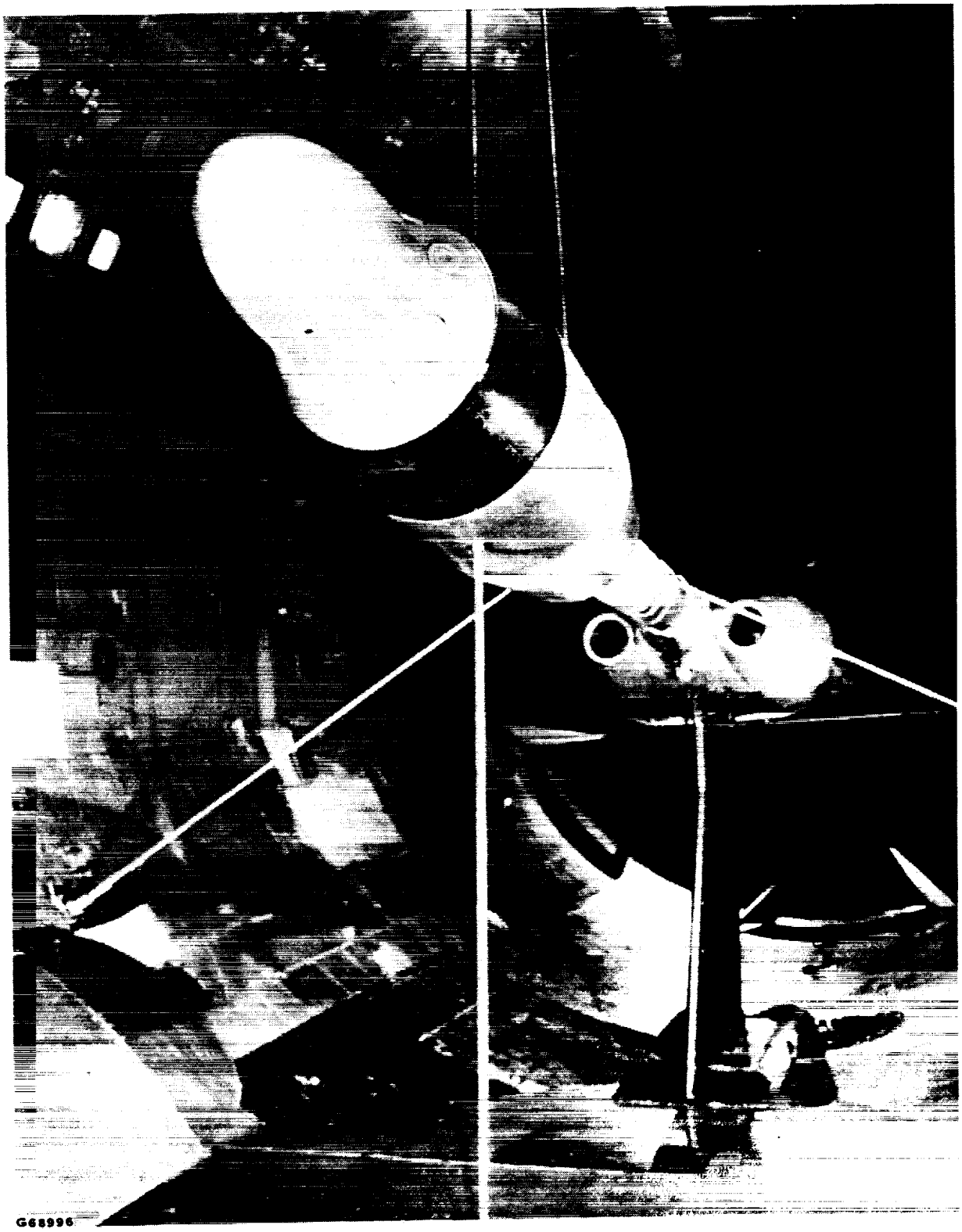

FIGURE 7-7. SPINNER /BODY TARE TEST

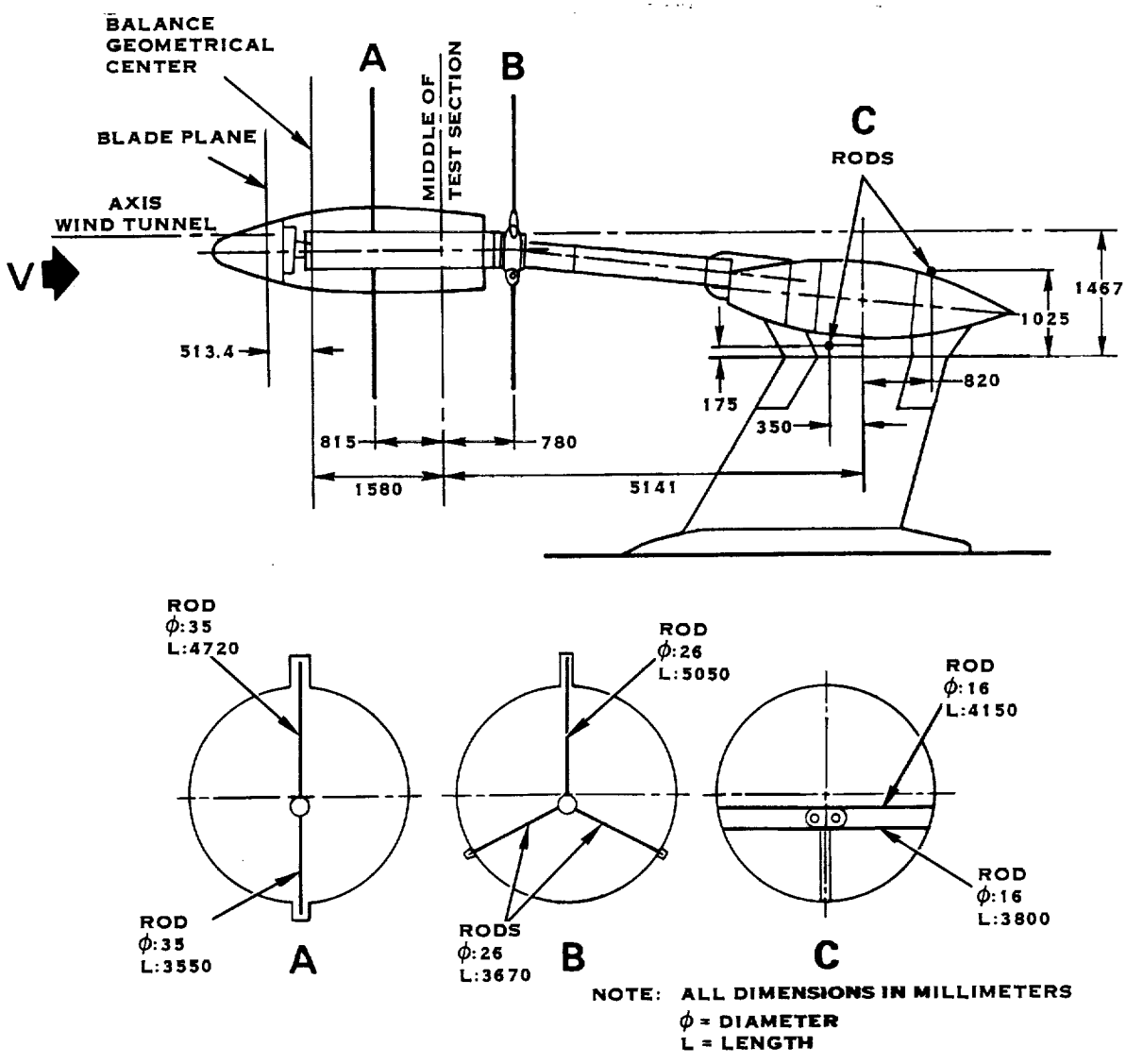

FIGURE 7-8. TEST RIG SUPPORT STRUCTURE FOR SPINNER/BODY TARE TEST

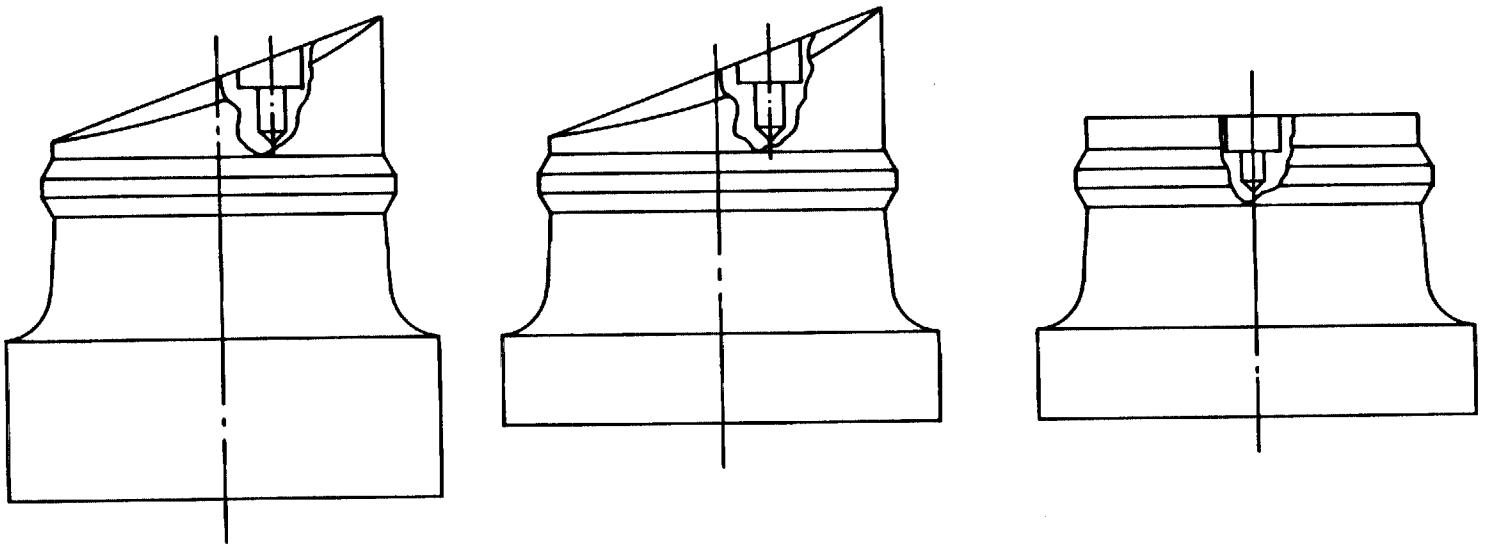

STEEL STUBS (2 EA.)
(H.S . PROVIDED)
P/N SK108344
S/N 1X
S/N 2X

ALUMINUM STUBS (4EA.)
(H. S. PROVIDED)
P/N SK108341
S/N 1X
S/N 2X
S/N 3X
S/N 4X

ALUMINUM STUBS (2EA)
(ONERA PROVIDED)

FIGURE 7-9. PROP-FAN BLADE STUBS

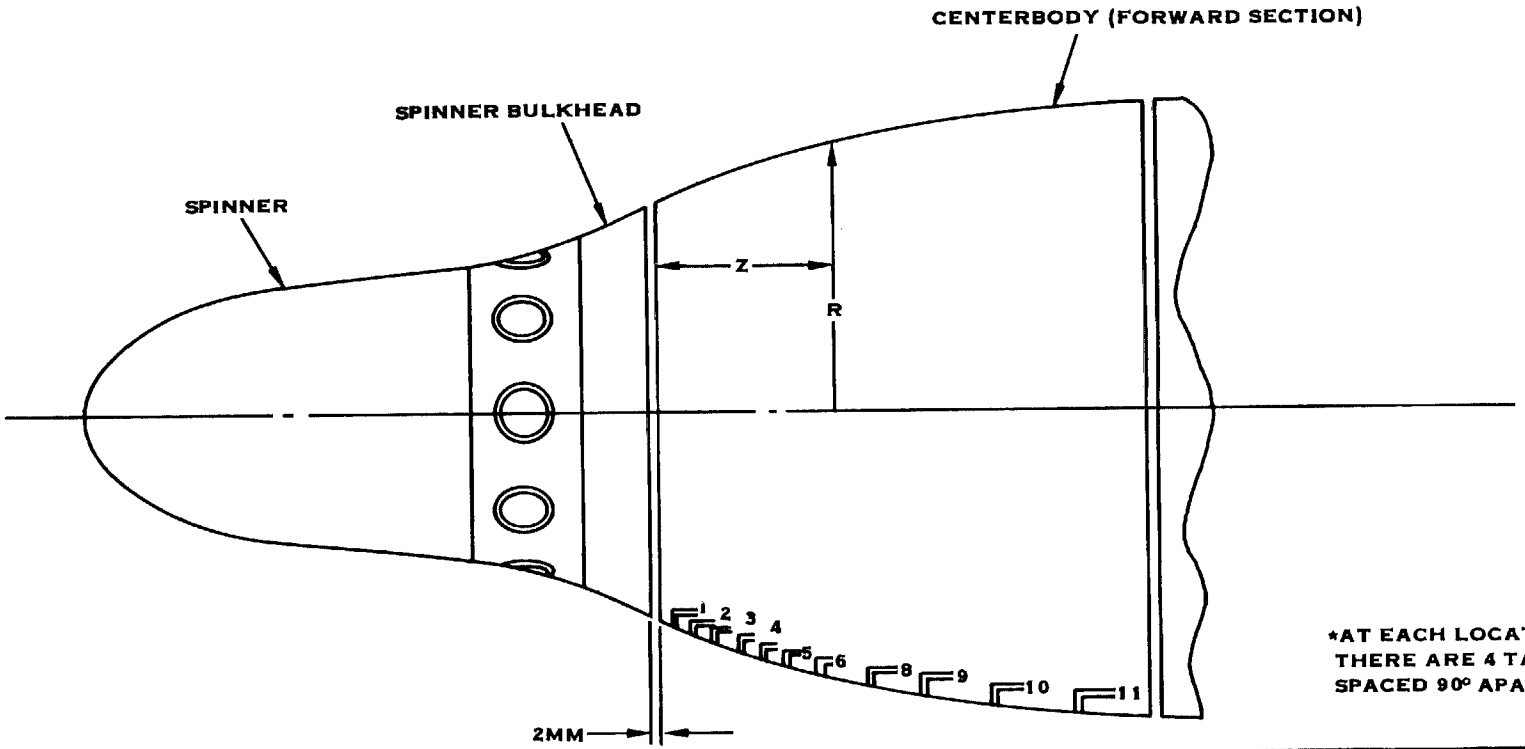

*AT EACH LOCATION, Z, THERE ARE 4 TAPS SPACED 90° APART

STATIC PRESSURE TAP NO.	R (MM)	*Z (MM)
1 , 30 , 59 , 88	411	13
2 , 31 , 60 , 89	419	38
3 , 32 , 61 , 90	427	64
4 , 33 , 62 , 91	436	94
5 , 34 , 63 , 92	444	128
6 , 35 , 64 , 93	451	159
7 , 36 , 65 , 94	459	202
8 , 37 , 66 , 95	467	253
9 , 38 , 67 , 96	474	311
10 , 39 , 68 , 97	481	395
11 , 40 , 69 , 98	485	529

FIGURE 7-10. CENTERBODY SURFACE PRESSURE TAP LOCATIONS (FORWARD SECTION)

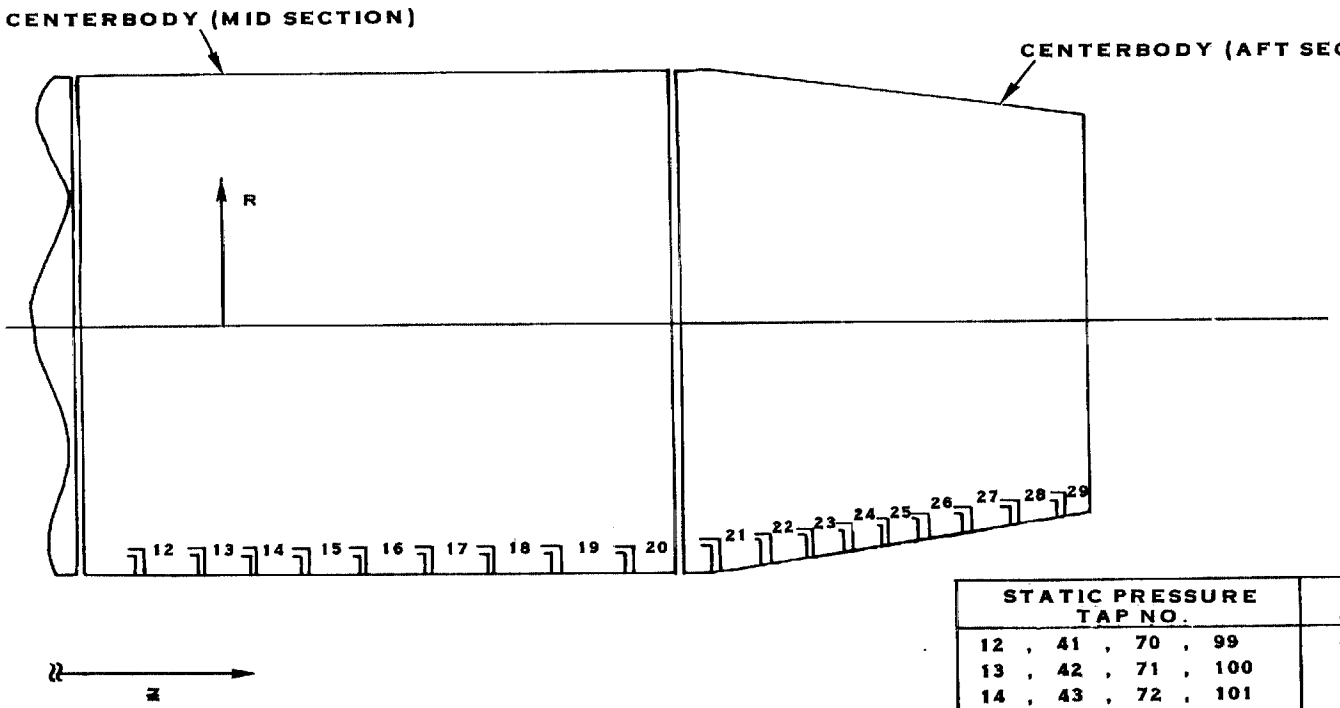

STATIC PRESSURE TAP NO.	R (MM)	Z* (MM)
12 , 41 , 70 , 99	485	665
13 , 42 , 71 , 100	485	765
14 , 43 , 72 , 101	485	865
15 , 44 , 73 , 102	485	965
16 , 45 , 74 , 103	485	1065
17 , 46 , 75 , 104	485	1165
18 , 47 , 76 , 105	485	1265
19 , 48 , 77 , 106	485	1365
20 , 49 , 78 , 107	485	1465
21 , 50 , 79 , 108	485	1565
22 , 51 , 80 , 109	478	1665
23 , 52 , 81 , 110	465	1765
24 , 53 , 82 , 111	452	1865
25 , 54 , 83 , 112	439	1965
26 , 55 , 84 , 113	426	2065
27 , 56 , 85 , 114	413	2165
28 , 57 , 86 , 115	401	2265
29 , 58 , 87 , 116	388	2365

* AT EACH LOCATION, Z, THERE ARE 4 TAPS SPACED 90° APART

FIGURE 7-11. CENTERBODY SURFACE STATIC PRESSURE TAP LOCATIONS (MID AND AFT SECTIONS)

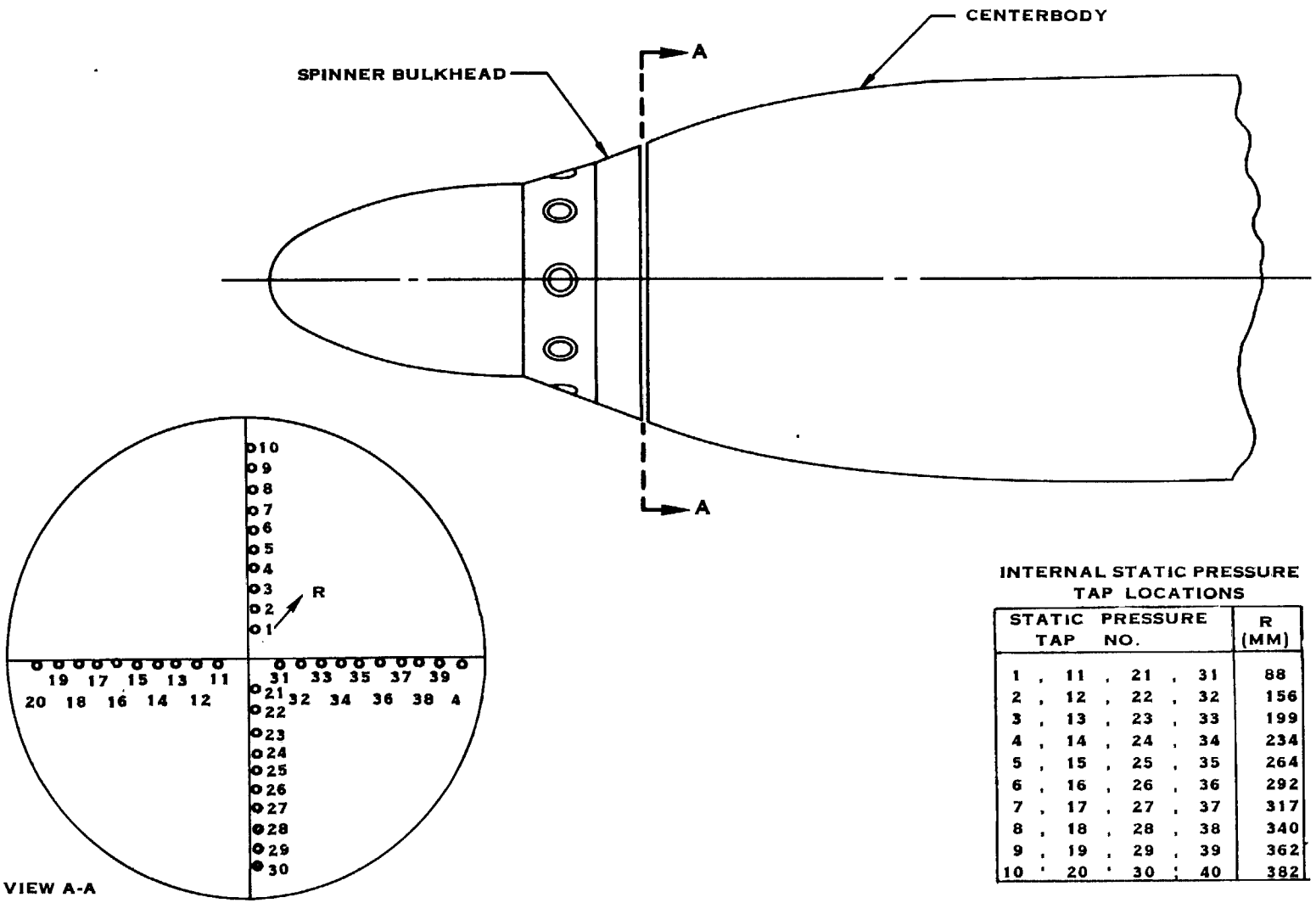

INTERNAL STATIC PRESSURE TAP LOCATIONS

STATIC PRESSURE TAP NO.				R (MM)
1	11	21	31	88
2	12	22	32	156
3	13	23	33	199
4	14	24	34	234
5	15	25	35	264
6	16	26	36	292
7	17	27	37	317
8	18	28	38	340
9	19	29	39	362
10	20	30	40	382

FIGURE 7-12. SPINNER BULKHEAD STATIC PRESSURE TAP LOCATIONS

Table 7-I. Spinner/Centerbody Drag Test Points

SPINNER/CENTERBODY DRAG TEST PT.	CORRECTED MACH NO.
242	.499
244	.789
246	.836
248	.834
250	.833
255	.800
257	.848
260	.789
262	.739
264	.686
266	.638
268	.590
270	.494
272	.447
274	.348
276	.244
287	.201
288	.201
289	.201
290	.201
291	.201
293	.298
294	.298
295	.298
296	.298
297	.298
299	.494
300	.494
302	.590
303	.590
305	.494
308	.298
309	.298
310	.298
311	.299
312	.298
314	.201
315	.201
316	.201
317	.201
318	.201

7.3.3 Discussion and Results

7.3.3.1 Spinner Drag

As depicted in Figure 7-13, the spinner drag (Ds) was measured directly from the axial force measured by the balance (F_B) with corrections for the back pressure force (F_{BP}) and the losses due to thermal effects in the flexible coupling (F_{TH}).

$$D_s = F_B - F_{BP} - F_{TH}$$

The axial force applied to the propeller shaft (F_B) was measured by three dynamometers T_1, T_2 and T_3 in the test rig balance as depicted in Figure 6-10. The losses (F_{TH}) due to the thermal effects of the flexible coupling were measured by strain gages bonded directly to the flex coupling. The back pressure force (F_{BP}) is the result of the difference between the free stream static pressure (P_o) and the integrated pressures in the space between the rear of the spinner bulkhead and the face of the centerbody (P_N), where a_N is an area weighting factor and A_s is the spinner base area.

$$F_{BP} = \left(\sum_{N=1}^{40} (a_N P_N) - P_o \right) A_s$$

$$A_s = .507 \text{ m}^2$$

Figure 7-14 presents the spinner drag coefficient (C_{SD}) as a function of corrected Mach number (M_{COR}). The spinner drag coefficient is given below and is expressed in terms of the spinner drag force (D_S), dynamic pressure (q_o) and projected spinner base area (A_S).

$$C_{SD} = \frac{D_S}{q_o A_S}$$

$$A_s = .519 \text{ m}^2$$

Since the spinner drag data was corrected for the back pressure effects, it represents the axial components of the forces applied by the static pressure acting normal to the spinner surface and the spinner boundary layer wall stress acting on the wetted area of the spinner. A quadratic equation was fitted to the spinner drag data, as shown below and on Figure 7-14, and was used to compute spinner drag corrections to measured thrust during Prop-Fan performance testing.

$$C_{SD} = 2.7699 M_{COR}^4 - 5.3225 M_{COR}^3 + 3.7727 M_{COR}^2 - 1.1215 M_{COR} + .2398$$

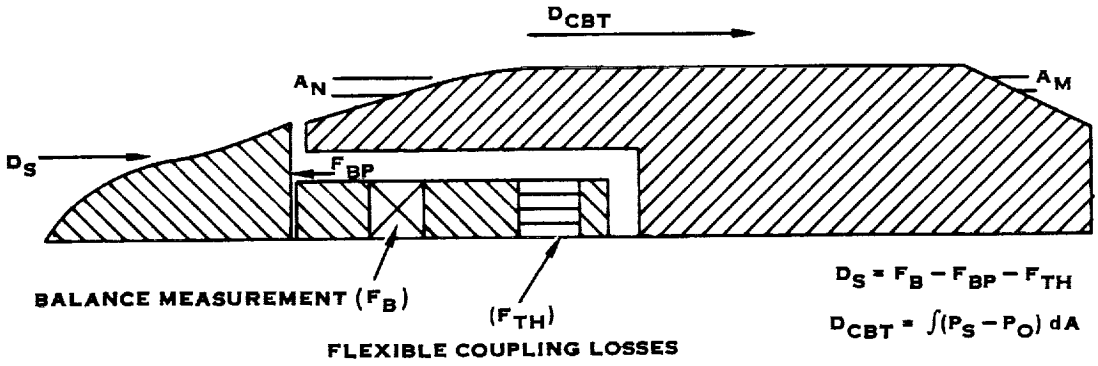

A. SPINNER/ CENTERBODY TARE TEST (WITHOUT BLADES)

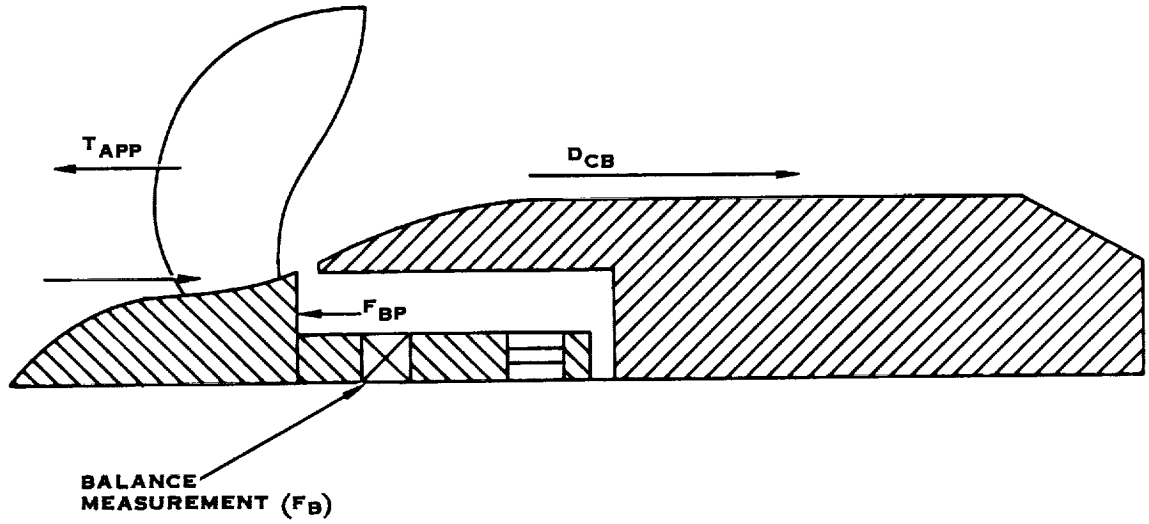

B. PROP FAN TEST PT. (WITH BLADES)

FIGURE 7-13. PROP-FAN TEST RIG FORCES

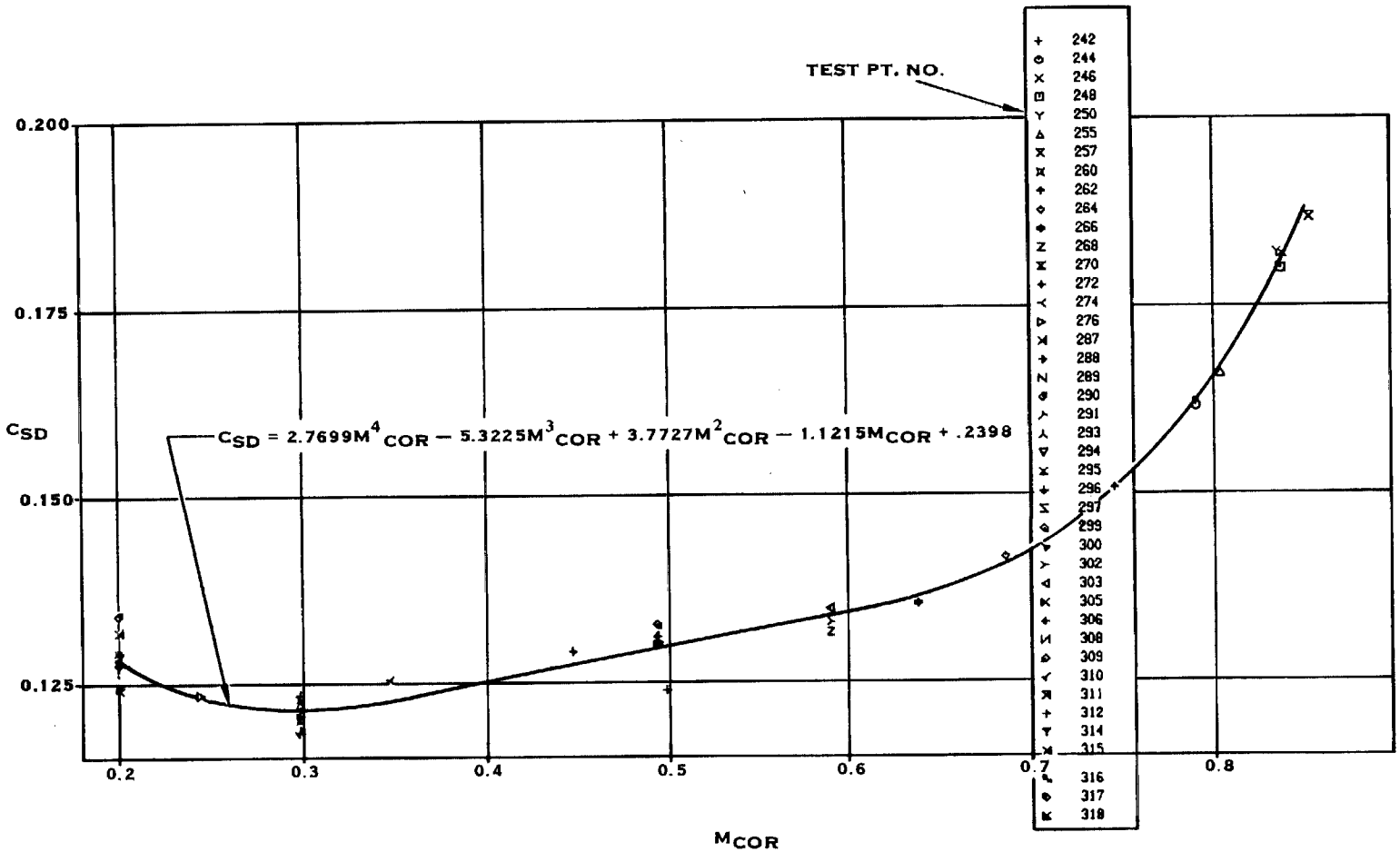

FIGURE 7-14. SPINNER DRAG COEFFICIENT VS. CORRECTED MACH NUMBER

7.3.3.1 (Continued)

The spinner drag coefficient, as expected, increased with Mach number for Mach numbers in the range from .3 to .85. However, an unexpected decrease in drag coefficient was observed between Mach .2 and Mach .3. The decrease in drag coefficient cannot be readily explained from the data that was collected. Theoretically, the drag should vary as the square of the velocity. The large number of data points taken at Mach .2 and Mach .3 does confirm that the decrease in spinner drag coefficient is a real phenomenon.

7.3.3.2 Centerbody Drag

As mentioned earlier, the Prop-Fan was tested in the presence of a centerbody which was designed to alleviate compressibility losses in the blade root sections. With the force measurement as shown in Figure 7-13, it has been shown that the Prop-Fan net thrust (T_{NET}) cannot be directly measured on the force balance (Reference 21). This is true because, as discussed in References 21 and 22, the thrust of the Prop-Fan blades changes the pressure acting on the centerbody, thereby changing the pressure drag. The presence of the body also causes an increase in thrust on the rotor equal in magnitude to the change in the centerbody drag. The change in centerbody drag is commonly referred to as the buoyancy force (BF). The measured Prop-Fan thrust has been classically referred to as apparent thrust (T_{APP}) and is the largest force component sensed by the balance. Since the increase in centerbody drag negates the increase in Prop-Fan thrust, there is no net increase in thrust produced by the Prop-Fan system. However, the thrust measurement (F_B), in Figure 7-13 (Views A and B), does not sense centerbody drag, therefore, measured or apparent trust (T_{APP}) is corrected by subtracting the buoyancy force, which is the difference between the centerbody drag measured at the Prop-Fan operating point of interest (D_{CB}) and the centerbody drag measured at the same Mach number without blades (D_{CBT}).

The centerbody pressure drag (D_{CBT}), was determined by pressure integration of the longitudinal rows of area-weighted static pressure taps. The integration requires a simple summation because the pressures are measured in the centers of equal annular areas.

$$D_{CBT} = \sum_{N=1}^{44} (P_N - P_O)A_N + \Sigma(P_M - P_O)A_M$$

WHERE:
- P_O = FREE STREAM STATIC PRESSURE
- P_N, P_M = STATIC PRESSURE AT TAP N, M
- A_N = INCREMENTAL FORWARD CENTERBODY AREA AT TAP N
- A_M = INCREMENTAL AFT CENTERBODY AREA AT TAP M

7.3.3.2 (Continued)

As a result of several last minute profile modifications, by ONERA, to the aft end of the Prop-Fan test rig centerbody, the local static pressure taps previously requested by Hamilton Standard were omitted. Therefore, the buoyancy force correction applied to the apparent thrust is in error. However, the change in the buoyancy force that would have occurred is small enough to result in no significant effect to the data. Therefore, the equation above is further simplified to the following:

$$D_{CBT} = \sum_{N=1}^{44} (P_N - P_o)A_N$$

Figure 7-13 presents the variation of centerbody drag coefficient without blades (C_{CBDT}) with corrected Mach number (M_{COR}). The centerbody drag coefficient without blades is given below and is expressed in terms of centerbody drag force without blades (D_{CBT}), dynamic pressure (q_o) and projected centerbody area (A_{CB}).

$$C_{CBDT} = \frac{D_{CBT}}{q_o A_{CB}}$$

$$A_{CB} = .22 \text{ m}^2$$

A quadratic equation was fitted to the centerbody drag, as shown below and on Figure 7-15 and was used to compute the buoyancy force correction to measured or apparent thrust during Prop-Fan performance testing.

$$C_{CBDT} = 7.6393M_{COR}^4 - 16.786M_{COR}^3 + 12.124M_{COR}^2 - 3.7165M_{COR} - .2320$$

It is observed from the data that the centerbody drag coefficient decreases with increasing Mach number. This indicated that the centerbody surface Mach numbers are increasing at a faster rate than the free stream velocity.

7.3.3.3 Performance Corrections

With the Prop-Fan blades installed and thrusting, as depicted in Figure 7-13, the balance measures the algebraic sum of the apparent thrust, the spinner drag, and the back pressure force. Therefore, the apparent thrust of the Prop-Fan is obtained as shown in the following equation:

$$T_{APP} = F_B - F_{BP} + D_S + F_{TH}$$

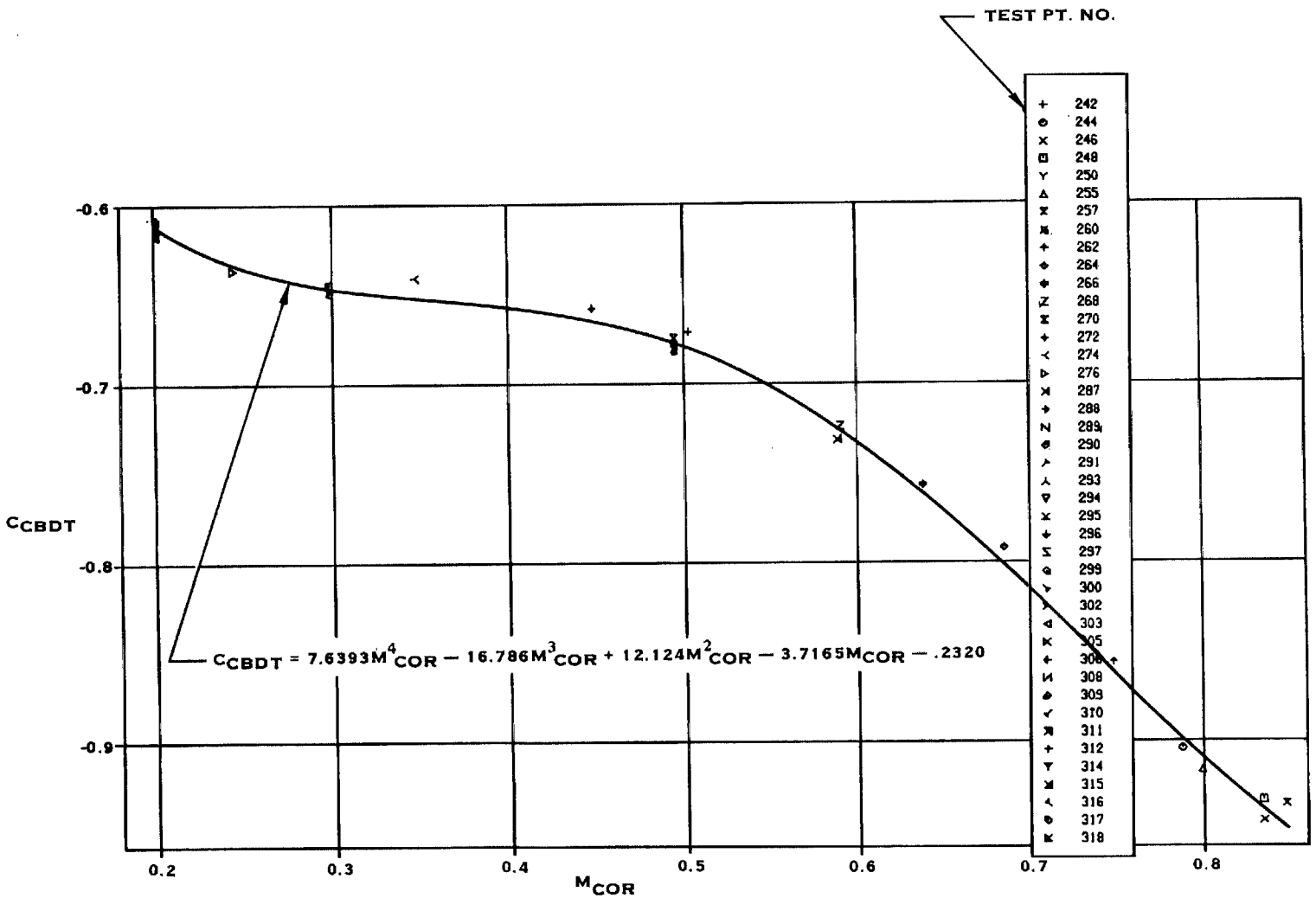

FIGURE 7-15. CENTERBODY DRAG COEFFICIENT VS. CORRECTED MACH NUMBER

7.3.3.3 (Continued)

As defined earlier, the centerbody drag is obtained from centerbody surface pressure integrations:

$$D_{CB} = \sum_{N=1}^{44} (P_N - P_O)A_N$$

Also, as mentioned previously, the buoyancy force was obtained from the difference between these and the tare run pressure integrations:

$$BF = D_{CB} - D_{CBT}$$

Finally, the net thrust (T_{NET}), which is defined as the propulsive force of the blades operating in the presence of the spinner and centerbody flow field without the increase in thrust due to the mutual interaction, is obtained by subtracting the buoyancy force from the apparent thrust:

$$T_{NET} = T_{APP} - BF$$

8.0 BLADE STRUCTURAL DYNAMIC EVALUATION

8.1 Test Objectives

8.1.1 Confirm that the SR-7L Prop-Fan was free of high speed blade flutter over the portion of its operating envelope that could be run in the ONERA S1-MA wind tunnel.

8.1.2 Evaluate the 1P blade strain sensitivity of the SR-7L Prop-Fan for a range of blade angles, rotational speeds, Mach Numbers and inflow angles.

8.1.3 Compare the measured and analytically predicted 1P blade strain responses of the SR-7L Prop-Fan for selected operating conditions.

8.2 Test Procedure

Testing of the SR-7L Large Scale Advanced Prop-Fan was conducted in the ONERA S1 atmospheric wind tunnel in Modane, France. The Prop-Fan was mounted so that the rotor plane was located in the throat of the wind tunnel. The tunnel throat was eight meters in diameter.

The drive system as described earlier in section 6.2, was supported by rods and cables attached to the tunnel walls as illustrated in Figures 8-1 and 8-2. A balance and torquemeter, also described in section 6.2, provided the capability to measure forces and moments acting on the Prop-Fan.

Test rig vibration was monitored by two sets of horizontal and vertical accelerometers. The accelerometers were located on the drive train housing in two planes aft of the Prop-Fan.

A stationary aerodynamic fairing was located downstream of the Prop-Fan. The fairing served as an extension of the external aerodynamic contour of the spinner. The fairing resulted in an approximate 35% blockage of the flow through the Prop-Fan rotor.

Power available from the test drive system was significantly lower than the rated power of the Prop-Fan. Therefore, in order to simulate operation at high power loading conditions, the Prop-Fan was run in two and four blade configurations as well as with eight blades. This allowed power loadings per blade to be achieved, which correspond to intermediate and high power operating points with eight blades. The disadvantage of operation with two and four blades was the negation of the inter-blade cascade effects which are present in the eight blade design. These effects tend to be destabilizing in that they lower the Mach Number at which the onset of classical flutter occurs.

The missing blades were replaced with stubs in the two and four blade configuration as depicted in Figure 7-9. The ends of the stubs were machined to match the external contour of the spinner. The Prop-Fan is shown in the two, four and eight blade configurations in Figures 8-3, 8-4 and 8-5.

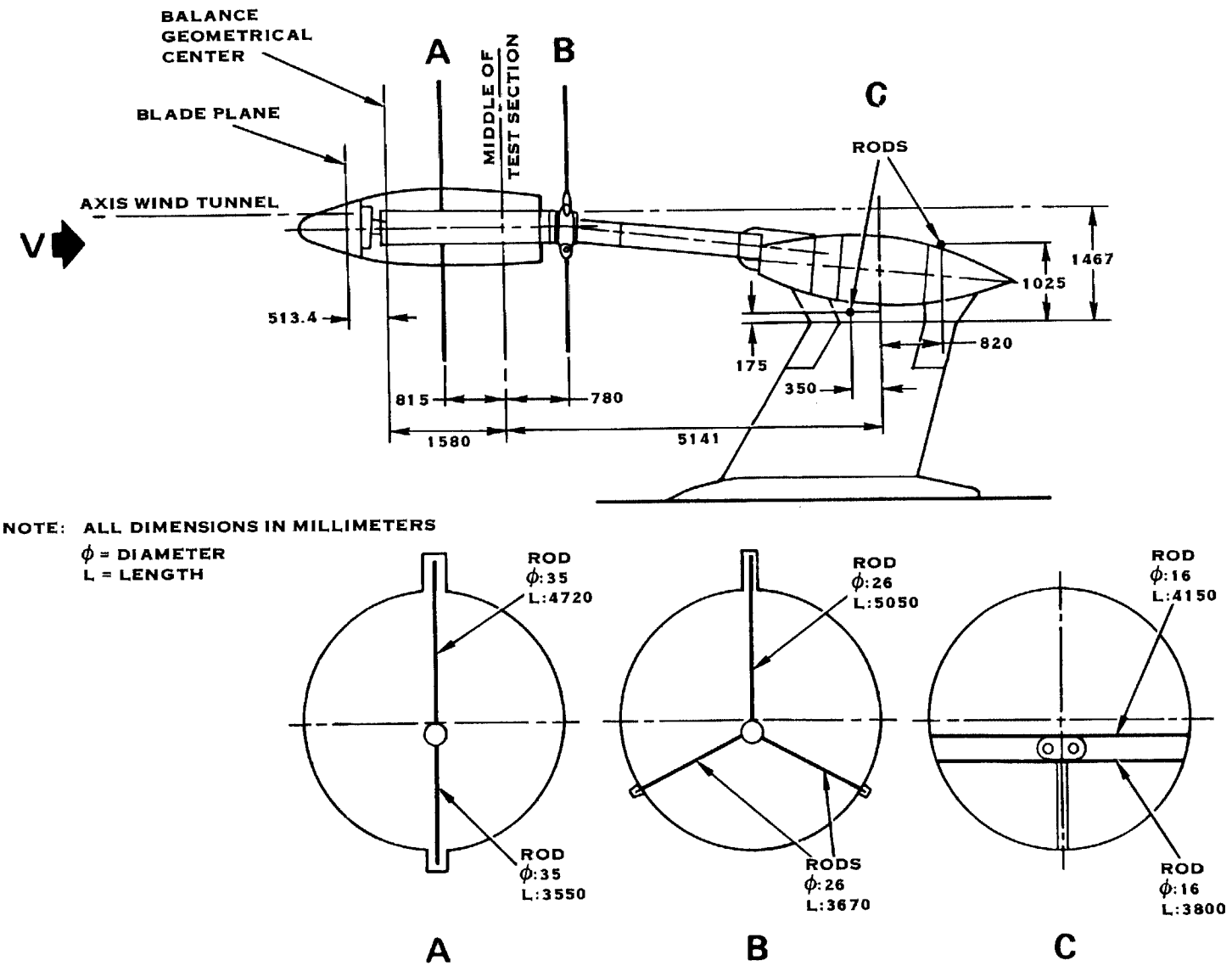

FIGURE 8-1. TEST RIG SUPPORT STRUCTURE FOR STRUCTURAL DYNAMIC EVALUATION (2 AND 4 BLADE CONFIGURATIONS)

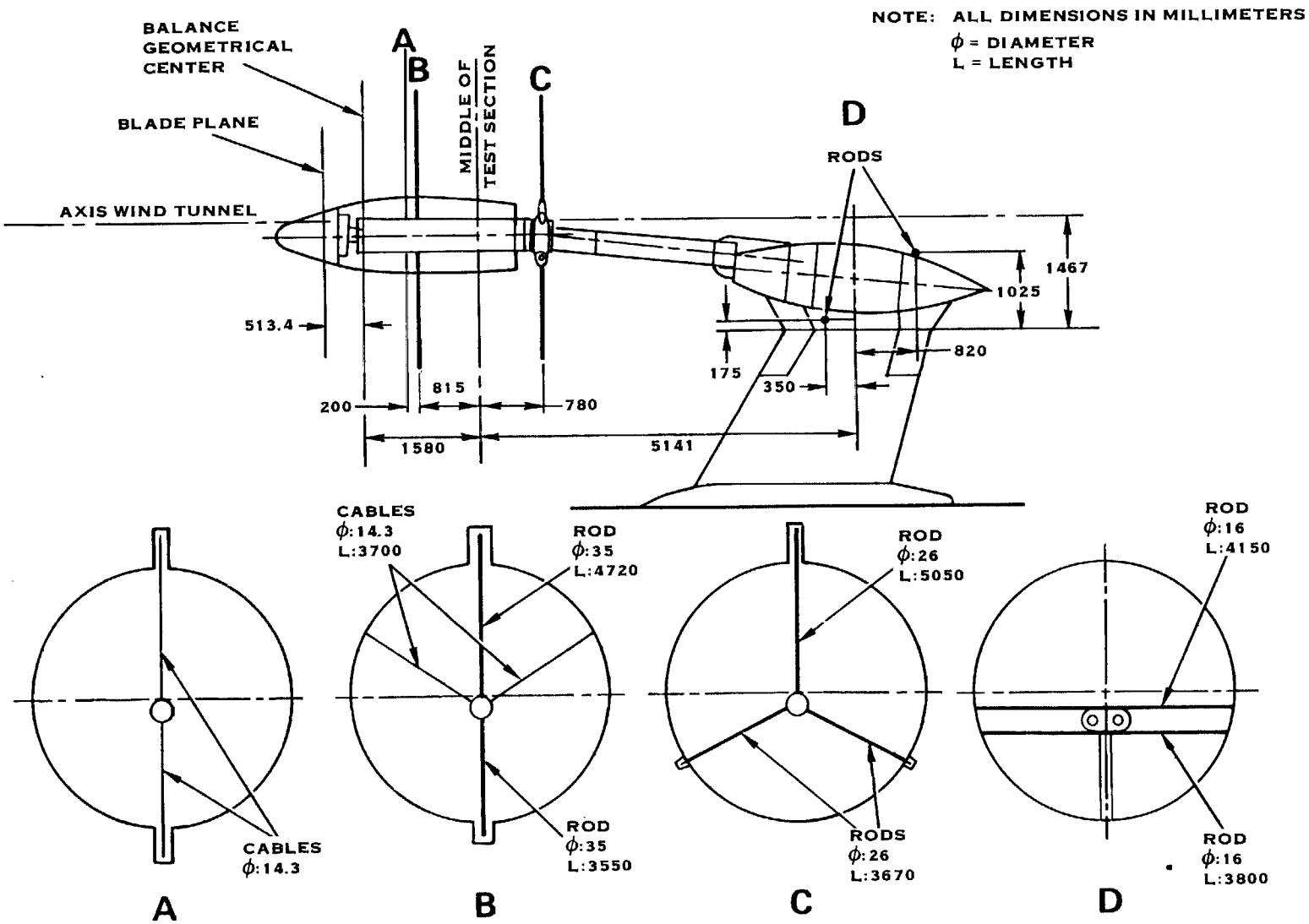

FIGURE 8-2. TEST RIG SUPPORT STRUCTURE FOR STRUCTURAL DYNAMIC EVALUATION (8 BLADE CONFIGURATION)

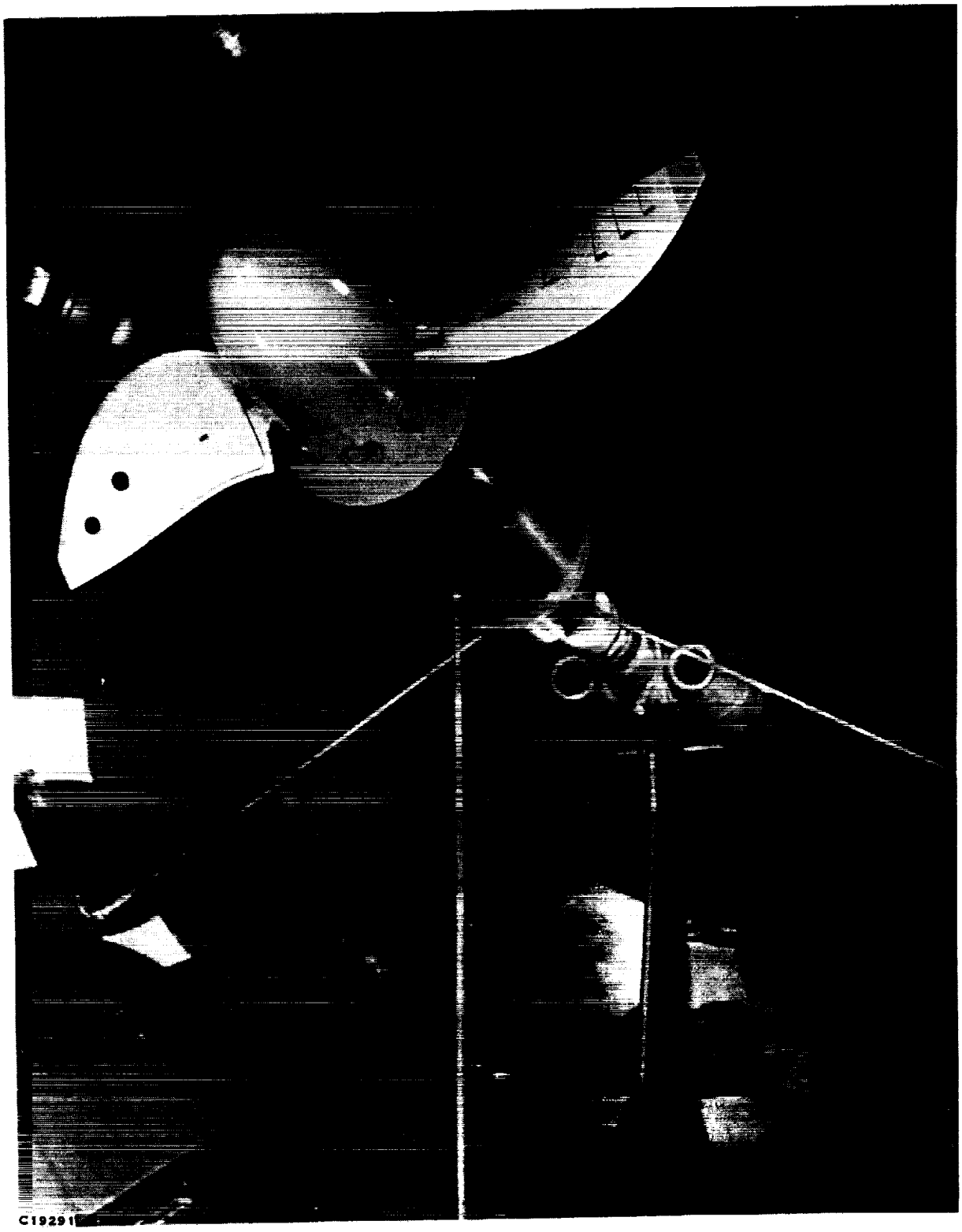

FIGURE 8-3. TWO BLADE TEST CONFIGURATION

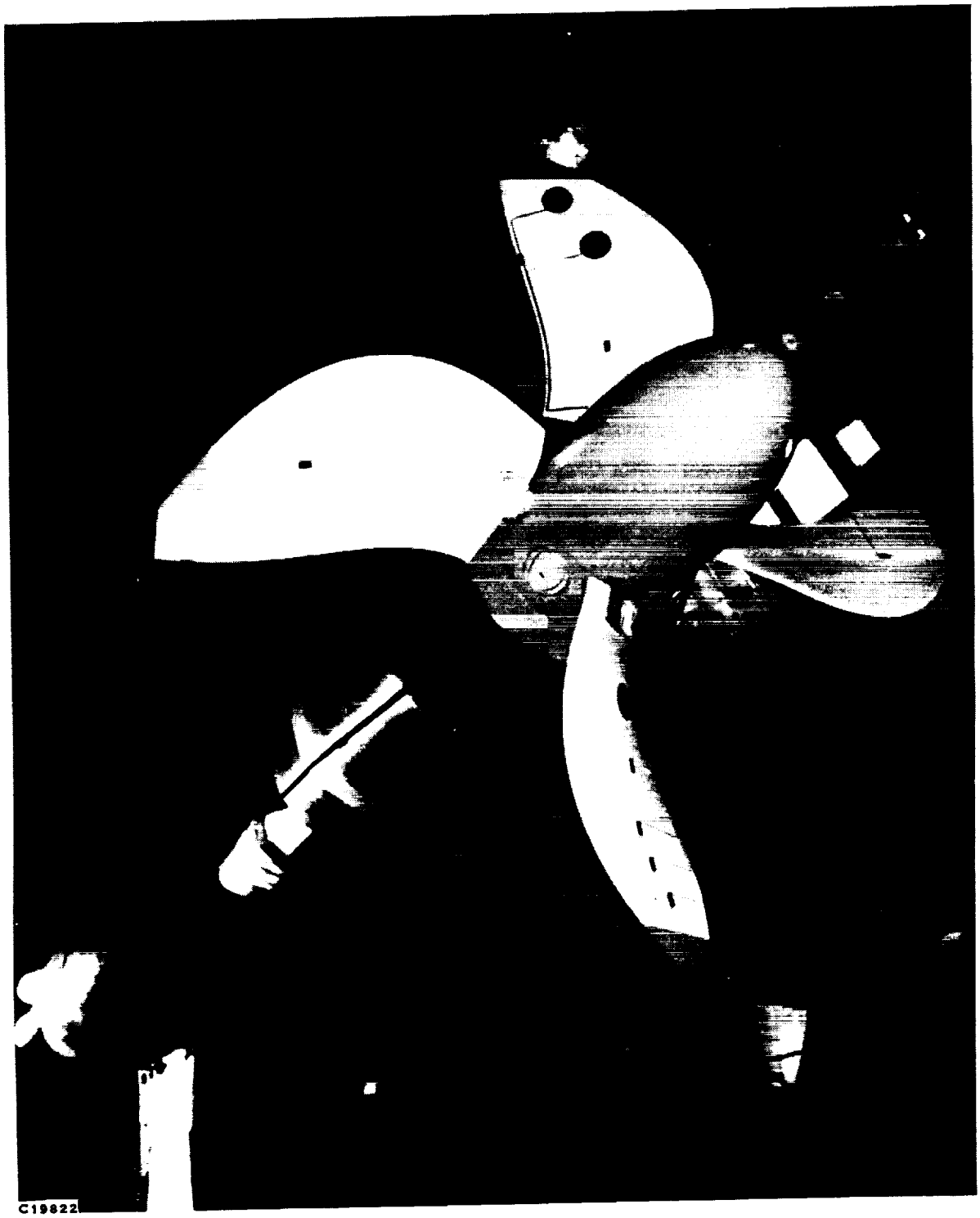

FIGURE 8-4. FOUR BLADE TEST CONFIGURATION

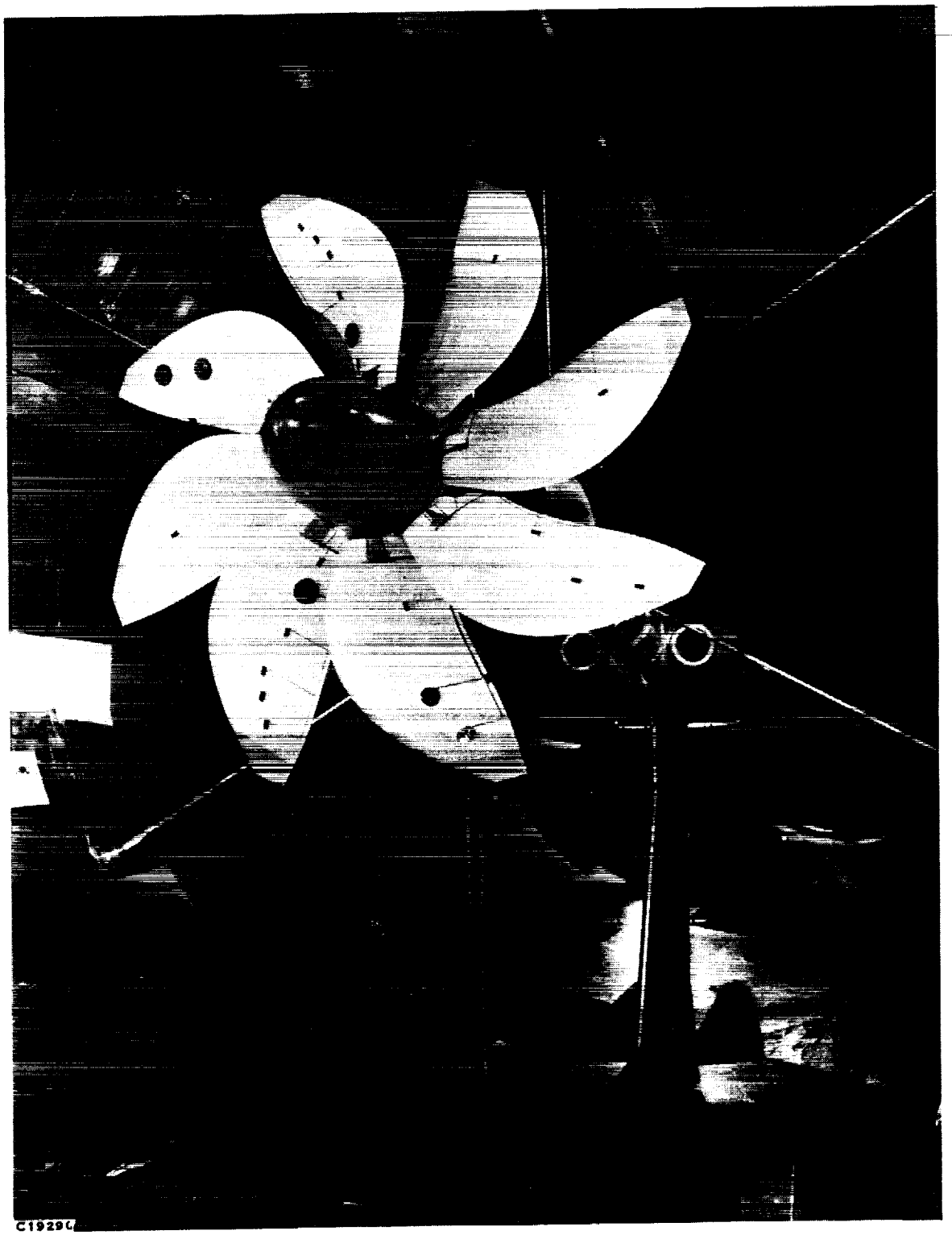

FIGURE 8-5. EIGHT BLADE TEST CONFIGURATION

8.2 (Continued)

The strain gage arrangements for the two, four and eight blade configurations are shown in Figures 8-6, 8-7 and 8-8. The blade surface gage locations were chosen either to correspond with the points of maximum strain for the blade normal modes or to provide the distribution of strain along the entire span of the blade. Blade shank gages were also used to measure vibratory bending moments.

The Prop-Fan was operated in a Beta control mode during the high speed wind tunnel testing. In this mode the blade pitch angle was selected by the operator using a manual control. The test procedure consisted of starting the Prop-Fan at a blade angle (β3/4) of 20° to 25° and increasing power to obtain 1200 RPM to 1500 RPM rotor speed with the tunnel flow drive system not operating. Mach number was then increased in increments. Following each increase in Mach number the blade angle was increased to maintain the rotor speed in the 1200 RPM to 1500 RPM range. At the Mach numbers of interest, test points were run at two or three different power settings and over a range of rotor speeds. Blade strain gage data was recorded for thirty seconds at each test point. Aerodynamic performance and test rig vibration data were also logged concurrently with the strain gage data.

8.3 Discussion and Results

8.3.1 General Discussion

During initial balance runs of the Prop-Fan, which was conducted at zero Mach number, test rig critical speeds were discovered at 360 RPM and 540 RPM. Both criticals were highly undamped, allowing rig vibration to grow rapidly if operation was attempted at these speeds. The critical speed at 360 RPM corresponded to the predicted rig first critical. Since both of these criticals were well below the planned test operating speeds, they did not pose a problem. No other critical speeds were apparent within the test rotational speed range. For the low rotational speeds at which dynamic balancing was accomplished, dynamometer vibratory stresses were the limiting factor rather than rig vibrations measured by the accelerometers. This may have resulted from relatively low accelerations causing large displacements due to the low frequency of the response.

Figures 8-9, 8-10 and 8-11 present a mapping of the test points run during structural dynamic testing. The test points acquired for the four blade configuration spanned the entire planned operating range. Power supplied to the Prop-Fan by the turbines was limited to 800 KW due to the elevated ambient temperature in the tunnel.

Operation between 1000 RPM and 1500 RPM resulted in high rig vibration for the two blade and the eight blade configurations. Therefore, this operating region had to be avoided. The vibration frequency was not 1P and was not believed to be caused by the Prop-Fan. With the exception of the 2 bladed configuration at 3° inflow angle (ψ), operation at inflow angles of 3° or 10° also resulted in a high level, low frequency vibration which precluded testing at those conditions.

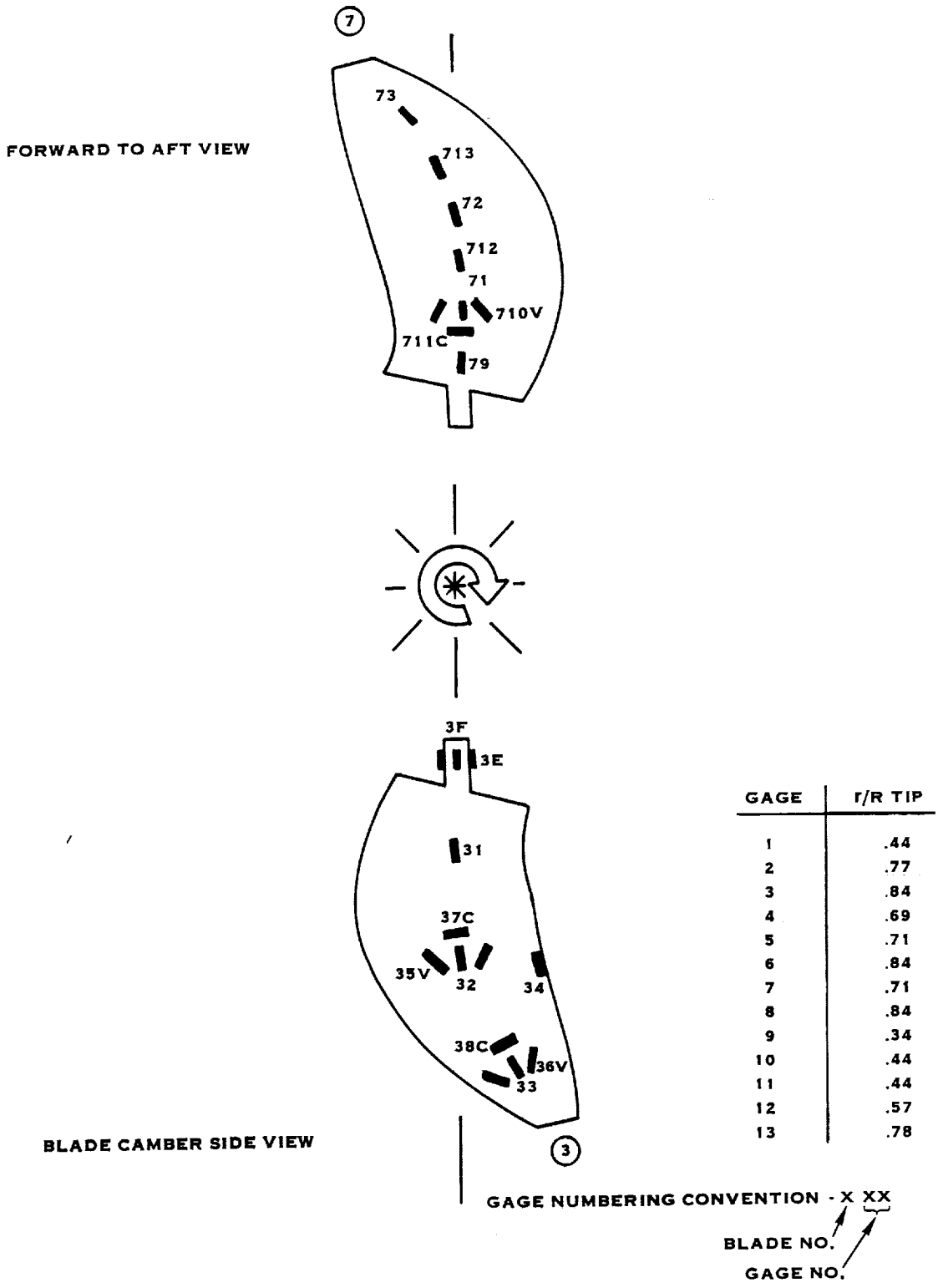

FIGURE 8-6. STRAIN GAGE ARRANGEMENT FOR TWO BLADE CONFIGURATION

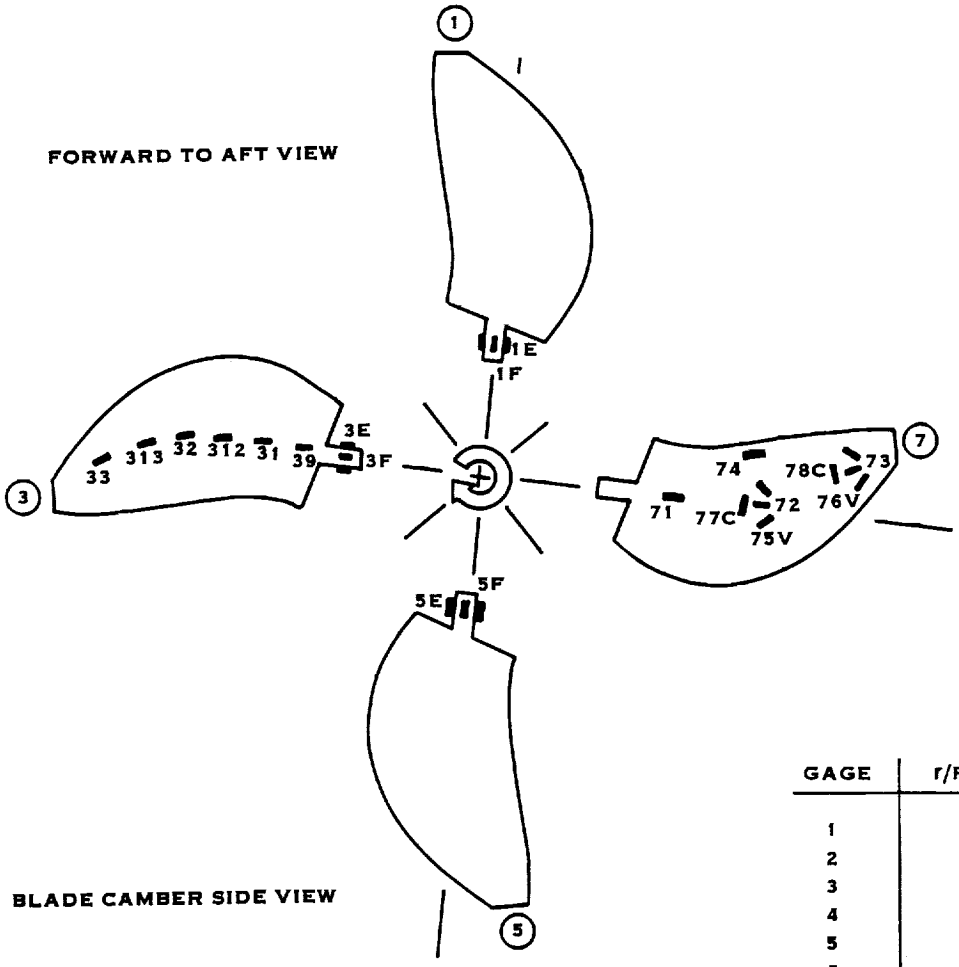

GAGE	r/R TIP
1	.44
2	.77
3	.84
4	.69
5	.71
6	.84
7	.71
8	.84
9	.34
10	.44
11	.44
12	.57
13	.78

GAGE NUMBERING CONVENTION - X XX

BLADE NO.

GAGE NO.

FIGURE 8-7. STRAIN GAGE ARRANGEMENT FOR FOUR BLADE CONFIGURATION

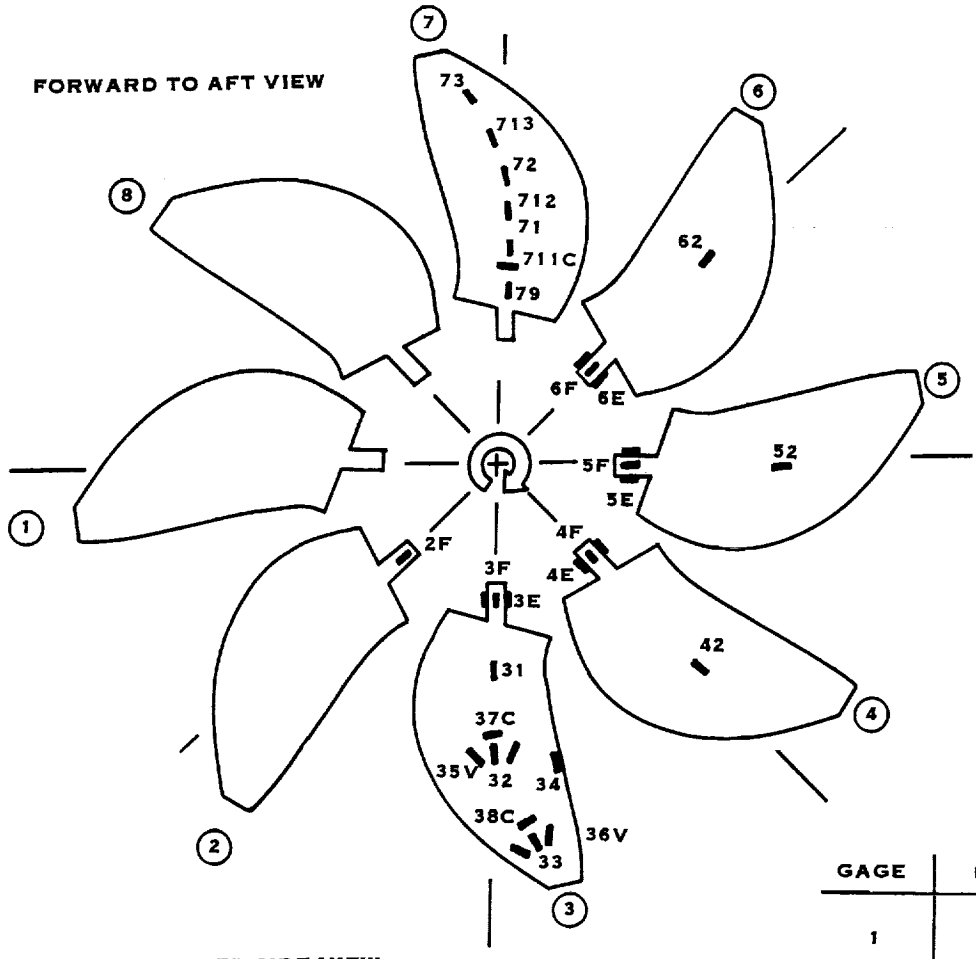

GAGE	r/R TIP
1	.44
2	.77
3	.84
4	.69
5	.71
6	.84
7	.71
8	.84
9	.34
10	.44
11	.44
12	.57
13	.78

GAGE NUMBERING CONVENTION - X XX

BLADE NO.

GAGE NO.

FIGURE 8-8. STRAIN GAGE ARRANGEMENT FOR EIGHT BLADE CONFIGURATION

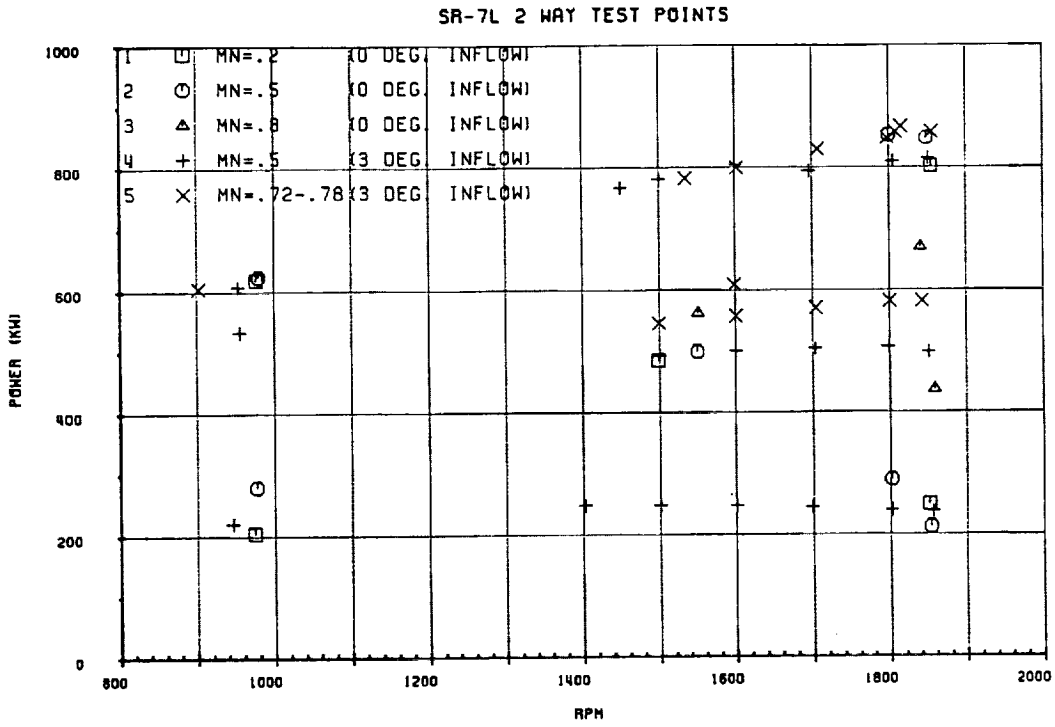

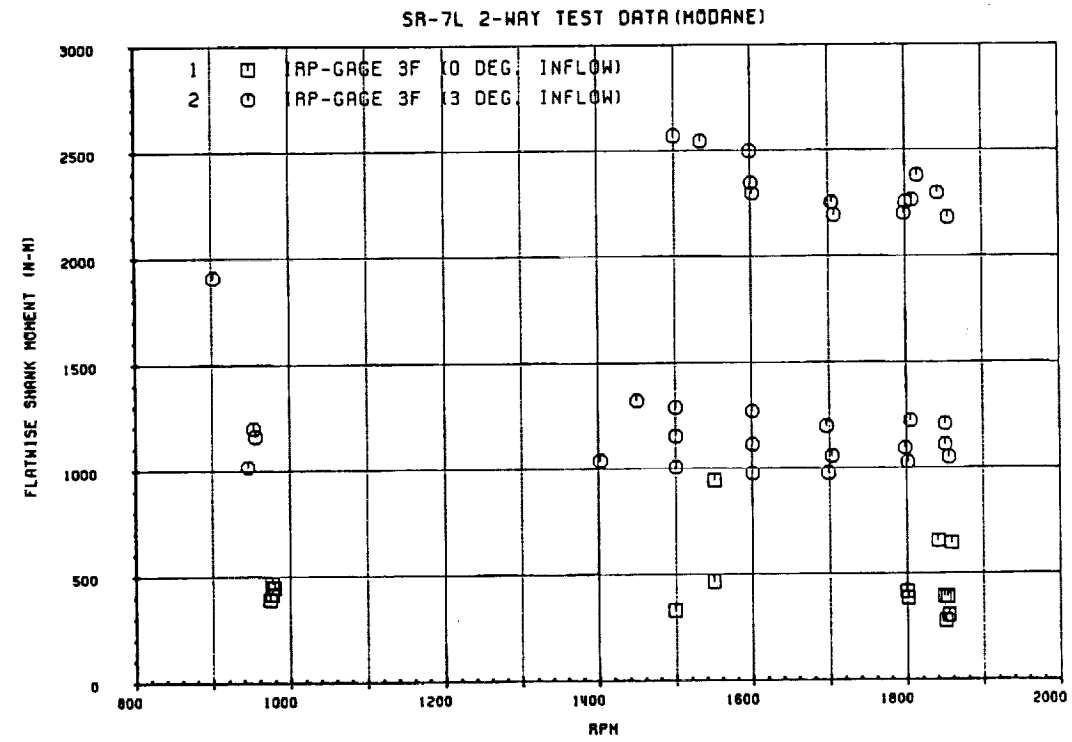

FIGURE 8-9, TEST POINTS AND BLADE SHANK MOMENTS (2 BLADE CONFIGURATION)

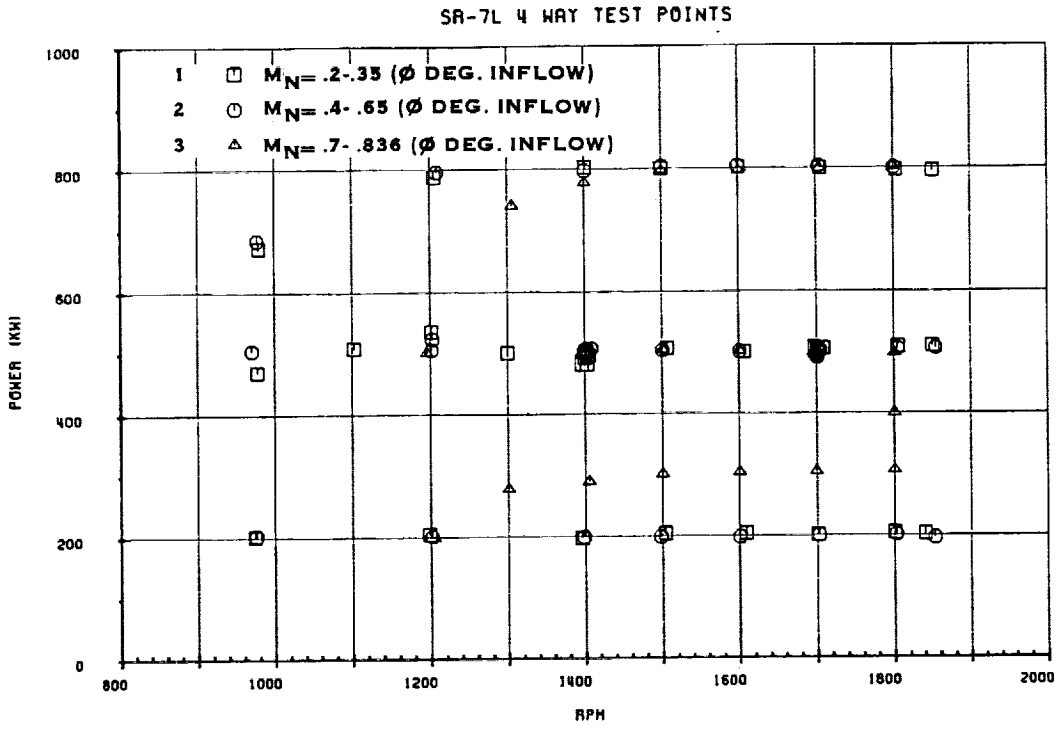

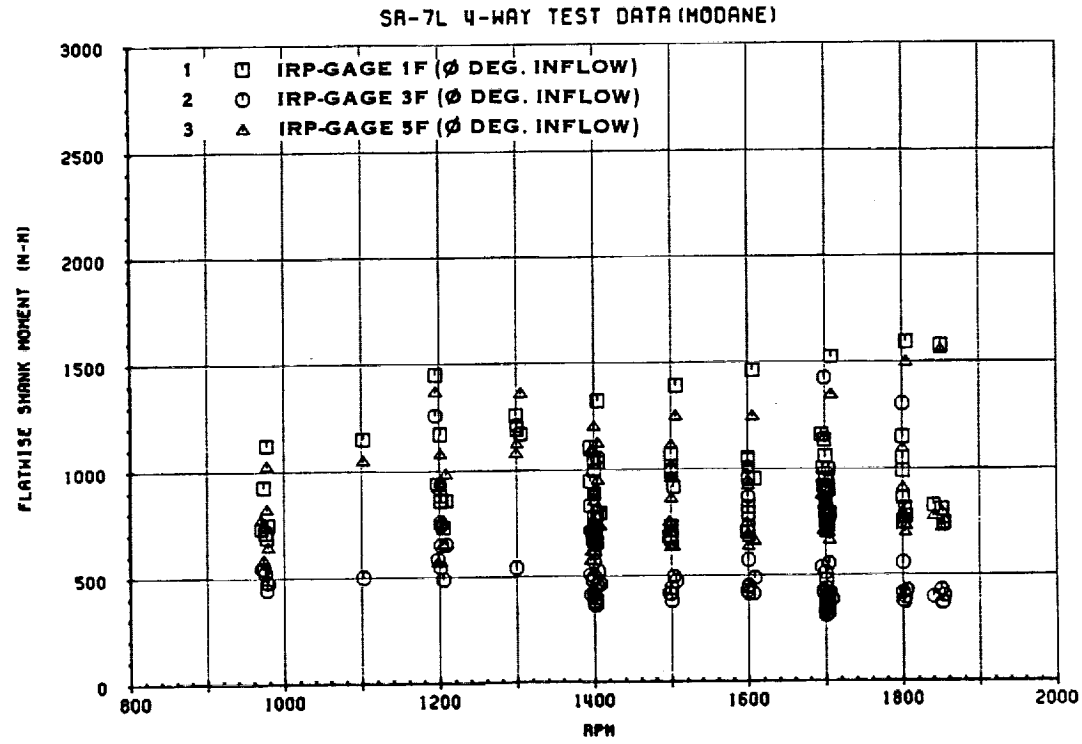

FIGURE 8-10. TEST POINTS AND BLADE SHANK MOMENTS (4 BLADE CONFIGURATION)

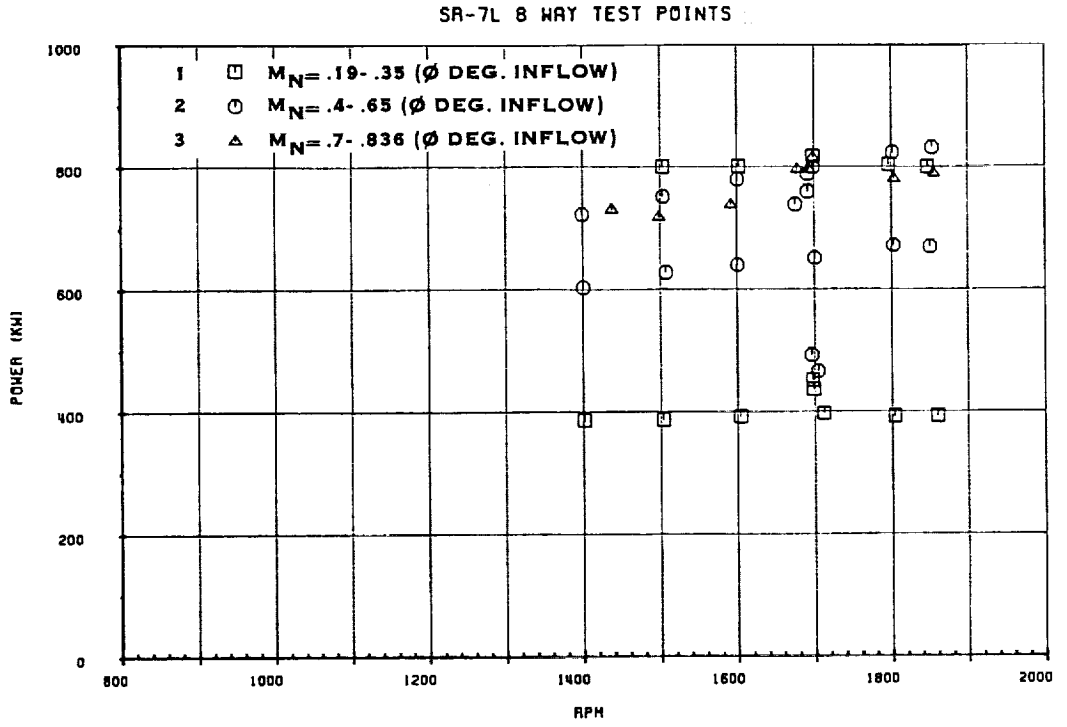

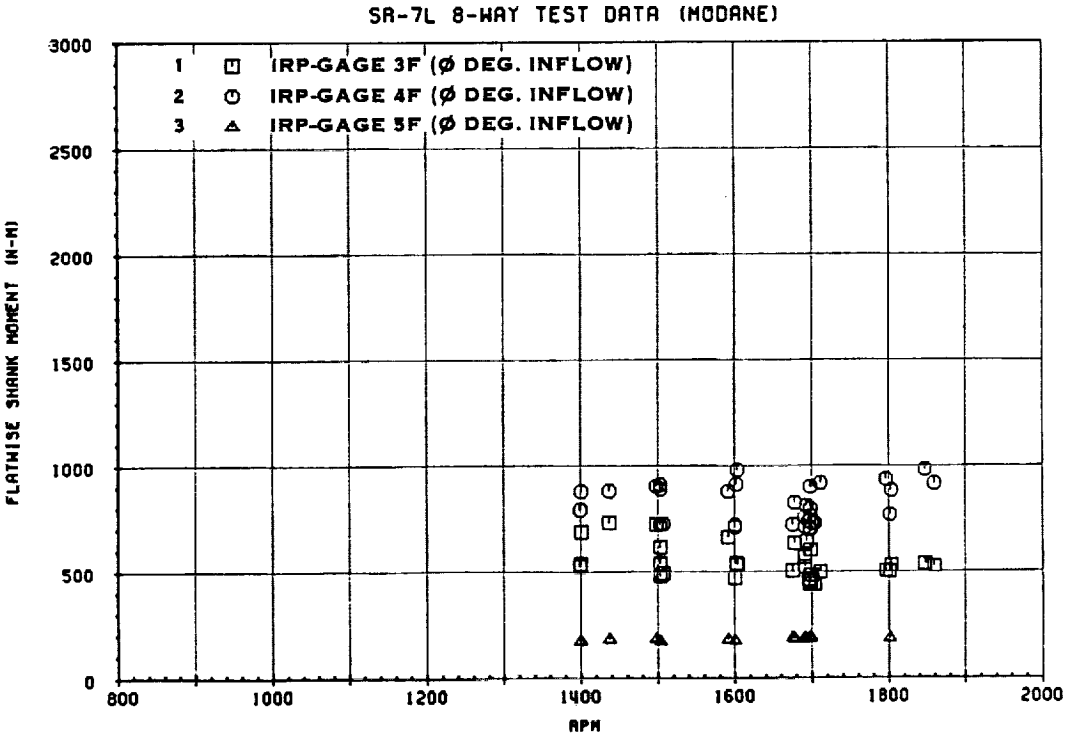

FIGURE 8-11. TEST POINTS AND BLADE SHANK MOMENTS (8 BLADE CONFIGURATION)

8.3.1 (Continued)

Mach numbers above .73 resulted in negative thrust for the eight blade configuration due to the low power available from the turbines. Since the balance was not designed for negative thrust, the maximum Mach number for the eight blade case was limited.

8.3.2 Data Reduction

The strain gage signals were recorded on magnetic tape for each of the gages shown in Figures 8-6, 8-7 and 8-8. These signals were then fed through a peak stress (strain) converter, a device which determines the peak vibratory strain occurring in a unit of time (.1 seconds for this data). The output of the peak stress (strain) converter is then statistically analyzed to obtain the average amplitude (mean) and standard deviation of each signal. The IRP (infrequently repeating peak) is defined, for the purposes of this report, as the mean plus twice the standard deviation. It is a conservative measure of the strain amplitude normally used to estimate blade fatigue life.

Figures 8-9, 8-10 and 8-11 show summaries of the conditions analyzed along with plots of the IRP shank moments for the 2, 4, and 8 bladed configurations. It can be seen that the highest values recorded were for the two bladed configuration with angular inflow (3 degrees). It is also noted that there are significant blade-to-blade differences. However, it was found that the data contained significant high frequency noise (several thousand HZ), which tended to artificially increase the IRP values. In general, no significant differences in strain gage signal were revealed between the two, four and eight blade configurations at uniform inflow angle, for the same gage (3F).

Figure 8-12 shows an example of the signal to noise problem and its variability between different gages. Because of the low response levels, the data reduction was not repeated with the noise filtered out.

Tables 8-I, 8-II, and 8-III show the conditions of the runs made along with some sample IRP tabulations, showing blade-to-blade variations.

Table 8-IV shows a tabulation of peak IRP values for each gage versus the limits determined based on the threshold at which blade fatigue damage begins to accumulate. Because of the high noise content, all of the IRP values (Figures 8-9, 8-10, 8-11 and Tables 8-I, 8-II, 8-III and 8-IV should be interpreted as conservative upper bounds on the strains actually felt by the blades. As such, the gages shown to be exceeding the limits should actually be interpreted as below the limits with the noise filtered out.

EXAMPLE: ONERA RUN NO. 559 :0° INFLOW ANGLE; 4 BLADE CONFIGURATION
(M_N = .2, 1500 RPM, 500KW)

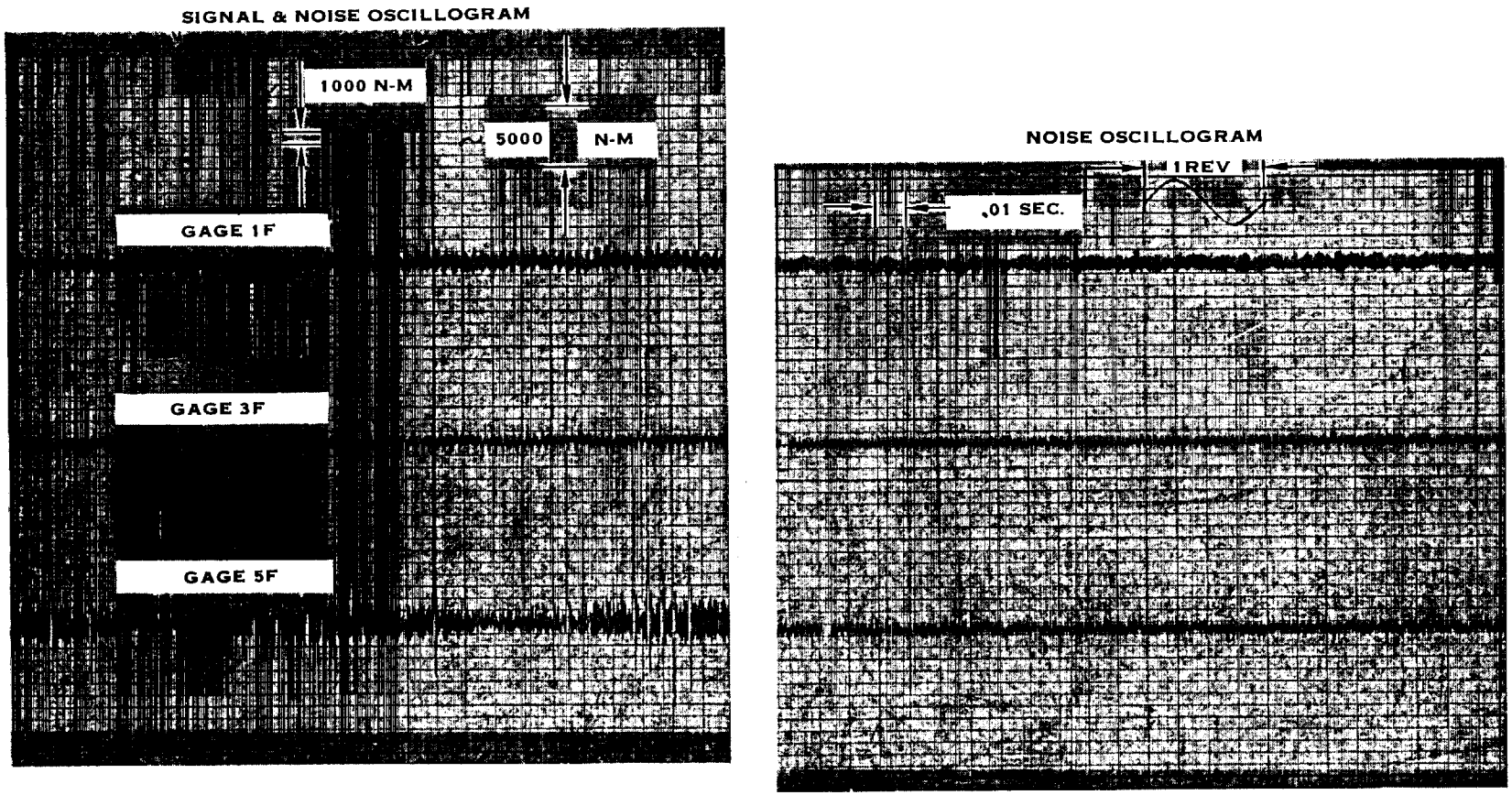

FIGURE 8-12. COMPARISON OF SIGNAL TO NOISE FOR FLATWISE SHANK MOMENT GAGES (0° INFLOW ANGLE)

TABLE 8-I. OPERATING CONDITIONS FOR $M_N > .1$ AND SAMPLE IRP TABULATIONS (2 BLADE CONFIGURATION)

DESCRIPTION	RUN NO.	O.N.E.R.A run no.	RPM	MACH NO.	THETA (at .75r/R) (deg.)	POWER (kW)	TORQUE (N-m)	IRP Gage 3F (N-m)	IRP Gage 31 microstrain	IRP Gage 71 microstrain	IRP Gage 33 microstrain	IRP Gage 73 microstrain
2 way(0 deg.)	3	1036.	973.	0.2000	41.10	204.0	2002.	392.	72.0	130.0	84.0	130.0
2 way(0 deg.)	4	1038.	976.	0.2000	54.10	619.0	6056.	416.	92.0	118.0	156.0	190.0
2 way(0 deg.)	5	1048.	1854.	0.2000	29.80	802.0	4131.	304.	72.0	94.0	56.0	96.0
2 way(0 deg.)	6	1050.	1498.	0.2000	29.90	485.0	3092.	332.	80.0	124.0	46.0	122.0
2 way(0 deg.)	7	1052.	1650.	0.2000	23.30	249.0	1285.	278.	70.0	86.0	42.0	80.0
2 way(0 deg.)	8	1081.	976.	0.5000	59.40	279.0	2730.	468.	88.0	244.0	98.0	
2 way(0 deg.)	9	1083.	979.	0.5000	63.50	624.0	6086.	446.	92.0	96.0	96.0	
2 way(0 deg.)	10	1105.	1549.	0.5000	46.20	499.0	3076.	464.	122.0	142.0	68.0	124.0
2 way(0 deg.)	11	1107.	1799.	0.5000	45.50	853.0	4528.	414.	96.0	100.0	80.0	100.0
2 way(0 deg.)	12	1109.	1848.	0.5000	44.90	848.0	4382.	392.	92.0	96.0	70.0	102.0
2 way(0 deg.)	13	1111.	1801.	0.5000	42.60	290.0	1538.	384.	94.0	98.0	50.0	82.0
2 way(0 deg.)	14	1114.	1852.	0.5000	41.20	212.0	1093.	388.	92.0	84.0	46.0	76.0
2 way(0 deg.)	15	1128.	1550.	0.8000	54.90	563.0	3468.	544.	294.0	292.0	182.0	228.0
2 way(0 deg.)	16	1132.	1840.	0.8000	55.00	670.0	3477.	654.	170.0		122.0	
2 way(0 deg.)	17	1134.	1858.	0.8000	54.80	437.0	2246.	644.	162.0		114.0	
2 way(3. deg.)	18	1162.	1500.	0.5000	46.90	492.0	3132.	1152.	368.0	338.0	184.0	259.0
2 way(3. deg.)	19	1164.	1600.	0.5000	46.50	500.0	2984.	1112.	266.0	274.0	142.0	190.0
2 way(3. deg.)	20	1166.	1703.	0.5000	45.00	504.0	2826.	1058.	232.0	236.0	136.0	176.0
2 way(3. deg.)	21	1168.	1798.	0.5000	43.40	507.0	2693.	1094.	238.0	244.0	130.0	162.0
2 way(3. deg.)	22	1170.	1850.	0.5000	42.70	498.0	2571.	1110.	232.0	236.0	122.0	154.0
2 way(3. deg.)	23	1172.	1850.	0.5000	43.90	815.0	4267.	1208.	256.0	250.0	150.0	180.0
2 way(3. deg.)	24	1174.	1805.	0.5000	43.00	810.0	4285.	1224.	264.0	260.0	146.0	184.0
2 way(3. deg.)	25	1176.	1696.	0.5000	44.50	794.0	4471.	1198.	278.0	274.0	154.0	184.0
2 way(3. deg.)	26	1178.	1600.	0.5000	46.60	805.0	4804.	1270.	302.0	306.0	172.0	216.0
2 way(3. deg.)	27	1180.	1500.	0.5000	48.80	781.0	4972.	1268.	334.0	352.0	212.0	250.0
2 way(3. deg.)	28	1182.	1450.	0.5000	50.10	767.0	5051.	1322.	348.0	368.0	208.0	260.0
2 way(3. deg.)	29	1184.	1402.	0.5000	47.20	248.0	1669.	1038.	270.0	304.0	162.0	206.0
2 way(3. deg.)	30	1186.	1500.	0.5000	46.90	248.0	1579.	1006.	248.0	262.0	146.0	168.0
2 way(3. deg.)	31	1188.	1600.	0.5000	45.30	247.0	1474.	976.	224.0	230.0	112.0	144.0
2 way(3. deg.)	32	1190.	1698.	0.5000	43.40	244.0	1372.	978.	220.0	220.0	114.0	136.0
2 way(3. deg.)	33	1192.	1801.	0.5000	42.10	239.0	1267.	1028.	218.0	214.0	112.0	134.0
2 way(3. deg.)	34	1194.	1855.	0.5000	41.40	237.0	1220.	1050.	218.0	214.0	100.0	126.0
2 way(3. deg.)	36	1198.	1598.	0.7800	55.30	609.0	3638.	2496.	618.0	616.0	322.0	372.0
2 way(3. deg.)	37	1200.	1600.	0.7500	55.20	558.0	3330.	2348.	600.0	590.0	296.0	346.0
2 way(3. deg.)	38	1202.	1499.	0.7500	55.40	546.0	3478.	2570.	694.0	692.0	370.0	412.0
2 way(3. deg.)	39	1204.	1704.	0.7500	54.80	571.0	3200.	2256.	524.0	520.0	302.0	328.0
2 way(3. deg.)	40	1206.	1800.	0.7500	54.00	582.0	3088.	2256.	478.0	476.0	256.0	270.0
2 way(3. deg.)	41	1208.	1843.	0.7500	53.30	582.0	3017.	2296.	486.0	488.0	236.0	288.0
2 way(3. deg.)	42	1210.	1602.	0.7230	53.80	800.0	4769.	2298.	592.0	592.0	318.0	340.0
2 way(3. deg.)	43	1212.	1534.	0.7230	54.80	783.0	4874.	2546.	706.0	710.0	404.0	438.0
2 way(3. deg.)	44	1214.	1707.	0.7240	54.80	830.0	4643.	2196.	506.0	508.0	262.0	290.0
2 way(3. deg.)	45	1216.	1798.	0.7250	53.80	848.0	4504.	2204.	480.0	474.0	270.0	298.0
2 way(3. deg.)	46	1218.	1855.	0.7240	53.30	856.0	4417.	2184.	462.0	454.0	208.0	254.0
2 way(3. deg.)	47	1220.	1808.	0.7420	53.30	858.0	4532.	2266.	490.0	488.0	260.0	296.0
2 way(3. deg.)	48	1222.	1815.	0.7630	53.30	867.0	4561.	2382.	524.0	526.0	258.0	294.0
2 way(3. deg.)	49	1230.	945.	0.5000	58.90	220.0	2223.	1016.	248.0	288.0	192.0	232.0
2 way(3. deg.)	50	1234.	955.	0.5000	63.10	533.0	5329.	1160.	302.0	346.0	218.0	250.0
2 way(3. deg.)	51	1236.	953.	0.5000	63.90	608.0	6092.	1198.	306.0	346.0	196.0	230.0
2 way(3. deg.)	52	1240.	902.	0.7200	69.10	605.0	6405.	1908.	528.0	562.0	56.0	438.0
STANDARD DEV.	**********	56.	304.	0.1678	8.67	220.3	1434.	730.	179.7	173.5	89.5	95.4
MINIMUM VALUE	**********	1036.	902.	0.2000	23.30	204.0	1093.	278.	70.0	86.0	42.0	76.0
AVERAGE VALUE	**********	1164.	1576.	0.5566	49.25	563.8	3508.	1257.	299.8	318.6	167.6	218.4
MAXIMUM VALUE	**********	1240.	1858.	0.8000	69.10	867.0	6405.	2570.	706.0	710.0	404.0	438.0

TABLE 8-II. OPERATING CONDITIONS FOR $M_N > .1$ AND SAMPLE IRP TABULATIONS (4 BLADE CONFIGURATION)

DESCRIPTION	RUN NO.	O.N.E.R.A run no.	RPM	MACH NO.	THETA (at .76r/R) (deg.)	POWER (kW)	TORQUE (N-m)	IRP Gage 1F (N-m)	IRP Gage 3F (N-m)	IRP Gage 5F (N-m)	IRP Gage 31 microstrain	IRP Gage 71 microstrain
4 way(0 deg.)	4	547.	977.	0.2000	41.40	469.0	4584.	1124.	482.	1024.	106.0	72.0
4 way(0 deg.)	5	549.	1102.	0.2000	40.60	508.0	4402.	1152.	502.	1048.	126.0	72.0
4 way(0 deg.)	6	551.	1201.	0.2000	37.79	535.0	4254.	1174.	546.	1078.	144.0	78.0
4 way(0 deg.)	7	555.	1299.	0.2000	34.90	500.0	3676.	1258.	542.	1080.	140.0	76.0
4 way(0 deg.)	8	557.	1405.	0.2000	32.30	495.0	3364.	1324.	524.	1126.	120.0	78.0
4 way(0 deg.)	9	559.	1506.	0.2000	30.10	506.0	3208.	1392.	474.	1248.	96.0	78.0
4 way(0 deg.)	10	563.	1606.	0.2000	28.30	500.0	2973.	1462.	414.	1246.	78.0	72.0
4 way(0 deg.)	11	565.	1706.	0.2000	26.56	505.0	2823.	1524.	386.	1344.	76.0	66.0
4 way(0 deg.)	12	567.	1805.	0.2000	25.38	508.0	2688.	1592.	428.	1494.	94.0	64.0
4 way(0 deg.)	13	569.	1850.	0.2000	25.15	509.0	2627.	1578.	428.	1552.	100.0	68.0
4 way(0 deg.)	20	585.	973.	0.2000	35.60	201.0	1973.	926.	546.	582.	118.0	76.0
4 way(0 deg.)	21	587.	1198.	0.2000	30.90	204.0	1626.	936.	584.	568.	118.0	88.0
4 way(0 deg.)	22	589.	1395.	0.2000	25.90	197.0	1349.	946.	506.	572.	96.0	94.0
4 way(0 deg.)	23	591.	1503.	0.2000	24.20	204.0	1296.	918.	496.	636.	86.0	88.0
4 way(0 deg.)	24	593.	1608.	0.2000	22.75	204.0	1211.	954.	488.	660.	90.0	80.0
4 way(0 deg.)	25	595.	1701.	0.2000	21.50	201.0	1128.	902.	474.	690.	86.0	66.0
4 way(0 deg.)	26	597.	1800.	0.2000	20.40	204.0	1082.	862.	416.	752.	76.0	66.0
4 way(0 deg.)	27	599.	1840.	0.2000	19.75	202.0	1048.	826.	396.	774.	74.0	64.0
4 way(0 deg.)	28	603.	1600.	0.2000	29.90	802.0	4786.	792.	444.	634.	84.0	94.0
4 way(0 deg.)	29	605.	1705.	0.2000	27.98	800.0	4481.	790.	418.	664.	78.0	80.0
4 way(0 deg.)	30	607.	1803.	0.2000	26.20	797.0	4221.	814.	394.	698.	76.0	72.0
4 way(0 deg.)	31	609.	1851.	0.2000	25.60	795.0	4101.	808.	366.	718.	72.0	70.0
4 way(0 deg.)	32	611.	1499.	0.2000	28.40	800.0	5096.	732.	414.	632.	82.0	94.0
4 way(0 deg.)	33	613.	1401.	0.2000	31.10	803.0	5473.	730.	436.	612.	92.0	90.0
4 way(0 deg.)	34	615.	1205.	0.2000	36.80	788.0	6245.	732.	490.	652.	124.0	84.0
4 way(0 deg.)	35	617.	979.	0.2000	44.60	672.0	6555.	748.	478.	642.	112.0	78.0
4 way(0 deg.)	36	621.	1202.	0.4000	46.75	523.0	4155.	862.	650.	748.	170.0	124.0
4 way(0 deg.)	37	623.	1600.	0.5000		501.0	2990.	822.	452.	672.	96.0	96.0
4 way(0 deg.)	38	625.	1701.	0.5000	45.80	499.0	2801.	800.	436.	704.	90.0	92.0
4 way(0 deg.)	39	627.	1804.	0.5000	44.25	504.0	2668.	776.	424.	728.	96.0	94.0
4 way(0 deg.)	40	629.	1854.	0.5000	43.60	505.0	2601.	744.	402.	752.	90.0	88.0
4 way(0 deg.)	41	631.	1500.	0.5000	44.75	503.0	3202.	688.	442.	698.	104.0	112.0
4 way(0 deg.)	42	633.	1398.	0.5000	46.75	502.0	3429.	694.	484.	736.	118.0	122.0
4 way(0 deg.)	43	635.	1201.	0.5000	51.40	505.0	4015.	884.	742.	942.	212.0	178.0
4 way(0 deg.)	44	639.	970.	0.5000	57.57	504.0	4962.	732.	546.	772.	146.0	126.0
4 way(0 deg.)	45	641.	1600.	0.5000	46.75	198.0	1182.	724.	414.	694.	92.0	96.0
4 way(0 deg.)	46	643.	1702.	0.5000	45.08	200.0	1122.	738.	406.	724.	86.0	88.0
4 way(0 deg.)	47	645.	1802.	0.5000	43.90	201.0	1065.	746.	372.	756.	84.0	84.0
4 way(0 deg.)	48	647.	1852.	0.5000	43.46	196.0	1011.	742.	372.	788.	80.0	84.0
4 way(0 deg.)	49	649.	1497.	0.5000	43.40	199.0	1269.	682.	416.	750.	96.0	102.0
4 way(0 deg.)	50	651.	1398.	0.5000	45.08	199.0	1359.	674.	478.	742.	116.0	116.0
4 way(0 deg.)	51	653.	1201.	0.5000	49.08	201.0	1598.	856.	756.	958.	218.0	170.0
4 way(0 deg.)	52	655.	975.	0.5000	54.75	202.0	1978.	714.	522.	744.	140.0	122.0
4 way(0 deg.)	53	657.	1598.	0.5000	49.07	804.0	4804.	704.	426.	744.	98.0	106.0
4 way(0 deg.)	54	659.	1703.	0.5000	47.73	804.0	4508.	732.	394.	760.	86.0	96.0
4 way(0 deg.)	55	663.	1800.	0.5000	46.16	800.0	4244.	742.	378.	780.	82.0	88.0
4 way(0 deg.)	60	691.	1697.	0.2000	22.70	507.0	2853.	920.	428.	708.	92.0	100.0
4 way(0 deg.)	61	693.	1396.	0.2000	25.50	481.0	3290.	830.	412.	616.	96.0	124.0

TABLE 8-II. (CONTINUED)

DESCRIPTION	RUN NO.	O.N.E.R.A run no.	RPM	MACH NO.	THETA (at .75r/R) (deg.)	POWER (kW)	TORQUE (N-m)	IRP Gage 1F (N-m)	IRP Gage 3F (N-m)	IRP Gage 5F (N-m)	IRP Gage 3T microstrain	IRP Gage 7T microstrain
4 way(0 deg.)	62	695.	1400.	0.2500	32.40	491.0	3349.	776.	416.	636.	94.0	118.0
4 way(0 deg.)	63	697.	1701.	0.2500	28.75	499.0	2801.	808.	344.	704.	82.0	102.0
4 way(0 deg.)	64	699.	1700.	0.3000	28.60	504.0	2831.	786.	332.	700.	82.0	102.0
4 way(0 deg.)	65	701.	1403.	0.3000	32.90	481.0	3274.	660.	364.	692.	90.0	118.0
4 way(0 deg.)	66	703.	1700.	0.3500	32.80	502.0	2820.	774.	308.	736.	82.0	106.0
4 way(0 deg.)	67	705.	1401.	0.3500	36.30	502.0	3422.	682.	372.	684.	82.0	124.0
4 way(0 deg.)	68	707.	1700.	0.4000	36.26	494.0	2775.	812.	312.	742.	84.0	112.0
4 way(0 deg.)	69	709.	1401.	0.4000	39.10	497.0	3388.	676.	362.	726.	94.0	130.0
4 way(0 deg.)	70	711.	1704.	0.4500	39.08	503.0	2819.	782.	322.	790.	84.0	116.0
4 way(0 deg.)	71	713.	1400.	0.4500	41.90	505.0	3444.	666.	382.	732.	94.0	134.0
4 way(0 deg.)	72	715.	1699.	0.5000	42.00	496.0	2788.	796.	326.	750.	90.0	118.0
4 way(0 deg.)	73	717.	1402.	0.5000	44.65	506.0	3446.	730.	396.	782.	108.0	140.0
4 way(0 deg.)	74	719.	1500.	0.5000	44.63	804.0	5118.	732.	382.	742.	102.0	136.0
4 way(0 deg.)	75	721.	1400.	0.5000	45.60	798.0	5443.	732.	414.	756.	114.0	148.0
4 way(0 deg.)	76	723.	1208.	0.5000	50.50	796.0	6292.	860.	652.	982.	192.0	186.0
4 way(0 deg.)	77	725.	977.	0.5000	57.20	685.0	6695.	690.	444.	820.	112.0	152.0
4 way(0 deg.)	81	741.	1700.	0.5500	41.30	490.0	2752.	886.	358.	706.	110.0	120.0
4 way(0 deg.)	82	745.	1408.	0.5500	45.80	506.0	3432.	796.	462.	732.	124.0	148.0
4 way(0 deg.)	83	747.	1704.	0.5700	45.70	500.0	2802.	902.	360.	698.	114.0	116.0
4 way(0 deg.)	84		1404.	0.5700	46.70	500.0	3401.	796.	456.	818.	132.0	154.0
4 way(0 deg.)	85	752.	1700.	0.6000	46.90	505.0	2837.	972.	370.	802.	122.0	120.0
4 way(0 deg.)	86	754.	1400.	0.6000	47.85	499.0	3404.	888.	496.	852.	158.0	168.0
4 way(0 deg.)	87	757.	1700.	0.6500	47.75	502.0	2820.	950.	384.	858.	128.0	130.0
4 way(0 deg.)	88		1400.	0.6500	47.67	501.0	3417.	996.	566.	886.	182.0	184.0
4 way(0 deg.)	89	763.	1697.	0.7000	48.50	495.0	2785.	1002.	414.	868.		134.0
4 way(0 deg.)	90	765.	1400.	0.7000	50.60	508.0	3465.	1034.	610.	900.		200.0
4 way(0 deg.)	91	767.	1700.	0.7500	50.60	497.0	2792.	1058.	512.	896.		152.0
4 way(0 deg.)	92	769.	1695.	0.8000	50.10	499.0	2811.	1160.	538.	874.		168.0
4 way(0 deg.)	93	771.	1800.	0.8000	49.90	497.0	2637.	1050.	558.	794.		168.0
4 way(0 deg.)	94	773.	1600.	0.8000	50.00	502.0	2996.	1052.	572.	944.		174.0
4 way(0 deg.)	95	775.	1500.	0.8000	50.10	504.0	3208.	1072.	656.	958.		212.0
4 way(0 deg.)	96	777.	1395.	0.8000	51.10	500.0	3423.	1108.	714.	1086.		244.0
4 way(0 deg.)	97	779.	1195.	0.8000	54.60	501.0		1450.	1260.	1366.		390.0
4 way(0 deg.)	108	847.	1704.	0.8000	53.80	800.0	4483.	996.	554.	956.		168.0
4 way(0 deg.)	109	849.	1800.	0.8000	53.80	802.0	4255.	990.	860.	910.		152.0
4 way(0 deg.)	110	851.	1400.	0.8000	53.80	797.0	4757.	952.	868.	1008.		174.0
4 way(0 deg.)	111	853.	1500.	0.8000	55.30	797.0	5074.	1014.	1000.	1114.		216.0
4 way(0 deg.)	112	855.	1400.	0.8000	56.40	778.0	5307.	1052.	1038.	1202.		250.0
4 way(0 deg.)	113	857.	1305.	0.8000	58.10	741.0	5422.	1172.	1176.	1360.		292.0
4 way(0 deg.)	114	859.	1698.	0.8000	56.20	305.0	1714.	1136.	1424.	1142.		180.0
4 way(0 deg.)	115	861.	1800.	0.8000	55.40	306.0	1623.	1150.	1304.	1094.		166.0
4 way(0 deg.)	116	863.	1600.	0.8000	55.40	304.0	1814.	1042.	1008.	922.		174.0
4 way(0 deg.)	117		1500.	0.8000	55.40	301.0	1916.	986.	986.	862.		206.0
4 way(0 deg.)	118	869.	1405.	0.8000	55.70	290.0	1971.	1034.	1060.	950.		242.0
4 way(0 deg.)	119	871.	1300.	0.8000	57.20	278.0	2042.	1196.	1214.	1124.		312.0
STANDARD DEV.	**********	91.2	237.	0.2209	10.71	191.4	1366.	218.	241.	210.	31.1	58.4
MINIMUM VALUE	**********	547.0	970.	0.2000	19.75	196.0	1011.	660.	308.	568.	72.0	64.0
AVERAGE VALUE	**********	684.9	1513.	0.4655	41.73	500.2	3233.	921.	541.	848.	106.8	128.7
MAXIMUM VALUE	**********	871.0	1854.	0.8000	58.10	804.0	6695.	1592.	1424.	1552.	218.0	390.0

TABLE 8-III. OPERATING CONDITIONS FOR $M_N > .1$ AND SAMPLE IRP TABULATIONS (8 BLADE CONFIGURATION)

DESCRIPTION	RUN NO.	O.N.E.R.A run no.	RPM	MACH NO.	THETA (at .75r/R) (deg.)	POWER (kW)	TORQUE (N-m)	IRP Gage 2F (N-m)	IRP Gage 3F (N-m)	IRP Gage 4F (N-m)	IRP Gage 33 microstrain
8 way(0 deg.)	64	1439.	1698.	0.1900	21.90	817.0	4595.	416.0	486.0	902.0	66.0
8 way(0 deg.)	65	1443.	1602.	0.1900	23.20	801.0	4775.	480.0	540.0	912.0	70.0
8 way(0 deg.)	66	1445.	1503.	0.1900	25.30	800.0	5083.	464.0	538.0	890.0	78.0
8 way(0 deg.)	67	1447.	1796.	0.1900	22.10	804.0	4275.	434.0	506.0	936.0	68.0
8 way(0 deg.)	68	1449.	1847.	0.1900	21.70	800.0	4136.	474.0	538.0	982.0	74.0
8 way(0 deg.)	69	1460.	1711.	0.1900	20.50	397.0	2216.	436.0	500.0	920.0	68.0
8 way(0 deg.)	70	1463.	1603.	0.1900	20.80	392.0	2335.	474.0	532.0	980.0	78.0
8 way(0 deg.)	71	1465.	1503.	0.1900	22.10	387.0	2459.	536.0	616.0	912.0	90.0
8 way(0 deg.)	72	1467.	1401.	0.1900	25.10	386.0	2631.	628.0	688.0	880.0	102.0
8 way(0 deg.)	73	1469.	1803.	0.1900	19.80	392.0	2076.	442.0	530.0	884.0	68.0
8 way(0 deg.)	74	1471.	1859.	0.1900	19.50	393.0	2019.	446.0	526.0	916.0	68.0
8 way(0 deg.)	75	1475.	1698.	0.3000	27.50	437.0	2458.	406.0	454.0	764.0	52.0
8 way(0 deg.)	76		1697.	0.3500	31.10	452.0	2543.	386.0	442.0	708.0	48.0
8 way(0 deg.)	77	1481.	1704.	0.4000	34.40	467.0	2617.	368.0	442.0	730.0	48.0
8 way(0 deg.)	79		1696.	0.4500	37.50	493.0	2776.	374.0	462.0	738.0	56.0
8 way(0 deg.)	80	1483.	1700.	0.5000	40.90	651.0	3657.	390.0	484.0	730.0	58.0
8 way(0 deg.)	81	1485.	1802.	0.5000	40.90	672.0	3561.				
8 way(0 deg.)	82	1487.	1850.	0.5000	40.90	670.0	3458.				
8 way(0 deg.)	83	1493.	1600.	0.5000	42.90	640.0	3820.	376.0	470.0	710.0	56.0
8 way(0 deg.)	84	1495.	1507.	0.5000	44.60	628.0	3979.	374.0	492.0	726.0	62.0
8 way(0 deg.)	85	1497.	1400.	0.5000	46.70	603.0	4113.	404.0	538.0	794.0	62.0
8 way(0 deg.)	86	1499.	1698.	0.5000	43.70	799.0	4493.	390.0	464.0	700.0	48.0
8 way(0 deg.)	87	1501.	1801.	0.5000	43.00	824.0	4369.	394.0	502.0	770.0	50.0
8 way(0 deg.)	88	1503.	1853.	0.5000	42.50	832.0	4288.				
8 way(0 deg.)	89	1505.	1600.	0.5000	43.60	780.0	4655.	370.0	470.0	720.0	50.0
8 way(0 deg.)	90	1507.	1503.	0.5000	45.30	752.0	4778.	368.0	478.0	722.0	52.0
8 way(0 deg.)	91	1509.	1399.	0.5000	47.20	723.0	4935.	400.0	524.0	792.0	58.0
8 way(0 deg.)	92	1511.	1675.	0.5730	45.10	739.0	4213.	406.0	504.0	724.0	54.0
8 way(0 deg.)	93	1513.	1691.	0.5990	45.70	760.0	4292.	418.0	524.0	712.0	54.0
8 way(0 deg.)	94		1691.	0.6490	47.30	789.0	4455.	472.0	570.0	758.0	68.0
8 way(0 deg.)	95	1517.	1698.	0.7030	49.40	815.0	4583.	498.0	604.0	800.0	90.0
8 way(0 deg.)	96		1678.	0.7220	50.20	796.0	4530.	524.0	636.0	826.0	86.0
8 way(0 deg.)	97	1519.	1693.	0.7200	50.70	796.0	4490.	518.0	642.0	812.0	94.0
8 way(0 deg.)	98	1521.	1591.	0.7200	51.70	739.0	4435.	566.0	662.0	880.0	88.0
8 way(0 deg.)	99	1523.	1498.	0.7300	53.10	719.0	4583.	618.0	722.0	904.0	110.0
8 way(0 deg.)	100	1525.	1437.	0.7300	54.10	731.0	4858.	624.0	732.0	882.0	110.0
8 way(0 deg.)	101	1527.	1803.	0.7300	52.60	781.0	4136.				
8 way(0 deg.)	102	1529.	1855.	0.7300	52.30	790.0	4067.				
STANDARD DEV.	**********	27.	136.	0.1975	11.66	157.6	924.	75.6	78.6	88.4	17.9
MINIMUM VALUE	**********	1439.	1399.	0.1900	19.50	386.0	2019.	368.0	442.0	700.0	48.0
AVERAGE VALUE	**********	1489.	1662.	0.4525	38.08	664.4	3835.	450.7	539.9	818.7	69.2
MAXIMUM VALUE	**********	1529.	1859.	0.7300	54.10	832.0	5083.	628.0	732.0	982.0	110.0

TABLE 8-IV. MEASURED VIBRATORY PEAKS VS. LIMITS

Gage Description	Peak IRP Strain observed for 8-way (0° inflow) fraction of limit	Peak IRP Strain observed for 4-way (0° inflow) fraction of limit	Peak IRP Strain observed for 2- way (0° inflow) fraction of limit	Peak IRP Stain observed for 2- way (3° inflow) fraction of limit
Radial Bending (44%r/R) Gage 1		.43	.33	.79
Radial Bending (71%r/R) Gage 2		1.12*	.48	1.05*
Radial Bending (84%r/R) Gage 3	.22	.45	.46	.88
Trailing Edge Bending Gage 4		.55	.6	1.01*
Shear (71%r/R) Gage 5	.04	.07	.05	.11
Shear (84%r/R) Gage 6	.05	.07	.08	.12
Chordwise (71%r/R) Gage 7	.22	.21	.16	.26
Chordwise (84%r/R) Gage 8	.36	.23	.20	.33
Radial Bending (34%r/R) Gage 9		.41	.30	.72
Shear (44%r/R) Gage 10				
Chordwise (44%r/R) Gage 11	.24			
Radial Bending (57%r/R) Gage 12	.26	.45	.49	1.11*
Radial Bending (78%r/R) Gage 13	.29	.29	.52	1.03*
Flatwise Shank Moment - Gage F	.29	.47	.28	.76
Edgewise Shank Moment - Gage E	.19	.22	.17	.27

* It is felt that because of the noise present, these values can be interpreted as within limits.

Notes: 1. The gage limits were set based on the strains reaching a threshold at which blade fatigue damage begins to accumulate (vibratory strain superimposed upon steady strain).

2. Because of the amount of noise in the strain signals, the IRP values listed here should be interpreted as conservative upper bounds on the strains actually felt by the blades.

8.3.2.1 Angular Inflow

As previously noted in section 2.0 and paragraph 8.3.2.1, the only angular inflow data obtained was for the two bladed configuration at 3° inflow angle. A spectral analysis of each strain gage signal was performed using an FFT (Fast Fourier Transform) algorithm. This analysis employed a Hanning window to help overcome leakage effects. Correlations were then made with the predictions of 1P response.

Table 8-V shows the P-order content obtained for the 3 degree conditions tested (shank moment and radial bending). It can be seen that the 2P component averaged about 25% of the 1P component (with 2P/1P approximately .54 near 1500 RPM) and that the 3P component was generally much smaller. It is noted that at least a portion of the excitation force driving the 2P response may have come from the test rig drive system. Twice per revolution vibration is characteristic of a shaft with universal joints. It is also likely that nonlinearities in the aerodynamic excitation, possibly due to observed vortex loading phenomena, or tunnel flow irregularities in the test section, are causes of higher order excitation. The aerodynamic analyses used for the predictions do not consider this effect.

The data digitized for the spectral analysis was sampled at constant time steps. Even small variations in RPM are known to result in substantially lowered P-order magnitudes. By synchronously sampling the data (digitizing at constant fractions of a cycle instead of constant time step) this problem can be overcome. This is known as a 'speed corrected' spectral analysis. However, since the RPM trace was not available for this test, this was not possible here. An alternative procedure was used for several strain gage results to double check the amplitudes obtained from the non 'speed corrected' spectral analysis. A calculation was made of the average amplitude of a band pass filtered (1P frequency mid band) strain record. This procedure is cumbersome but should produce conservative strains because the amplitudes are those generated by a peak stress converter (with a finite reset rate). Table 8-VI shows that the band pass filtered values are typically 10% higher than the spectral values. Even with no RPM variation, the spectral magnitudes are known to be up to 16% low, due to the effect known as leakage (with a Hanning window as employed here) in digital signal processing terminology. It is concluded that the actual magnitudes are within 10% (higher) of the spectral values.

Figures 8-13 and 8-14 show the trends of 1P response (shank moment and blade bending) with respect to power, RPM and Mach number for the 2 bladed configuration at 3° inflow angle. As expected, the response increased with power and Mach number. Variations of RPM are influenced by system resonances. Figure 8-15 shows the variation of bending strain with spanwise location. Again, the trends are believable and consistent with the data collected during the four and eight blade structural testing.

TABLE 8-V. P-ORDER CONTENT OF STRAIN GAGE OUTPUT AT 3° INFLOW ANGLE (2 BLADE CONFIGURATION)

DESCRIPTION	O.N.E.R.A. RUN NO.	POWER (kW)	RPM	MACH NO.	1P FLATWISE SHANK MOMENT GAGE 3F N-m	2P FLATWISE SHANK MOMENT GAGE 3F N-m	3P FLATWISE SHANK MOMENT GAGE 3F N-m	1P SPANWISE STRAIN(44%r) GAGE 31 microstrain	2P SPANWISE STRAIN(44%r) GAGE 31 microstrain	3P SPANWISE STRAIN(44%r) GAGE 31 microstrain
2 way(3.deg.)	1162	492.0	1500.	0.5000	854.	389.2	0.0	206.0	132.0	0.0000E+00
2 way(3.deg.)	1164	501.0	1606.	0.5000	778.	244.0	0.0	182.0	80.0	0.0000E+00
2 way(3.deg.)	1166	505.0	1703.	0.5000	813.	98.8	0.0	182.0	30.0	0.0000E+00
2 way(3.deg.)	1168	507.0	1798.	0.5000	851.	156.8	0.0	186.0	54.0	0.0000E+00
2 way(3.deg.)	1170	499.0	1858.	0.5000	799.	116.2	0.0	172.0	38.0	0.0000E+00
2 way(3.deg.)	1172	817.0	1850.	0.5010	912.	95.8	0.0	200.0	28.0	0.0000E+00
2 way(3.deg.)	1174	811.0	1805.	0.5000	979.	133.6	0.0	218.0	40.0	0.0000E+00
2 way(3.deg.)	1176	794.0	1673.	0.5000	897.	171.4	0.0	204.0	56.0	0.0000E+00
2 way(3.deg.)	1178	806.0	1600.	0.5000	929.	296.2	0.0	220.0	100.0	0.0000E+00
2 way(3.deg.)	1180	782.0	1500.	0.5000	981.	357.2	0.0	242.0	128.0	0.0000E+00
2 way(3.deg.)	1182	768.0	1450.	0.5000	947.	296.2	0.0	236.0	106.0	0.0000E+00
2 way(3.deg.)	1184	248.0	1392.	0.5000	732.	223.6	0.0	176.0	80.0	0.0000E+00
2 way(3.deg.)	1186	249.0	1500.	0.5010	758.	278.8	0.0	180.0	96.0	0.0000E+00
2 way(3.deg.)	1188	247.0	1600.	0.5000	729.	154.0	0.0	164.0	50.0	0.0000E+00
2 way(3.deg.)	1190	244.0	1698.	0.5000	714.	142.2	0.0	158.0	48.0	0.0000E+00
2 way(3.deg.)	1192	240.0	1801.	0.4990	790.	124.8	0.0	168.0	40.0	0.0000E+00
2 way(3.deg.)	1194	237.0	1855.	0.4990	761.	107.4	0.0	160.0	34.0	0.0000E+00
2 way(3.deg.)	1198	608.0	1598.	0.7800	1885.	490.8	92.9	442.0	176.0	0.0000E+00
2 way(3.deg.)	1200	559.0	1600.	0.7490	1707.	702.8	0.0	398.0	246.0	0.0000E+00
2 way(3.deg.)	1202	546.0	1499.	0.7490	1890.	755.0	0.0	460.0	274.0	0.0000E+00
2 way(3.deg.)	1204	568.0	1704.	0.7490	1757.	325.2	113.2	396.0	110.0	0.0000E+00
2 way(3.deg.)	1206	580.0	1800.	0.7520	1870.	217.8	124.9	406.0	74.0	0.0000E+00
2 way(3.deg.)	1208	582.0	1840.	0.7500	1681.	232.4	130.7	360.0	78.0	0.0000E+00
2 way(3.deg.)	1210	802.0	1602.	0.7240	1699.	688.2	0.0	402.0	242.0	0.0000E+00
2 way(3.deg.)	1212	784.0	1534.	0.7230	1632.	882.8	0.0	396.0	318.0	0.0000E+00
2 way(3.deg.)	1214	828.0	1707.	0.7240	1734.	383.4	0.0	396.0	134.0	0.0000E+00
2 way(3.deg.)	1216	849.0	1798.	0.7240	1832.	226.4	151.0	406.0	76.0	0.0000E+00
2 way(3.deg.)	1218	858.0	1855.	0.7240	1710.	180.0	98.7	370.0	60.0	0.0000E+00
2 way(3.deg.)	1222	868.0	1815.	0.7600	1954.	325.2	122.0	428.0	110.0	0.0000E+00
2 way(3.deg.)	1230	221.0	945.	0.5000	659.	101.6	0.0	178.0	40.0	0.0000E+00
2 way(3.deg.)	1234	534.0	955.	0.5010	862.	0.0	0.0	244.0	0.0	0.0000E+00
2 way(3.deg.)	1236	609.0	953.	0.5010	880.	0.0	0.0	248.0	0.0	0.0000E+00
2 way(3.deg.)	1240	605.0	902.	0.7200	1617.	113.2	0.0	456.0	54.0	0.0000E+00
STANDARD DEV.	**********	214.0	273.	0.1181	467.	211.9	49.4	107.9	76.3	0.0000E+00
MINIMUM VALUE	**********	221.0	902.	0.4990	659.	0.0	0.0	158.0	0.0	0.0000E+00
AVERAGE VALUE	**********	580.3	1585.	0.5948	1200.	273.1	25.3	280.0	94.9	0.0000E+00
MAXIMUM VALUE	**********	868.0	1858.	0.7800	1954.	882.8	151.0	460.0	318.0	0.0000E+00

C-2

TABLE 8-VI COMPARISON OF 1P CONTENT OF STRAIN GAGE OUTPUT OBTAINED BY TWO METHODS

	RUN#1176 Using Band Pass Filter (1)	RUN#1176 From Spectral Analysis (2)	RUN#1176 Ratio (1)/(2)	RUN#1190 Using Band Pass Filter (3)	RUN#1190 From Spectral Analysis (4)	RUN#1190 Ratio (3)/(4)	RUN#1214 Using Band Pass Filter (5)	RUN#1214 From Spectral Analysis (6)	RUN#1214 Ratio (5)/(6)
Gage 3F (N-m)	496.0	449.0	1.11	397.0	357.0	1.11	929.0	867.0	1.07
Gage 31(microstrain)	113.0	102.0	1.11	85.0	79.0	1.08	211.0	198.0	1.07
Gage 71(microstrain)	110.0	100.0	1.10	85.0	76.0	1.12	208.0	194.0	1.07
Gage 72(microstrain)	76.0	70.0	1.09	50.0	47.0	1.06	116.0	110.0	1.06
Gage 73(microstrain)	65.0	59.0	1.10	37.0	33.0	1.12	92.0	87.0	1.06

- Method 1-Spectral Analysis-values obtained via an FFT routine employing a Hanning window(not speed corrected)
- Method 2-Band Pass Filter-values obtained from the data sample average of the output from a peak stress converter after filtering the signal with a 1P band pass filter
- Conclusion -actual amplitudes within 10%(higher) of the spectral values

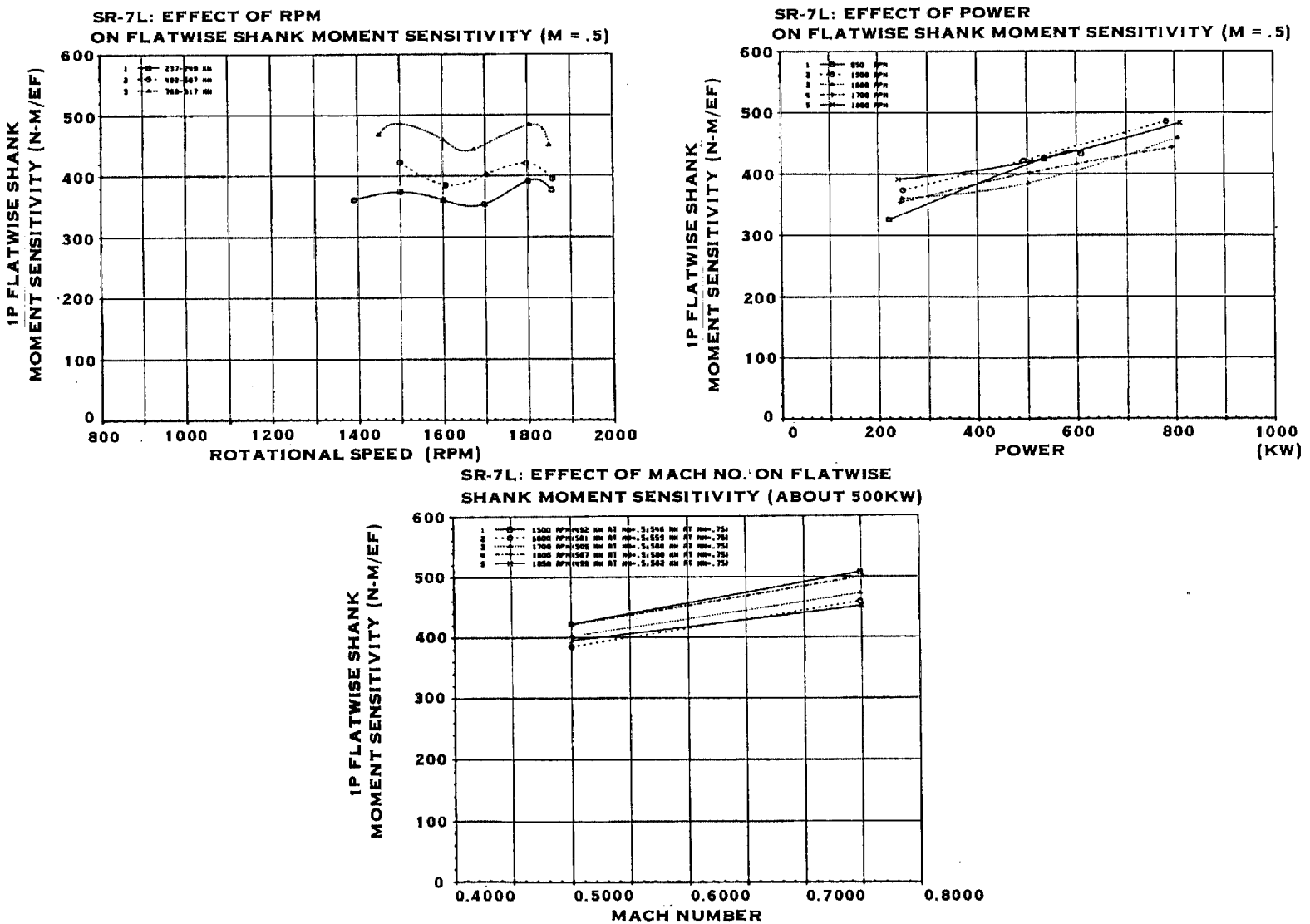

FIGURE 8-13. TRENDS OF 1P RESPONSE, 2 BLADES, 3° ANGULAR INFLOW (SHANK MOMENT)

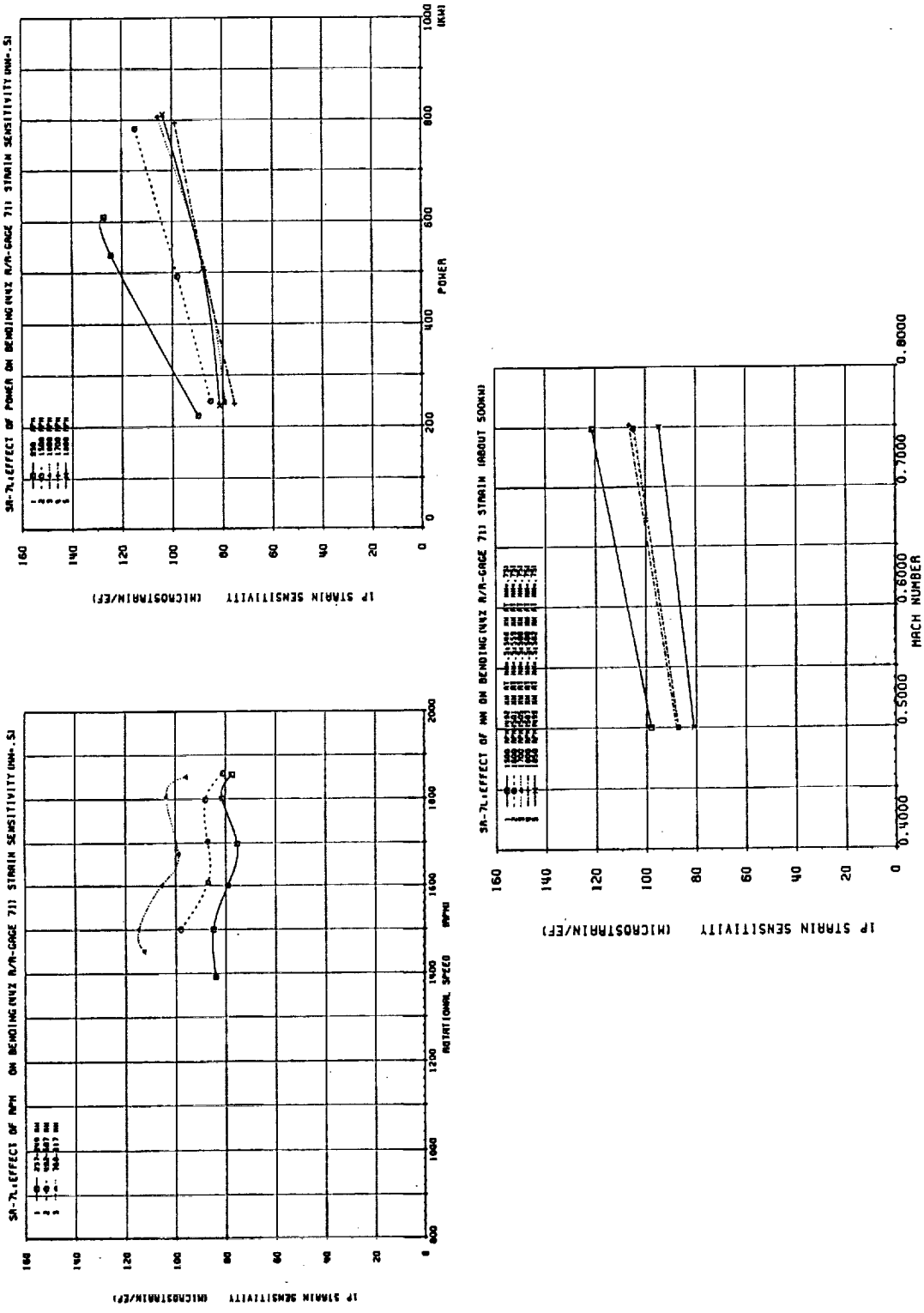

FIGURE 8-14. TRENDS OF 1P RESPONSE, 2 BLADES, 3° ANGULAR INFLOW (RADIAL BENDING)

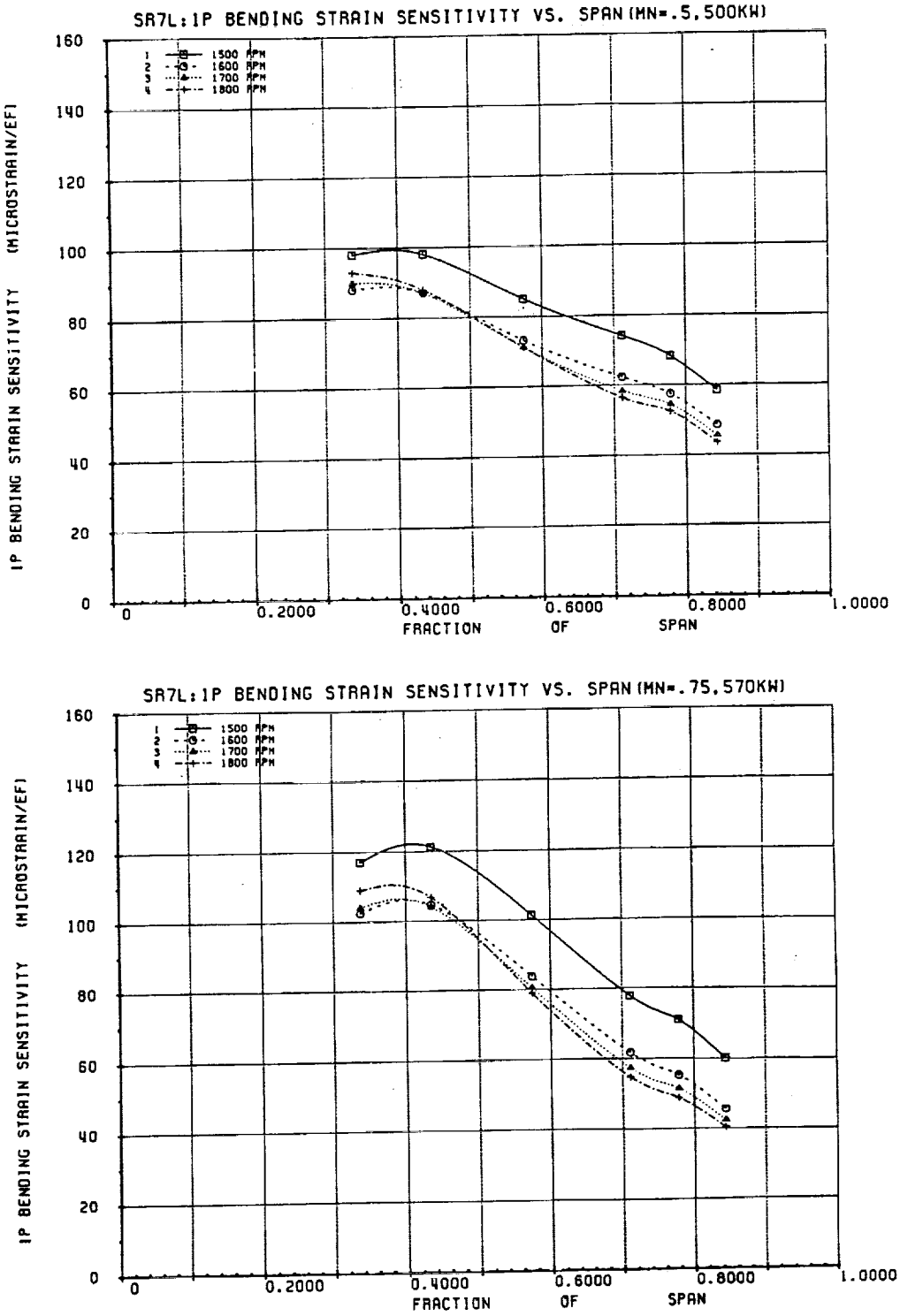

FIGURE 8-15. RADIAL BENDING VS SPAN, 2 BLADES, 3° ANGULAR INFLOW

8.3.2.1 (Continued)

The plotted values were normalized with respect to E.F. (excitation factor) which is defined as:

$$E.F. = \psi\ (V_T/644.8)^2(\rho/\rho_o)$$

Where ψ is the inflow angle in degrees, V_T the true airspeed in Km/HR, ρ the air density, and ρ_o the air density at standard sea level conditions.

Only the 1P component of the response has been plotted to investigate trends. The IRP values include the higher order content as well as unfiltered noise.

8.3.2.2 Analytical Method

A finite element model of the SR-7L blade was developed during the design phase. The same model was used here to predict 1P response for correlation with test. The steady state aerodynamic loads were calculated using the HS computer code H444. The steady air loads along with centrifugal loads, were applied to the model which was analyzed using the in-house finite element code, BESTRAN (Reference 23). From this solution the differential stiffness matrix was obtained and added to the structural stiffness matrix. The differential stiffness matrix represents the additional stiffness of the blade under centrifugal loading. The unsteady (1P) airloads were then calculated using the HS computer code H337. The loads were applied to the finite element model and displacements and surface strains predicted.

Mohr's circle relationships were employed to calculate strains in the direction of the gages for correlation with test. Shank moments were calculated using the reaction loads at the root of the blade and assuming a linear variation of moment up to the shank location.

The H444 and H337 codes are both aerodynamic 'strip' analyses that have been calibrated to predict the steady and unsteady airloads on swept Prop-Fan blades. The H444 code employs a Goldstein formulation to calculate induced velocities, whereas the H337 code uses a skewed wake theory. Two-dimensional, compressible airfoil data was used by both codes to predict the aerodynamic loads. Triangular plate elements were used in the BESTRAN code to do the finite element analysis. Each component of the composite blade (i.e., shells, spar, foam, sheath) were represented by separate plate elements. They were all tied together using constraints based on plane-sections remaining plane. Further detail on the codes and their use can be found in the LAP Blade Design Report (Reference 14).

Figure 8-16 illustrates a Campbell diagram of the SR-7L blade. Shown are BESTRAN frequencies compared with test values. It is assumed that the RPM range tested was far enough away from 1P resonance that the influence of damping on strain magnitudes can be neglected.

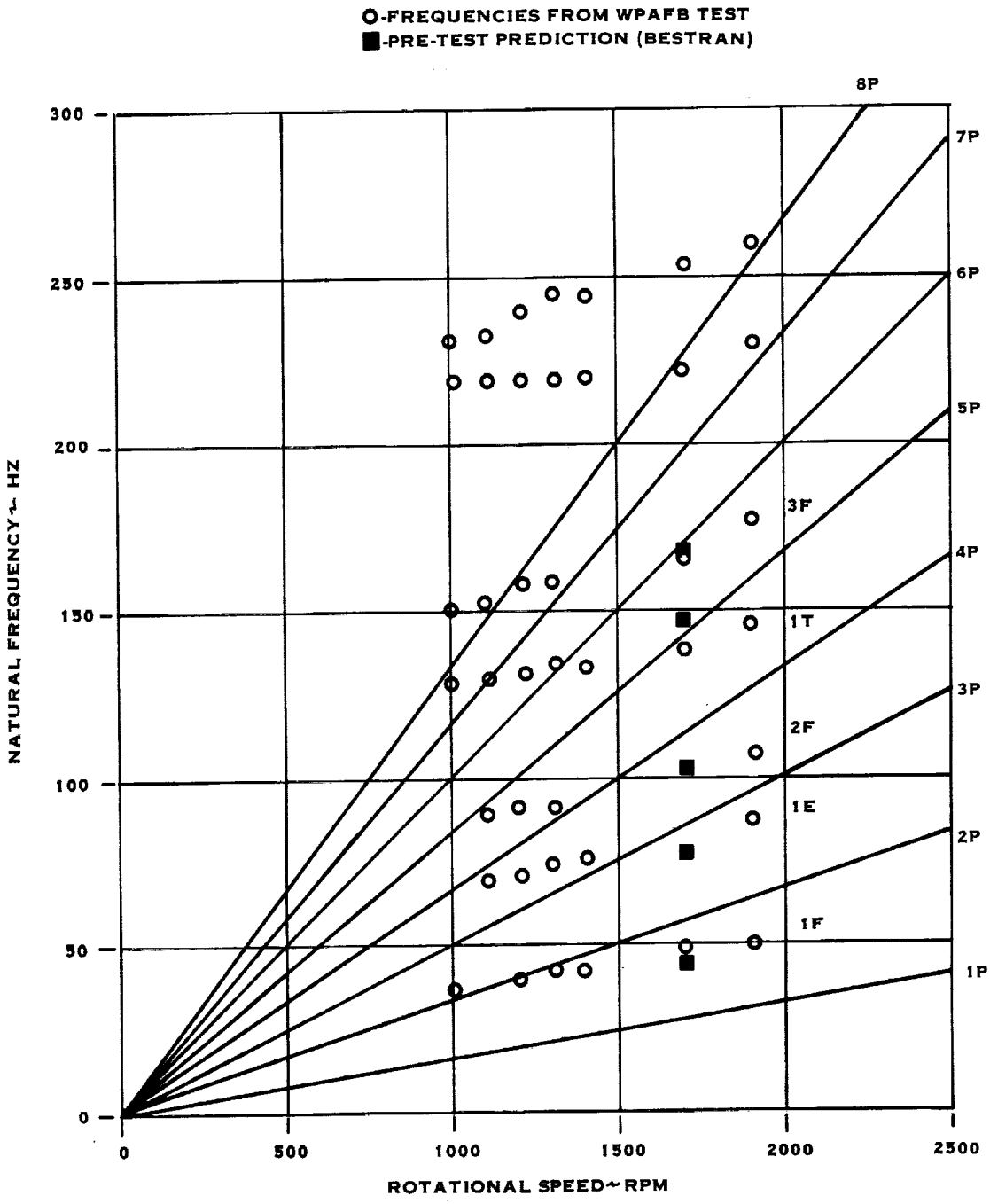

FIGURE 8-16 COMPARISON OF SR-7L NATURAL FREQUENCY TEST RESULTS TO PREDICTIONS

8.3.2.3 Test vs. Analysis

Three cases were chosen to analyze and compare to test. The conditions were picked to study the influence of power and Mach number variations on the predicted strains. Case 1 (run #1176) was at 1673 RPM, 794 KW, .5 M_N. Case 2 (run #1190) was at 1698 RPM, 244 KW, .5 M_N. Case 3 (run #1214) was at 1707 RPM, 829 KW, .724 M_N.

The IP gage strains were calculated using the methods outlined in the previous section. Comparisons were then made to the values obtained from a spectral analysis of the test data. See Figures 8-6, 8-7 and 8-8 for gage locations. Figure 8-17 shows the variation of radial bending strain as a function of spanwise location. As can be seen the correlation is quite reasonable with the in-board predicted strains being about 30% too high. However, as previously noted in paragraph 8.3.2.1, the 'measured' strain levels are felt to be up to 10% low.

Figure 8-18 shows the correlation of shank moments and root radial bending (gages F and 1) as a function of power, (holding RPM and Mach number). Both the test and analysis show the expected trend of increased 1P response with increased power. The test values are consistently below those calculated. Figure 8-19 shows the same quantities plotted against Mach number (holding RPM and power). The trends are consistent with expectations (higher response with increased Mach number). Table 8-VII shows a comparison of all the strain gage results for the three conditions. As noted from the plots, the correlation with radial bending strains and shank moments is quite reasonable. However, the correlation is rather poor with the gage placed near the trailing edge, and also with the chordwise and shear gages. This is consistent with previous experience. It is felt that these values are affected more by local distributions of aerodynamic loads, whereas the radial gages are strained by an integration of loads outboard of a given gage. Further study is needed to better define the local load distributions in order to more closely correlate with the measured strains.

8.3.2.4 Blade Flutter

Prior to the high speed wind tunnel test, an unstalled flutter analysis was conducted for the two, four and eight bladed Prop-Fan configurations. The analysis indicated that the Prop-Fan would be free from unstalled flutter throughout the wind tunnel test operating envelope. The tests confirmed the predictions in that no flutter or tendency to flutter was measured or observed. The wind tunnel test results were also a good indicator that no unstalled flutter would occur during the subsequent flight test program. Though the maximum Mach number achieved for the eight bladed configuration was limited to .73, the resulting dynamic pressure at the tunnel's effective pressure altitude of 4,360 meters (14,000 ft.) is greater than the maximum dynamic pressure expected for the flight test.

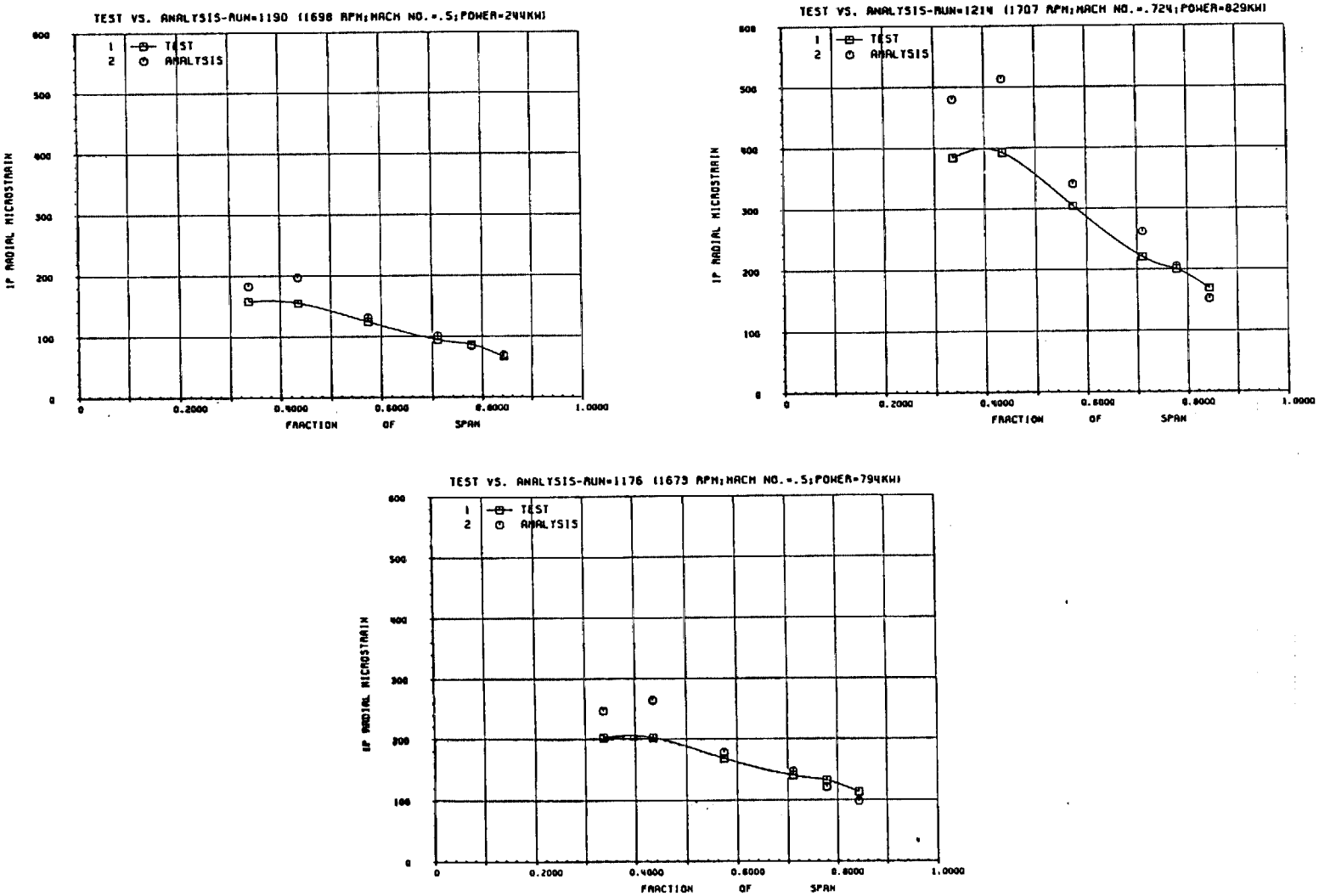

FIGURE 8-17. TEST VS ANALYSIS (RADIAL BENDING VS SPAN)

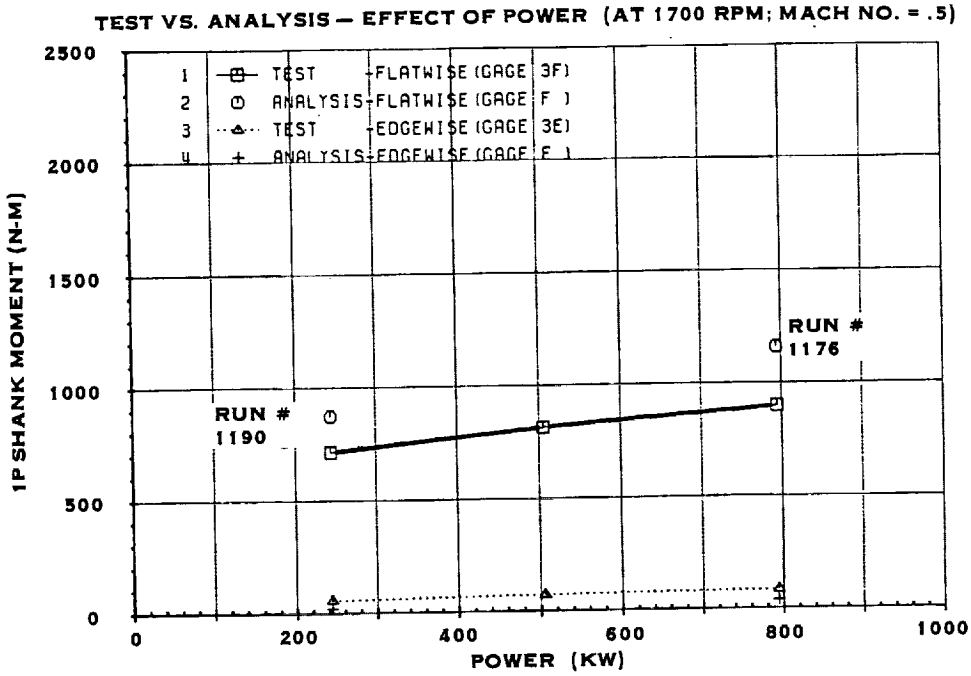

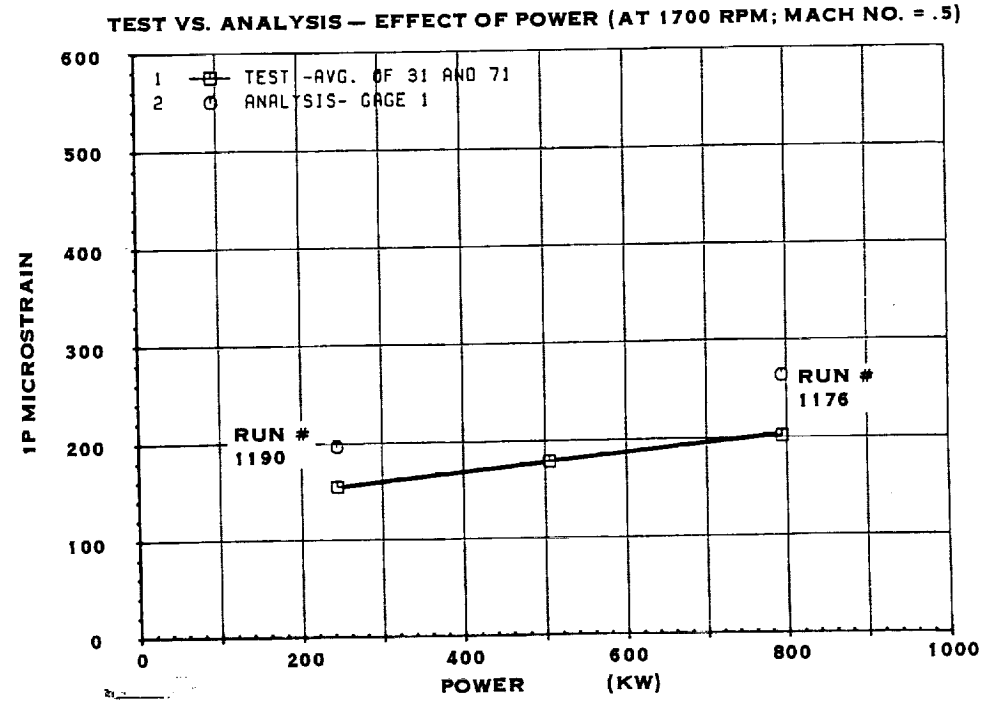

FIGURE 8-18. TEST VS. ANALYSIS (EFFECT OF POWER)

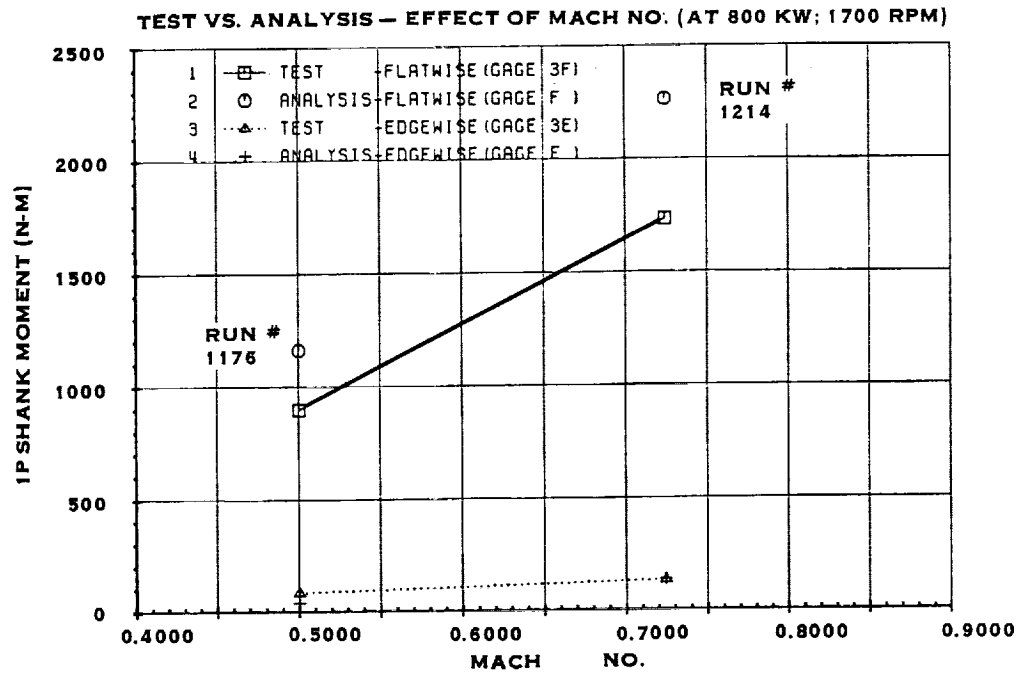

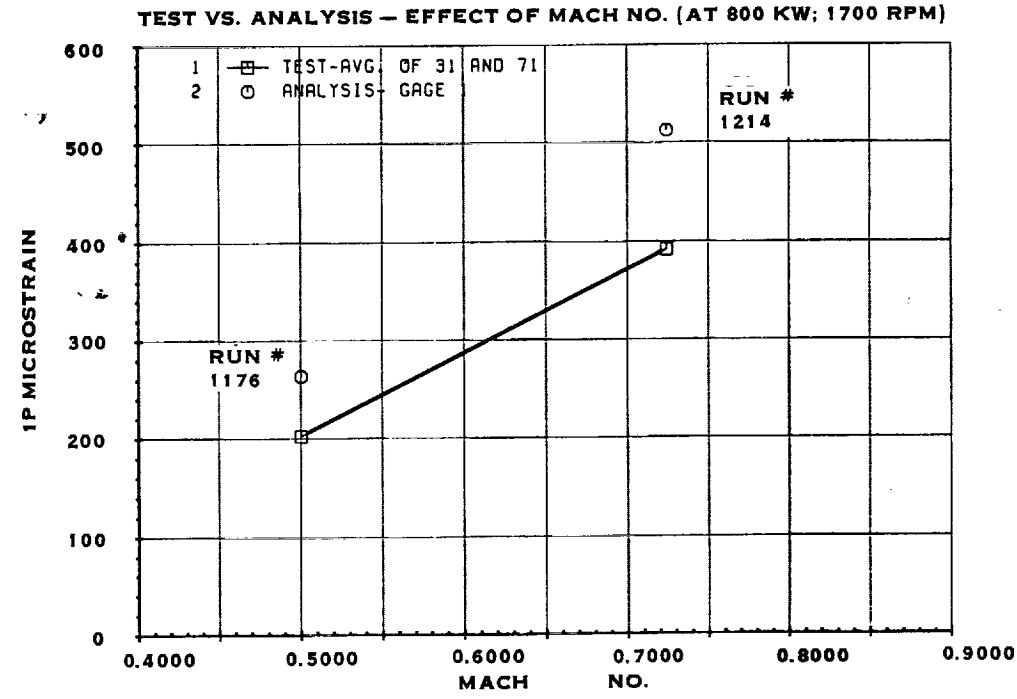

FIGURE 8-19. TEST VS. ANALYSIS (EFFECT OF MACH NO.)

Gage Description	RUN#1176 Analysis from BESTRAN (1)	RUN#1176 Test -from Spectral Analysis (2)	RUN#1176 Ratio (1)/(2)	RUN#1190 Analysis from BESTRAN (3)	RUN#1190 Test-from Spectral Analysis (4)	RUN#1190 Ratio (3)/(4)	RUN#1214 Analysis from BESTRAN (5)	RUN#1214 Test-from Spectral Analysis (6)	RUN#1214 Ratio (5)/(6)	
Flatwise Shank Moment Gage F - (N-m)	1160.	897.0	1.29	874.0	714.0	1.224	2265.	1734.	1.31	REASONABLE CORRELATION
Radial Bending-34%r/R Gage 9 - microstrain	246.	202.0	1.22	183.0	158.0	1.158	480.	384.	1.25	
Radial Bending - 44%r/R Gage 1 microstrain	264.	202.0	1.31	197.0	155.0	1.271	513.	392.	1.31	
Radial Bending - 57%r/R Gage 12 - microstrain	178.	168.0	1.06	131.0	124.0	1.056	340.	304.	1.12	
Radial Bending - 71%r/R Gage 2 - microstrain	147.	140.0	1.05	101.0	94.0	1.074	262.	220.	1.19	
Radial Bending - 78%r/R Gage 13 - microstrain	121	132.0	0.92	84.0	86.0	0.977	205.	200.	1.03	
Radial Bending - 84%r/R Gage 3 - microstrain	98.	113.0	0.87	69.0	66.0	1.045	152.	169.	0.90	
Edgewise Shank Moment Gage E - (N-m)	37.	83.0	0.45	19.0	56.0	0.339	135.	132.	1.02	POOR CORRELATION
Trailing Edge Bending Gage 4 - microstrain	44.	64.0	0.69	1.0	38.0	0.026	76.	184.	0.41	
Shear - 71%r/R Gage 5V-microstrain	117.	20.0	5.85	66.0	16.0	4.125	209.	24.	8.71	
Shear - 84%r/R Gage 6V-microstrain	169.	28.0	6.04	89.0	20.0	4.450	282.	24.	11.75	
Chordwise - 84%r/R Gage 8C - microstrain	44.	22.0	2.00	25.0	0.0		71.	16.	4.44	

Notes: 1. See figures 8-17, 8-18 and 8-19 for plots of the radial bending and flatwise shank results.
2. Test Values from Spectral Analysis (see Figure 8-12). Analysis from H337 (aerodynamic) and Bestran (structural).

TABLE 8-VII. COMPARISON OF TEST VS. ANALYSIS (1P)

8.3.2.4 (Continued)

The maximum Mach numbers achieved for the two and four bladed Prop-Fan configurations were .80 and .84, respectively. Though these configurations did not permit the effects of blade cascade to be evaluated, they did demonstrate the Prop-Fan's resistance to unstalled flutter onset for subsequent blade surface pressure testing.

8.3.2.5 Whirl Flutter

Due to the flexibility of the ONERA test rig, whirl flutter was a concern for this test. These concerns were reinforced when initial calculations of the installations' stability showed whirl flutter to occur within the operating envelope. For the initial computations, the forward support structure, shown in view A of Figure 8-1 and views A and B in Figure 8-2, had a three rod configuration that resulted in undesireable symetrical pitch and yaw stiffness. To stabilize the two and four bladed configurations, a two rod support structure, as depicted in view A of Figure 8-1, was utilized. The two rod configuration, which provided asymetrical pitch and yaw stiffness, resulted in a more stabilized system. The computations also demonstrated the need to add cables, as shown in view A of Figure 8-2, for the eight bladed configuration to increase structural damping while improving the distribution of the pitch and yaw stiffness. The end result of these rig modifications was successful completion of the wind tunnel test with no whirl flutter instabilities encountered.

9.0 AERODYNAMIC PERFORMANCE EVALUATION

9.1 Test Objective

To measure the aerodynamic performance of the SR-7L Prop-Fan for a range of blade angles, rotational speeds and Mach numbers.

9.2 Test Procedure

Aerodynamic performance data (thrust and power) was measured concurrently with the structural dynamic data. As a result, the data includes losses in performance resulting from the presence of the strain gages and strain gage wires on the aerodynamic surfaces of the blade. Installation of the gages was accomplished so as to minimize these losses.

Power available from the two turbine engines driving the Prop-Fan in the wind tunnel was significantly lower than the rated power of the Prop-Fan. Therefore, testing was conducted using two and four blade configurations as well as eight blades. The two and four blade configurations permitted operation at power loadings per blade that correspond to high and intermediate power operating points respectively for the eight blade Prop-Fan design. The disadvantage to this approach is that the eight blade performance cannot be easily extrapolated from the two or four blade test results. This is due to the aerodynamic interaction between the blades. This interaction is more significant for the eight blade design than for the two or four blade configurations, due to the reduced spacing between blades. Unfortunately the aerodynamic performance data for the 2 blade configuration was limited, and rather than attempt to project the full power eight blade performance from the the two and four blade test results, the available results are compared to analytical predictions. This serves to verify the analytical techniques and provides confidence that the predictions for the eight blade high power performance may also be correct.

The missing blades were replaced with stubs (see Figure 7-9) in the two and four blade configurations. The ends of the stubs were machined to match the external contour of the spinner.

The Prop-Fan was operated in the Beta Control mode during the aerodynamic performance testing. In this mode, Hamilton Standard personnel were able to change the blade pitch angle during testing by means of an increase/decrease pitch switch located in the control room. For a fixed Mach number and a constant power supplied by the turbines, the Prop-Fan rotational speed was varied by increasing or decreasing blade pitch angle. At the Mach numbers of interest, aerodynamic performance data was collected for two or three different power settings and over a range of rotational speeds. Approximately 140 performance data points were collected.

9.3 Discussion and Results

9.3.1 Data Reduction Procedure

The blade pitch angle (β3/4) was measured and recorded for each test point. An electrical signal proportional to blade angle was provided by means of a potentiometer mounted on the rotating side of the Prop-Fan. The potentiometer shaft was positioned by the rotation of the No. 7 blade retaining ring through a cable and pulley arrangement (Figure 5-3). Figure 9-1 demonstrates the linearity of the output of the blade angle measurement potentiometer as monitored during a pre-test calibration check.

The Prop-Fan rotational speed was measured by use of a 1P pickup. The sensor was triggered by a gear mounted on the test rig drive shaft. The rotational speed was averaged over ten revolutions.

The power absorbed by the Prop-Fan (BHP) was determined by multiplying the torque supplied to the Prop-Fan (Q_{COR}) by the rotational speed (N). Torque supplied to the Prop-Fan (Q_{COR}) was computed by subtracting the measured frictional losses in the balance (Q_{FL}) from the torque measured by the torquemeter (Q_{MEAS}).

$$BHP = N \times Q_{COR}$$

Where: $Q_{COR} = Q_{MEAS} - Q_{FL}$

The net trust (Q_{NET}) determined during testing is the uninstalled thrust of the Prop-Fan rotor, operating in the presence of a spinner and centerbody and is computed from the following equation:

$$Q_{NET} = F_B + F_{TH} - F_{BP} + D_S - BF$$

Where:

F_B = axial force measured by the balance
F_{TH} = losses due to thermal effects
F_{BP} = back pressure force
D_S = spinner drag
BF = buoyancy force

The temperature correction term (F_{TH}) compensates for the effects of changes in temperature on the balance strain gages.

The back pressure term (F_{BP}) corrects for the increase in measured thrust due to the differential between the pressure behind the spinner bulkhead and the free stream pressure. The back pressure force is calculated by multiplying the difference between the average pressure measured by the taps shown in Figure 7-10 and the free steam pressure by the projected area of the spinner bulkhead.

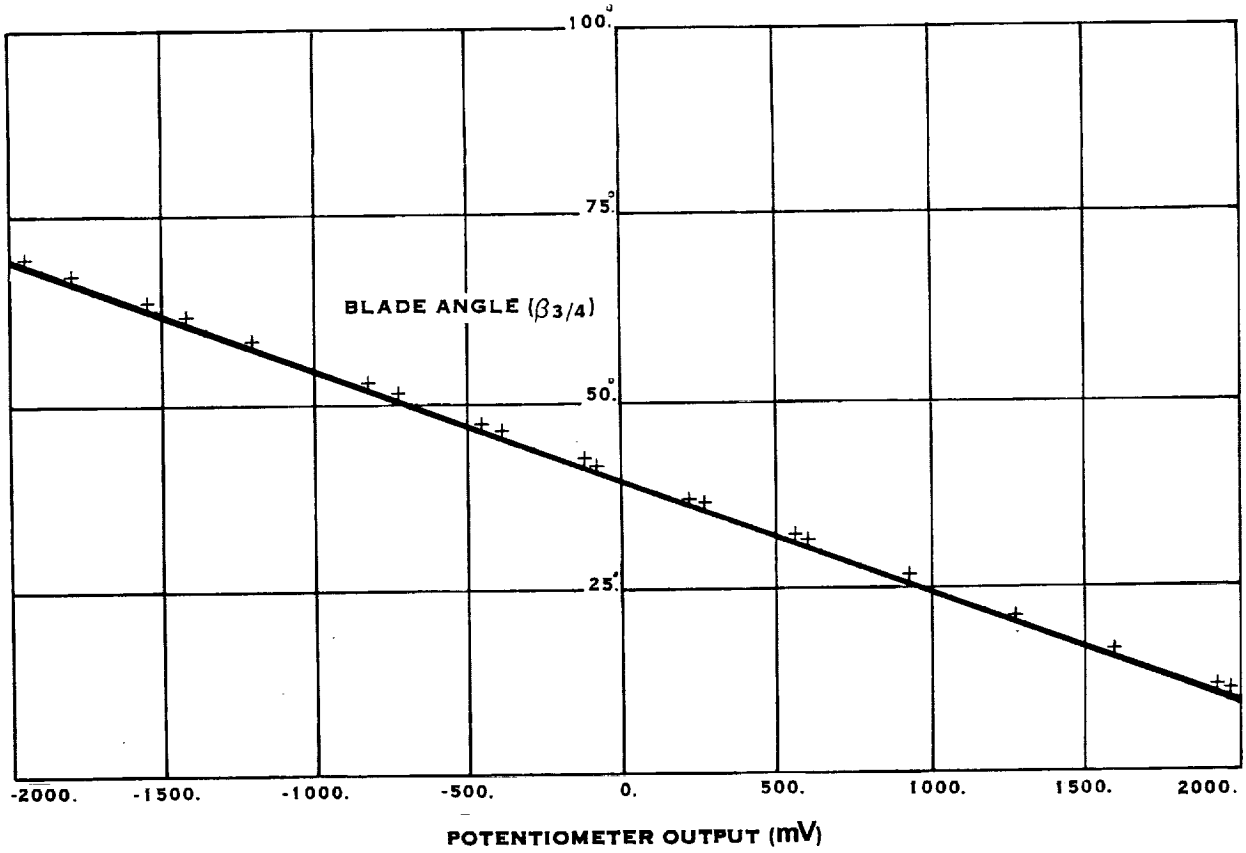

FIGURE 9-1. LAP BLADE ANGLE POTENTIOMETER OUTPUT

9.3.1 (Continued)

The spinner drag force (D_s) is computed by multiplying the spinner drag coefficient by the free stream dynamic pressure and the reference area of the spinner, as defined in paragraph 7.3.3.1. The spinner drag coefficient was determined as a function of Mach number during the spinner drag test (Figure 7-14).

The buoyancy force term (BF) eliminates the apparent increase in thrust caused by the interaction between the Prop-Fan rotor and the centerbody. The buoyancy force is determined by measuring the centerbody drag at the performance test point of interest and subtracting the centerbody drag without blades for the same Mach number. The centerbody drag was determined during performance testing by integrating the difference between the pressures measured by the taps shown in Figure 7-10 and the free stream static pressure over the surface of the centerbody. (See paragraph 7.3.3.2). The centerbody drag without blades was computed by multiplying the centerbody drag coefficient by the free stream dynamic pressure and the centerbody reference area. The centerbody drag coefficient was determined as a function of Mach number during the spinner drag test as depicted in Figure 7-15.

Mach number was established from the ratio of static pressure (measured four meters upstream of the Prop-Fan rotor) to stagnation pressure. Static pressure was also measured in the plane of rotation as a backup. The ratio of static-to-stagnation pressure was correlated with data taken during a pre-test calibration in order to compute the Mach number (see Paragraph 7.2). The Prandlt-Young correction was applied to the computed Mach number to compensate for the effects of the tunnel walls and the thrust produced by the Prop-Fan.

9.3.2 Data Presentation

The most complete aerodynamic performance data was acquired for the four blade Prop-Fan configuration. Operational problems encountered with the test rig, while running the two and eight blade configuration, limited the operating envelope for these configurations. The rig operational problems were addressed earlier in section 8.0. The structural failure of the centerbody during the test also significantly delayed the test program. Therefore, in order to expedite the program, the test points were limited to the boundaries and a few interior points of the operating envelopes for the two and eight blade configurations.

9.3.2 (Continued)

The aerodynamic performance data was nondimensionalized for analysis according to the following set of equations.

(POWER COEFFICIENT)

$$Cp = \frac{BHP\ (\rho_o/\rho)}{5.674\ (ND/1000)^3 D^2}$$

(NET THRUST COEFFICIENT)

$$C_{TNET} = \frac{T_{NET}(\rho_o/\rho)}{340.42\ (ND/1000)^2 D^2}$$

(ADVANCE RATIO)

$$J = 60\ \frac{V}{ND}$$

Where:

BHP = power, KW
T_{NET} = net thrust, N
D = Prop-Fan diameter, m
ρ_o/ρ = density ratio, sea level to ambient
N = rotational speed, RPM
V = free stream velocity, m/sec

It should be emphasized that the performance data was acquired only during structural testing where blade angle was continually varied to maintain a constant power level. Accordingly, the data was plotted as curves of power coefficient and net thrust coefficient versus advance ratio to eliminate blade angle (ß3/4) as a variable. If desired, this data can be converted to efficiency (η) by the relationship:

(EFFICIENCY)

$$\eta = \frac{C_{TNET}}{C_P} \times J$$

The power and thrust coefficient data as a function of advance ratio are presented for the four blade configuration in Figures 9-2, 9-3 and 9-4 and for the two blade configuration in Figure 9-5. The data was then cross-plotted to derive the more conventional maps of C_{TNET} versus C_P. Plots of C_{TNET} versus C_P for the two, four and eight blade cases are presented in Figures 9-6, 9-7, 9-8, 9-9 and 9-10. The limited scope of the two blade and eight blade data is apparent. Data taken at 3° inflow angle rather than at 0° is presented for the two blade configuration, because a better distribution of test points was run at that angle. Examination of these plots shows that the net thrust coefficient exhibits smooth consistent variations with power coefficient and advance ratio.

SR-7L WIND TUNNEL PERFORMANCE DATA

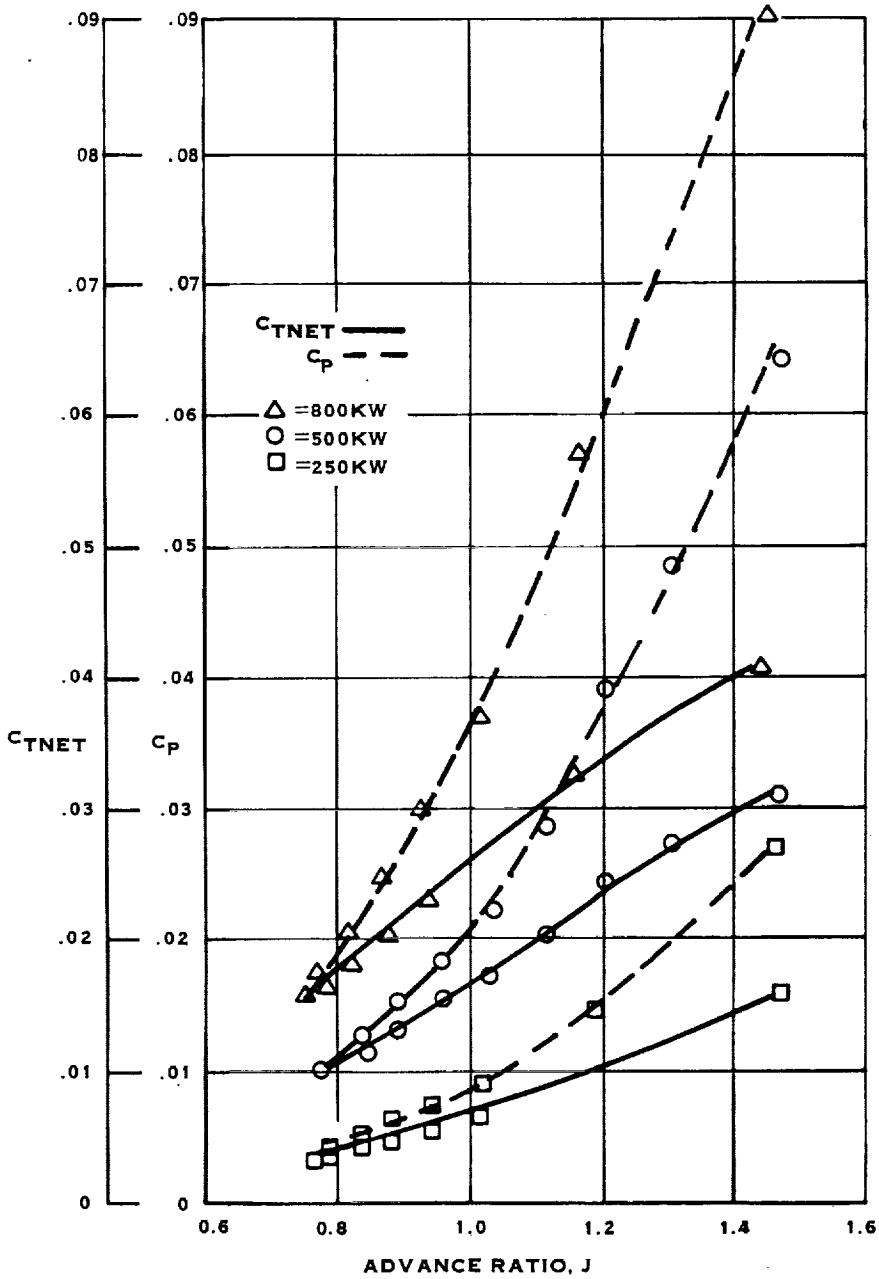

FIGURE 9-2. C_P AND C_{TNET} VS J, 4 BLADES, $M_N = .2$, $\psi = 0°$

SR-7L WIND TUNNEL PERFORMANCE DATA

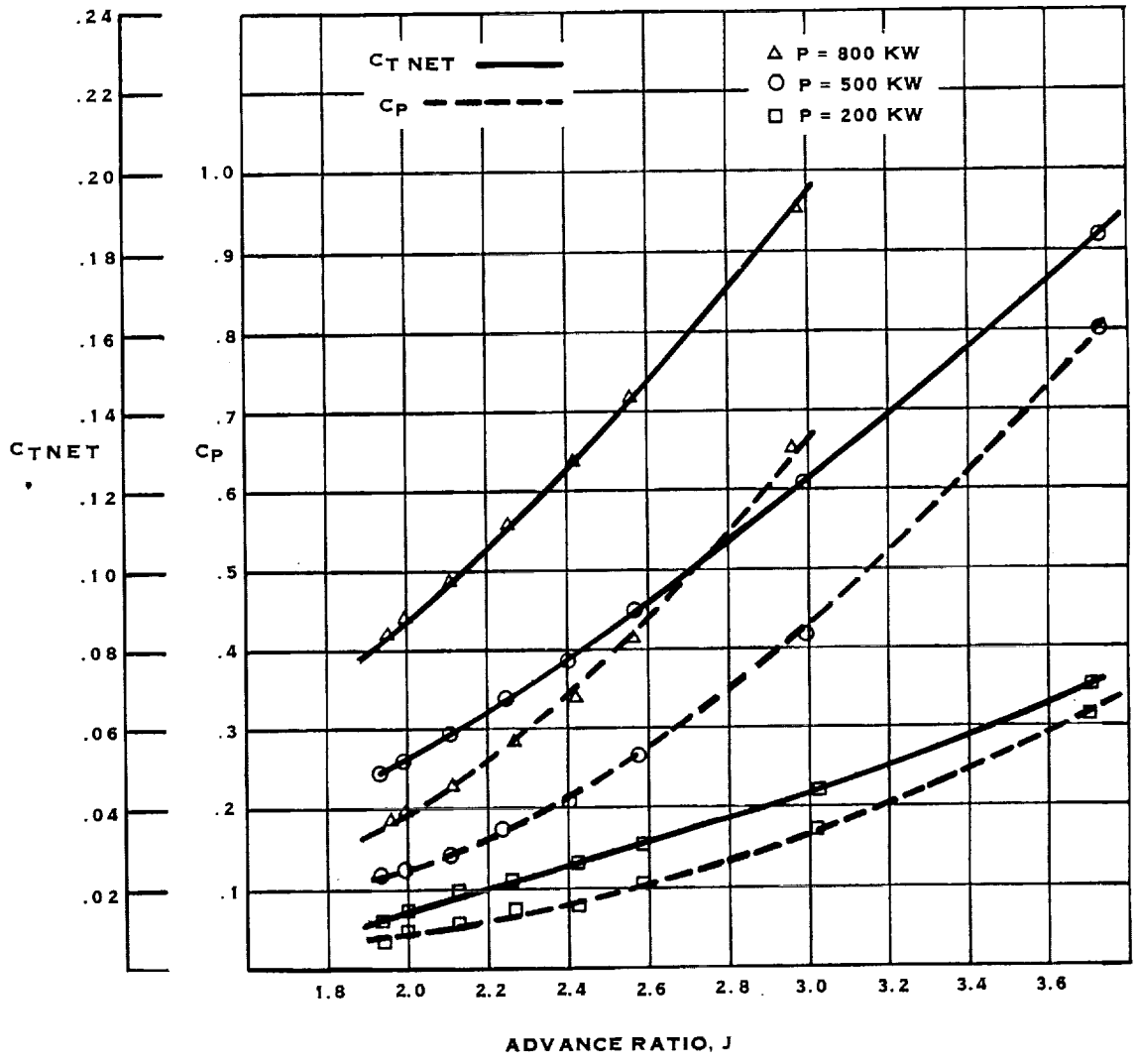

FIGURE 9-3. C_P AND C_{TNET} VS. J, 4 BLADES, M_N = .5, ψ = 0°

SR-7L WIND TUNNEL PERFORMANCE DATA

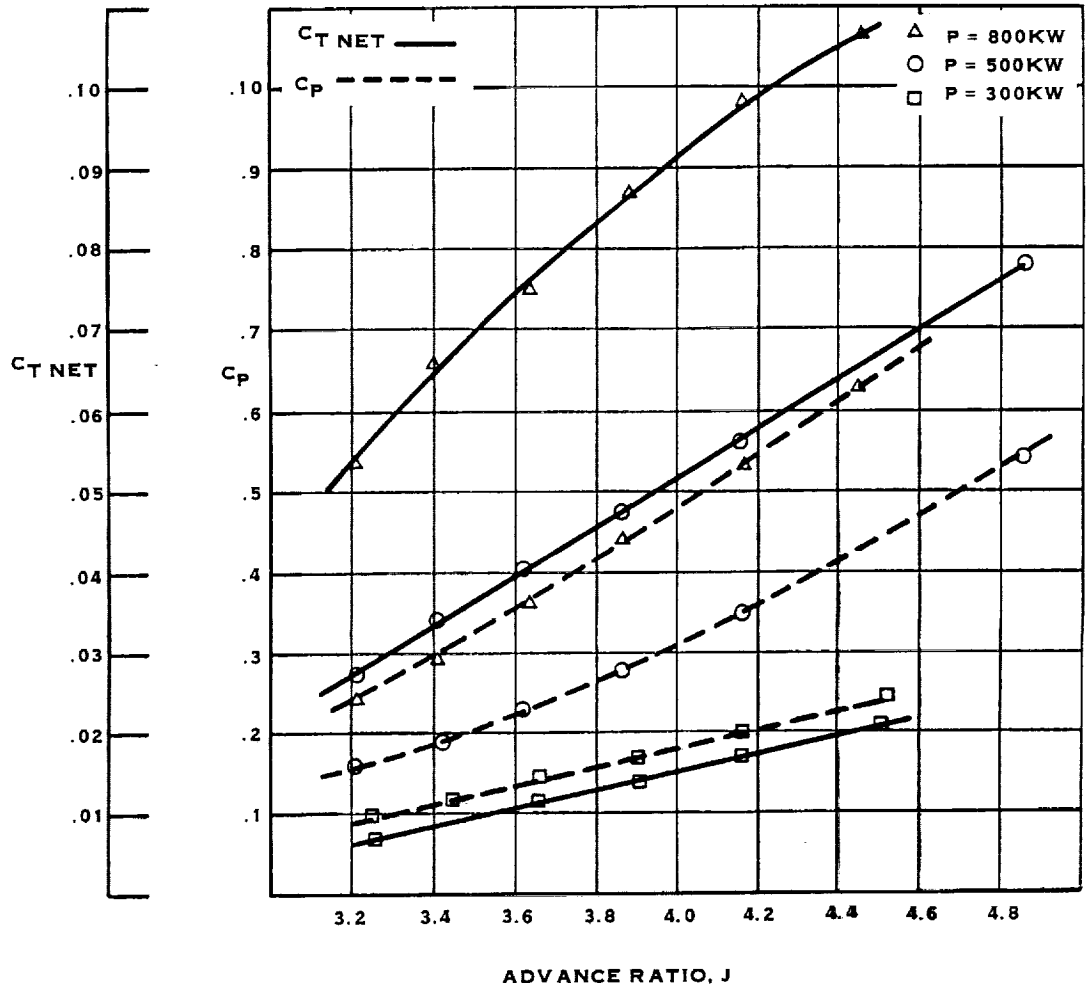

FIGURE 9-4. C_P AND C_{TNET} VS. J, 4 BLADES, $M_N = .8$, $\psi = 0°$

SR-7L WIND TUNNEL PERFORMANCE DATA

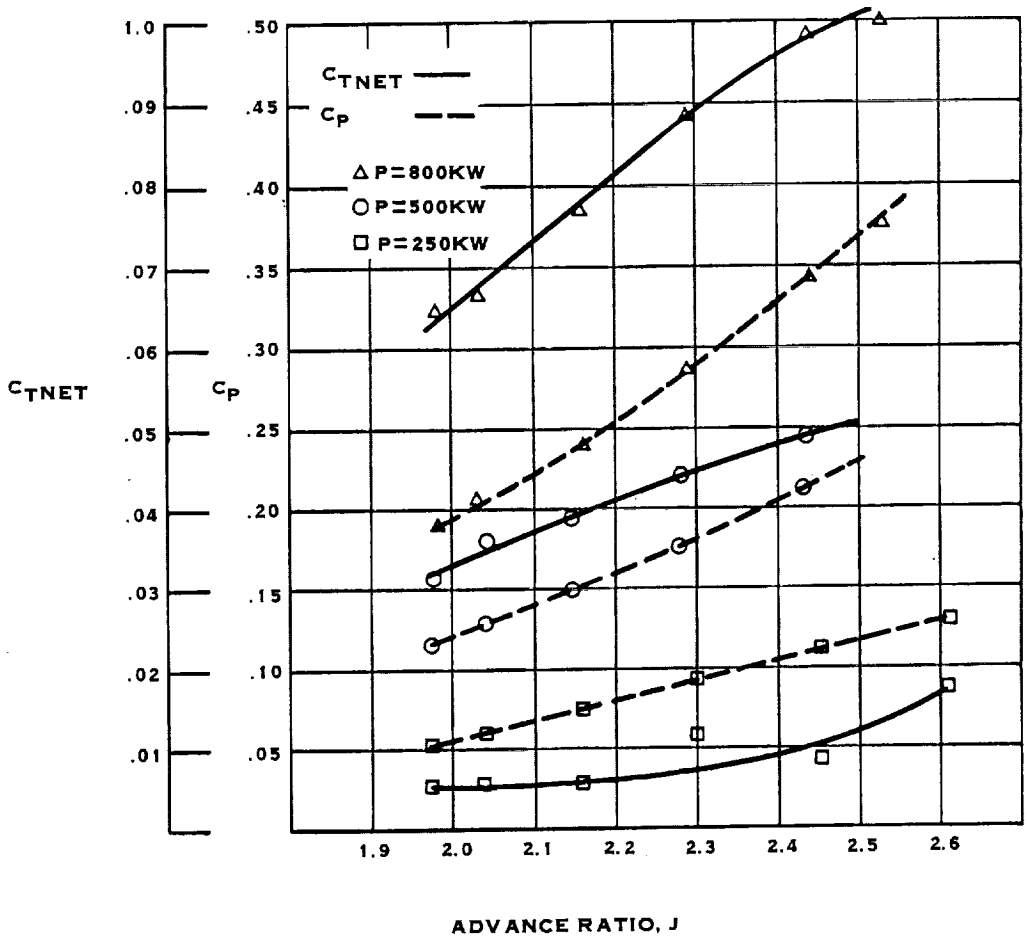

FIGURE 9-5. C_P AND C_{TNET} VS J, 2 BLADES, M_N = .5, ψ=3°

SR-7L WIND TUNNEL PERFORMANCE DATA

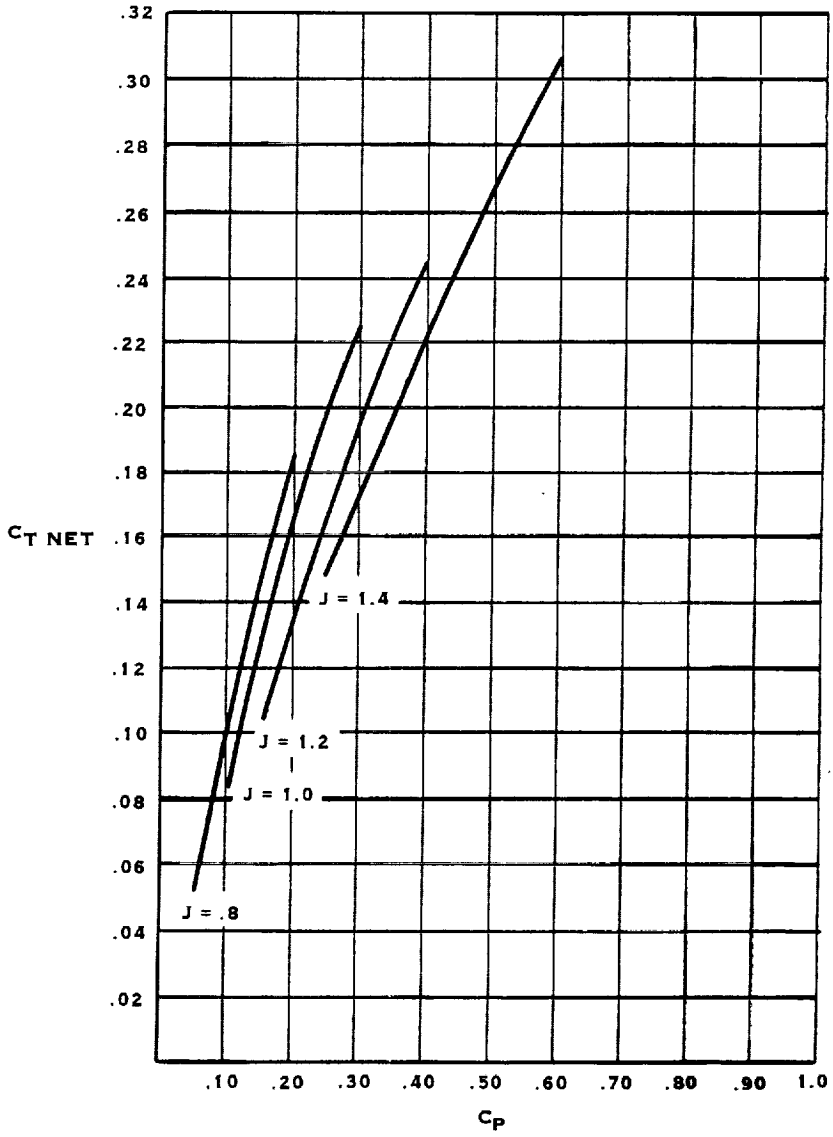

FIGURE 9-6. C_{TNET} VS C_P, CONSTANT J, 4 BLADES, M_N = .2

SR-7L WIND TUNNEL PERFORMANCE DATA

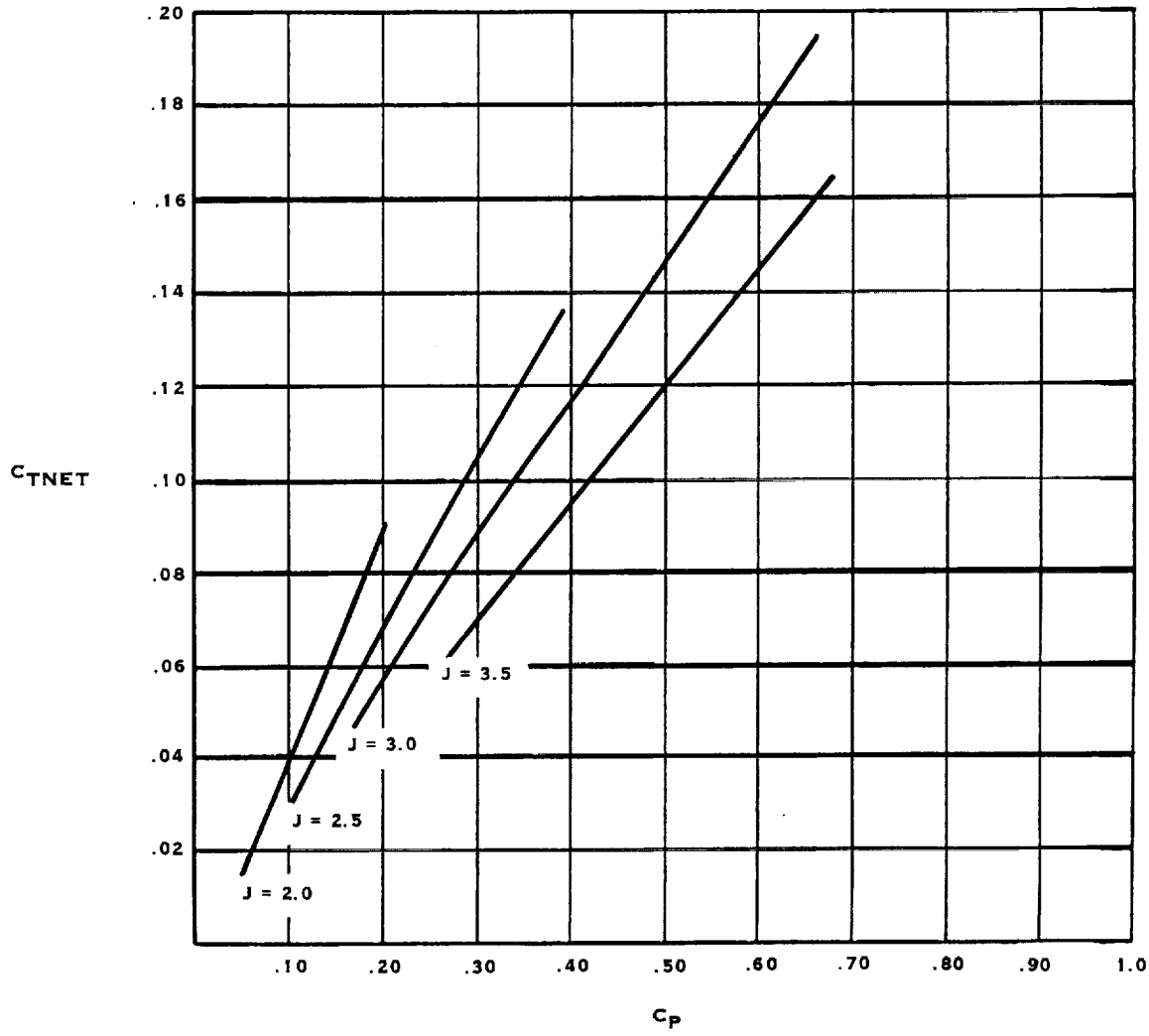

FIGURE 9-7. C_{TNET} VS C_P, CONSTANT J, 4 BLADES, $M_N = .5, \psi = 0°$

SR-7L WIND TUNNEL PERFORMANCE DATA

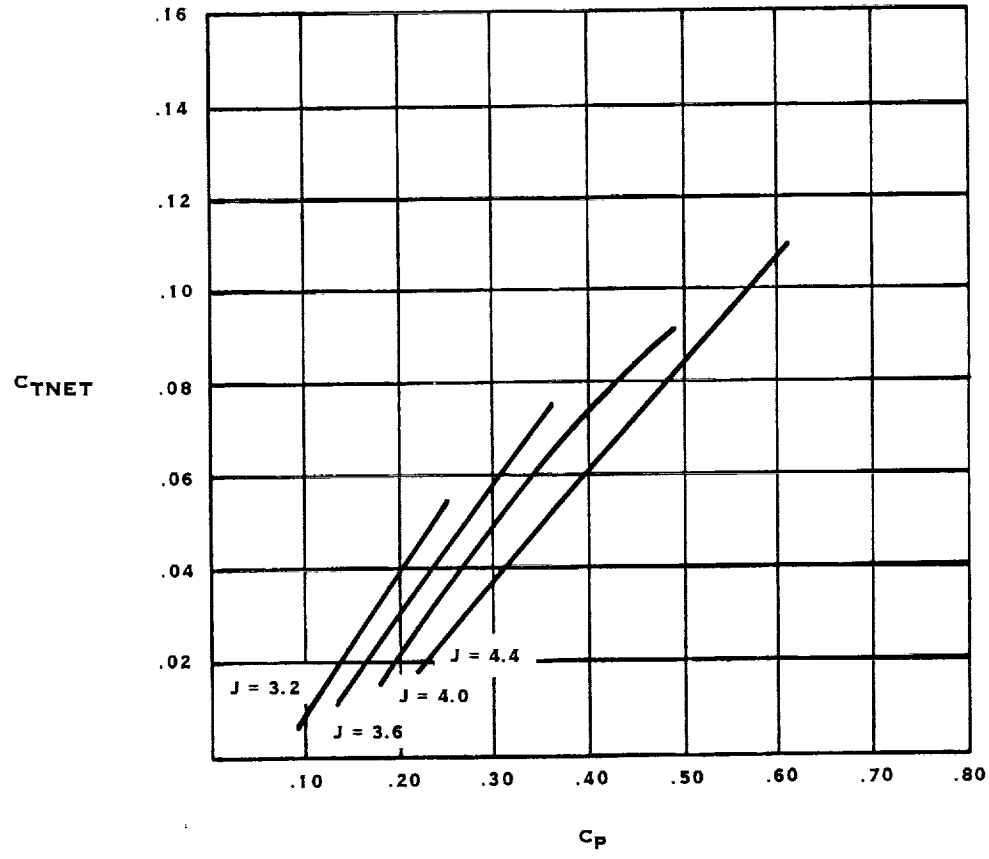

FIGURE 9-8. C_{TNET} VS C_P, CONSTANT J, 4 BLADES, M_N = .8, ψ =0

SR-7L WIND TUNNEL PERFORMANCE DATA

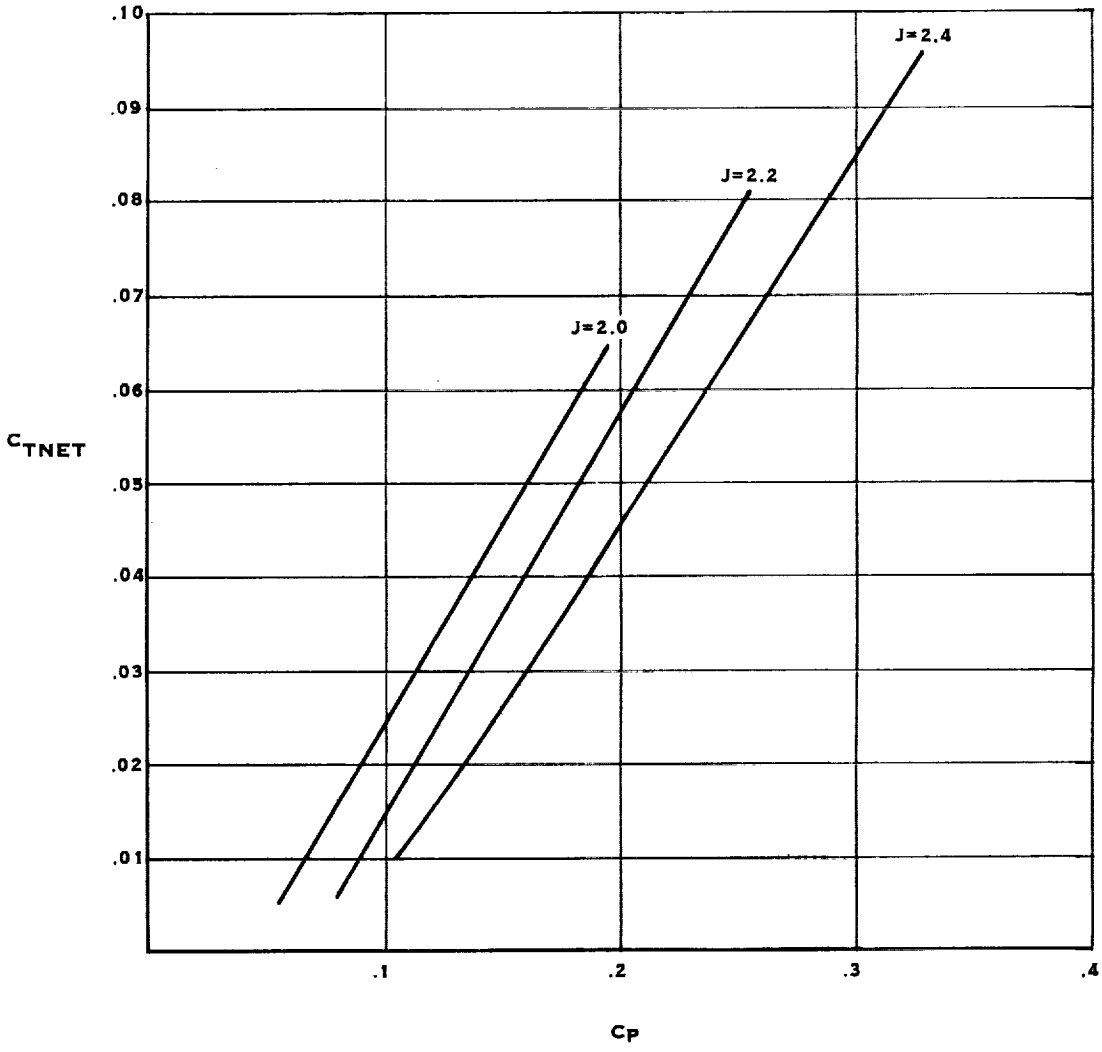

FIGURE 9-9. C_{TNET} VS C_P, CONSTANT J, 2 BLADES, $M_N = .5$, $\psi = 3^\circ$

SR-7L WIND TUNNEL PERFORMANCE DATA

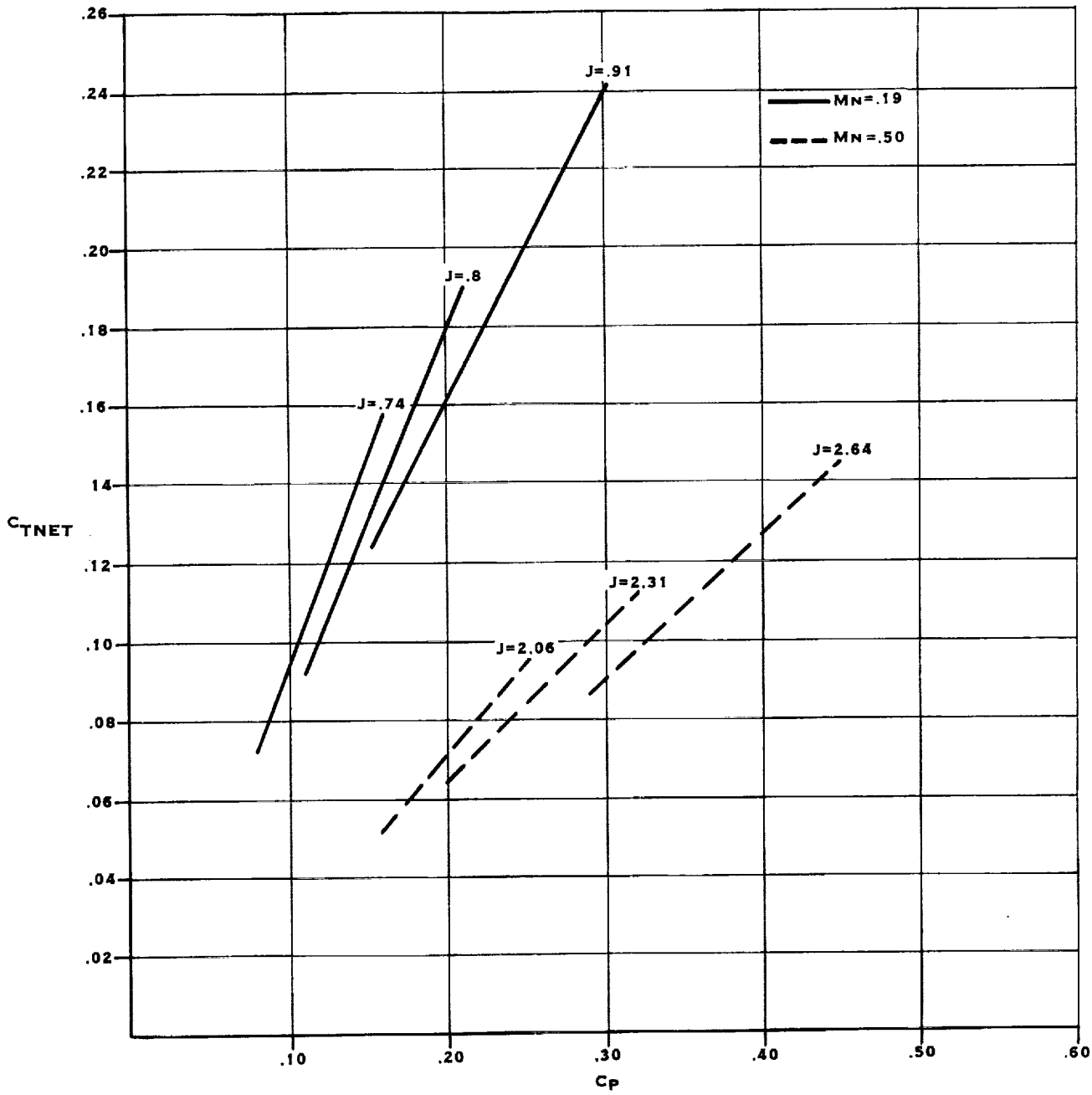

FIGURE 9-10. C_{TNET} VS C_P, CONSTANT J, 8 BLADES, $\psi = 0°$

9.3.2 (Continued)

The four blade and eight blade data was cross-plotted again to obtain curves of net thrust coefficient versus advance ratio for a constant power coefficient. Comparison of Figures 9-11 and 9-12 shows that for the same advance ratio and power coefficient, a higher net thrust coefficient is obtained with the four blade configuration than with eight blades. Therefore, as expected, the four blade configuration, at lower power loadings, is more efficient than the eight blade Prop-Fan.

Comparisons of the calculated and experimentally determined performance of the four and eight blade Prop-Fan configurations are shown in Figures 9-13 and 9-14. These calculations were made using a refined lifting line method. The predicted and measured performance agree very well for the four blade configuration over the entire range of test points. Although the performance of the eight blade Prop-Fan design was underpredicted at Mach 0.5, good agreement between measurement and prediction was obtained at Mach numbers of .70 and .73. Moreover, the trends of thrust with power are predicted accurately.

SR-7L WIND TUNNEL PERFORMANCE DATA

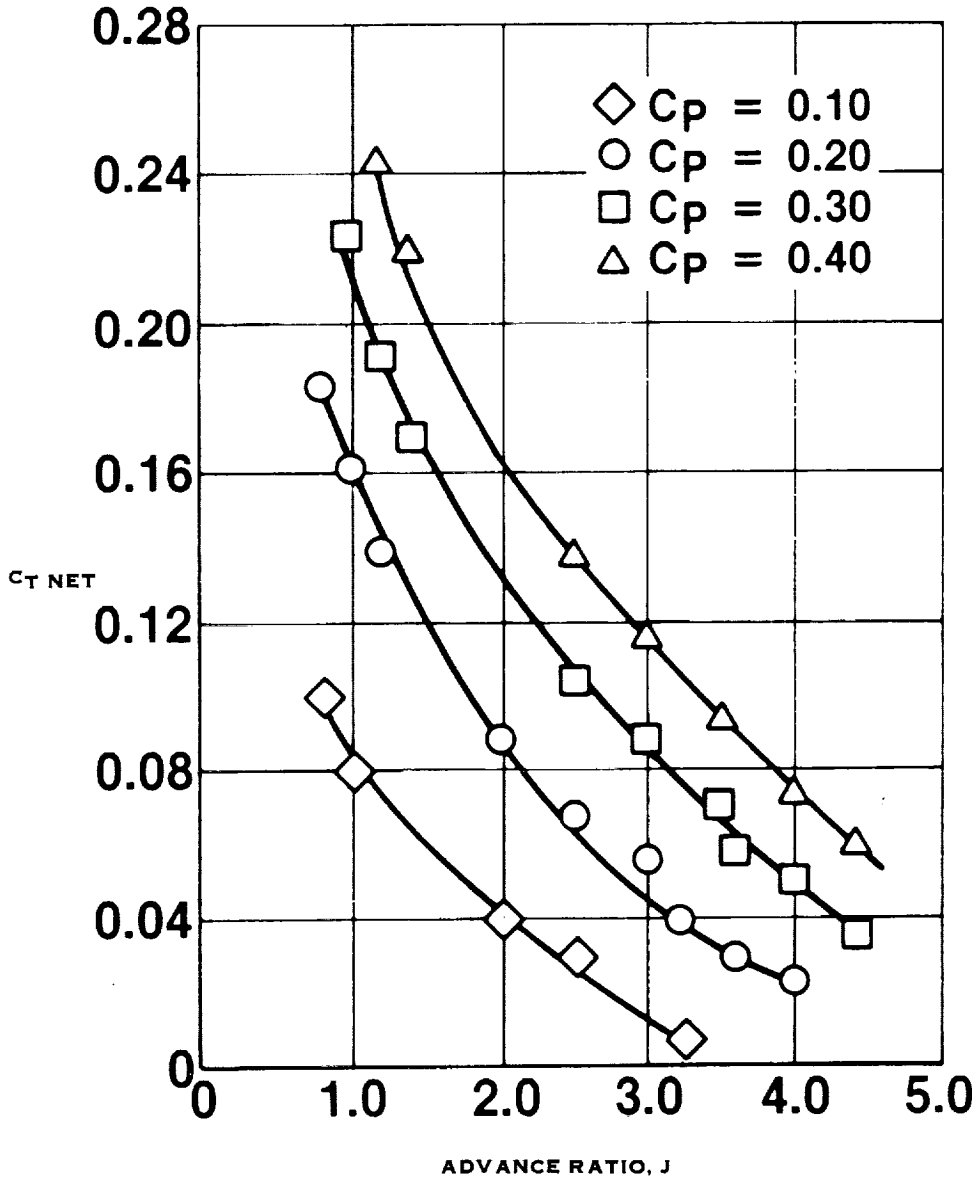

FIGURE 9-11. C_{TNET} VS J, CONSTANT C_P, 4 BLADES, $\psi = 0°$

SR-7L WIND TUNNEL PERFORMANCE DATA

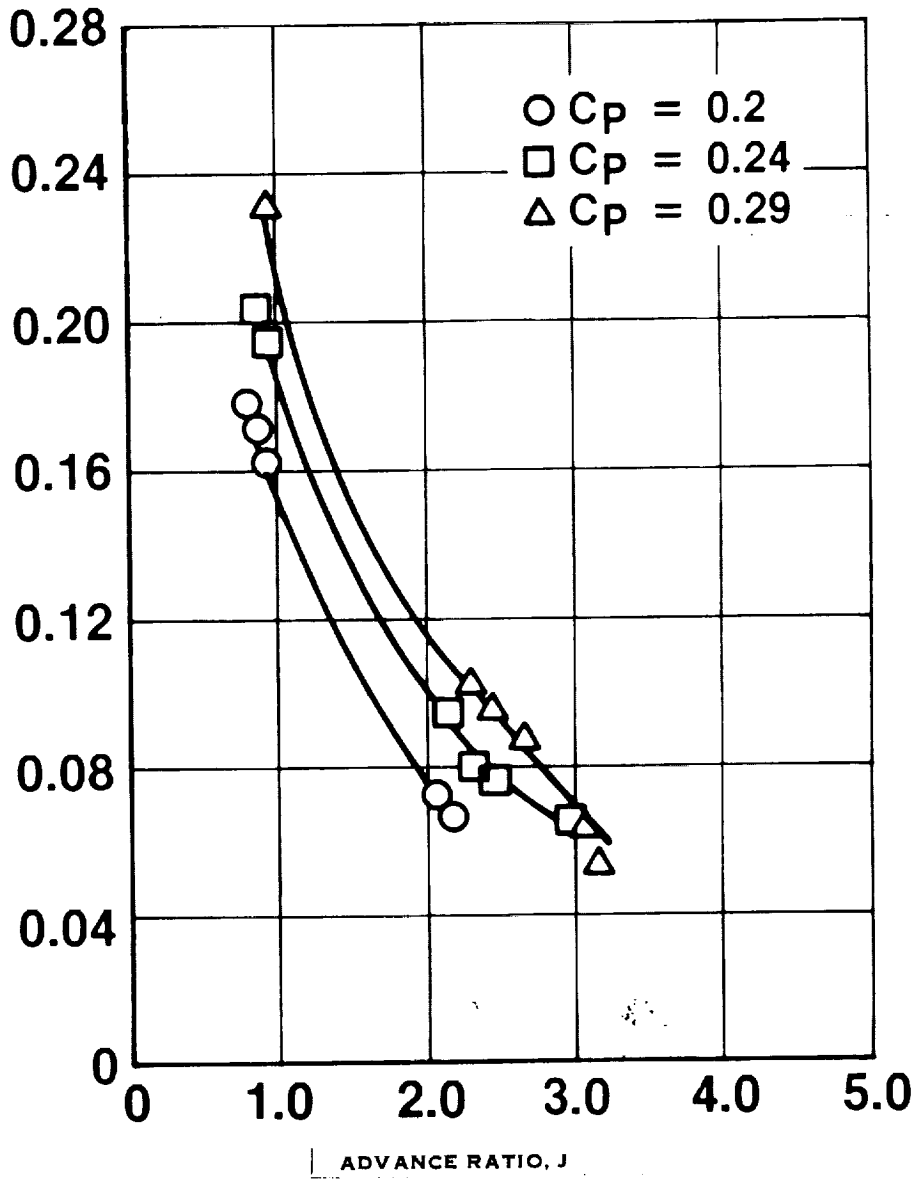

FIGURE 9-12. C_{TNET} VS. J, CONSTANT Cp, 8 BLADES, $\psi = 0°$

SR-7L WIND TUNNEL PERFORMANCE DATA

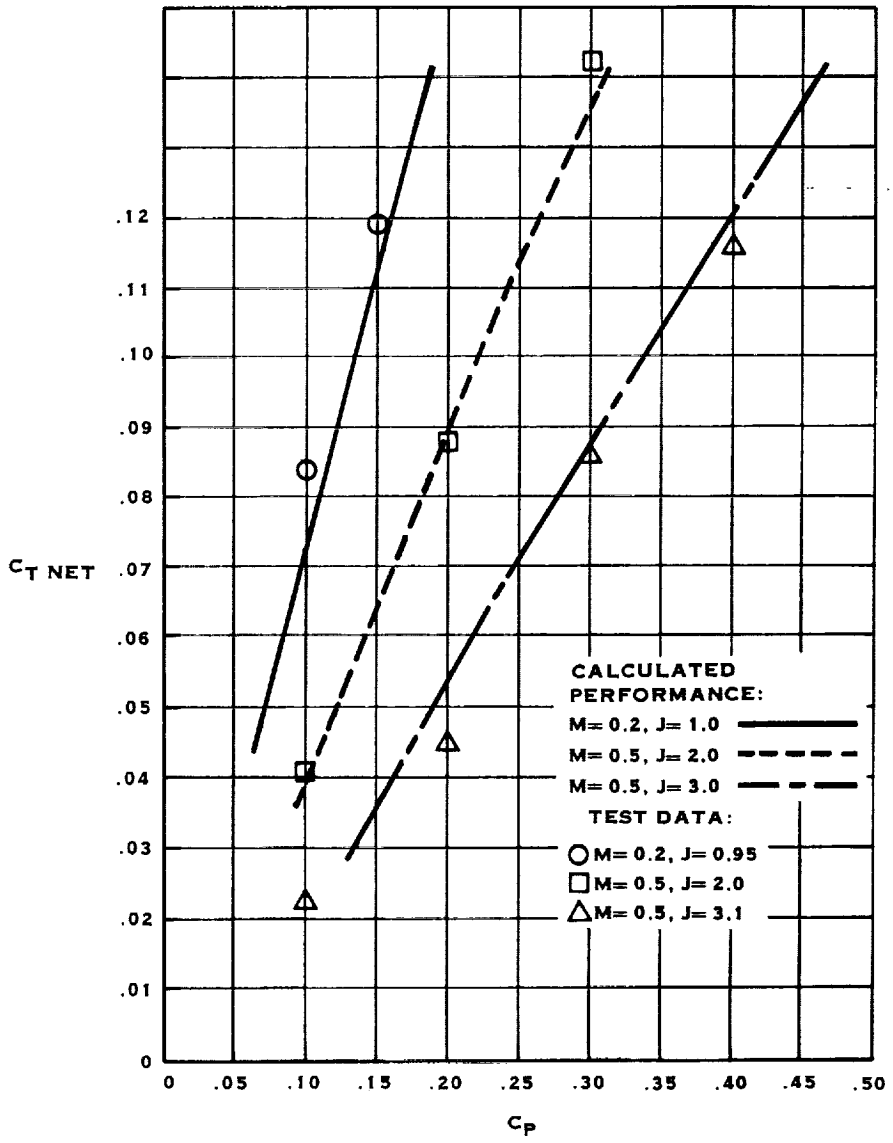

FIGURE 9-13. COMPARISON OF MEASURED AND PREDICTED PERFORMANCE, 4 BLADES

SR-7L WIND TUNNEL PERFORMANCE DATA

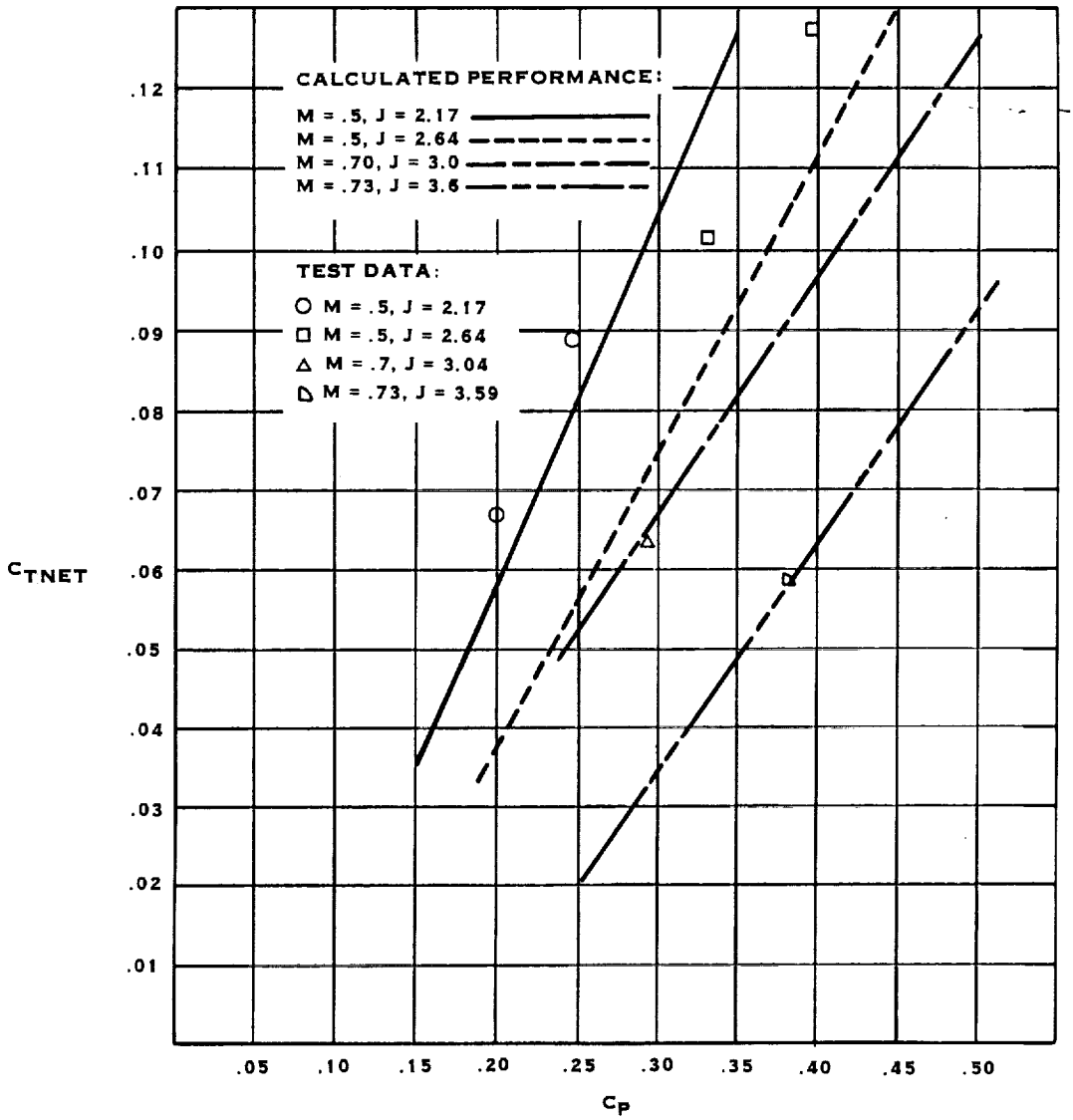

FIGURE 9-14. COMPARISON OF MEASURED AND PREDICTED PERFORMANCE, 8 BLADES

10.0 BLADE SURFACE STEADY PRESSURE MEASUREMENT

10.1 Test Objective

To measure the steady pressure distribution on the surface of the SR-7L Prop-Fan blade for a range of blade angles, rotational speeds, and simulated flight Mach numbers.

10.2 Test Procedure

In preparation for blade surface steady pressure testing, the Prop-Fan was installed on the drive system, as described in section 6.2, and supported as shown in Figures 10-1 and 10-2.

As noted earlier in section 2.0, collection of blade surface steady pressure test data was interrupted during the first tunnel entry in early 1986 and had to be rescheduled for a second tunnel entry in early 1987. Though the steady pressure test data collected was quite limited as a result of the interruption, enough information was obtained to indicate that a revised pressure tap layout was desirable. A new steady pressure blade incorporating an improved pressure tap layout was fabricated for use during the second tunnel entry. It provided a much higher density of surface pressure taps in areas on the blade where the local steady pressures were more sensitive to changing operating conditions.

The steady pressure measurement blade (S/N 009) was installed in blade position 7. For balancing purposes, a counterweight blade (S/N 058) was installed in position number 3, as shown in Figure 10-3. As a precaution, signals from 2 shank mounted strain gages were monitored throughout the test. Special contour matching blade stubs were installed in the remaining 6 hub arm bores. The test rig power capabilities necessitated conducting all testing using a 2 bladed Prop-Fan configuration, thereby permitting operation at power loadings per blade corresponding approximately to the take-off and cruise conditions of the eight blade Prop-Fan design.

The Prop-Fan was operated in the beta control mode during the entire test. In this mode, Hamilton Standard personnel were able to change the blade pitch angle during testing by means of an increase/decrease pitch switch located in the control room. For a fixed Mach number and a constant power supplied by the turbines, the Prop-Fan rotational speed was varied by increasing or decreasing blade pitch angle.

The blade pitch angle ($\beta 3/4$) was measured and recorded for each test point. An electrical signal proportional to blade angle was provided by means of a potentiometer mounted on the rotating side of the Prop-Fan as illustrated in Figure 5-3.

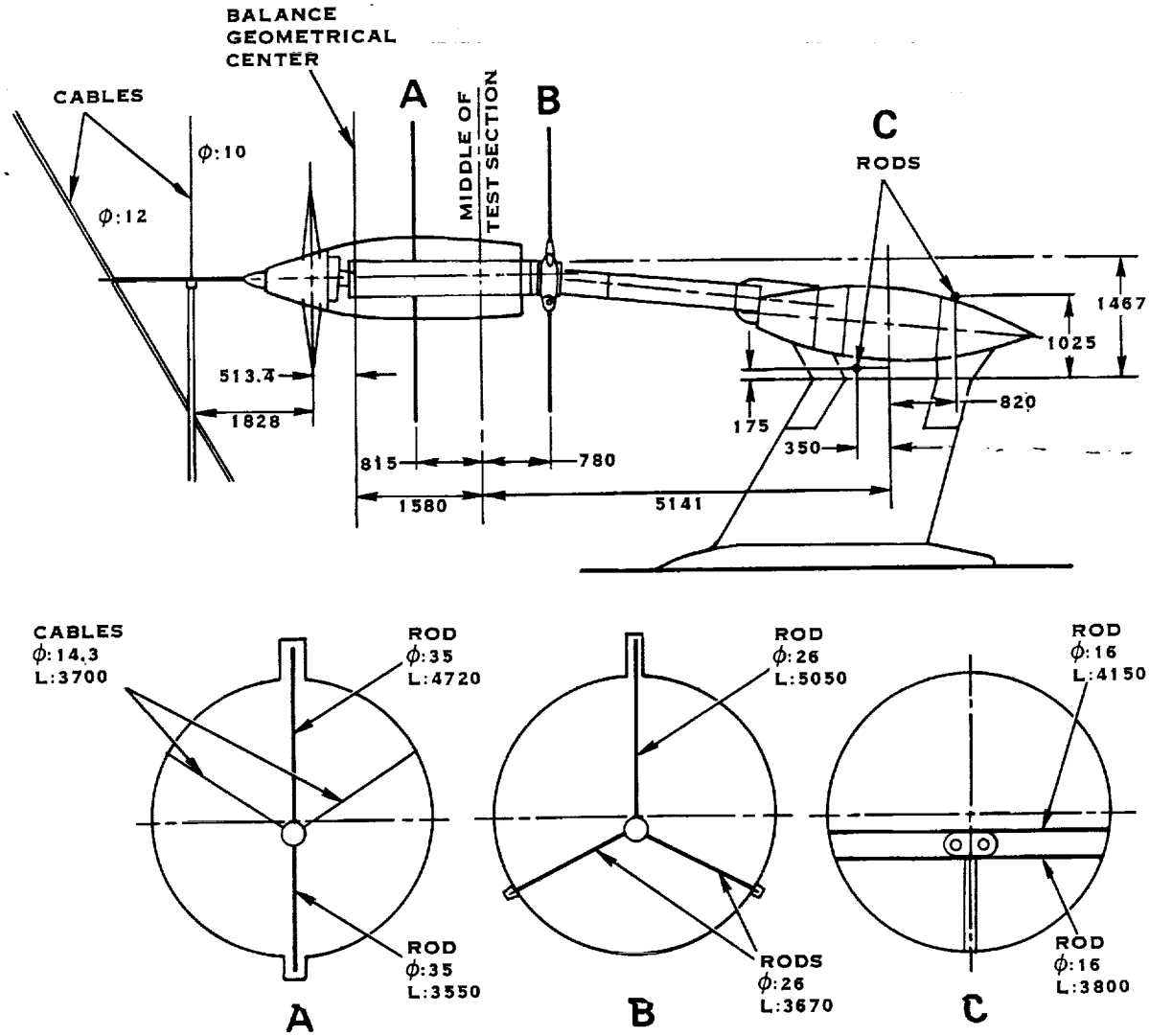

NOTE: ALL DIMENSIONS IN MILLIMETERS
φ = DIAMETER
L = LENGTH

RE 10-1. STEADY PRESS-

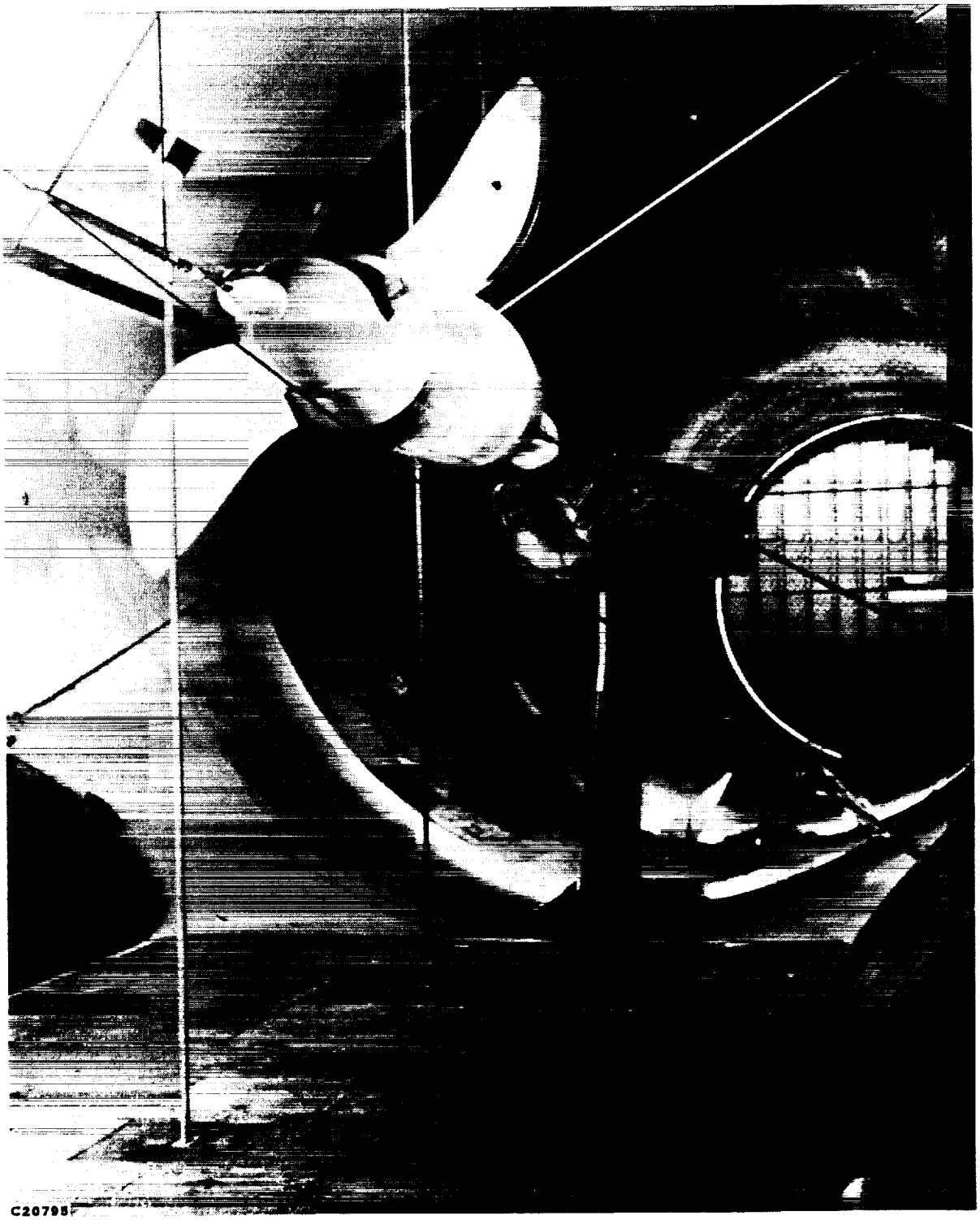

FIGURE 10-2. PROP-FAN STEADY PRESSURE TEST SET-UP

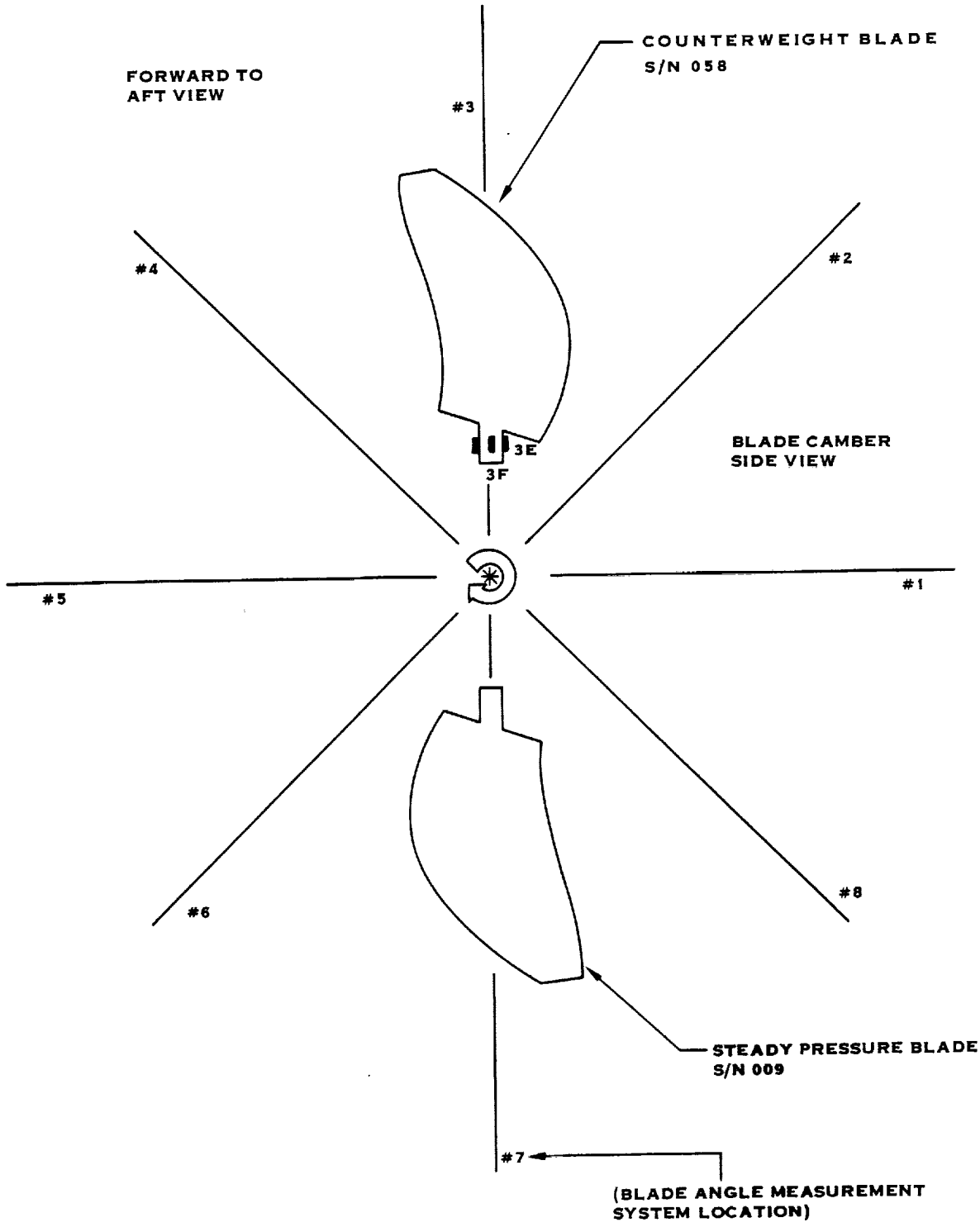

FIGURE 10-3. LAP BLADE INSTALLATION
STEADY PRESSURE TEST (2 BLADE)

10.2 (Continued)

The Prop-Fan rotational speed was measured by use of a 1P pickup. The sensor was triggered by a gear mounted on the test rig drive shaft. The rotational speed was averaged over ten revolutions.

The power absorbed by the Prop-Fan was determined by multiplying the torque supplied to the Prop-Fan by the rotational speed. Torque supplied to the Prop-Fan was computed by accounting for the measured frictional losses in the test rig relative to the torque measured by the torquemeter.

Collection of blade surface steady pressure data was accomplished by utilizing a specially instrumented SR-7L blade as illustrated in Figures 10-4 and 10-5, coupled with a Scanivalve™ pressure measurement system. Thirteen rows of pressure taps were located on both the face and camber sides of the steady pressure measurement blade. The pressure tap location and numbering scheme used for data acquisition and reduction are depicted in Figures 10-6, 10-7 and 10-8. This numbering scheme differs from that in the referenced test plan. The pressure tap channels which span the blade were fabricated by bonding a thin plastic skin to a channelized adhesive layer. Each channel was connected to a tube embedded in the root of the blade which led out to the blade shank. The tubes were connected to the Scanivalve mounted on the dome cap of the Prop-Fan, protruding through the nose of the spinner. One Scanivalve channel was provided for each tube. The stationary portion of the Scanivalve contained a pressure transducer that could be scanned by remote command to monitor one channel at a time. This arrangement allowed pressure measurements to be made at only one radial station per run. Pressure measurements were made by masking off all the rows of pressure taps except at the section of interest. The Scanivalve was then cycled through all channels to record the pressures at one radial station. Thirteen runs were required at each Prop-Fan operating point to obtain a complete pressure map for the blade surface at the operating point.

The Scanivalve was enclosed in an aerodynamic fairing to maintain a well behaved inflow to the Prop-Fan. The umbilical, which connected the Scanivalve to the control and monitoring equipment outside the tunnel, was enclosed in a conduit with an airfoil shaped cross-section. This also minimized disturbance of the flow.

Table 10-I lists the operating conditions that were run during the test along with tolerances showing the maximum variation in the parameters allowed when testing at different radial stations. In general, the procedure for setting a specific test condition was to set Mach number and then adjust the rotor speed and blade angle, to obtain the desired power coefficient and advance ratio.

FIGURE 10-4. LAP STEADY PRESSURE BLADE (CAMBER SIDE)

FIGURE 10-5. LAP STEADY PRESSURE BLADE (FACE SIDE)

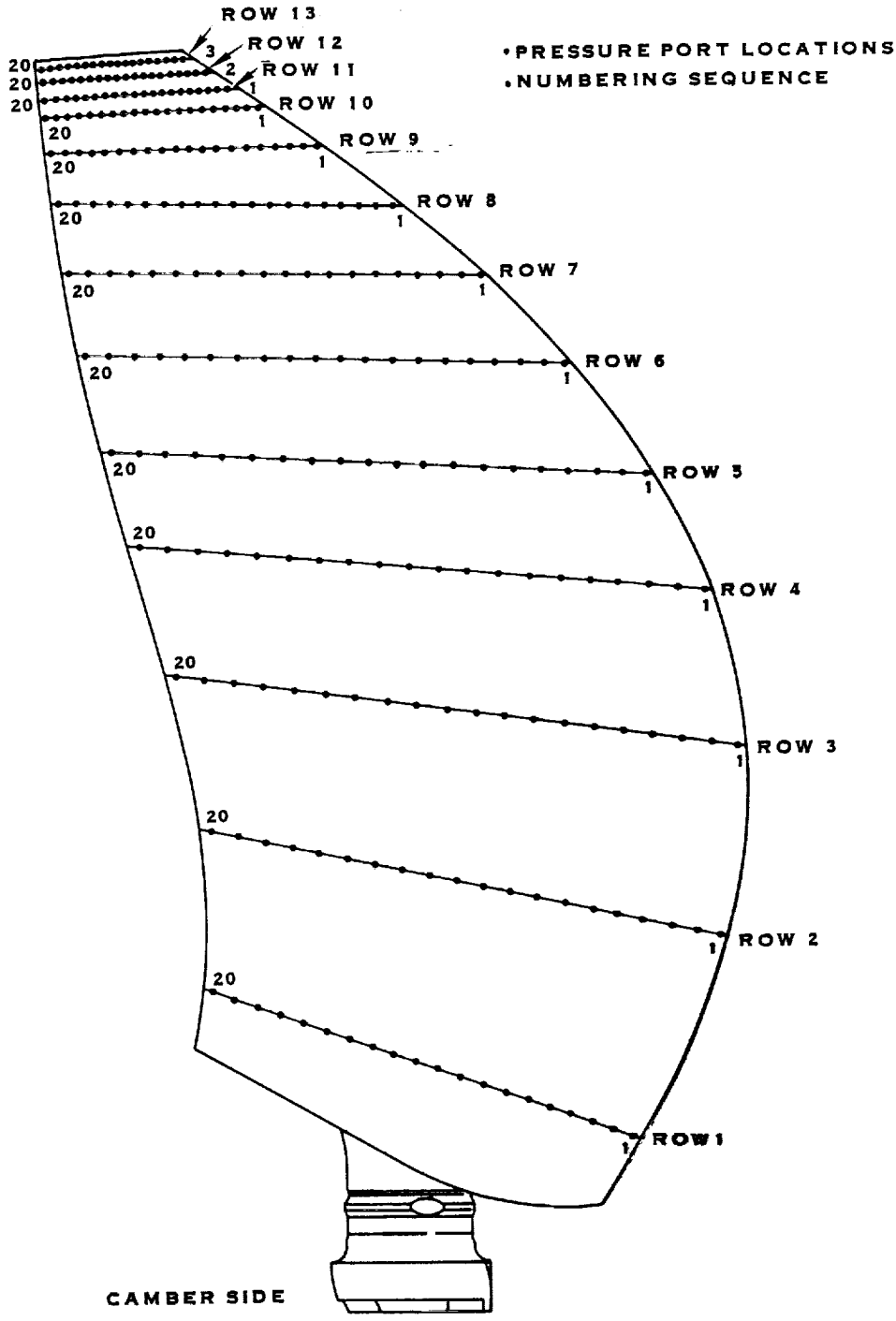

FIGURE 10-6. STEADY PRESSURE BLADE

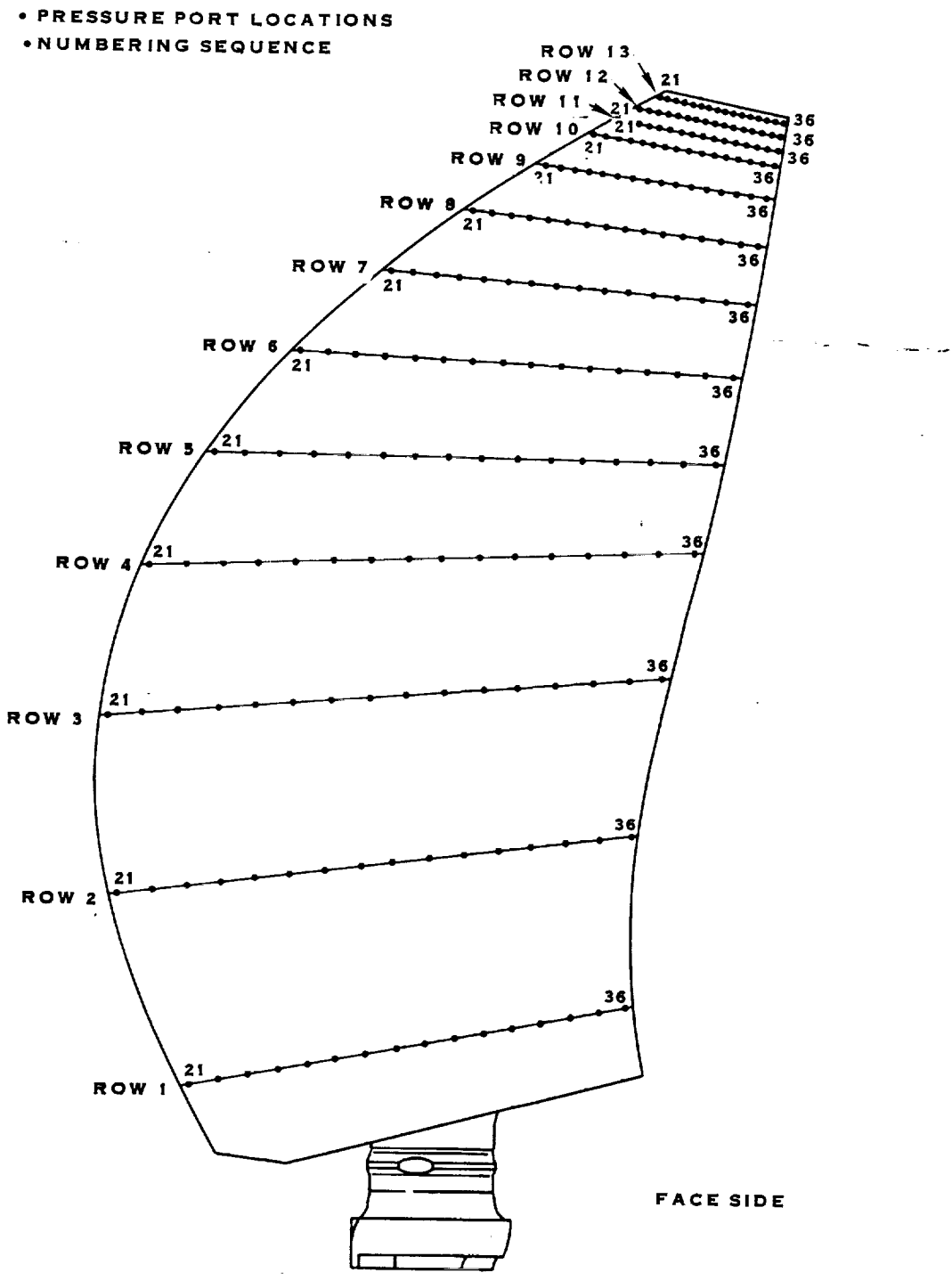

FIGURE 10-7. STEADY PRESSURE BLADE

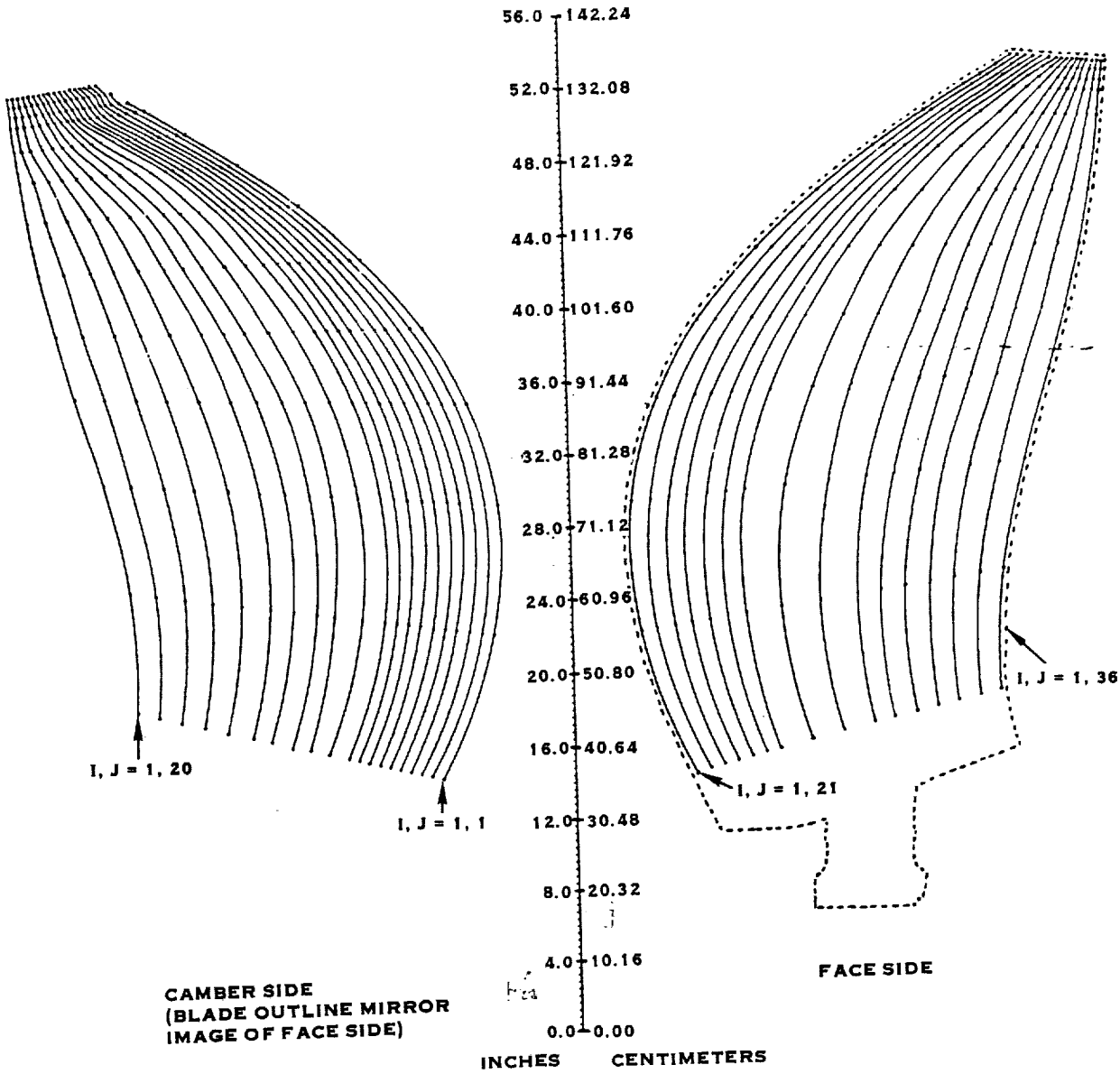

NOTE: THE VERTICAL SCALE REPRESENTS THE DISTANCE ALONG THE BLADE PITCH CHANGE AXIS FROM THE PROPFAN CENTER LINE.

FIGURE 10-8. ARRANGEMENT OF THE PRESSURE TAPS ON THE BLADE SURFACE – PROJECTED VIEW

TABLE 10-I. OPERATING CONDITIONS FOR BLADE STEADY PRESSURE TESTING (2 BLADE LAP PROPELLER)

Condition No.	M Mach No.	J Advance Ratio ±.2	β Blade Angle ±.10°	C_p Power Coefficient ±.2	N RPM ±
1	.01	.08	13.80°	.079	1200
2	.02	.14	15.70°	.093	1200
3	.02	.15	18.78°	.152	1200
4	.03	.18	21.60°	.204	1200
5	.20	.88	25.65°	.098	1665
6	.20	.88	30.40°	.251	1651
7	.50	3.065	57.51°	.649	1186
8	.50	3.055	54.95°	.360	1190
9	.50	3.063	50.86°	.108	1185
10*	.60	3.066	54.98°	.226	1436
11*	.70	3.055	55.00°	.229	1685
12*	.78	3.07	54.97°	.223	1840
13*	.78	3.20	54.98°	.112	1782

* RADIAL STATIONS 2,4 AND 10 WERE NOT RUN AT THIS CONDITION.

10.2 (Continued)

After establishing the operating condition, the basic wind tunnel and Prop-Fan parameters (tunnel static temperature and pressure, Mach number and rotor speed) were logged into the microcomputer, a record number was assigned for filing purposes, and the scanivalve was activated. The scanivalve then ran through a calibration sequence followed by the pressure data scan. The data were then plotted in preliminary form and reviewed. If the data contained questionable features, a second scan was performed or hand scanning of individual suspicious points was made.

Test points 1 through 4 in Table 10-I approximate static conditions of increasing power and were selected to provide information on leading edge vortex flow (there was no applied tunnel flow for these points, although there was some Prop-Fan induced flow). Points 5 and 6 were selected to investigate take-off conditions; points 7 through 9 covered a wide range of power loading conditions at 0.50 Mach number and bracket through the design cruise power loading. Points 10 through 13 were selected to investigate transonic flow characteristics and were all at relatively low power due to rig limitations. For these points, power coefficient and advance ratio were held constant while Mach number was varied.

10.3 Discussion and Results

10.3.1 Data Reduction

10.3.1.1 Data Format

The pressure data were reduced to coefficient form and plotted during the test using a microcomputer system to provide the test personnel with a basis for judging the quality of the data following each scan. This preliminary data reduction included an approximate correction (described below) for the centrifugal pumping in the tubes and channels that led from the scanivalve to the pressure taps. The pressure coefficient formula that was used is:

$$C_p = \frac{P_c - P_o}{0.5\rho(V_o^2 + V_t^2)}$$

Where:

P_c = Corrected Blade Surface Pressure
P_o = Tunnel Static Pressure
ρ = Air Density
V_o = Tunnel Velocity
V_t = Tangential Velocity at Pressure Tap Radius

10.3.1.1. (Continued)

For each radial station the mid-chord radius (for a prescribed blade angle of 50.0 degrees) was used in determining the approximate centrifugal correction and the tangential velocity. It should be noted, however, that the radii of the pressure taps at each station vary along the blade chord, and furthermore, the radius of any given tap varies with blade angle. In addition, the values describing the chordwise distribution of the pressure taps, which were stored in the microcomputer, were nominal rather than measured values, and did not represent the precise distributions. The final data reduction at Hamilton Standard will account rigorously for these effects, and will be presented in a separate NASA Contractor Report (Reference 24).

10.3.1.2 Discussion of Problems

Before reviewing the data, it is necessary to address three basic test problems, each of which had some effect on the data presented in this report. The problems are as follows in decreasing order of severity:

1. Particle impacts resulting in failure of the tape seal over rows of dormant pressure taps or resulting in venting of individual channels.

2. Crack formation in the plastic skin which seals the channels on the blade surface.

3. Reference pressure transients which interrupted the scan sequence.

Particle impacts on the steady pressure blade occurred on several occasions during the test. In most cases the impacts resulted in little or no damage, however, four cases of damage to the tape which sealed the dormant rows of pressure taps occurred and two cases of channel venting occurred due to direct particle impingement on a specific channel. The data affected by tape seal failure were limited to radial stations 3, 6, 11 and 13 at Mach numbers generally greater than 0.20. Channel venting due to direct particle impact resulted on channels 26 and 29 and was repaired following the runs in which it occurred. The data that were compromised by impact events will be eliminated from the final data package.

Prior to the second test run (radial station 13), cracks were found in the camber side plastic skin layer, between radial stations 6 and 8, and 9 and 10, on the blade. The cracks, which are believed to have been catalyzed by the application of a cleaning solvent that "shocked" and embrittled the plastic, were not present following the first run (radial station 5); they were found immediately after applying the solvent. Continued blade checks showed high leak rates on channels 2 through 8. To correct the leak problem a series of tape strips was applied to the cracked areas, sealing them off and establishing acceptable leak rates. Testing continued with this configuration and leak rates were monitored following every other run. The fix was found to be satisfactory on all channels, although channel 2 required further repair as the test progressed. In general this problem is not considered to have compromised the data.

10.3.1.2 (Continued)

Reference pressure transients occurred during several data scans. Fortunately, this phenomenon was quite evident in the on-line pressure coefficient plots, so scans that were affected were either rerun entirely or hand scanned to pick up the affected points. Therefore this problem is considered to be of minimal consequence to the test data.

10.3.2 Discussion of Result

The entire spectrum of data is summarized in Figures 10-9 through 10-21; each figure shows all of the measured pressure distributions for a specific test condition, and is in the form of the on-line data reduction. These figures are presented in order of increasing Mach number. For Mach numbers where two or more power settings were run, the figures are sub-ordered by increasing power. Radial stations 2, 4, and 10 are left blank for Mach numbers greater than 0.50 because no data were collected due to limited test time. Radial stations with data points which may be eliminated or replaced with hand logged values, for the final data package, are marked with an asterisk.

Figures 10-9 through 10-12 show the pressure distributions for the nominal static operating condition. The pressure loading is seen to increase with increasing applied power, as expected, and the presence of leading edge vortex flow is suggested in Figures 10-11 and 10-12 by the negative pressure hump that spans along the camber side leading edge; the vortex then appears to sweep across the chord in between the 90 and 95 percent radius, resulting in very high loading in that region.

The data at these static operating conditions contain some inconsistencies. For example, when running radial station 6 the data was found to diverge from the trends at the neighboring stations. The cause of this inconsistency is not certain, however, it is noted that the actual Mach number was not zero (due to the Prop-Fan induced flow) and was variable during the "static" runs (Mach No. varied from 0.02 to 0.04). Though the reason for the Mach number variation is not known for sure, it was revealed during a daily tunnel inspection that a portion of the tunnel flow straightening honeycomb had been blown out. Subsequent running with the Prop-Fan driving the tunnel resulted in somewhat higher Mach numbers. To investigate this problem further radial station 7 was rerun for conditions 2 and 4. Comparisons of the pressure distributions or these runs are given in Figures 10-22 and 10-23. It is clear from this comparison that a repeatability problem existed for some of the static point data.

Figures 10-13 through 10-21 and Figure 10-24 show the pressure distributions for the remaining operating conditions. The data at these conditions show good repeatability. For example, Figure 10-24 shows radial station 8 which was scanned twice at 0.20 Mach number, first on the climb up to 0.78 Mach number (in accordance with the test plan sequence), and then on the decent, approaching shutdown. The results are seen to be nearly identical.

10.3.2 (Continued)

Some of the aerodynamic effects that are apparent in Figures 10-13 through 10-21 are leading edge vortex loading at 0.20 Mach number for the take-off case (Figure 10-14), inverted leading edge pressure distributions for the low power cases at high Mach numbers (Figures 10-15, 10-18, 10-19, 10-20 and 10-21) and evidence of trailing edge shock waves at the outboard stations at high Mach numbers (evident by the trailing edge pressure jump in Figures 10-19, 10-20 and 10-21. The inverted leading edge pressure distributions, as noted above, are typical for cambered airfoil sections operating at incidence below the design angle of attack value.

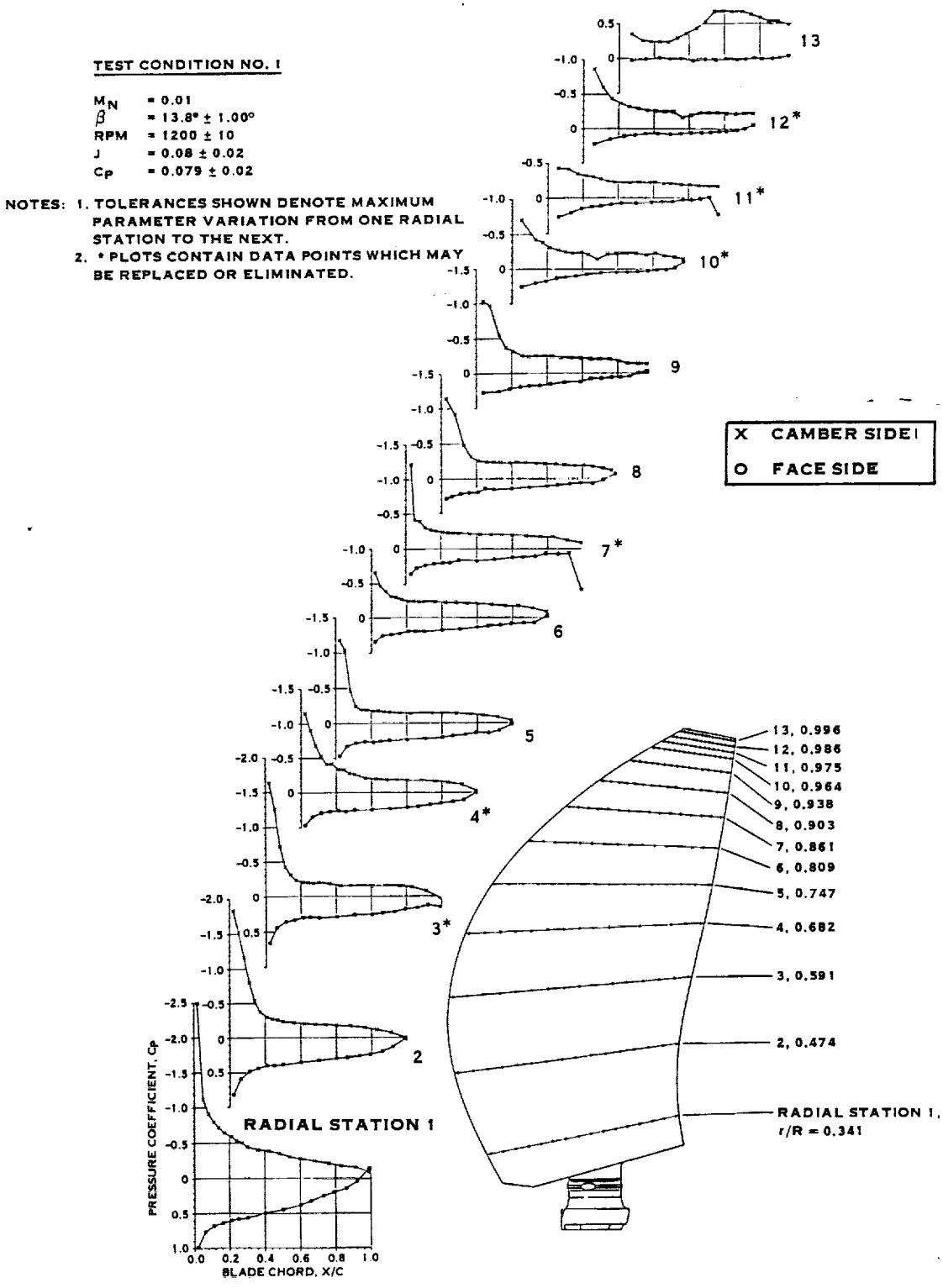

FIGURE 10-9. LAP SR-7L STEADY PRESSURE DISTRIBUTION (ON-LINE DATA)

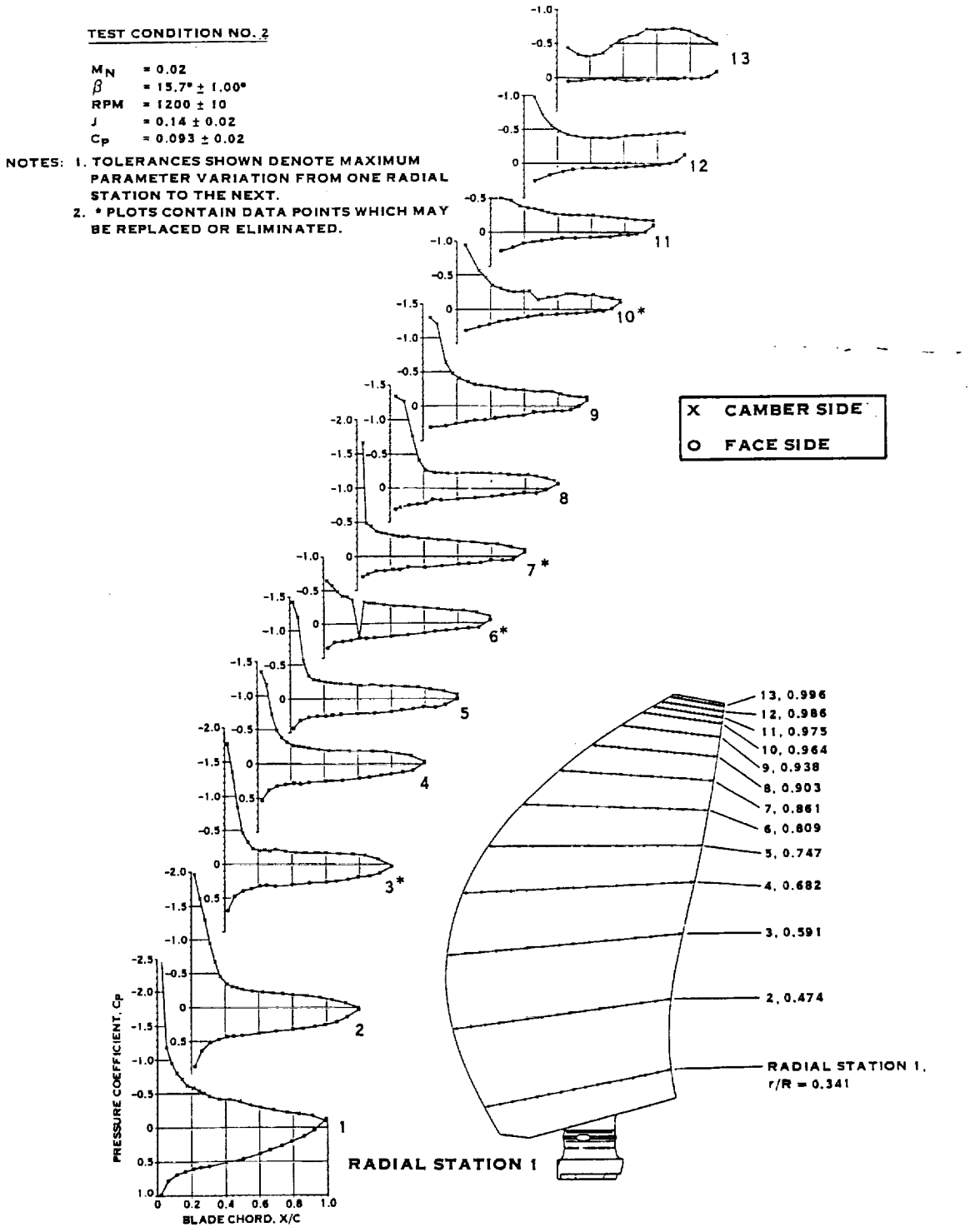

FIGURE 10-10. LAP SR-7L STEADY PRESSURE DISTRIBUTION (ON-LINE DATA)

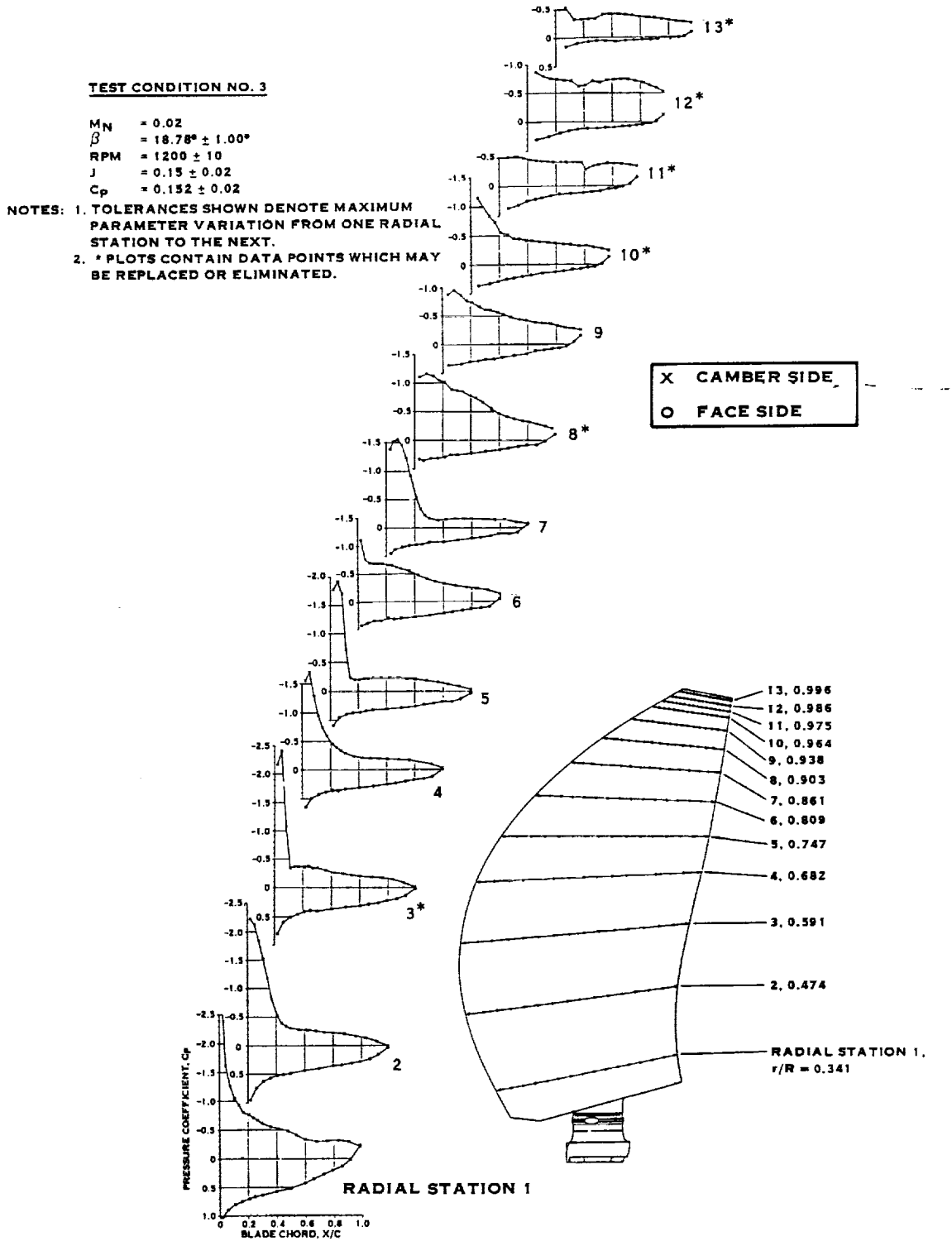

FIGURE 10-11. LAP SR-7L STEADY PRESSURE DISTRIBUTION (ON-LINE DATA)

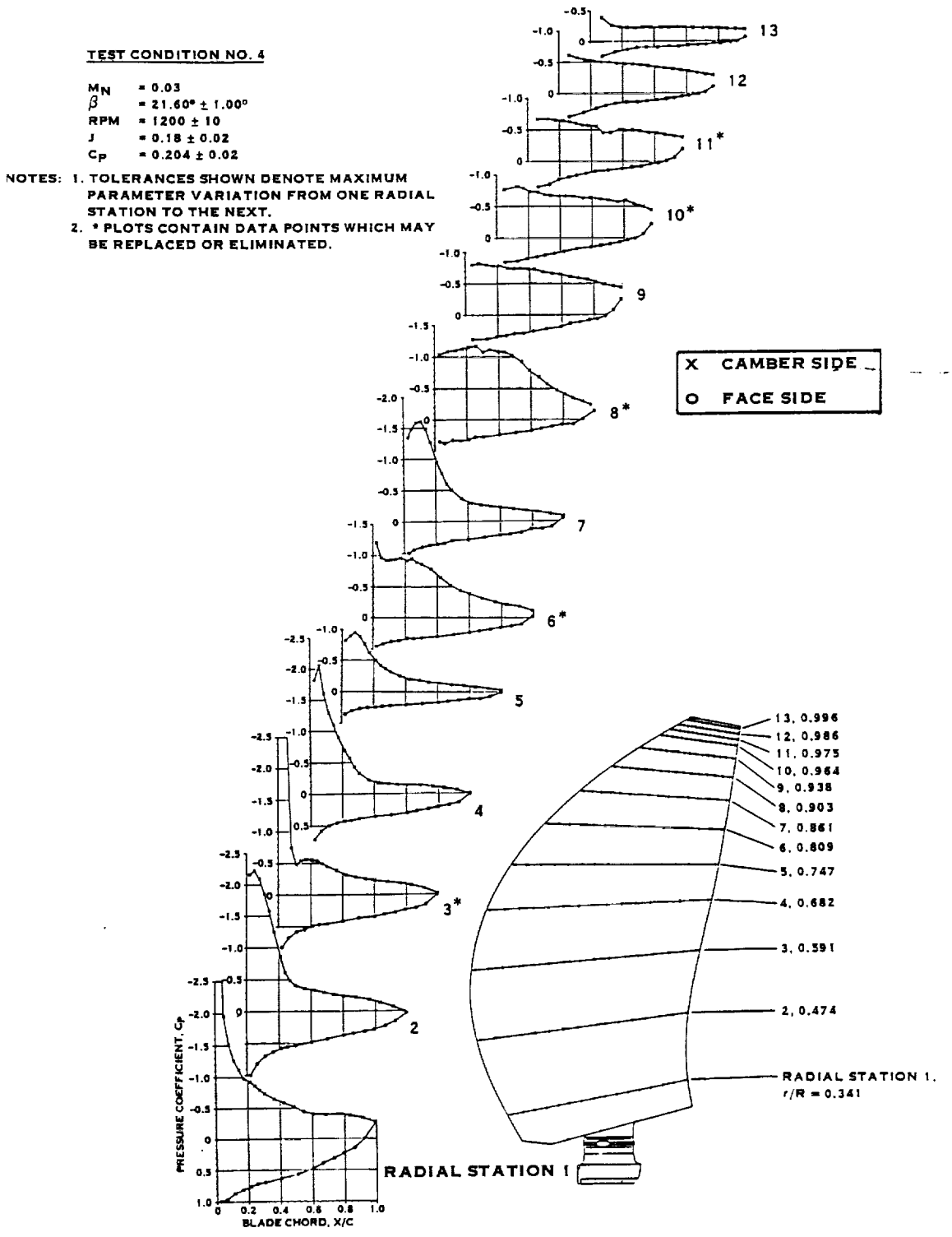

FIGURE 10-12. LAP SR-7L STEADY PRESSURE DISTRIBUTION (ON-LINE DATA)

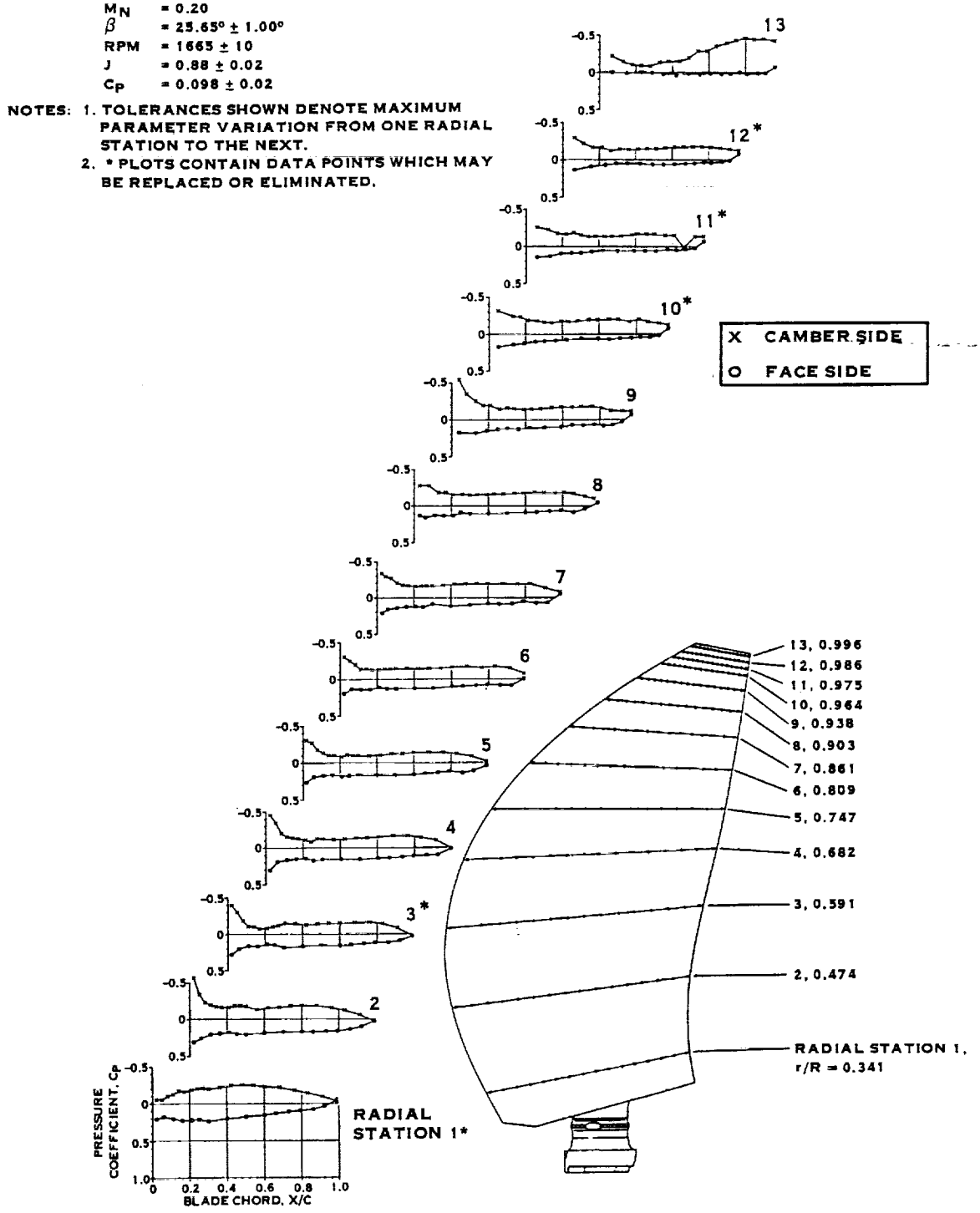

FIGURE 10-13. LAP SR-7L STEADY PRESSURE DISTRIBUTION (ON-LINE DATA)

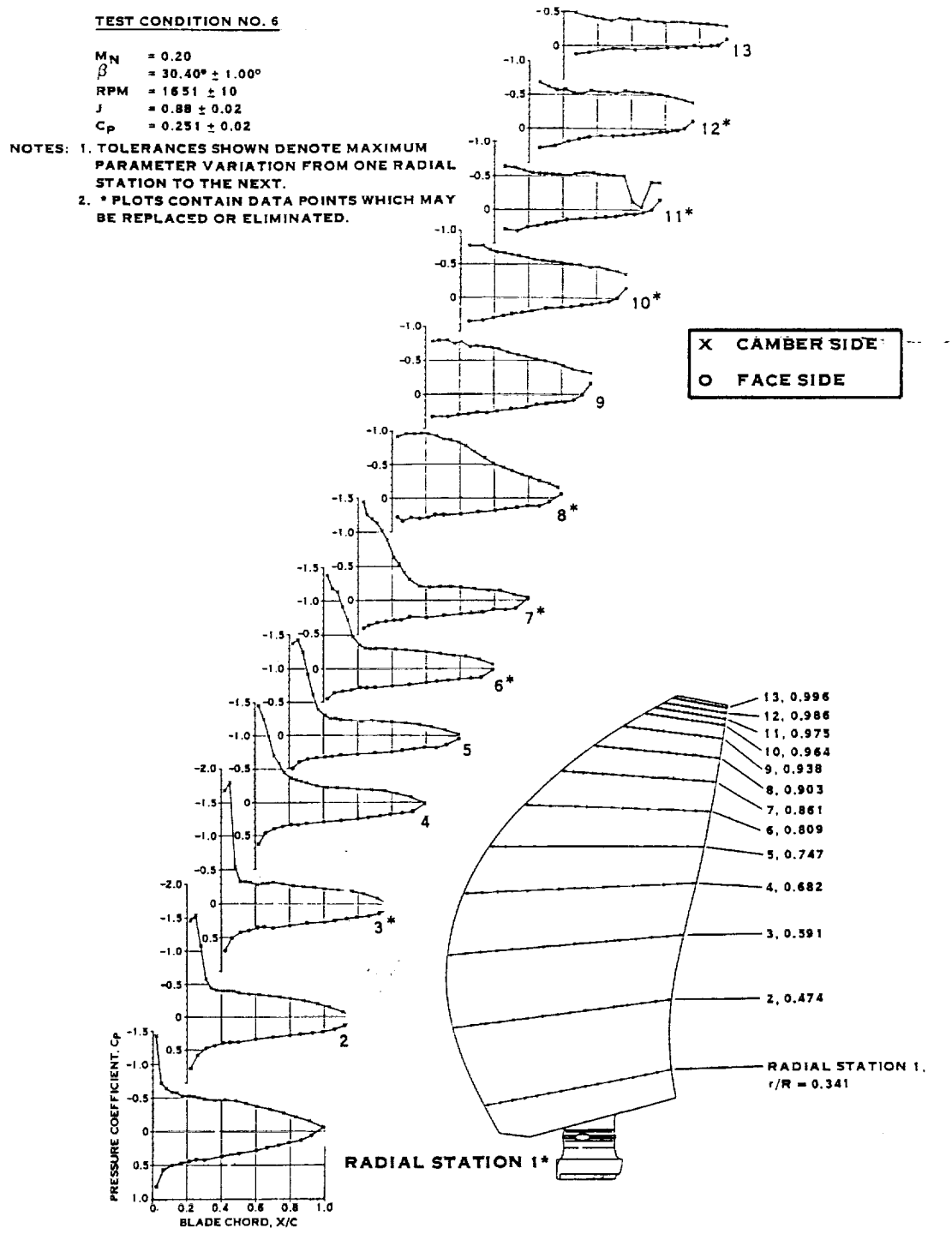

FIGURE 10-14. LAP SR-7L STEADY PRESSURE DISTRIBUTION (ON-LINE DATA)

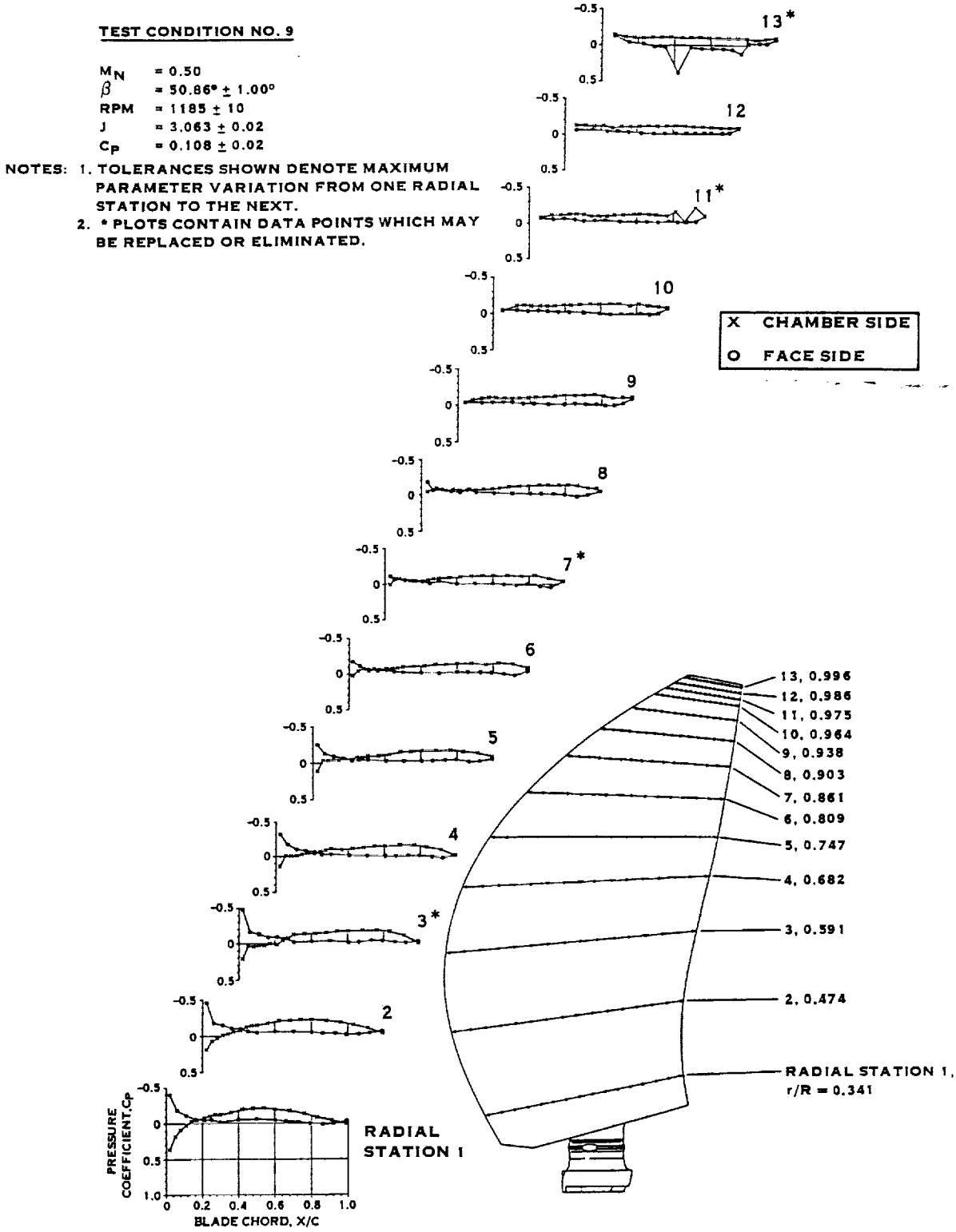

FIGURE 10-15. LAP SR-7L STEADY PRESSURE DISTRIBUTION (ON-LINE DATA)

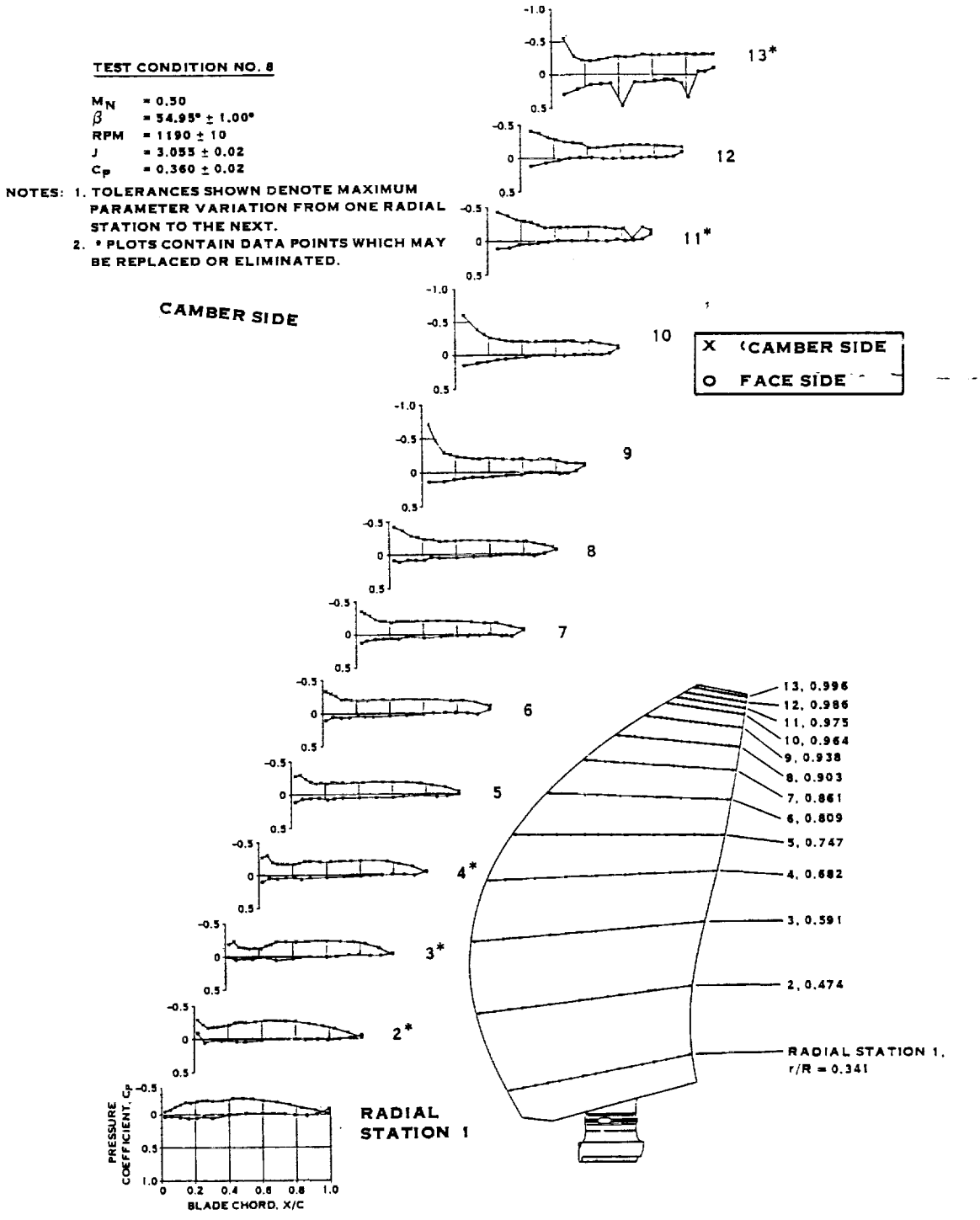

FIGURE 10-16. LAP SR-7L STEADY PRESSURE DISTRIBUTION (ON-LINE DATA)

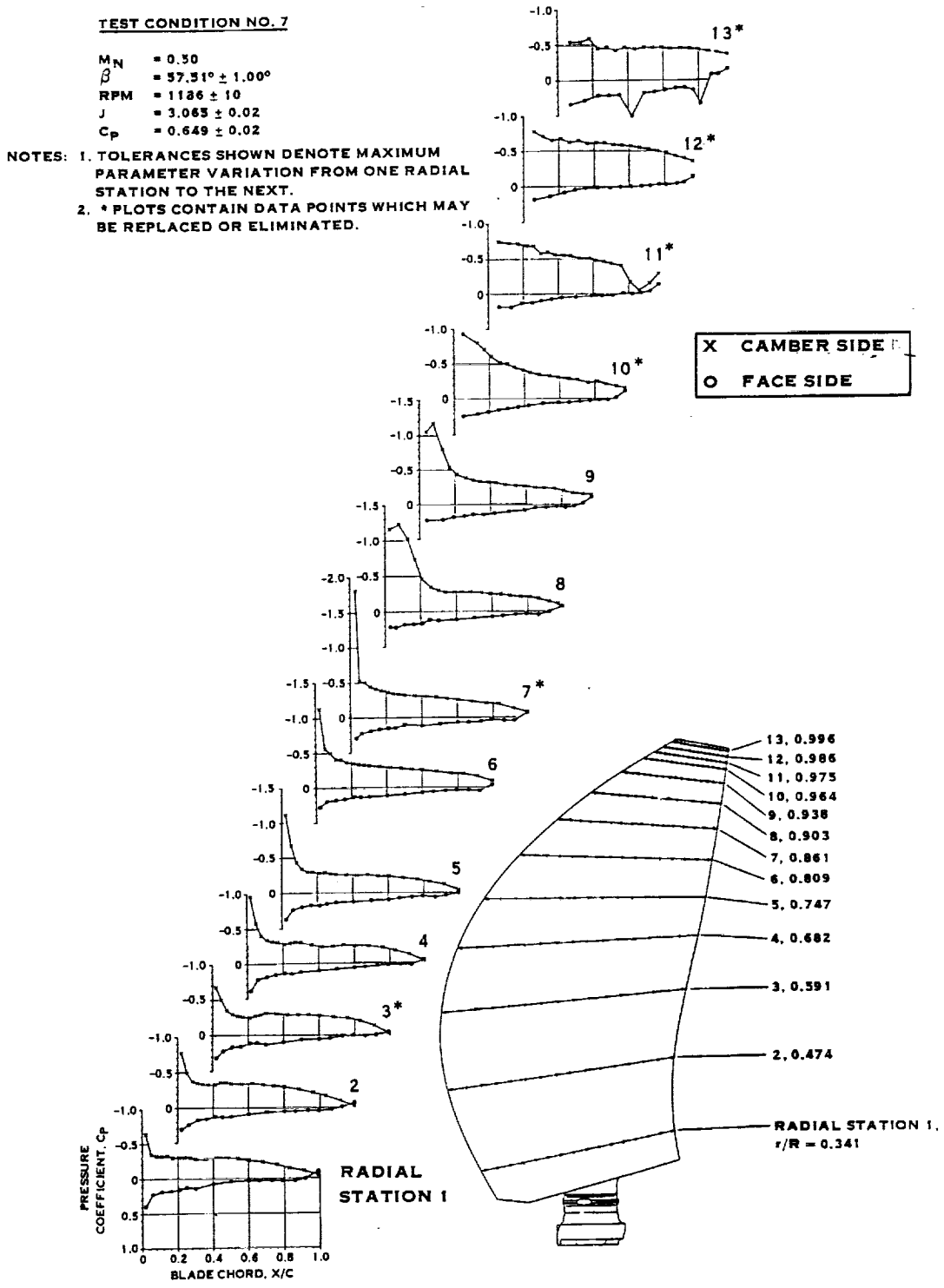

FIGURE 10-17. LAP SR-7L STEADY PRESSURE DISTRIBUTION (ON-LINE DATA)

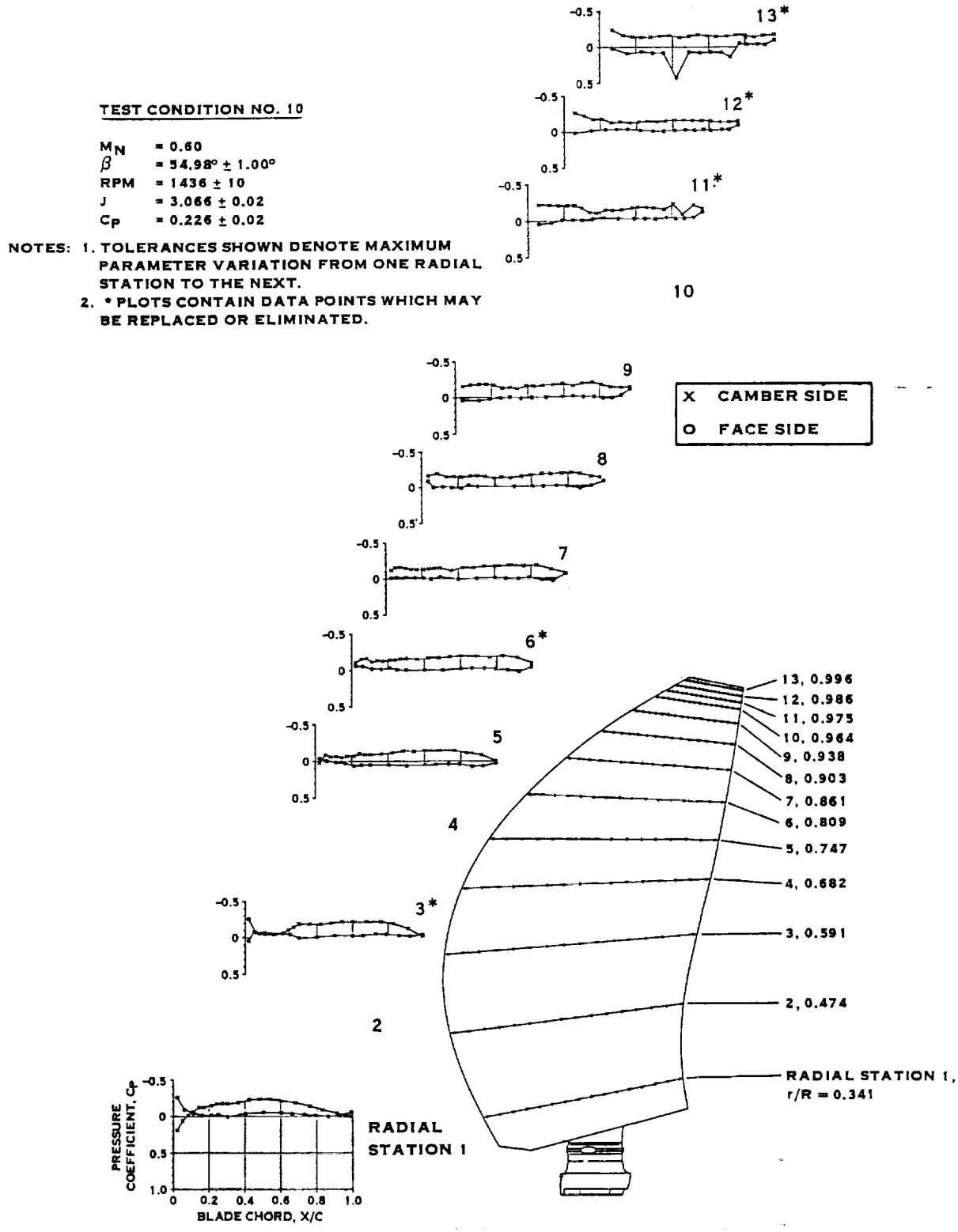

FIGURE 10-18. LAP SR-7L STEADY PRESSURE DISTRIBUTION (ON-LINE DATA)

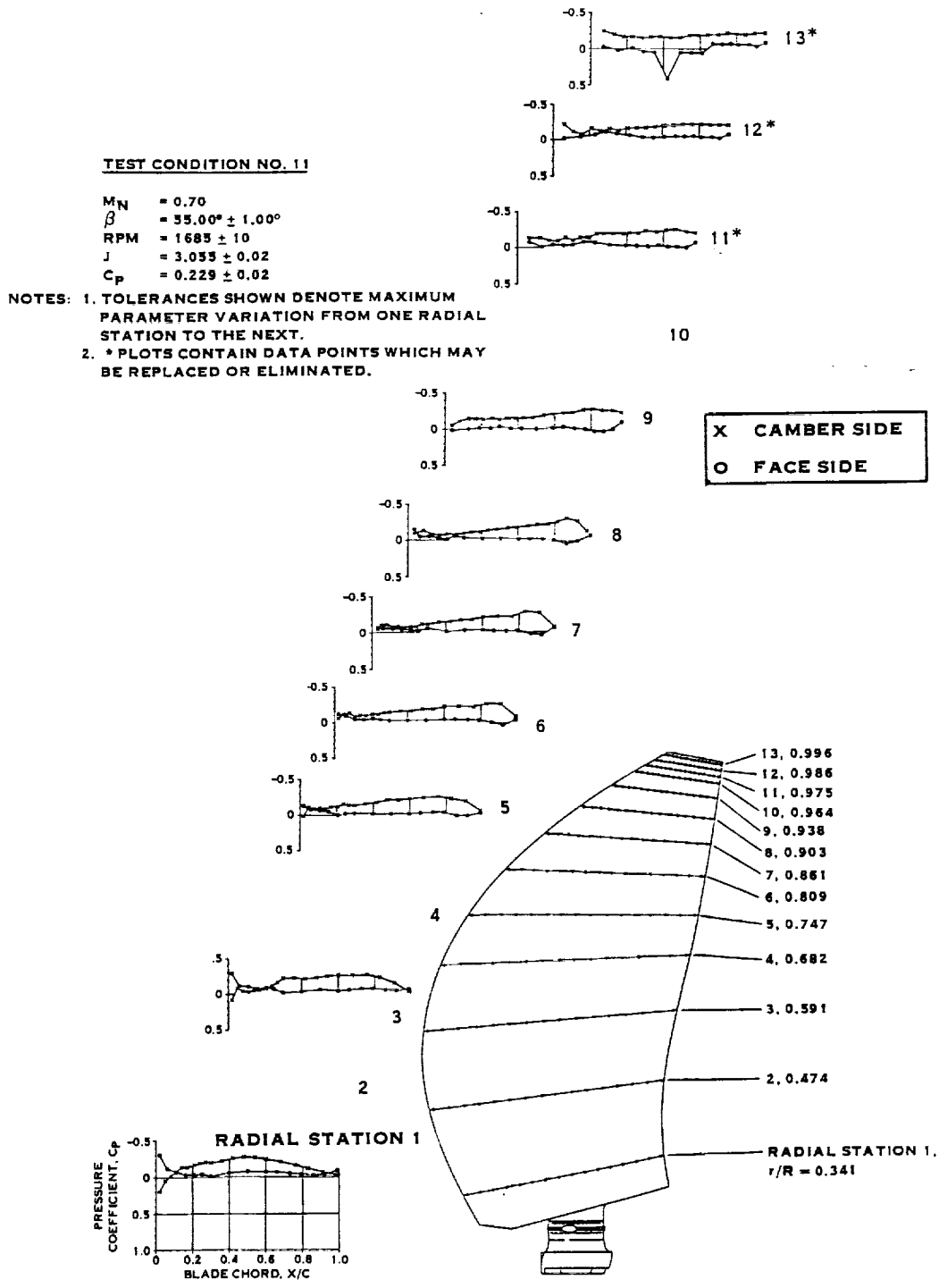

FIGURE 10-19. LAP SR-7L STEADY PRESSURE DISTRIBUTION (ON-LINE DATA)

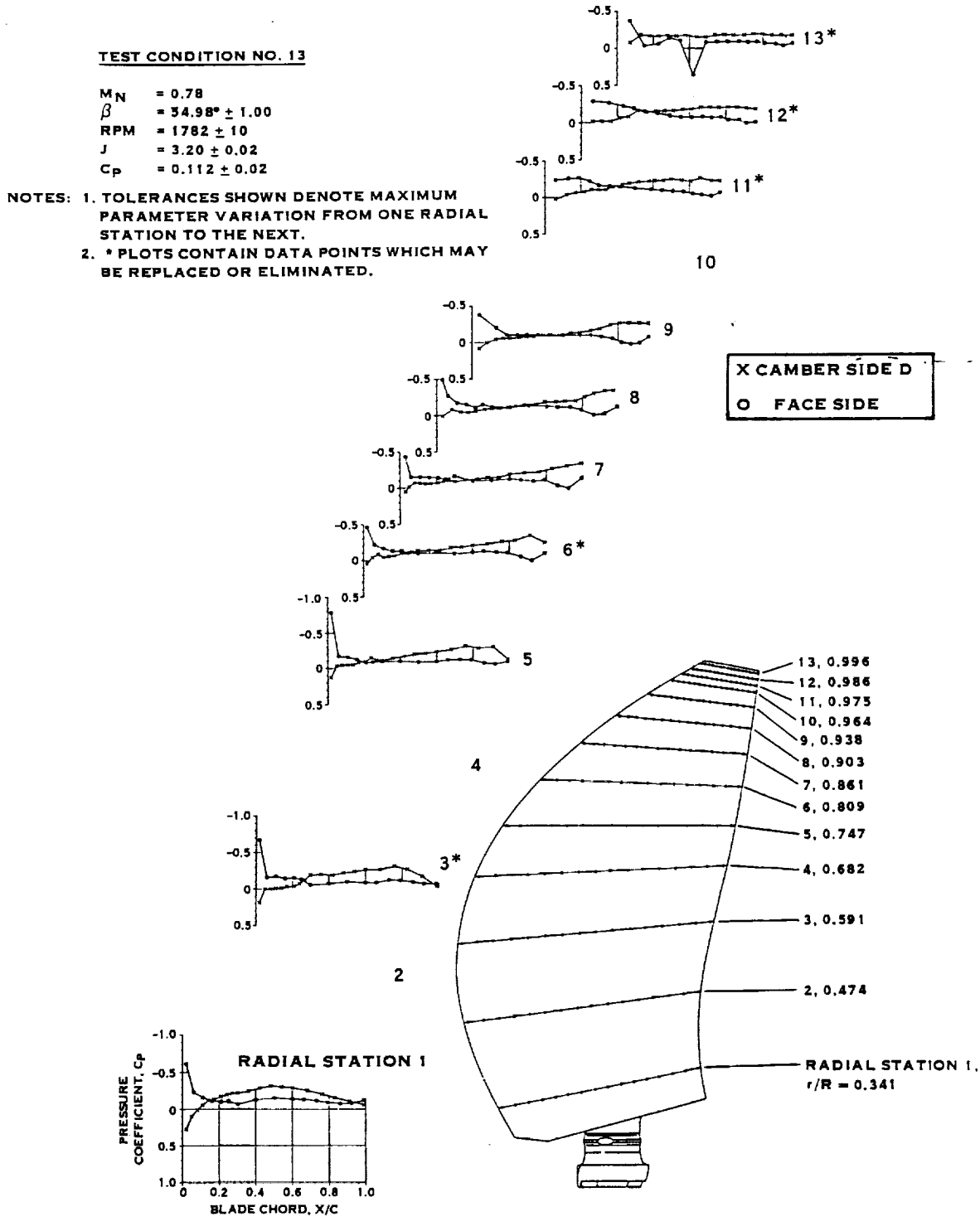

FIGURE 10-20. LAP SR-7L STEADY PRESSURE DISTRIBUTION (ON-LINE DATA)

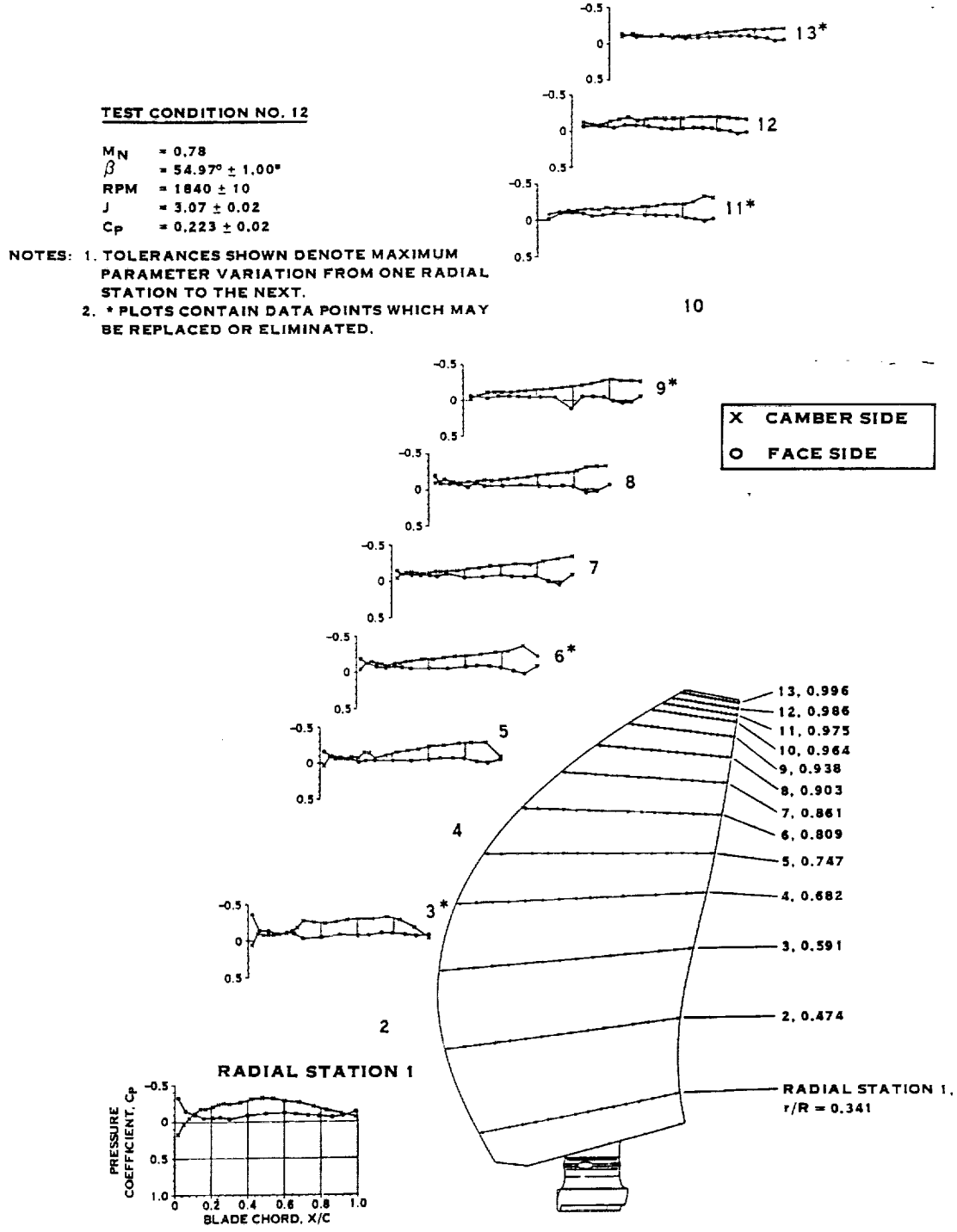

FIGURE 10-21. LAP SR-7L STEADY PRESSURE DISTRIBUTION (ON-LINE DATA)

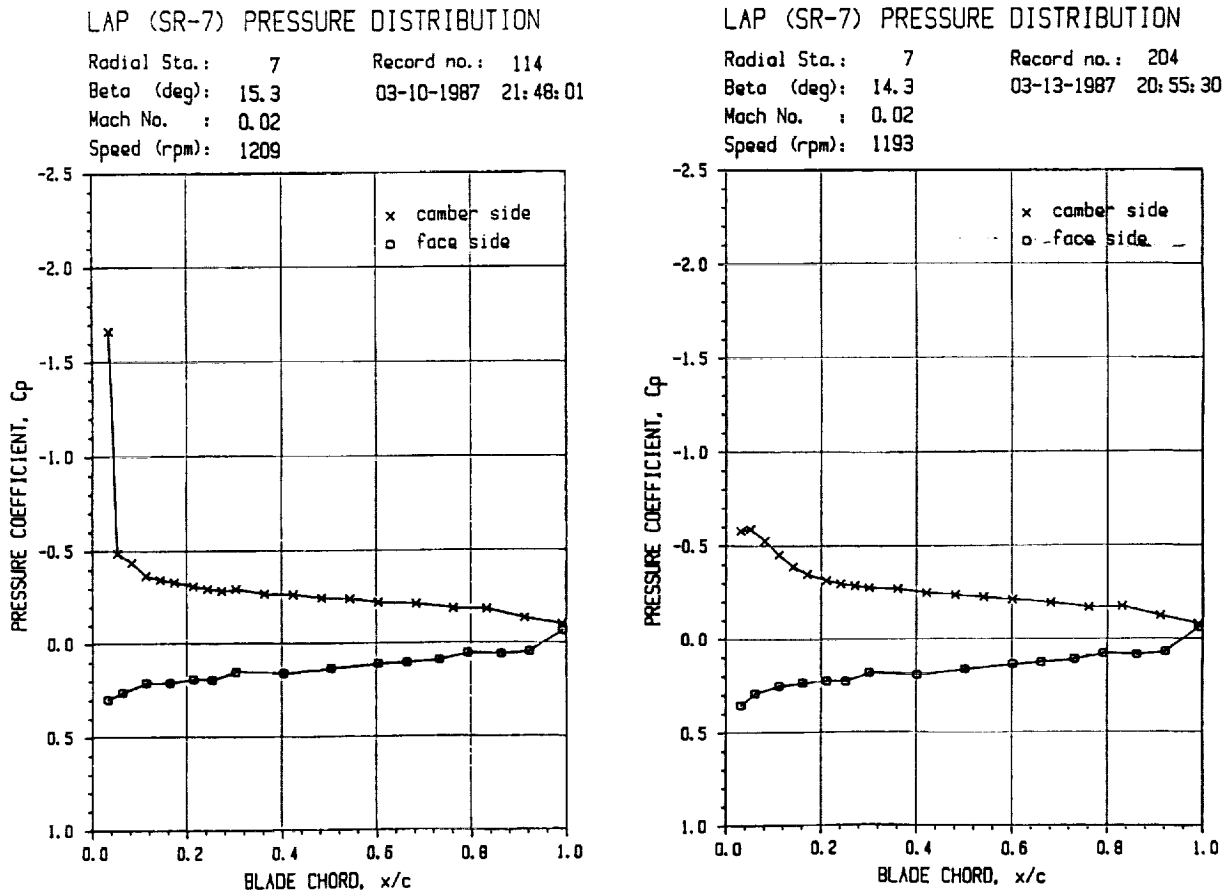

FIGURE 10-22. REPEATABILITY PROBLEM FOR STATIC LOW POWER POINT

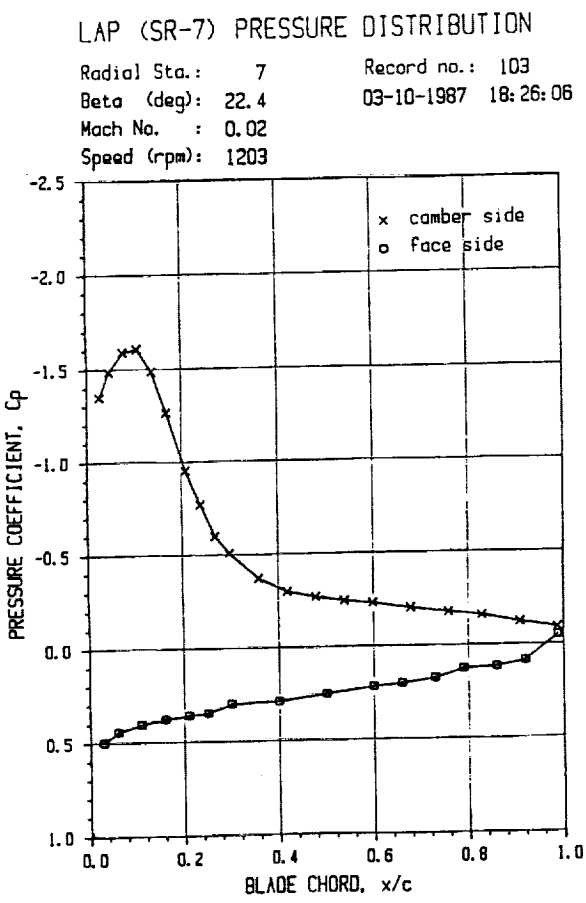

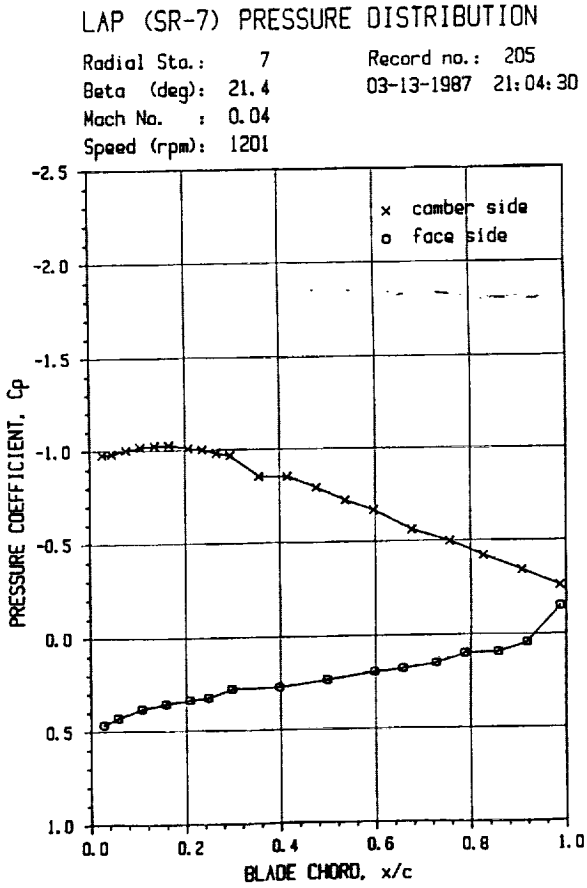

FIGURE 10-23. REPEATABILITY PROBLEM FOR STATIC HIGH POWER POINT

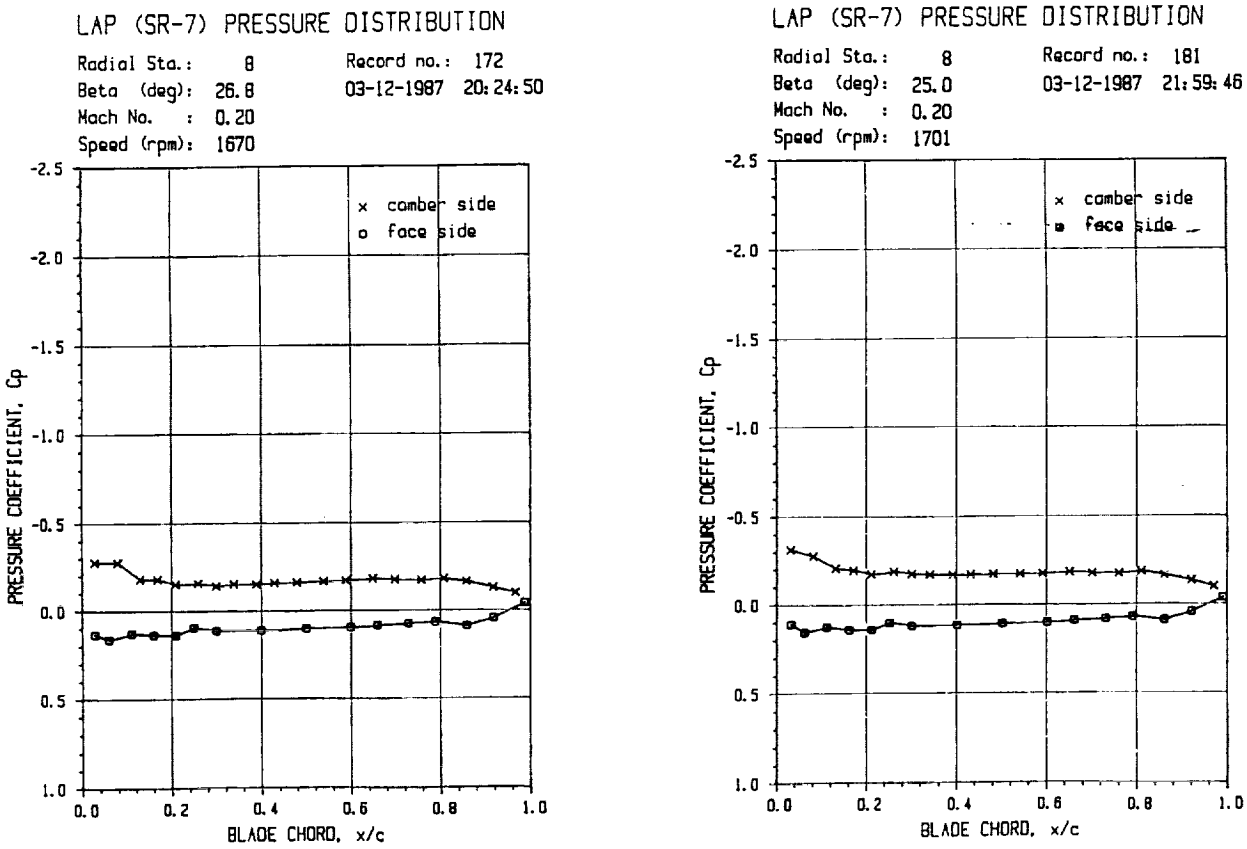

FIGURE 10-24. ILLUSTRATION OF REPEATABILITY AT 0.20 MACH NUMBER

11.0 BLADE SURFACE UNSTEADY PRESSURE MEASUREMENT

11.1 Test Objectives

11.1.1 Measure the unsteady pressure distribution on the surface of the SR-7L Prop-Fan blade for a range of blade angles, rotational speeds, and simulated flight Mach numbers for axial and angular inflow conditions.

11.1.2 Evaluate the effect of a wake in the propeller inflow on the unsteady pressure distribution on the surface of a blade.

11.2 Test Procedure

In preparation for blade surface unsteady pressure testing, the Prop-Fan was installed on the drive system as described in section 6.2, and supported as shown in Figures 11-1 and 11-2. Table 11-I shows the conditions that were tested.

The unsteady pressure measurement blade (S/N 054) was installed in blade position 3. For balancing purposes, the steady pressure measurement blade (S/N 009) was installed in position number 7, as shown in Figure 11-3. As a precaution, signals from 2 strain gages located on the shank of the unsteady pressure blade were monitored throughout the test. Special contour matching blade stubs were installed in the remaining 6 hub arm bores. The test rig power capabilities and tunnel time constraints necessitated conducting all testing using a 2 bladed Prop-Fan configuration, thereby permitting operation at power loadings per blade corresponding approximately to the take-off and cruise conditions of the eight blade Prop-Fan design.

The Prop-Fan was operated in the beta control mode during the entire test. In this mode, Hamilton Standard personnel were able to change the blade pitch angle during testing by means of an increase/decrease pitch switch located in the control room. For a fixed Mach number and a constant power supplied by the turbines, the Prop-Fan rotational speed was varied by increasing or decreasing blade pitch angle.

The blade pitch angle (ß3/4) was measured and recorded for each test point. An electrical signal proportional to blade angle was provided by means of a potentiometer mounted on the rotating side of the Prop-Fan as illustrated in Figure 5-3.

The Prop-Fan rotational speed was measured by use of a 1P pickup. The sensor was triggered by a gear mounted on the test rig drive shaft. The rotational speed was averaged over ten revolutions.

The power absorbed by the Prop-Fan was determined by multiplying the torque supplied to the Prop-Fan by the rotational speed. Torque supplied to the Prop-Fan was computed by accounting for the measured frictional losses in the test rig relative to the torque measured by the torquemeter.

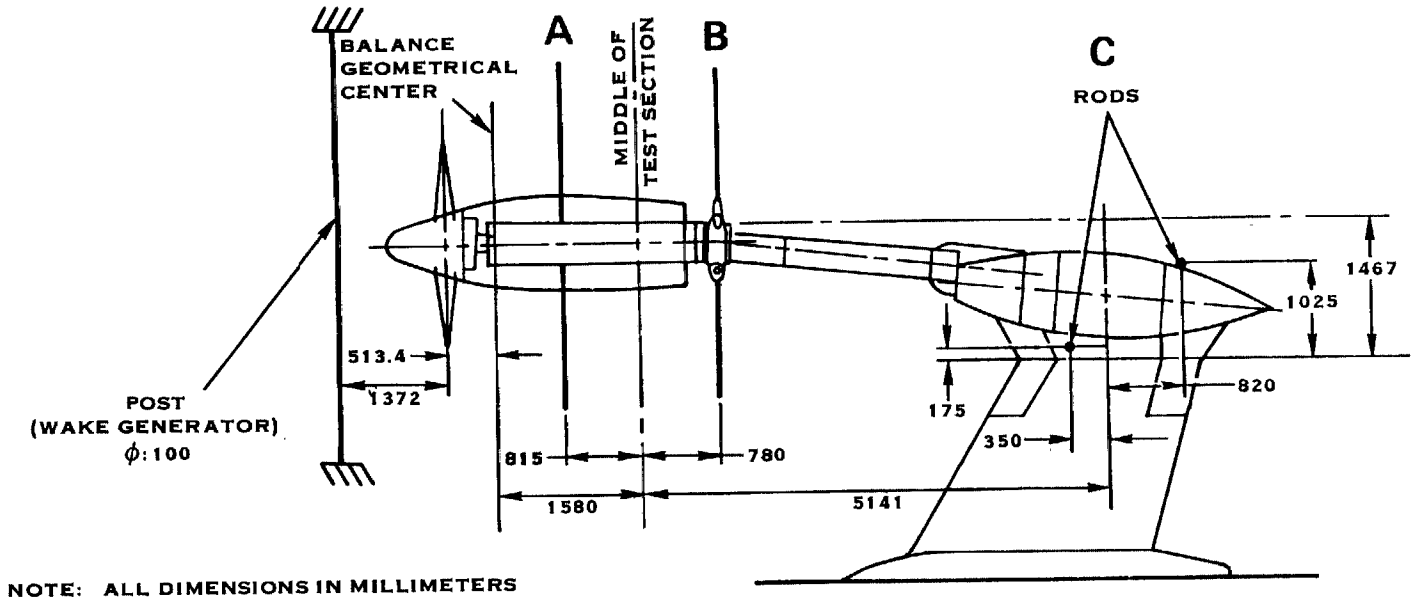

NOTE: ALL DIMENSIONS IN MILLIMETERS
ϕ= DIAMETER
L= LENGTH

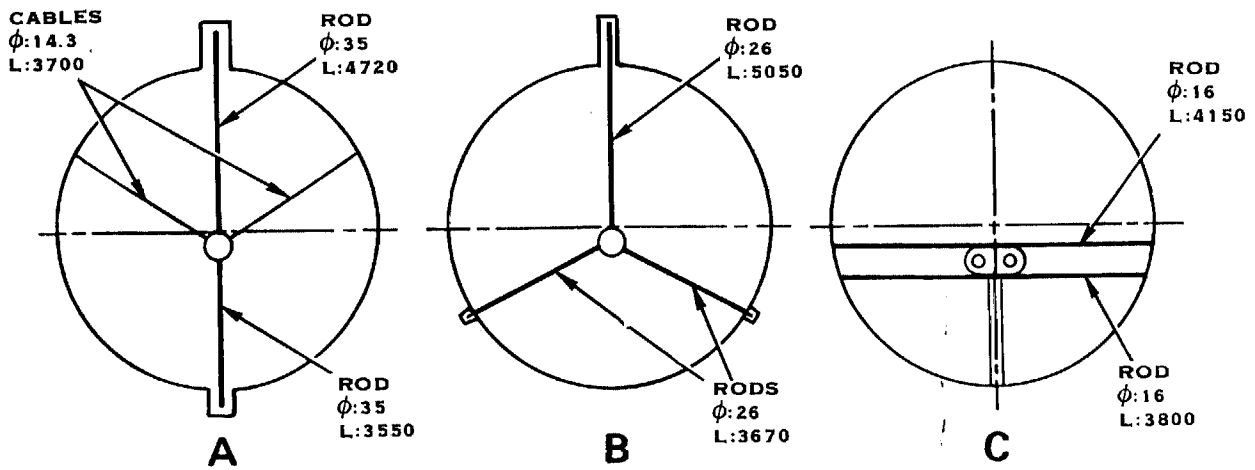

FIGURE 11-1. UNSTEADY PRESSURE TEST RIG SUPPORT STRUCTURE

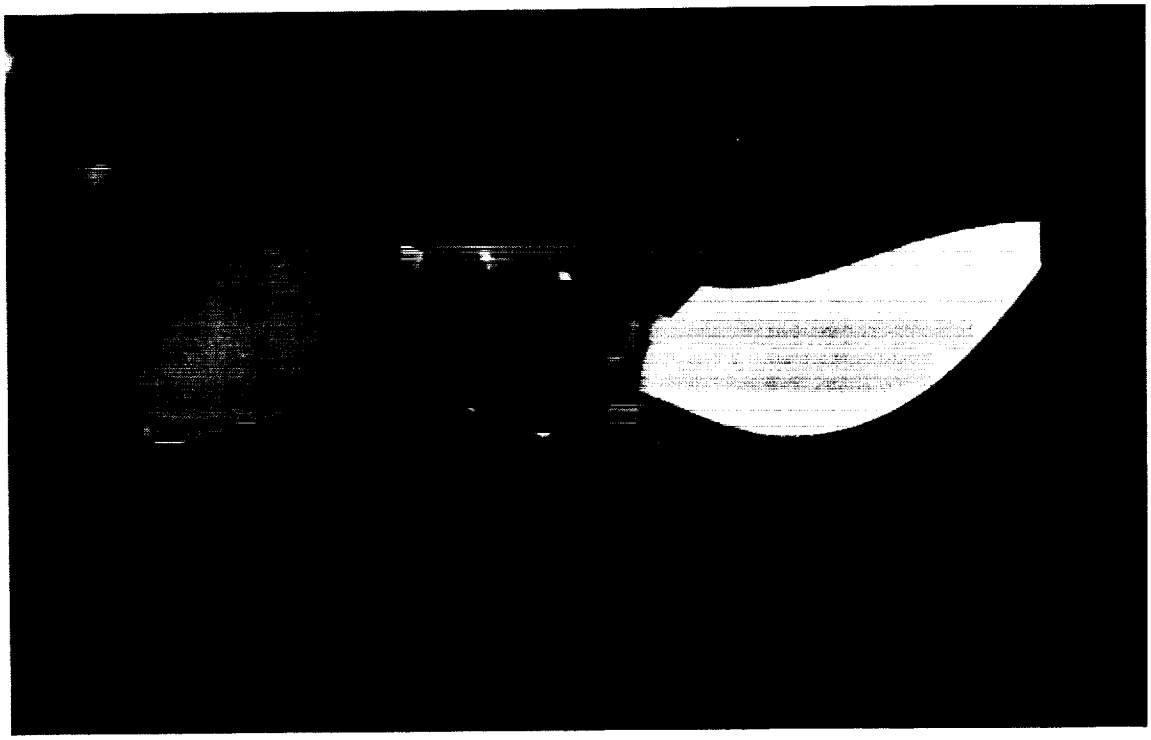

FIGURE11-2. PROP-FAN UNSTEADY PRESSURE TEST SET-UP

TABLE 11-I. OPERATING CONDITIONS FOR BLADE UNSTEADY PRESSURE TEST (2 BLADE LAP PROPELLER)

Condition No.	M Mach No.	J Advance Ratio ±.02	β Blade Angle ±1.00°	C_p Power Coefficient ±.02	N RPM ±10
2	.02	.14	15.70°	.093	1200
3	.02	.15	18.78°	.152	1200
4	.03	.18	21.60°	.204	1200
5	.20	.88	25.65°	.098	1665
5A	.20	.88	27.19°	.15	1684
5B	.20	.88	29.50°	.20	1684
6	.20	.88	30.40°	.251	1651
7	.50	3.065	57.51°	.649	1186
8	.50	3.055	54.95°	.360	1190
9	.50	3.063	50.86°	.108	1185
10	.60	3.066	54.98°	.226	1436
11	.70	3.055	55.00°	.229	1685

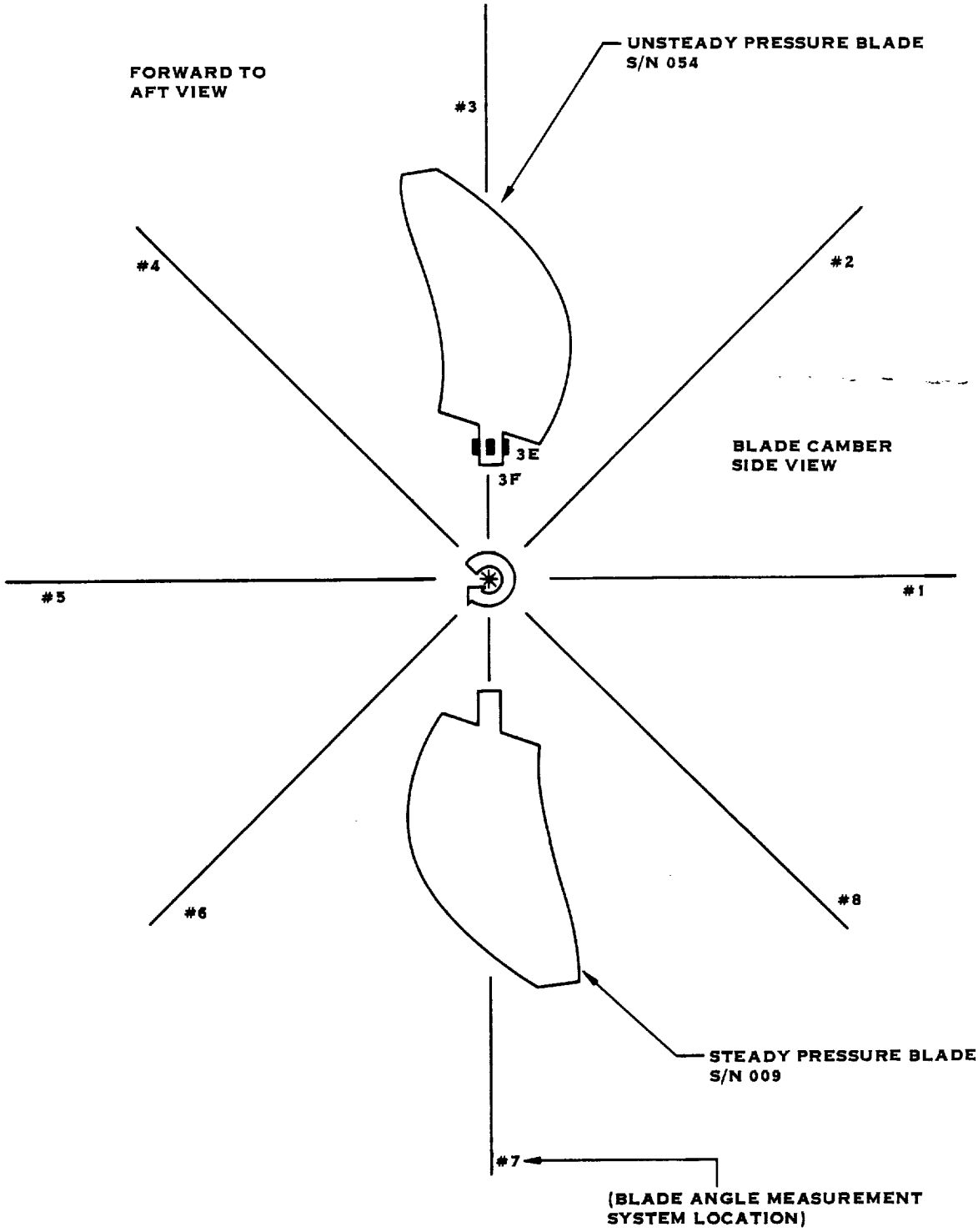

FIGURE 11-3. LAP BLADE INSTALLATION
UNSTEADY PRESSURE TEST (2 BLADE)

11.2 (Continued)

Mach number was established from the ratio of static pressure, measured four meters upstream of the Prop-Fan rotor, to stagnation pressure. Static pressure was also measured in the plane of rotation as a backup. The ratio of static to stagnation pressure was correlated with data taken during a pre-test calibration in order to compute the Mach number. The Prandlt-Young correction was applied to the computed Mach number to compensate for the effects of the tunnel walls and the thrust produced by the Prop-Fan.

Collection of blade surface unsteady pressure data was accomplished by utilizing a specially instrumented SR-7L blade as illustrated in Figures 11-4 and 11-5, coupled with an FM multiplex data acquisition system. Twenty-six high frequency response pressure transducers were installed in two rows on the face and camber sides of the unsteady pressure blade. The pressure transducer location and the numbering scheme used for data acquisition and reduction are depicted in Figures 11-6 and 11-7.

The pressure transducers were mounted flush with the blade surface as depicted in Figure 11-8. The signal and excitation wires from each transducer were connected to signal conditioning electronics located in the cuff of the blade. The signal wires also passed through attenuating resistors mounted on the blade root. The function of the attenuating resistors was to establish the gain for the pressure signals.

The unsteady pressure signals were transmitted from the rotating to the stationary field through the FM multiplex data acquisition system provided for the SR-7L Prop-Fan. The signals were monitored on a four-channel oscilloscope and recorded on a 14-track IRIG tape recorder.

The frequency response of the system was DC to 1000 Hz. Prior to the High Speed Wind Tunnel Test an evaluation program was conducted to determine the sensitivity of the transducers to temperature, strain, vibration, and centrifugal loading. The results of this test program indicated a maximum 2% of full scale error due to temperature in the range from 0 to 130°F and a maximum .92% of full scale error due to all other factors.

Generation of the wake in the Prop-Fan inflow was accomplished by erecting a vertical steel cylinder upstream of the rotor. The cylinder was 100mm (3.93 inches) in diameter and was located such that its centerline intersected the Prop-Fan axis of rotation at a distance of 1.372m (54.02 inches) upstream of the rotor plane. The wake generated by the cylinder was intended to create a twice per revolution (2P) disturbance for the instrumented blade to pass through. Figure 11-9 shows the Prop-Fan with the cylinder in place.

FIGURE 11-4. LAP UNSTEADY PRESSURE BLADE(CAMBER SIDE)

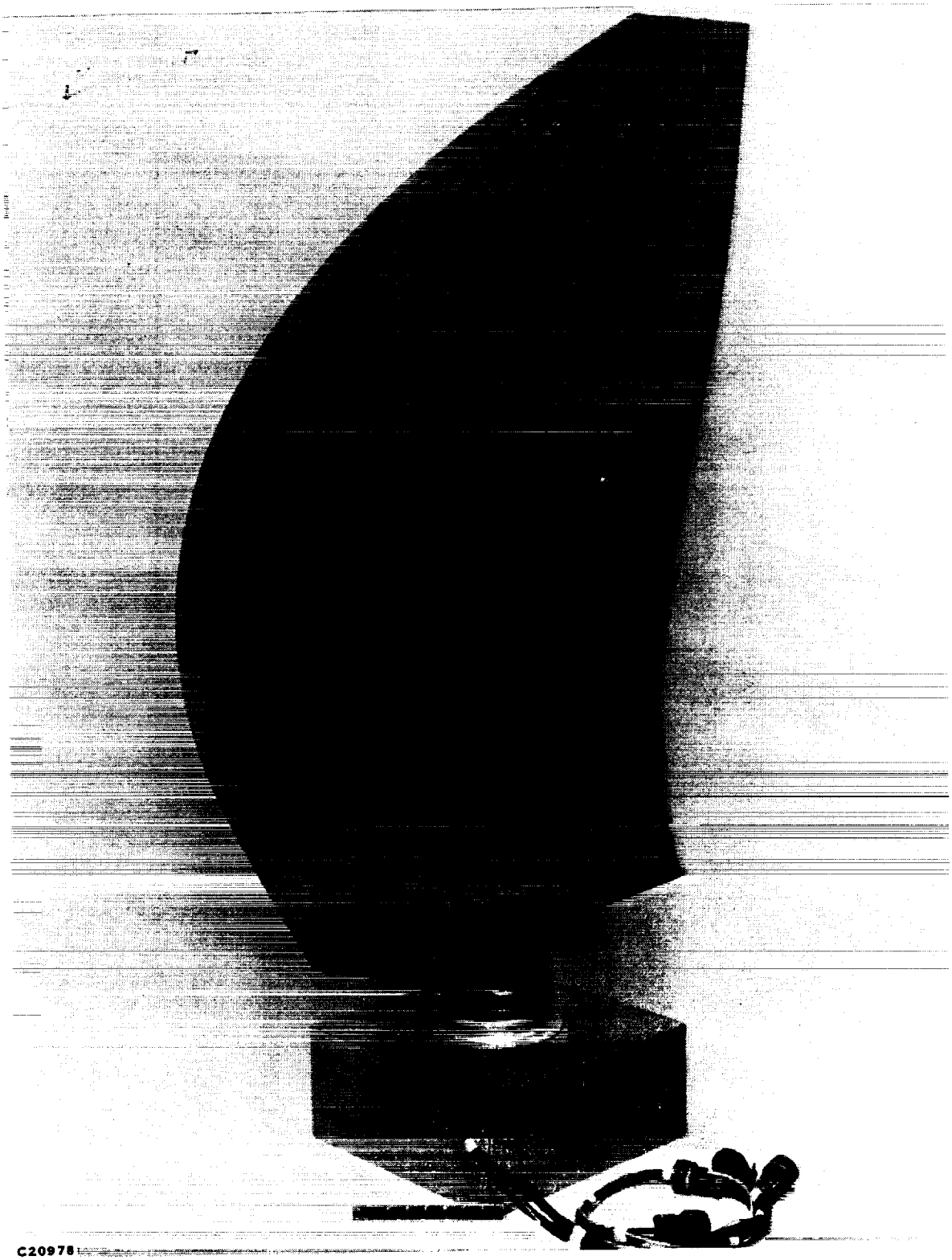

FIGURE 11-5. LAP UNSTEADY PRESSURE BLADE (FACE SIDE)

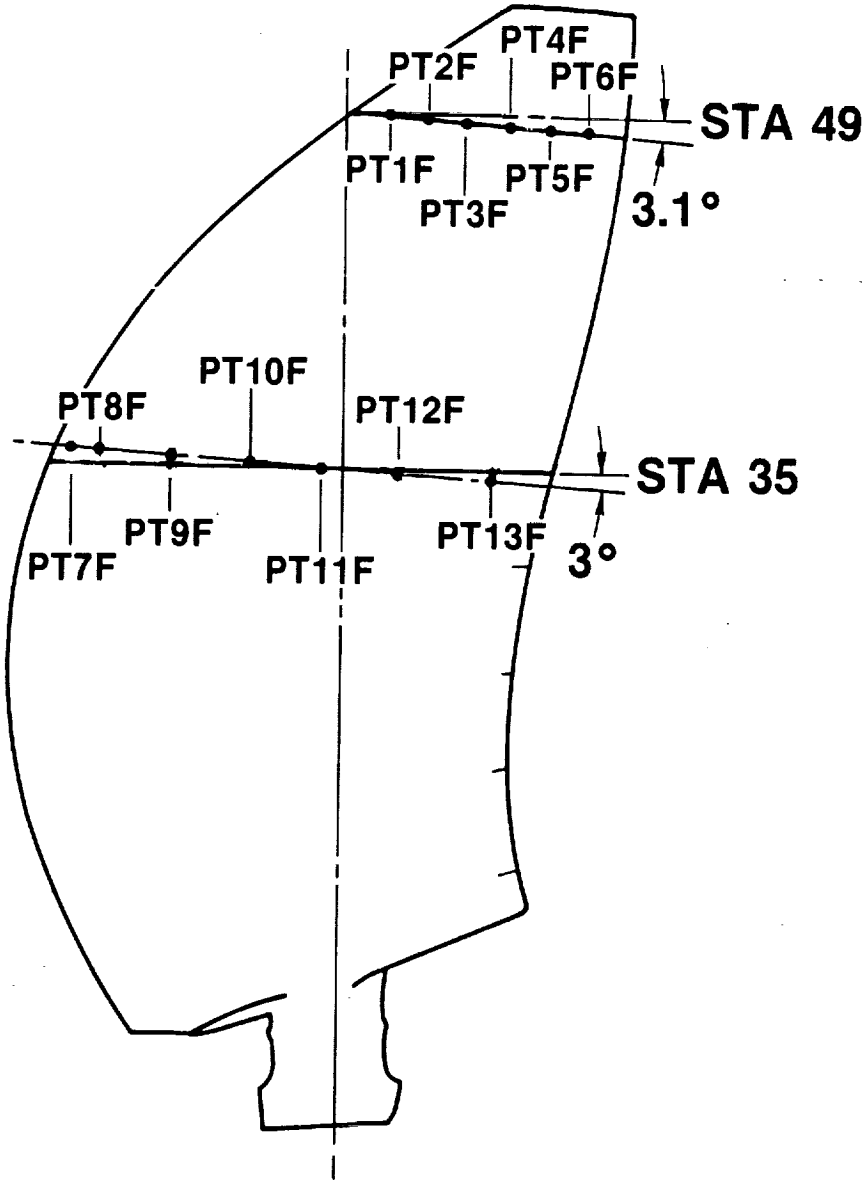

FIGURE 11-6 UNSTEADY PRESSURE BLADE, FACE SIDE TRANSDUCER LOCATIONS

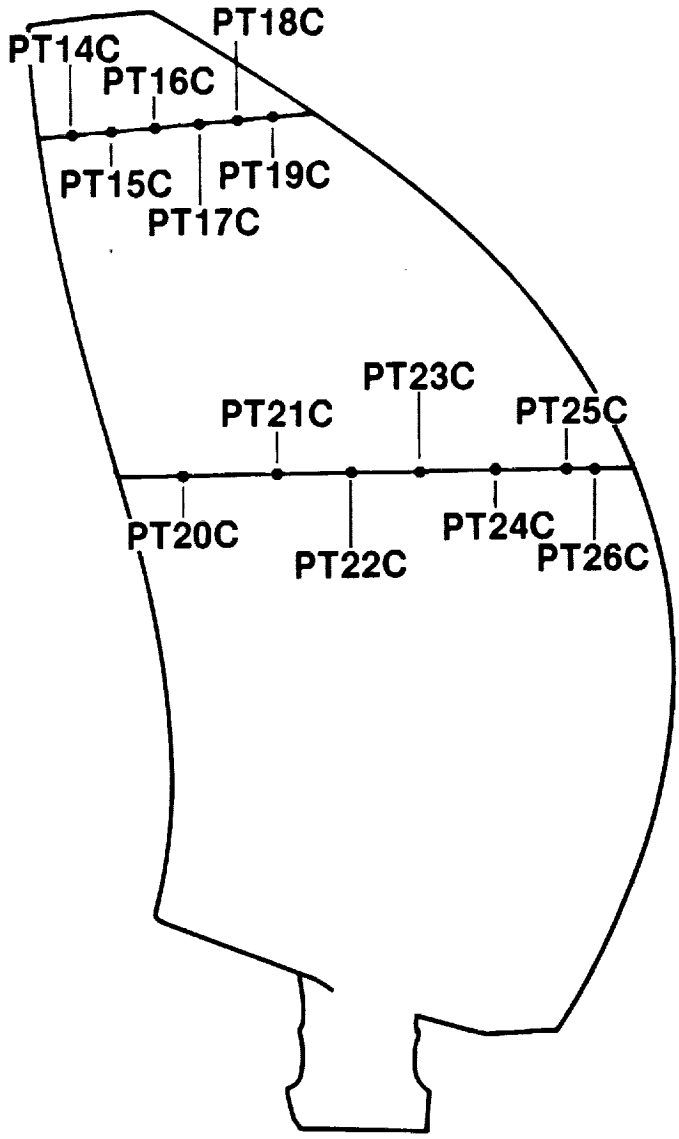

FIGURE 11-7 UNSTEADY PRESSURE BLADE, CAMBER SIDE TRANSDUCER LOCATIONS

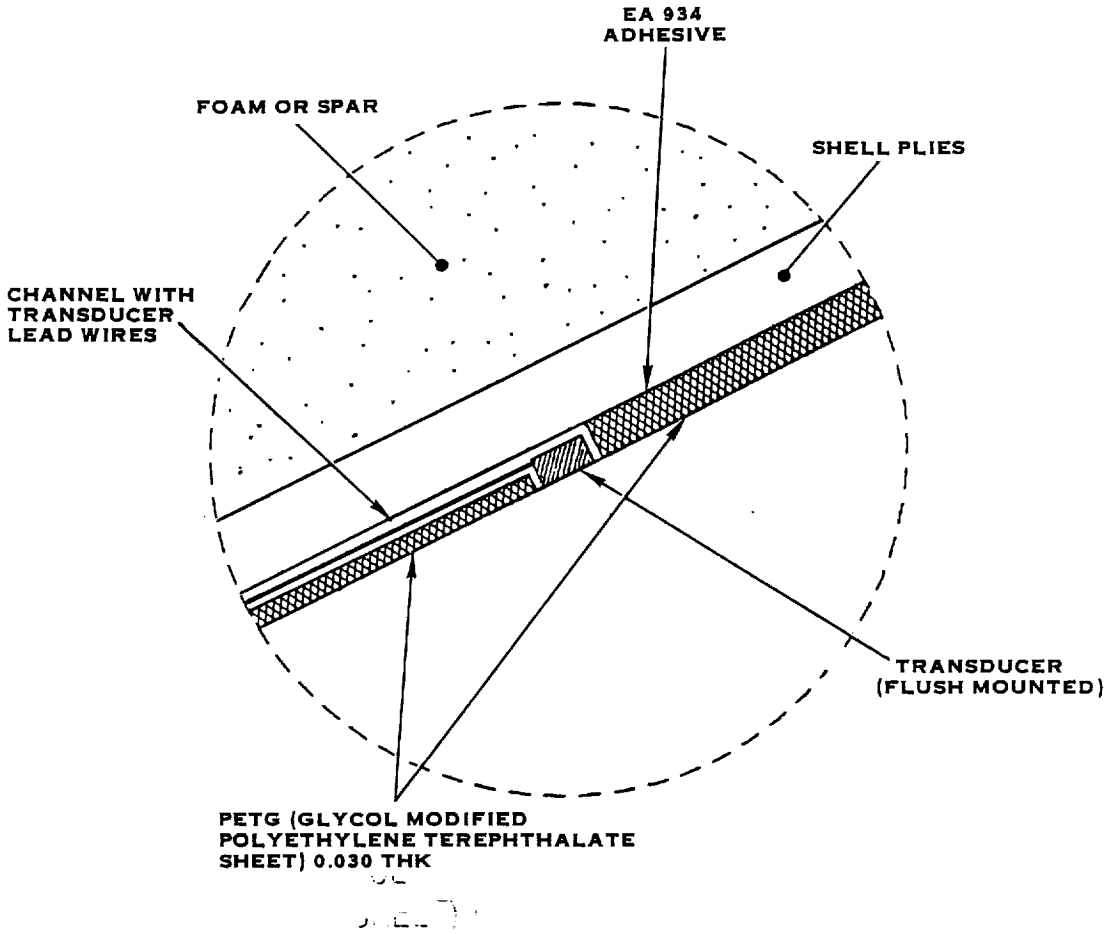

FIGURE 11-8 LAP SR-7L UNSTEADY PRESSURE BLADE TRANSDUCER MOUNTING

FIGURE 11-9. UNSTEADY PRESSURE TEST SET-UP WITH WAKE GENERATOR

11.2 (Continued)

The complete range of Prop-Fan operating conditions that were tested is given in Table 11-I. Because of time limitations, the range of conditions tested was reduced for the zero degree inflow cases with and without the cylinder. In addition, transducer wire problems resulted in intermittent and nonexistent signals on several sensors. The resulting series of test conditions for which signals were recorded is given for each transducer in Table 11-II.

11.3 Discussion and Results

To provide an illustration of the data collected during the test, examples are given in Figure 11-10 of the periodic variations in pressure (with corresponding frequency spectra) which were measured on the camber side of the blade at the 90% radius, 56% chord point (pressure transducer number PT16C). Here the three inflow cases are compared for the Prop-Fan operating condition defined below.

Mach number,	$M_N = 0.20$
Advance Ratio,	$J = 0.883$
Power Coefficient,	$Cp = 0.250$
Blade Angle,	$\beta = 32°$

This operating point is representative of the Prop-Fan take off condition.

The pressure versus time plots at the left in Figure 11-10 were obtained from a signal enhancing waveform analyzer. Sampling was initiated by the recorded once per revolution pip signal and waveforms from 1024 revolutions were averaged. Thus the repetitive portion of the pressure waveform is enhanced and the random part is suppressed. The spectra, shown at the right in Figure 11-10, were obtained via digital Fourier transform analysis. Successive time slices were transformed and averaged for 4.8 seconds. Each spectrum contains 400 frequency points spaced linearly from 0 to 500 Hertz.

Preliminary interpretation of Figure 11-10 is as follows:

In interpreting the waveforms, a transducer can be considered to be scanning the inlet flow as it rotates. Since the blade position is known as a function of time, the time axis can be converted to angular position. The six and twelve o'clock positions are indicated on the bottom trace. For the trace at the top of Figure 11-10, representing clean inflow, the signal level should be low, corresponding to a low distortion level. However, a small sinusoidal component can be seen in the waveform and spectrum that must be caused by a residual flow angularity in the tunnel. This can be considered a background level and must be subtracted from the data for the 3° angular inflow and for the cylinder wakes.

TABLE 11-II. CHART OF TRANSDUCERS FROM WHICH DATA WAS ACQUIRED VERSUS TEST CONDITION

✓ INDICATES THAT DATA WAS ACQUIRED

TRANSDUCER	0° INFLOW ANGLE WITHOUT CYLINDER								3° INFLOW ANGLE WITHOUT CYLINDER											0° INFLOW ANGLE WITH CYLINDER					
OPERATING CONDITION	4	5	5A	5B	6	7	8	9	2	3	4	5	5A	5B	6	7	8	9	10	11	4	5	5A	5B	6	9
PT1F																										
PT2F	✓	✓	✓	✓	✓	✓	✓	✓	✓	✓	✓	✓	✓	✓	✓	✓	✓	✓	✓		✓	✓	✓	✓		✓
PT3F																										
PT4F																										
PT5F	✓		✓	✓	✓	✓	✓	✓	✓	✓	✓	✓	✓	✓	✓	✓	✓	✓	✓		✓					✓
PT6F	✓	✓	✓	✓	✓	✓	✓	✓	✓	✓	✓	✓	✓	✓	✓	✓	✓	✓	✓		✓	✓	✓	✓		✓
PT7F																										
PT8F	✓	✓	✓	✓	✓	✓	✓	✓	✓	✓	✓	✓	✓	✓	✓	✓	✓	✓	✓	✓	✓	✓	✓	✓	✓	✓
PT9F		✓				✓	✓	✓	✓	✓	✓	✓	✓	✓	✓	✓	✓	✓	✓							✓
PT10F	✓	✓	✓	✓	✓	✓	✓	✓	✓	✓	✓	✓	✓	✓	✓	✓	✓	✓	✓		✓	✓	✓	✓	✓	✓
PT11F			✓	✓	✓	✓	✓	✓	✓	✓	✓	✓	✓	✓	✓	✓	✓	✓	✓							✓
PT12F			✓	✓	✓	✓	✓	✓	✓	✓	✓	✓	✓	✓	✓	✓	✓	✓	✓		✓	✓	✓	✓		✓
PT13F	✓	✓	✓	✓	✓	✓	✓	✓	✓	✓	✓	✓	✓	✓	✓	✓	✓	✓	✓		✓	✓	✓	✓		✓
PT14C																										
PT15C			✓	✓	✓	✓	✓	✓	✓	✓	✓	✓	✓	✓	✓	✓	✓	✓	✓		✓				✓	✓
PT16C	✓	✓	✓	✓	✓	✓	✓	✓	✓	✓	✓	✓	✓	✓	✓	✓	✓	✓	✓		✓	✓	✓	✓	✓	✓
PT17C									✓	✓	✓	✓	✓	✓	✓	✓	✓	✓	✓							
PT18C	✓								✓	✓	✓	✓	✓	✓	✓	✓	✓	✓	✓		✓					
PT19C																										
PT20C	✓	✓	✓	✓	✓	✓	✓	✓	✓	✓	✓	✓	✓	✓	✓	✓	✓	✓	✓	✓	✓	✓	✓	✓	✓	✓
PT21C									✓	✓	✓	✓	✓	✓	✓	✓	✓	✓	✓							
PT22C																										
PT23C			✓	✓	✓	✓	✓	✓	✓	✓	✓	✓	✓	✓	✓	✓	✓	✓	✓						✓	✓
PT24C			✓	✓	✓	✓	✓	✓	✓	✓	✓	✓	✓	✓	✓	✓	✓	✓	✓						✓	✓
PT25C			✓	✓	✓	✓	✓	✓	✓	✓	✓	✓	✓	✓	✓	✓	✓	✓	✓						✓	✓
PT26C			✓	✓	✓	✓	✓	✓	✓	✓	✓	✓	✓	✓	✓	✓	✓	✓	✓						✓	✓

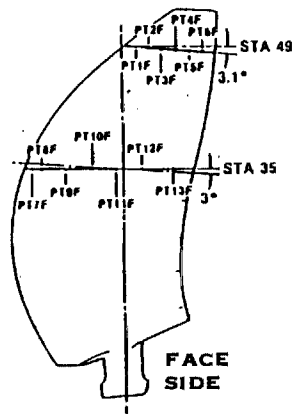

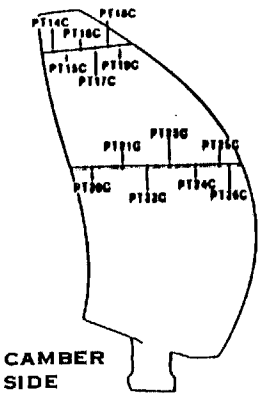

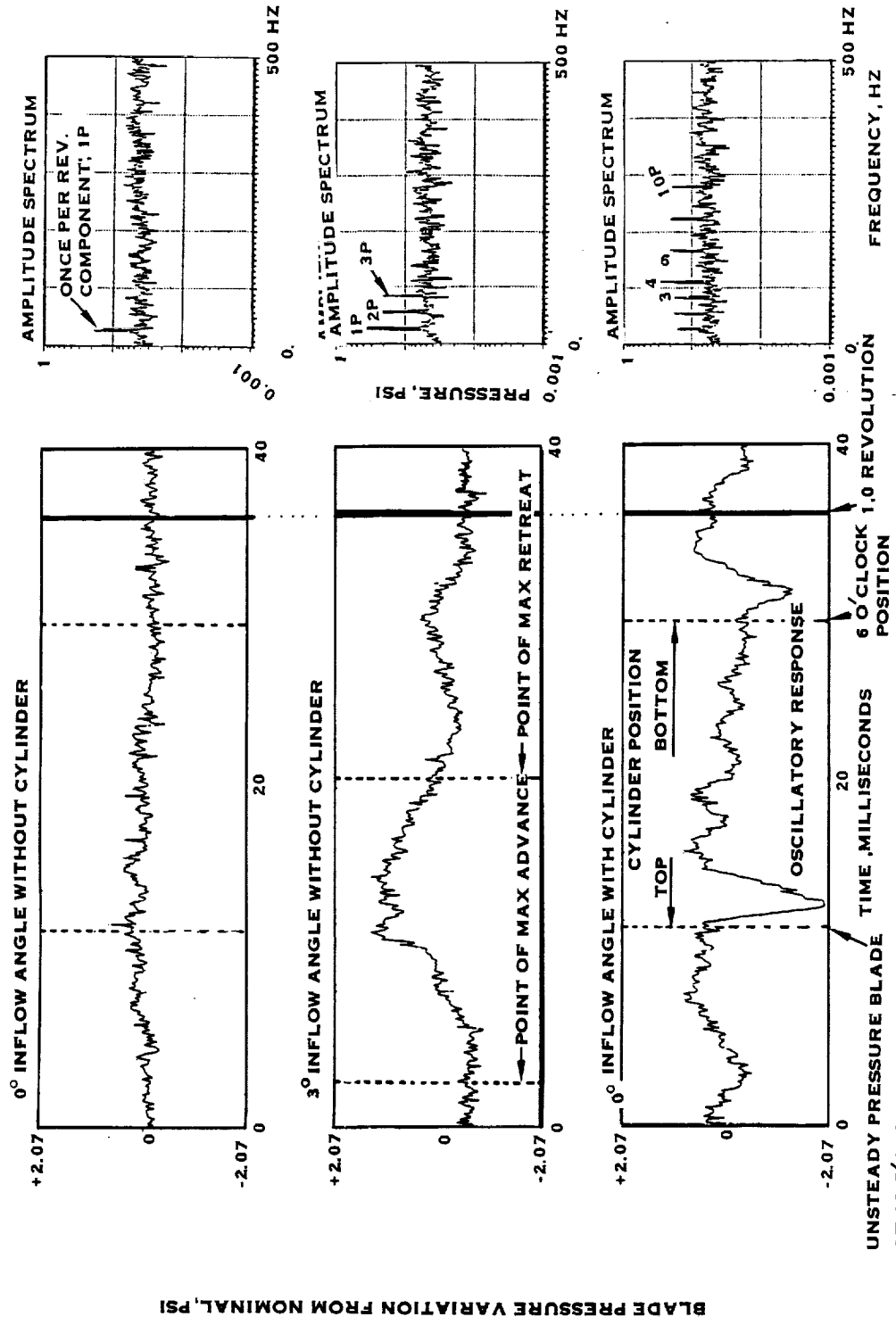

FIGURE 11-10. EXAMPLES OF THE MEASURED UNSTEADY PRESSURES

11.3 (Continued)

In the data for the 3° angular inflow, the angle of attack seen by the instrumented blade should be nearly a pure sine wave at the once per revolution (1P) frequency. Simplistic analysis would indicate that the blade pressure response should also be sinusoidal. The waveform and spectrum show that this is far from true. Figure 11-11 illustrates the terms "advancing" and "retreating" for angular inflow. Further evaluation of the data at other positions on the blade is required to identify the source of this non-sinusoidal behavior.

For the data with the cylinder wake, the blade pressure should respond with a pulse each time the blade passes through a wake at the top and bottom of the revolution. This behavior is observed in the bottom trace, but the pulse magnitudes are surprisingly different at the top and bottom positions. Another interesting feature of the data for cylinder wakes is the oscillating response after the wake pulse.

Sinusoidal response was observed on the pressure (face) side of the blade in all cases examined for angular inflow conditions.

Sinusoidal response was also observed on the suction (camber) side of the blade under low loading conditions. However, under high loading conditions, non-sinusoidal behavior is present. The non-sinusoidal response appears to be a result of leading edge and tip vortices which may be distorting the response. Another possibility is the formation and breakdown of the vortices as the angular inflow or wake inflow modulates the angle of attack.

An analysis of the blade unsteady surface pressure data will be presented in a separate NASA Contractor Report (Reference 25).

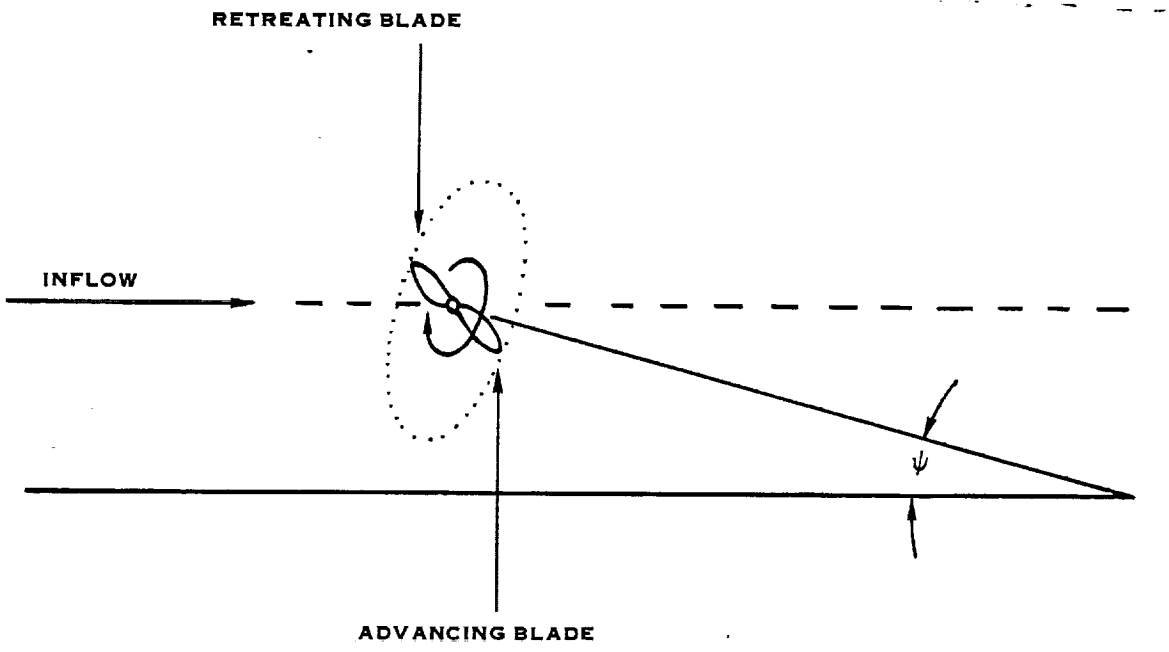

FIGURE 11-11. ILLUSTRATION OF THE TERMS "ADVANCING" AND "RETREATING" FOR ANGULAR INFLOW

12.0 CONCLUSIONS

The High Speed Wind Tunnel Test has provided an extensive evaluation of the operating characteristics of the SR-7L Large-Scale Advanced Prop-Fan. All the test objectives, set forth in the Plan of Test 267X-135 Rev. D, regarding acquisition of data were accomplished and 102 hours of operating experience were attained. No problems were uncovered that would have been considered an impedance to the planned follow-on PTA Flight Test. ONERA drive system constraints and testing problems precluded running all desired test points, however, those points successfully run did provide a wealth of aerodynamic performance, structural dynamic, steady and unsteady blade pressure information. Further areas of investigation are indicated that should ultimately result in highly accurate aerodynamic design and performance prediction methods. The conclusions and recommendations derived from each phase of the High Speed Wind Tunnel Test are presented in the following sections. Two separate low number NASA Contractor Reports will be published providing a more detailed evaluation of the blade surface steady and unsteady pressure tests.

12.1 Blade Structural Dynamic Evaluation

The SR-7L Prop-Fan was found to be free of high speed blade flutter over the entire operating envelope tested. All the measured blade surface and blade shank strains were below the allowables set prior to testing. These allowable levels were set to avoid accumulation of fatigue damage to the blades, therefore, no fatigue damage to the blades was incurred.

Reasonable correlation was found between the measured and analytically predicted 1P blade bending strains for the SR-7L blade. Results confirmed that 1P strain peaks inboard on the blade and lessens near the tip. Also, blade strains were found to increase with power and Mach number (all other variables held constant).

The interpretation of IRP (infrequently repeating peak) strain values was made difficult due to a significant amount of high frequency (>25P) noise in the signals. In general, this type noise is easily filtered out, however, this could not be done for the zero inflow angle data due to the low signal response levels. The angular inflow (3°) strains were determined from spectral analysis, the amplitudes of which were not affected by "noise" outside the frequency range of interest.

Significant 2P blade vibratory response was also measured for the 3° angular inflow case. The amplitude of the 2P response averaged approximately 25% of the 1P component response. It is concluded that at least a portion of the excitation force driving the 2P response was generated by the test rig drive system. Twice per revolution vibration is characteristic of a shaft with a universal joint. It is also noted that nonlinearities in the aerodynamic excitation, possibly due to observed vortex loading phenomena or tunnel inflow irregularities, are causes of higher order excitation.

12.1 (Continued)

Because RPM traces were not available for the data reduction effort, the harmonic content of the blade strains was determined from a "non-speed corrected" spectral analysis. The spectrum values were compared to values obtained from calculations of amplitude of the 1P bandpass filtered signals. It was concluded that the blade strain magnitudes from the spectral analysis were within 10% (low) of the actual magnitudes.

For comparison purposes, 1P strain predictions were also made for the angular inflow cases. Due to test constraints, angular inflow test data collection was limited to a 2 bladed Prop-Fan configuration at 3° inflow angle. Predictions were 16 to 31% higher than test data for the inboard response (flatwise shank moment and radial bending) and up to 13% lower than test for the outboard bending response. This is considered reasonable correlation, especially when it is considered that the measured values were perhaps up to 10% lower than correct. (See previous conclusion). As with earlier testing of the SR-7A 2 ft. diameter aeroelastic model, correlation of root response was marginal for the trailing edge, shear and chordwise gages (Reference 26).

12.2 Aerodynamic Performance Evaluation

Measured aerodynamic performance of the SR-7L Prop-Fan corresponded well with analytical predictions for the four blade configuration over the entire range of points tested. Similarly, good agreement between measured and predicted performance was found for the eight blade configuration at Mach numbers of .70 and .73. However, performance of the eight blade configuration was slightly underpredicted at .50 Mach number. The characteristic shape of the LAP performance curves were similar to those observed for the SR-7A aeroelastic model wind tunnel tests (Reference 27).

12.3 Blade Surface Steady Pressure Measurement

Steady pressure distributions were successfully measured on the blade surface at all of the 13 radial stations for Mach numbers of 0.03, 0.20 and 0.50, and at all radial stations except 2, 4 and 10 for Mach numbers of 0.60, 0.70 and 0.78. Subsequently, an uncertainty analysis was performed, which demonstrated that the measurement errors and uncertainties involved in this test, were acceptable.

Studies of the sensitivity of the correction for centrifugal loading on the column of air in the blade's pressure tap channels showed that the assumptions used in processing the data were valid.

During operation at approximate static rotor conditions, the inflow Mach number was 0.03 $\pm$0.015, where $\pm$0.015 is the maximum station-to-station variation in the Mach number. The pressure distributions were found to be very sensitive to Mach number for these conditions, so some respective station-to-station pressure distribution inconsistencies exist in these data.

12.3 (Continued)

The chordwise pressure loading is found to move aft with increasing relative Mach number for the 0.60, 0.70 and 0.78 Mach number cases.

Evidence of tip edge and leading edge vortex flows were found in the static rotor data and the 0.20 Mach number data.

The inverted leading edge pressure distributions observed during the low power high Mach number conditions, are typical for cambered airfoil sections operating at incidence below the design angle of attack value.

Evidence of trailing edge shock waves is present at the outboard radial stations in the 0.70 and 0.78 Mach number data.

12.4 Blade Surface Unsteady Pressure Measurement

Unsteady blade surface pressure data were successfully measured over the following range of conditions:

- Angular Inflow (3°) $0.02 \leq M_N \leq 0.70$
- Uniform Inflow (0°) $0.02 \leq M_N \leq 0.50$
- Inflow with Wake $0.03 \leq M_N \leq 0.50$

The uniform inflow data shows evidence of distortion. This appears to be a result of test section inlet asymmetry.

The angular inflow and wake data clearly shows unsteady pressure response. A dominant once-per-revolution response is evident in the angular inflow data while the wake data illustrates twice-per-revolution response as the instrumented blade passes the wake generating post.

Sinusoidal response was observed on the pressure (face) side of the blade in all cases examined for angular inflow conditions.

Sinusoidal response was observed on the suction (camber) side of the blade under low loading conditions. However, under high loading conditions, non-sinusoidal behavior is present. The non-sinusoidal response appears to be a result of leading edge and tip vortices which may be distorting the response. Another possibility is the formation and breakdown of the vortices as the angular inflow or wake inflow modulates the angle of attack.

LIST OF SYMBOLS

LIST OF SYMBOLS

A	-	area
A_N	-	incremental forward centerbody area at tap N
A_M	-	incremental aft centerbody area at tap M
AF	-	blade activity factor = $6250 \int_{\text{Hub/tip}}^{1.0} (b/D)\, X^3 dX$
a	-	area weighting factor
BHP	-	brake horsepower, KW
BF	-	buoyancy force, N
C_{CBDT}	-	centerbody drag coefficient without blades = $\frac{D_{CBT}}{q_o\,(A_{CB})}$
C_{CBDW}	-	centerbody drag coefficient with blades = $\frac{D_{CB}}{q_o\,(A_{CB})}$
C_{SD}	-	spinner drag coefficient = $\frac{D_S}{q_o\,(A_S)}$
C_P	-	power coefficient = $\frac{P}{\rho_o N^3 D^5}$
C_T	-	thrust coefficient = $\frac{T}{\rho_o N^2 D^4}$
C_{TNET}	-	net thrust coefficient = $\frac{T_{APP} - BF}{\rho_o N^2 D^4}$
c	-	speed of sound, m/sec
D	-	drag, N
D	-	diameter, m
EF	-	excitation factor = $\psi(V_T/644.8)^2(\rho/\rho_o)$

F	-	force, N
IRP	-	infrequently repeating peak
J	-	advance ratio = $60 \frac{V}{ND}$
M	-	Mach number
N	-	rotational speed, RPM
P	-	power, watt
P	-	pressure, N/cm^2
PA	-	pressure forces in the form $(P-P_o)$ Area, N
P_o	-	freestream static pressure, N/cm^2
P_N, P_M	-	static pressure at tap N, M
P_T	-	total pressure, N/cm^2
P_{STAG}	-	stagnation pressure, N/cm^2
Q	-	torque, N·m
q_o	-	dynamic pressure, N/cm^2
r	-	radius, m
r/R	-	fractional radius
SHP	-	shaft horsepower
T	-	thrust, N
T_{STAG}	-	stagnation temperature, °K
T_s	-	static temperature, °K
T_t	-	total temperature, °K
V	-	velocity, m/sec
ß	-	blade angle, deg
η	-	efficiency

ρ	-	mass density, Kg/m^3
ψ	-	inflow angle, deg
τ	-	$\frac{\text{thrust}}{\rho(\text{disc area})V^2}$
α	-	$\frac{\text{disc area}}{\text{tunnel cross-section area}}$

Subscripts

APP	-	apparent
B	-	balance
BP	-	back pressure
CB	-	centerbody
CBT	-	centerbody tare
C, COR	-	corrected
FL	-	functional losses
MEAS	-	measured
N	-	number
NET	-	net
o	-	free stream
S	-	spinner
t	-	tangential
T	-	true
TH	-	thermal effects
TNET	-	net thrust

REFERENCES

REFERENCES

1. J.B. Whitlow and G.K. Sievers, "Fuel Savings Potential of the NASA Advanced Turboprop Program," NASA TM-83736, 1984.

2. J.F. Dugan, Jr., NASA LeRC, B.S. Gatzen and W.M. Adamson, United Technologies, "Prop-Fan Propulsion - Its Status and Potential", SAE Paper 780995, November 1978.

3. "Cost/Benefit Tradeoffs for Reducing the Energy Consumption of the Commercial Air Transportation System, Douglas Aircraft Co; NASA Ames Contract NAS2-8618, NASA CR-137925 Summary Report, June 1976.

4. "Study of the Cost/Benefit Tradeoffs for Reducing the Energy Consumption of the Commercial Air Transportation System", Lockheed-California Company, NASA Ames Contract NAS2-8612, NASA CR-137927 Summary Report, August 1976.

5. "Energy Consumption Characteristics of Transports Using the Prop-Fan Concept", Boeing Commercial Airplane Company, NASA Ames Contract NAS2-9104, NASA CR-137938 Summary Report, October 1976,

6. "Study of Unconventional Aircraft Engines Designed for Low Energy Consumption", Pratt-Whitney Aircraft, NASA Lewis Contract NAS3-19465, NASA CR-135065 Final Report, June 1976.

7. "Study of Cost/Benefit Tradeoffs for Reducing the Energy Consumption of the Commercial Air Transportation System", United Airlines, NASA Ames Contract NAS2-8625, NASA CR-137891, June 1976.

8. "Study of Unconventional Aircraft Engines Designed for Low Energy Consumption", General Electric Co., NASA CR-135136, December 1976.

9. "Fuel Conservation Merits of Advanced Turboprop Transport Aircraft", Lockheed-California, NAS2-8612, NASA CR-152096 August 1977.

10. NASA Tech. Mem. 83736 "Fuel Saving Potential of NASA Advanced TurboProp Program", September 1984.

11. D.C. Mikkelson, G.A. Mitchell, and L.J. Bober, "Summary of Recent NASA Propeller Research", NASA TM-83733, 1984.

12. NASA CR 3505 "Evaluation of Wind Tunnel Performance Testing of an Advanced 45° Swept Eight Bladed Propeller at Mach numbers from .45 to .85", Hamilton Standard Division, Windsor Locks, CT, March 1982.

13. C.L. DeGeorge, J.E. Turnberg, H.S. Wainauski, "Large-Scale Advanced Prop-Fan (LAP) Static Rotor Test Report", Hamilton Standard Division UTC, Windsor Locks, CT (NASA CR-180848).

14. W.E. Sullivan, J.E. Turnberg, J.A. Violette, "Large-Scale Advanced Prop-Fan (LAP) Blade Design," Hamilton Standard Division, Windsor Locks, CT, (NASA CR-174790).

15. R.A. Schwartz, P. Carvalho, M.J. Cutler, "Large-Scale Advanced Prop-Fan (LAP) Pitch Change Actuator and Control Design Report", Hamilton Standard Division, Windsor Locks, CT, January 1986 (NASA CR-174788).

16. M. Soule, "Large-Scale Advanced Prop-Fan (LAP) Hub/Blade Retention Design Report," Hamilton Standard Division, Windsor Locks, CT (NASA CR-174786).

17. B. Huth, "System Design and Integration of the Large-Scale Advanced Prop-Fan, "Hamilton Standard Division, Windsor Locks, CT, August 1984, (NASA CR-174789).

18. Pierre, M. "Characteristiques et Possibilite de la Grand Soufflerie Sonique de Modane-Avrieux," ONERA Technical Note 134, 1968.

19. Masson, A. "Essair D'Helices dans la Grande Soufflerie de Modane-Avrieux," ONERA Technical Note 161, 1970.

20. Pope, A., "Wind-Tunnel Testing," John Wiley and Sons, 1954.

21. R.M. Reynolds, R.I. Sammonds and G.C. Kenyon, "An Investigation of a Four Blade Single-Rotation Propeller in Combination with an NACA 2-Series, D-Type Cowling at Mach numbers up to 0.83", NASA RM A53B06, April 13, 1953.

22. H.Glauert, "Airplane Propellers, Body and Wing Interference", Volume IV, Division 2, Chapter VIII, Aerodynamic Theory, W.F. Durand, editor Juluis Springer (Berlin), 1935 (Dover reprint 1963).

23. "BESTRAN User's Guide, Auxiliary Program ST570", D.C. Jennings, December 14, 1977.

24. Bushnell, P.R., "Measurement of the Steady Surface Pressure Distribution on a Single Rotation Large Scale Advanced Prop-Fan Blade at Mach numbers from 0.03 to 0.78", (NASA CR-182124).

25. Bushnell, P.R., Gruber, M.E., and Parzych, D.J., "Measurement of the Unsteady Surface Pressure Distribution on a Single Rotation Large Scale Advanced Prop-Fan Blade at Mach numbers from 0.03 to 0.70", (NASA CR-182123).

26. D. Nagle, S. Auyeung, J. Turnberg, "SR-7A Aeroelastic Model Design Report", Hamilton Standard Division UTC, Windsor Locks, CT (NASA CR-174791).

27. G. Stefko, G. Rose, G. Podboy, "Wind Tunnel Performance Results of an Aeroelastically Scaled 2/9 Model of the PTA Flight Test Prop-Fan", AIAA-87-1893.

APPENDIX A

CHRONOLOGICAL HISTORY OF TEST

APPENDIX A

CHRONOLOGICAL HISTORY OF TEST

Testing of the LAP Prop-Fan started on February 20, 1986 and continued until April 9, 1986. The test was terminated at this point following the discovery of severe fretting corrosion in the ONERA drive shaft retention area. During this time period, 55 hours and 3 minutes of test time were accumulated.

Testing resumed on February 27, 1987 and continued until March 19, 1987. The intent of the second phase of testing was to collect blade steady and unsteady surface pressure data utilizing a 2 blade configuration. Testing was successfully completed after accumulating an additional 47 hours and 10 minutes of test time.

The following tabulation provides a chronological history of the entire High Speed Wind Tunnel Test conducted at the ONERA facility in Modane, France.

CHRONOLOGICAL HISTORY OF TEST

Date	Event	Test Time (Hr. : Min.)	Accum. Test Time (Hr. : Min.)
January 13, 1986	H.S. personnel at tunnel - ONERA setting up on test rig.	-	-
January 14, 1986	H.S. stationary instrumentation installed - ONERA working on drive system.	-	-
January 15, 1986	ONERA continues work on test rig.	-	-
January 16, 1986	Prop-Fan arrives - uncrated and set-up initiated.	-	-
January 17, 1986	ONERA working on test rig - H.S. continues test setup.	-	-
January 20, 1986	Rig ready for Prop-Fan installation	-	-
January 21, 1986	Prop-Fan installation underway.	-	-
January 22, 1986	ONERA continues chariot work - H.S. continues installation of Prop-Fan.	-	-
January 23, 1986	Stubs installed - Instrumentation set-up underway.	-	-
January 24, 1986	Tiedown continues - Centerbody being installed.	-	-
January 27, 1986	Rig rods/cable installation underway - Stubs shimmed for shake test with dry prop.	-	-
January 28, 1986	ONERA working on support system.	-	-

CHRONOLOGICAL HISTORY OF TEST (Continued)

Date	Event	Test Time (Hr. : Min.)	Accum. Test Time (Hr. : Min.)
January 29, 1986	Chariot moved into tunnel loop - Shake test set-up continues.	-	-
January 30, 1986	Shake test initiated.	-	-
January 31, 1986	Shake test continued.	-	-
February 3, 1986	Shake test continued.	-	-
February 4, 1986	Shake test continued - ONERA trial fitting blockage.	-	-
February 5, 1986	Shake test continued.	-	-
February 6, 1986	Shake test completed - Initiated set-up for spinner drag test.	-	-
February 7, 1986	H.S. continued work on Prop-Fan - ONERA preparing for tare test.	-	-
February 10, 1986	Preparation continued for tare test.	-	-
February 11, 1986	Preparation continued.	-	-
February 12, 1986	Tunnel blowdown completed - Completed tare test for M_N = .2, .35.	-	-
February 13, 1986	Tunnel inspected - Ran tunnel cal to M_N = .85.	-	-
February 14, 1986	Spinner drag test started at 1220 hrs - Test completed up to M_N = .85.	-	-

CHRONOLOGICAL HISTORY OF TEST (Continued)

Date	Event	Test Time (Hr. : Min.)	Accum. Test Time (Hr. : Min.)
February 17, 1986	Started blade installation for 4 blade test.	-	-
February 18, 1986	Completed installation and checkout of blades.	-	-
February 19, 1986	Prop-Fan serviced with oil - replaced No. 3 blade seal - installed brush block and beta cable.	-	-
February 20, 1986	Safety meeting held - Engine oil loss during initial runs.	:34	:34
February 21, 1986	Balance runs made without air - problems with power supply.	1:00	1:34
February 24, 1986	Dynamic balance achieved - problems with blade angle calibration.	2:25	3:59
February 25, 1986	Tunnel power failed during first attempt to run with wind - Computer memory lost - subsequent engine problem - Completed M_N = .2.	1:03	5:02
February 26, 1986	H.S. instrumentation problems - Completed M_N = .35, .50	3:33	8:35
February 27, 1986	Continued points up to M_N = .80.	5:43	14:18
February 28, 1986	Improved balance - Ran to M_N = .836 before laminated centerbody tore loose. Testing terminated temporarily to repair damage to blades, rig and tunnel.	3:41	17:59
March 1 thru March 12, 1986	H.S. repairing 2 damaged blades at H.S. ONERA rebuilding centerbody.	-	17:59

CHRONOLOGICAL HISTORY OF TEST (Continued)

Date	Event	Test Time (Hr. : Min.)	Accum. Test Time (Hr. : Min.)
March 13, 1986	H.S. personnel at tunnel - Began installing blades (2 blade test).	-	17:69
March 14, 1986	Began balance runs - Centerbody installation completed.	:07	18:06
March 16, 1986	Continued work on Prop-Fan instrumentation.	-	18:06
March 17, 1986	Adjustments made to centerbody - Balance runs continued - Support cables (30°) installed.	:19	18:27
March 18, 1986	2 blade test started - Heavy rig vib. - cables removed - RPM sweep to 1855, M_N = 0.2.	4:35	23:02
March 19, 1986	Completed test points to M_N = .8. Rig angle of attack to be changed to 3°.	5:34	28:36
March 20, 1986	Improved prop balance - Completed test points to M_N = .78 with 3° inflow. Angle of attack to be changed to 10°.	5:29	34:05
March 21, 1986	During initial prop balance run, high rig vibration - Prop balance good - returning to 0° inflow.	:30	34:35
March 22, 1986	Installing blades for 8 blade test.	-	34:35
March 23, 1986	Blade installation and instrumentation continued.	-	34:35

CHRONOLOGICAL HISTORY OF TEST (Continued)

Date	Event	Test Time (Hr. : Min.)	Accum. Test Time (Hr. : Min.)
March 24, 1986	Support structures installed - Balance runs initiated.	:10	34:45
March 25, 1986	Support structures rearranged - Heavy rig vibrations.	1:30	36:15
March 26, 1986	Balance runs continued - Ran M_N = .2 points. Rig unstable between 1000 to 1500 RPM.	2:37	38:52
March 27, 1986	Completed points at M_N = .2, .5, .73. Can't run at M_N = .8 due to negative thrust on test rig.	3:22	42:14
March 28, 1986	Tap test revealed delamination of S/N 057 (No. 7) blade. Set-up for steady pressure test initiated.	-	42:14
April 1, 1986	Scanivalve installation underway.	-	42:14
April 2, 1986	Delaminated blade being repaired on site - Scanivalve work continued.	-	42:14
April 3, 1986	Work on blade and Scanivalve continued.	-	42:14
April 4, 1986	Balance runs initiated - Completed M_N = 0 test points.	2:11	44:25
April 7, 1986	Prop unbalance drifts during runs - Additional balance runs made - Completed test points up to M_N = .45 before Scanivalve support cable failed - Umbilical severed.	4:25	48:50

CHRONOLOGICAL HISTORY OF TEST (Continued)

Date	Event	Test Time (Hr. : Min.)	Accum. Test Time (Hr. : Min.)
April 8, 1986	Back-up scanivalve installed - ONERA modifying damaged support hardware - Ran test points for M_N = 0, .3.	4:56	53:46
April 9, 1986	Unusual high rig vibration continues - runout measurements taken at end of day - Decided to terminate testing.	1:17	55:03
April 10, 1986	Minimum body disassembled to determine reason for rig vibration - No significant discoveries yet.	-	55:03
April 11, 1986	Continued teardown - Nothing found - Chariot removed from test section.	-	55:03
April 14, 1986	Continued teardown and disassembly.	-	55:03
April 15, 1986	Prop-Fan disassembly completed.	-	55:03
April 16, 1986	Severe fretting corrosion found on test rig cone seat.	-	55:03

NOTE: (Testing Resumed in 1st QTR 1987 to Complete Steady and Unsteady Pressure Testing)

January 28, 1987	H.S. personnel at tunnel - ONERA continues setting up test rig with new drive shaft.	-	55:03
January 29, 1987	Began Prop-Fan assembly.	-	55:03
January 30, 1987	Completed Prop-Fan installation.	-	55:03

CHRONOLOGICAL HISTORY OF TEST (Continued)

Date	Event	Test Time (Hr. : Min.)	Accum. Test Time (Hr. : Min.)
February 2-8, 1987	ONERA conducted vibration tests during this period	-	55:03
February 9, 1987	H.S. personnel at tunnel - Instrumentation installation begins - Completed shake tests.	-	55:03
February 10, 1987	Instrumentation set-up continues.	-	55:03
February 11, 1987	Chariot moved into tunnel - Support cables installed.	-	55:03
February 12, 1987	Tunnel calibration initiated.	-	55:03
February 13, 1987	Tunnel calibration completed - Trial set-up of wake generator and checkout to M_N = .83.	-	55:03
February 16, 1987	Continued wake generator checkout - Completed in evening - Wake generator removed.	-	55:03
February 17, 1987	Chariot removed from tunnel - Scanivalve set-up underway.	-	55:03
February 18, 1987	Continued scanivalve set-up.	-	55:03
February 19, 1987	Scanivalve set-up continued - Check out of restraint design underway - Chariot installed in tunnel.	-	55:03
February 20, 1987	Ran tunnel to M_N = .83 to check scanivalve restraint.	-	55:03

CHRONOLOGICAL HISTORY OF TEST (Continued)

Date	Event	Test Time (Hr. : Min.)	Accum. Test Time (Hr. : Min.)
February 23, 1987	Installed both pressure blades - Trouble-shooting instrumentation.	-	55:03
February 24, 1987	Completed blade hook-up - Continued working on instrumentation problems.	-	55:03
February 25, 1987	Continued tiedown of instrumentation and scanivalve.	-	55:03
February 26, 1987	NASA representative at tunnel - Instrumen-tation troubleshooting continued.	-	55:03
February 27, 1987	Initialed balance runs - Damage incurred to unsteady pressure blade - Completed test points for $M_N = 0$.	1:57	57:00
February 28, 1987	Replaced unsteady pressure blade with counterweight blade - Continued trouble-shooting steady pressure blade problem.	-	57:00
March 2, 1987	Troubleshooting scanivalve continued - Initial balance runs made.	2:33	59:33
March 3, 1987	Continued troubleshooting scanivalve - Continued attempts to improve balance.	:43	60:16
March 4, 1987	Balance problems continued - Work continued on scanivalve.	1:53	62:09
March 5, 1987	Scanivalves swapped - Attempted 2 plane dynamic balance - Good balance achieved - Scanivalve working flawlessly.	2:00	64:09

CHRONOLOGICAL HISTORY OF TEST (Continued)

Date	Event	Test Time (Hr. : Min.)	Accum. Test Time (Hr. : Min.)
March 6, 1987	Steady pressure testing initiated - Completed Row No. 5 to M_N = .78.	3:57	68:06
March 9, 1987	Completed Rows 13 and 11 - FOD on S.P.B.	5:15	73:21
March 10, 1987	Completed Rows 9 and 7 - FOD continues.	5:34	78:55
March 11, 1987	Engine fuel problem - Completed Rows 12 and 3.	5:18	84:13
March 12, 1987	Completed Rows 10, 1 and 8.	6:07	90:20
March 13, 1987	Completed Row 6 - Ran points for Rows 4, 7 and 2 - Discovered debris loose in tunnel - Steady pressure testing completed.	6:04	96:24
March 14, 1987	Troubleshooting problems with unsteady pressure blade.	-	96:24
March 16, 1987	Completed work on blade - Blade installed and tied down.	-	96:24
March 17, 1987	Balance runs made - Inflow angle at 3° - Began collecting data up to M_N = .7.	2:02	98:26
March 18, 1987	Inflow angle returned to 0° - Wake generator installed - Collected data up to M_N = .5.	1:19	99:45
March 19, 1987	Reran test points up to M_N = .5 - Removed wake generator - Collected remaining test-points up to M_N = .5 - Unsteady pressure test completed.	2:28	102:13

CHRONOLOGICAL HISTORY OF TEST (Continued)

Date	Event	Test Time (Hr. : Min.)	Accum. Test Time (Hr. : Min.)
March 20, 1987	Removed Chariot - Disassembled Prop-Fan.	-	102:13
March 23, 1987	Equipment prepared for shipment.	-	102:13

1. Report No.	2. Government Accession No.	3. Recipient's Catalog No.
NASA CR 182125		

4. Title and Subtitle

LARGE-SCALE ADVANCED PROP-FAN (LAP)
HIGH SPEED WIND TUNNEL TEST

5. Report Date: JULY 1988

6. Performing Organization Code: 73030

7. Author(s): William A. Campbell, Peter Arseneaux, Harold S. Wainauski

8. Performing Organization Report No.: HSER 11894

9. Performing Organization Name and Address
HAMILITON STANDARD DIVISION
UNITED TECHNOLOGIES CORPORATION
ONE HAMILTON ROAD
WINDSOR LOCKS, CT 06096

10. Work Unit No.: 535-03-01

11. Contract or Grant No.: NAS3-23051

12. Sponsoring Agency Name and Address
NASA Lewis Research Center
21000 Brookpark Rd.
Cleveland, Ohio 44135

13. Type of Report and Period Covered: CONTRACTOR REPORT

14. Sponsoring Agency Code

15. Supplementary Notes
Project Manager: J. Notardonato, Advanced Turboprop Project Office
NASA Lewis Research Center
Cleveland, OH 44135

16. Abstract

High Speed Wind Tunnel testing of the SR-7L Large Scale Advanced Prop-Fan (LAP) is herein reported. The LAP is a 2.74 meter (9.0 FT) diameter, 8-bladed tractor type rated for 4475 KW (6,000 SHP) at 1698 RPM. It was designed and built by Hamilton Standard under contract to the NASA Lewis Research Center. The LAP employs thin swept blades to provide efficient propulsion at flight speeds up to Mach .85.

Testing was conducted in the ONERA SIMA Atmospheric Wind Tunnel in Modane, France. The test objectives were to confirm the LAP is free from high speed classical flutter, determine the structural and aerodynamic response to angular inflow, measure blade surface pressures (static and dynamic) and evaluate the aerodynamic performance at various blade angles, rotational speeds and Mach numbers.

The measured structural and aerodynamic performance of the LAP correlated well with analytical predictions thereby providing confidence in the computer prediction codes used for design. There were no signs of classical flutter throughout all phases of the test up to and including the 0.84 maximum Mach number achieved. Steady and unsteady blade surface pressures were successfully measured for a wide range of Mach numbers, inflow angles, rotational speeds and blade angles. No barriers were discovered that would prevent proceeding with the PTA (Prop-Fan Test Assessment) Flight Test Program scheduled for early 1987.

17. Key Words (Suggested by Author(s))	18. Distribution Statement
Advanced Turboprop Prop-Fan Energy Efficient Propeller High Speed Wind Tunnel	This document will remain under distributic limitation until July 1989.

19. Security Classif. (of this report)	20. Security Classif. (of this page)	21. No. of Pages	22. Price*
UNCLASSIFIED	UNCLASSIFIED	193	

[redacted]